UNIVERSITEIT VAN PRETORIA
UNIVERSITY OF PRETORIA
YUNIBESITHI YA PRETORIA

Cellular effects of Coenzyme Q10 and Resveratrol in the SJL/J dysferlinopathy mouse model

By

Marnie Potgieter

Submitted in partial fulfillment of the requirements for the degree

Doctor of Philosophy

(PhD)

In the faculty of Health Sciences

Department of Anatomy

University of Pretoria

South Africa

Supervisor: **Prof E Pretorius**

Co-supervisor: **Dr M Beukes**

Department of Anatomy

Faculty of Health Sciences

2009

UNIVERSITEIT VAN PRETORIA
UNIVERSITY OF PRETORIA
YUNIBESITHI YA PRETORIA

Cellular effects of Coenzyme Q10 and Resveratrol in the SJL/J dysferlinopathy mouse model

By

Marnie Potgieter

Supervisor: Prof E Pretorius

Co-supervisor: Dr M Beukes

Department: Anatomy

Degree: Doctor of Philosophy

Abstract

The muscular dystrophies (MDs) are genetic disorders of muscle degeneration due to mutations in genes that encode a wide variety of proteins. Dysferlinopathy encompasses a large variety of neuromuscular diseases characterized by the absence of dysferlin in skeletal muscle and an autosomal recessive mode of inheritance. Dysferlinopathy can manifest as limb girdle muscular dystrophy type 2B (LGMD 2B), Miyoshi myopathy (MM) or distal myopathy with anterior tibial onset (DMAT). The first symptoms usually appear during the second or third decade of life as clumsiness when running, fatigue when walking long distances and difficulty in climbing stairs. Progression of the disease eventually leads to a loss of ambulation.

A deficit in membrane-repair machinery in dysferlinopathy suggested a direct role for dysferlin in the Ca^{2+}-dependent membrane-repair process. Recently, dysferlin has also been implicated in the process of chemotaxis. Evidence exists that free radical mediated injury contributes to the pathogenesis of muscle necrosis in the muscular dystrophies. The imbalance of free radical synthesis and antioxidant capacity has been suggested to contribute to the necrotic process.

It is therefore imperative to explore the effect of antioxidant supplementation in the MDs. The present study followed a novel approach in investigating the cellular effects afforded by the supplementation of the SJL/J mouse model for dysferlinopathy with the antioxidants, Coenzyme

Q10 (CoQ10) and resveratrol. The study aimed to determine, at cellular level, the histopathology and ultrastructural changes in the SJL/J mouse model following a 90 day trial with antioxidant supplementation. In addition to studying the morphology, the study paid attention to non-specific parameters. The study mainly focused on the histopathology and ultrastructural alterations in the SJLL/J mouse. In addition the oxidative stress index of the affected quadriceps muscle was determined.

The outcome provides evidence that increased oxidative stress levels are present in the SJL/J mouse. Antioxidant supplementation with CoQ10 at 120mg/kg/day or a resveratrol/CoQ10 combination supplementation at 40 and 60mg/kg/day, decreased the levels of oxidative stress and dystrophic markers at a cellular level. In addition, increased physical strength was observed. This thesis provides evidence to create a new platform for combination therapeutic strategies.

UNIVERSITEIT VAN PRETORIA
UNIVERSITY OF PRETORIA
YUNIBESITHI YA PRETORIA

Declaration

I, Marnie Potgieter, hereby declare that this thesis entitled:

Cellular effects of Coenzyme Q10 and Resveratrol in the SJL/J dysferlinopathy mouse model

which I herewith submit to the University of Pretoria for the Degree of Doctor of Philosophy in Anatomy, is my own original work and has never been submitted for any academic award to any other tertiary institution for any degree.

30 November 2009

Date

Marnie Potgieter

I will praise thee; for I am fearfully and wonderfully made: marvellous are thy works; and that my soul knoweth right well.

Psalm 139:14

Ek wil U loof, want U het my op 'n wonderbaarlike wyse geskep. Wat U gedoen het vervul my met verwondering.

Acknowledgements

Praise be to my Father in Heaven. Thank you, dear Lord for the opportunity, not only to walk on Thy ways in this world, but for carrying me when I get tired. Thank you for not only allowing me to dream, and for making them true, but for giving me this precious opportunity to live a dream.

Thank you to my Mother and Father for your love, constant support, and motivation throughout the years. Thank you for all the opportunities you gave me in life, it is because of you that I could achieve this great milestone. Thank you for all your prayers. My dear Mother, thank you for being my best friend and for always being just a phone call away. Thank you for always making sure that I have all I could ever need and more, throughout my life. You are God's ever-flowering rose in my garden of hope. Thank you for the sketches that you've made for this thesis. It adds a very special touch.

Piet and Faan, my dear brothers. You have always been a great inspiration to me. Thank you for your love and support, and for believing in me.

Johan. How will I ever be able to put the gratitude in my heart to words. Thank you for always being by my side; for your love, support, and motivation. Thank you for always being there when I needed you most. For sacrificing so many things you could have had in life, to make sure I have all I needed.

In loving memory of dearest Grandfather, Piet Potgieter. How I wish I could share with you this dream that you have made possible for me. I am so grateful for all the wonderful times I had with you. For all the things I have learnt from you, and for all you have done for me. I know you were my greatest admirer; you were also my greatest hero. Your legendary colours paint a rainbow in my sky every day. You will forever live on in my heart, and I will always try to do what you have so masterly done as a way of living; to give without ever expecting anything in return, and to love, as if you have never been hurt.

Prof Resia Pretorius, my study leader and supervisor for four years. Thank you for your valuable contribution to make this dream come true. Thank you for the opportunity that you have given me to accomplish this milestone. Thank you for so unselfishly sacrificing your time to help me through this thesis.

Dr Mervyn Beukes, co-supervisor for the study. Thank you for all the long hours spent in the lab with me. Thank you for your words of encouragement towards the end when I struggled to keep up.

Dr Roland Auer, head of UPBRC at the time, Michelle Auer and Santa Meyer (veterinary technologists). Thank you for your commitment and dedication to make the animal study a huge success. I am grateful for all the time you have spent so selflessly to make this possible for me. Thank

you for always doing more than was expected from you. Thank you to Arno Louw, UPBRC, for all you have done to get the tensile strength test meter in time.

I owe gratitude to the staff of the Department of Anatomy, and the head of the department, Prof Jan Meiring, for having me as a student and for the great opportunity to build my carreer in science. Also to the Department of Biochemistry, Prof Jan Verschoor, Prof Zeno Appostolides, Nicolene Fourie, and Sandra van Wyngaardt. Thank you for having me as a guest student, for making your facilities available to me, and for your friendliness during the numerous hours I have spent in your labs.

I am also in debted to the Unit for Electron Microscopy. I am grateful for the opportunity that I had to spend so many hours in the facility, to have learnt so many things. Thank you to the staff, for all your assistance and support. Uncle Chris, thank you for being the shoulder I could cry on whenever I got tired. Thank you for your advice and encouragement. Thank you for always making me feel so at home in the facility.

Warren Vieira, I'm forever in debted to you. Thank you for all the assistance with the stats. Thank you for always being willing to help and for being available whenever I needed you.

Nanette, thank you for your constant motivation and encouragement, and for all assistance that you've offered so selflessly during the course of my study. Thank you for so many good years of friendship. We have now accomplished what we have started some four years ago. I am proud of you!

My true and trusted friend, Fiona. I thank you for all your support; for helping me out in a time when I needed you most. I greatly appreciate all you have done for me.

My dear friend Jana, thank you for all your prayers and constant support in good times and in bad. I am so grateful that the Lord, our God, has given me this precious friendship; a sister to run with me in this challenging race to the purpose of life on earth.

Wendy, thank you very much for the white blood cell counts

Mrs Janis de Graaf, thank you very much for the numerous hours that you have sacrificed to help me with the grammar.

To all my friends and family, thank you for your love and support.

TABLE OF CONTENTS

LIST OF FIGURES

LIST OF TABLES AND TEXT BOXES

LIST OF ABBREVIATIONS AND SYMBOLS

%	percentage
®	registered sign
°C	degrees celcius
µl	microliter
µm	micrometer
10q24	the gene location for *MYOF*
11q12-13	gene location for AHNAK
14q32	gene location for AHNAK nucleoprotein 2
2p13	gene location for *DYSF*
8-OH-dG	8-hydroxy-deoxyguanosine
A/J	Albino mouse strain with spontaneous progressive muscular dystrophy due to dysferlin mutation
aa	amino acids
A-band	anisotropic band
$ABTS^{+}$	2,2'-azinobis(3-ethylbenzothiazoline sulphonate)
ADP	Adenosine diphosphate
$ADP\text{-}Fe^{3+}$	Adenosine diposphate iron tri-oxide
AED	animal equivalent dose
ANOVA	Analysis of variance
ATP	Adenosine triphosphate
AU	arbitrary units
Balb/c	albino, laboratory-bred strain of the house mouse
BAR	family of genes
BHP	tert-butylhydroperoxide
BHT	butylated hydroxytoluene
Bin-1	conserved member of the BAR family of genes implicated in myoblast differentiation and membrane deformation
BMD	Becker muscular dystrophy
bp	base pair
BSA	Body surface area
BW755c	
c.elegans	*Caenorhabditis elegans*
C2C12	myoblast mouse cell line
Ca^{2+}	Calcium
CAT	catalase
CAV3	caveolin 3 gene
$CD4^{+}$	A glycoprotein expressed on the surface of T helper cells (cluster of differentiation)

cDNA	complementary deoxyribonucleic acid
CH	calponin homology
CK	Creatine kinase
CMD/MDC	Congenital muscular dystrophies
Co	Company
CO_2	Carbon dioxide
CoQ	Coenzyme Q
CoQ10	Coenzyme Q10
COQ2	OH-benzoate prenyl-transferase gene
$CoQH_2$	reduced form of CoQ10/ubiquinol
COX	cyclooxygenase
CPK	creatine phosphokinase
CT	computed tomography
C-terminal	carboxy terinal
Cu,Zn SOD	Copper/Zinc superoxide dismutase
DACM	distal anterior compartment myopathy
DAPC	dystrophin associated protein complex
DFBN9	a specific type of autosomal recessive deafness in humans
DGC	Dystrophin-glycoprotein complex
DHEA	dehydroepiandosterone
DHPR	dihydropyridine receptor
DM	Myotonic dystrophy
DMAT	Distal myopathy with anterior tibial onset
DMD	Duchenne muscular dystrophy
DNA	deoxyribonucleic aced
DPC	dystrophin protein complex
DTT	1,4-Dithiothreitol
dy/dy	homozygous dystrophic mouse strain with dy mutation, suggested to be a mutation in the M-chain gene; animals display a more severe phenotype than the mdx mouse
DYSF	dysferlin gene
Dysf^{im}	Allele responsible for decreased levels of dysferlin in SJL/J mice; inflammatory myopathy allele
E	Expect value. The E-value is a parameter that describes the number of hits on can 'expect' to see by chance when searching a database of a particular sized.
EAE	experimental autoimmune encephalitis
EAM	Autoimmune myositis
EBD	extensor digitorum brevis
ECM	extra cellular matrix
EDL	extensor digitorum longus
EDMD	Emery-Dreifuss muscular dystrophy
EDTA	ethylenediaminetetraacetic acid

EHL	extensor hallicus longus
EM	electron microscopy
F28+	28th generation
F4/80	an antibody used to identify mouse macrophages
FA	focal adhesion
FDA	Food and Drug Administration
FER-1	*C. elegans* ferlin-1 gene
FER-1	nematode protein ferlin-1
FER1L1	dysferlin
FER1L2	otoferlin
FER1L3	myoferlin
FER1L4-6	proteins that are predicted form the human and mouse genomic sequences but have not yet been characterized
FKRP	Fukutin-related protein
FSHD	Facioscapulohumeral dystrophy
g	gauge
g	gram
Glocuse-6-P	glucose-6-phosphate
Gluconate-6-P	Gluconate-6-phosphate
GM-CSF	monocyte-colony stimulating factor
GPx	glutathione peroxidase
GRMD	golden retriever muscular dystrophy
GSH	glutathione
H	Hydrogen
H_2O_2	hydrogen peroxide
HED	human equivalent dose
HEPA	high efficiency particulate air
HMG-CoA	3-hydroxy-3-methylglutaryl-coenzyme A
H-zone	*Heller* zone
I-band	isotropic band
IFCC	International Federation of Clinical Chemistry and Laboratory Medicine
IFN-γ	interferon-γ
IgE	immunoglobulin E
IL	interleukin
ILK	integrin-linked kinase
IU	international units
IVC	individually ventilated microisolator-cages
IκBα	nuclear factor of kappa light polypeptide gene enhancer in B-cells inhibitor, alpha
K	conversion factor
K_2PO_4	potassium phosphate
Kb	kilobyte

KCl	potassium chloride
kDa	kilodalton
kg	kilogram
Km	The K_m factor, body weight (kg) divided by BSA (m^2), is used to convert the mg/kg dose used in a study to an mg/m^2 dose
kV	kilo volt
$L^{\bullet}$	Carbon-centered radical
LARGE	The LARGE gene was so named because it covers over 660 kb of genomic DNA; the protein it encodes is a putative glycosyltransferase.
LDH	Lactate dehydrogenase
LGMD	Limb girdle muscular dystrophy
LGMD 2B	Limb girdle muscular dystrophy type 2B
$LOO^{\bullet}$	lipid peroxyl radicals
LOOH	lipid hyperoxide
M	molar
MAC	membrane attack complex
MCK	myosin creatinine phosphokinase
MD(s)	Muscular dystrophy/dystrophies
MDA	Malondialdehyde
mdx	Dystrophin-deficient mouse model for Duchenne muscular dystrophy
mg/kg	milligram per kilogram
mg/kg/day	milligram per kilogram per day
mg/m^2	milligram per square meter
MHC-1	myosin heavy chain class I
min	minutes
ml	millilitre
M-line	*mittel* line
mm	millimetre
mM	millimolar
MM	Miyoshi myopathy
mmol/g	millimoles per gram
Mn-SOD	Manganese superoxide dismutase
MRC	Medical Research Council
MRC-5	human lung cell line
MRI	magnetic resonance imaging
mRNA	messenger ribonucleic acid
MYOF	the gene for myoferlin
n	sample size
Na_2CO_3	sodium carbonate
NAD^+	nicotinamide adenine dinucleotide
NADPH	nicotinamide adenine dinucleotide phosphate

NCL-Hamlet	Mouse monoclonal antibody against dysferlin
NF-κB	nuclear factor kappa-light-chain-enhancer of activated B cells
NK	natural killer
nm	nanometer
nmol/g	nanomoles per gram
NO•	nitric oxide
NOS	nitric oxide synthase
N-terminal	Nuclear terminal
O_2^-	superoxide
O_3	singlet oxygen
OGHD	oxoglutarate dehydrogenase
OH^-	hydroxyl radical
OH	hydroxide
$ONOO^-$	peroxynitrite
OPMD	Oculopharyngeal muscular dystrophy
OSI	oxidative stress index
OsO_4	osmium tetroxide
PA	Pennsylvania
PBS	Phosphate buffered saline
PD	proximodistal phenotype
pH	measure of the acidity or basicity / potential of Hydrogen
POMT1	Protein O-linked mannose β-1,2-N-acetylglucosaminyltransferase.
PT	posterior tibial
PUFA	polyunsaturated fatty acids
P-value	level of significance / probability value
r^2-value	coefficient of determination
RNA	Ribonucleic acid
ROS	reactive oxygen species
Rpm	revolutions per minute
RuO_4	ruthenium tetroxide
S100A10	a protein encoded by the *S100A10* human gene
S100A11	a protein encoded by the *S100A11* human gene
SD	standard deviation
SE	standard error
sec	seconds
SEM	scanning electron microscopy
SH3	domain in myoferlin that may mediate interactions with other proteins
SJL/J	Swiss Jim Lambert; Dysferlin-deficient strain of Swiss mice; animal model for dysferlinopathy

SJL/Olac	SJL strain obtained by the Clinical Research Centre, Harrow from the Jackson Laboratory, Bar Harbor in 1975, to OLAC, now Harlan Laboratories in 1977. This strain is now known as SJL/JOlaHsd
SOD	superoxide dismutase
SR	sarcoplasmic reticulum
STIR	short-time-inversion-recovery
SWR/J	Swiss mice used widely in research as general purpose strain
TA	anterior tibial/tibialis anterior
TAS	Total antioxidant status
TBA	thiobarbituric acid
TBARS	TBA reactive substances
TCA	trichloroacetic acid
TCAP	Telethonin, a protein that interacts with, or “caps”, another protein in muscle called titin.
TEM	transmission electron microscopy
TNF	tumor necrosis factor
TNFα	tumor necrosis factor-α
TNFα(-/-)	TNFα null mice
TRIM 32	One of 37 TRIM proteins containing a tripartite motif (TRIM).
T-tubule	transverse tubule
U/l	unit per liter
UPBRC	University of Pretoria’s Biomedical Research Centre
USA	United States of America
UV	ultra violet
WW	a protein-binding domain on the dystrophin protein that include two conserved moieties of tryptophan, with W representing the letter code of tryptophan
Z-disc	*Zwishenscheibe* disc
ZNF9	Zinc finger protein 9.

When you love what you're doing, it's hard not to.

Michael S Pepper

Chapter 1

Introduction

Muscular dystrophy (MD) is a class of muscular disorders, classified by its specific mode of inheritance, gene mutation, and muscle groups affected by the pathological progression. First identified in the 17th century, this class of disorders remains a subject in need of continuous research as no effective treatment is available to date.

Dysferlinopathy is sub-classified as a limb girdle type of muscular dystrophy, inherited in an autosomal recessive way. It is affecting the musculature of the pelvic and shoulder girdles. Onset of this muscle deteriorating genetic disease varies from as early as the 2nd decade of life to as late as the 8th decade. Identification of the gene mutated in the dysferlinopathies (Bashir *et al*., 1998; Liu *et al*., 1998), just over a decade ago, created high expectations for an intervention in the limitations inevitably suffered by those affected. Yet, the answer to a full life for dysferlinopathy patients remains to be unravelled. One of the goals of MD research is underscored by the understanding of how sarcolemmal damage is initiated. How it is repaired, and how the sarcolemma can be protected, or the damage minimized by pharmacologic or therapeutic intervention (Lovering *et al*., 2005). The present study follows an in-line approach by employing a neutraceutical treatment strategy.

The mutation in the dysferlin gene results in a deficiency of the protein dysferlin. Dysferlin has been shown to be involved in membrane repair machinery (Bansal *et al*., 2003), and has lately also been implicated in the process of chemotaxis (Chiu *et al*., 2009). From this point of view, and considering its interactions with numerous other proteins as reviewed in chapter 2 of this thesis, it seems likely that dysferlin may also be involved in other cellular processes, and responses, yet to be determined. The deficiency in this protein eventually leads to muscle cell necrosis, muscle deterioration, and in due course, loss of ambulation.

A major focus of biological research, as it is known today, is to elucidate the molecular and cellular mechanisms that underlie human health and disease (Doran *et al*., 2007), and to aim at manipulating the alterations in disease towards a normal phenotype. The possible diversity in the function of dysferlin and the even more diverse cellular effects brought about by its deficiency; render it viable to explore alternative treatment strategies that focus on the cellular effects, rather than the mechanism of the pathology itself. To address the cellular effects caused by dysferlin deficiency at microscopic level will comprise amongst others, the effective inflection of the cellular environment

to maintain cell stability for longer and reduction of the rate of dystrophic progression. Rather than repairing the membrane defect or the defective chemotactic response. The present study follows an alternative approach in applying antioxidant supplementation to provide relief to a cellular environment possibly subjected to oxidative stress.

Professor Karl Folkers was one of the pioneers who realized the body's need for optimal levels of the antioxidant, Coenzyme Q10 (CoQ10). In two successful double-blind trials, Folkers and Simonsen, 1995, were able to show that CoQ10 administration results in definite improved physical performance in a variety of muscular dystrophies. Folkers' team demonstrated CoQ10 to be therapeutically beneficial to a range of dystrophies and atrophies, probably attributed to its essentiality in the bioenergetics of life (Folkers and Simonsen, 1995). Evidence of its deficiency in the muscular dystrophies (Folkers and Simonsen, 1995) renders CoQ10 ideal for an alternative therapeutic approach in the dysferlinopathies.

Deficiency of CoQ10 was recently demonstrated to be an autosomal recessive disorder with heterogenous phenotypic manifestations and genetic background (Gempel *et al*., 2007). Primary CoQ10 deficiency is considered the only treatable mitochondrial disorder, since patients have a response to oral CoQ10 supplementation (Montini *et al*., 2008). In order for CoQ10 to maintain its physiological properties in biological systems, the need exists for optimum levels of the coenzyme in order to meet the metabolic demand. Literature is expanding with reports focusing on the deficiency of CoQ10 in the body.

Folkers and Simonsen, 1995, reported that the muscular dystrophies may have one or more significant vitamin deficiencies of those vitamins required in the biosynthesis of CoQ10 and that these additional diverse deficiencies may be major for the dystrophies. In 1985, Folkers and co-workers showed a deficiency of CoQ10 in muscle mitochondria of muscular dystrophy patients (Folkers *et al*., 1985). Folkers and Simonsen, 1995, suggested that patients suffering from muscular dystrophies should be treated with CoQ10, indefinitely. Available evidence indicates that, owing to its metabolic roles, CoQ10 could positively influence the natural course of disease and potentially enhance the effect of other treatments by correcting some metabolic derangements (Littarru and Tiano, 2005). Metabolic derangements are often not causative; they are known to be the consequences of secondary aspects of diseases (Littarru and Tiano, 2005). Because of its pivotal role in bioenergetics in all cells of the body, numerous systems are affected when the availability of CoQ10 becomes limited. It might therefore be imperative to explore the effect of CoQ10 supplementation in the MDs.

The statement by Bermúdez-Crespo and López in 2007 that it takes a broad, comprehensive and systematic approach to understand biology that is generally unbiased and not dependent on existing knowledge, encouraged the approach followed in the present study. A novel approach in investigating the cellular effects brought about by the supplementation of the SJL/J mouse model for dysferlinopathy with the antioxidants CoQ10 and resveratrol was followed. The main focus of the study was to determine, on a cellular level, the histopathology and ultrastructural changes in the SJL/J mouse model following a 90 day trial with antioxidant supplementation. In addition to studying the morphology, the study also paid attention to parameters that are non- or less-specific to the dysferlinopathies. The SJL/J mouse model was decided upon as the animal model of choice in the present study since a reduction in dysferlin protein in SJL/J mice, consistent with the dysferlin reduction in dysferlinopathy patients renders this model ideal for dysferlinopathy research (Bittner *et al*., 1999).

Non-specific parameters in the present context are regarded as factors that are not directly related to muscle cell structure and not directly affecting histopathology in dysferlin-deficient muscular dystrophy. These parameters include body weight, physical strength, the levels of inflammatory leukocytes at the haematopoietic level, and creatine kinase (CK) and lactic dehydrogenase (LDH) levels in the blood.

The body weight of the mouse is a measure of muscle mass as well as of overall well-being (Li *et al*., 2005), and was measured twice weekly in accordance with the quality assurance of the study, to maintain the animals in optimal condition. Force transduction strength testing is a non-invasive procedure that allows extremely quantitative assessment of treatment (Weller *et al*., 1997). In addition, the tensile strength test is a useful method for assessing disease progression in the SJL/J mouse model, and the effect of different treatments on physical strength.

Massively elevated serum levels of muscle enzymes, including CK, LDH, and aldolase, have been reported in early stage dysferlinopathy (reviewed by Urtizberea *et al*., 2008). In addition, serum CK levels of SJL/J mice have been found to increase along with exacerbation of the inflammatory changes (Nemoto *et al*., 2007).

Leucocytes travel out of the circulatory system in order to elicit an immune response in the tissues where needed. It follows that increased demand for particular leucocytes in various sites is reflected by increased numbers in the circulation. It was therefore decided to carry out a quantitative analysis of white blood cell counts, blood CK and LDH levels, as well as the weight change and tensile

strength of animals in present study. This was done to establish how these parameters were affected by antioxidant supplementation.

Both histo- and ultrastructural pathology have been well established in dysferlinopathy patients (Selcen *et al*., 2001; Fanin and Angelini, 2002; Cenacchi *et al*., 2005) and dysferlin-deficient animal models (Weller *et al*., 1997; Bittner *et al*., 1999; Bansal *et al*., 2003). Nevertheless, the effect of antioxidant supplementation on this level has not been described previously. Therefore, this thesis includes a chapter on the histopathology where the morphology of all groups was compared to reveal the effect of antioxidants. Chapter 5 also investigated the variation that occurred in the muscle fiber size of SJL/J quadriceps and gastrocnemius muscles and the alteration in the variation pattern afforded by antioxidant supplementation.

This thesis elaborated on the histopathological findings by including a chapter on the ultrastructure of the affected quadriceps muscles. The ultrastructural study included the ultrastructural hallmarks of the disease that has previously been described (Selcen *et al*., 2001; Cenacchi *et al*., 2005), but also paid attention to non-specific alterations at the ultrastructural level of the SJL/J mouse. Non-specific alterations were expected to provide insight on possible alternative ongoing pathological processes, or metabolic disturbances, as an effect of the disease. The strong qualitative focus of these two chapters forms the core of the present thesis and provides a detailed outline of muscle morphology, and how it is affected by dysferlin-deficiency in the SJL/J mouse model. It furthermore provided evidence that justified the investigation of the last experimental chapter of this thesis which includes the analysis of oxidative stress levels in the animals.

It has previously been reported that oxidative stress is primarily involved in the patho-meganistic muscle deterioration in the mdx mouse model for dystrophin-deficient MD (Disatnik *et al*., 1998). The lack of previous findings to support this notion in the SJL/J mouse model supported the initiative to determine the levels of oxidative stress in this model. The final experimental chapter of this thesis, therefore, provides an investigation into the level of oxidative stress in the quadriceps muscle of SJL/J mice and how these levels were affected by antioxidant supplementation.

The aim of the study was to determine whether the supplementation of two potent antioxidants, namely resveratrol and CoQ10, could render any benefit to the SJL/J mouse model for dysferlinopathy, when administered as a single daily dose. The study investigated this objective by studying the cellular effects afforded by the antioxidant supplementation in the SJL/J mouse model.

In order to reach this aim the study objectives that underlined the above methodological approach can be summarized as follows: The implementation and execution of a 90 day antioxidant supplementation trial with the SJL/J mouse model to study:

a. Non-specific parameters, including:
    i. Animal weight as a parameter of animal well-being during the course of the trial
    ii. Tensile strength as a parameter of disease progression and physical strength of SJL/J mice
    iii. Enzyme levels of creatine kinase and lactate dehydrogenase in the blood
    iv. White blood cell counts as indicating factor for ongoing inflammatory events

b. Histopathology
    i. As a qualitative parameter for morphological characteristics in the SJL/J mouse on light microscopic level
    ii. As a quantitative parameter for morphometric assessment of fiber size variation

c. Ultrastructure, to study hallmarks of the disease in the SJL/J mouse, and to pay attention to non-specific alterations, and what they might imply

d. Oxidative stress levels in quadriceps muscles by measuring the levels of malondialdehyde (MDA) and the total antioxidant status (TAS). Calculation of the oxidative stress index (OSI) from these two parameters gives a quantitative indication of the degree of oxidative stress.

Also, to establish how these parameters are affected by the antioxidant supplementation with CoQ10 and resveratrol, alone and in combination, at various concentrations.

Two different concentrations of CoQ10, one concentration of resveratrol, and a combination of CoQ10 and resveratrol were utilized. The combination preparation consisted of the same concentration CoQ10 used as the lower dose tested, and the same concentration of resveratrol, as the single supplementation dose administered. It is expected that beneficial effects afforded by the supplementation with antioxidants will be more pronounced with supplementation of the high dose CoQ10, and the combination of resveratrol/CoQ10.

The following hypothesis was formulated upon execution of the present study:

The supplementation of SJL/J mice with the antioxidants CoQ10 and resveratrol will be beneficial to the animals, and the beneficial effect will be evident at cellular level.

This thesis concludes with a summary of the outcome of the present study and how these findings might be implicated in future development of therapeutic strategies.

Chapter 2

Literature Review

2.1 INTRODUCTION

The muscular dystrophies (MDs) are a genetic group of disorders of muscle degeneration due to mutations in genes that encode a wide variety of proteins. These proteins include extracellular matrix proteins, transmembrane and membrane-associated proteins, cytoplasmic enzymes, and nuclear matrix proteins (Cohn and Campbell, 2000). The diseases vary enormously in terms of severity, age of onset, selective muscle involvement, and inheritance pattern. Even different mutations of single genes may cause dystrophies that range from the mildest to the most severe (Rando, 2002). Despite these variabilities, the most significant common feature among all of these disorders is necrotic degeneration of skeletal muscle cells, leading to, sooner or later, a loss of ambulation in the affected. Intensive investigation of the literature in this chapter will provide a comprehensive overview of the muscular dystrophies. It will more specifically shed light on the specific molecular events and mechanisms involved in the course of the dysferlinopathies.

Evidence of oxidative stress as the primary pathogenic factor contributing to the dystrophic process, and the progression of the disease condition, has been reported in dystrophin-deficient MD (Murphy and Kehrer, 1989; Disatnik *et al*., 1998). Although this has not yet been proved in the dysferlinopathies, it seems likely to be relevant. Considering its less aggressive pathologic course, compared to DMD, such an observation would strengthen the possibility that the application of antioxidant supplementation in dysferlin-deficient subjects may render significant value in the dysferlinopathies.

It therefore the aim of the present study to determine, on a cellular level, how the morphology and ultrastructure in dysferlin-deficient SJL/J mouse muscle, will be affected by antioxidant supplementation. In order to proceed, it is of the essence to have an in depth understanding of the disease and its pathologic progression. A detailed review of the specific mechanisms, unravelled to date, in the dysferlinopathies, as well as their involvement in the pathogenesis and disease progression, is presented.

2.2 MUSCULAR DYSTROPHY

The muscular dystrophies are a heterogeneous group of inherited disorders characterized by progressive weakness and degeneration of skeletal muscles. Although known for the selective involvement of skeletal muscles, this selectivity in the MDs is not restricted only to weakness, but also extends to muscle wasting and enlargement (Pradhan, 2006). They have traditionally been classified by clinical presentation, mode of inheritance, age of onset, and overall progression. The development of molecular genetic mapping techniques has shown that a number of clinically similar conditions are linked to a variety of distinct single-gene disorders. So far, the MDs have been mapped to at least 29 different genetic loci, that give rise to at least 34 different clinical disorders (Dalkilic and Kunkel, 2003), and additional information is accumulating rapidly (Lovering *et al*., 2005). Muscular dystrophy includes a spectrum of disorders caused by loss of the linkage between the extracellular matrix and the actin cytoskeleton (Laval and Bushby, 2004).

Duchenne muscular dystrophy (DMD), is the most common form of MD, affecting approximately one in 3 500 newborn males worldwide (Biggar *et al*., 2001; Metules, 2002; Wagner, 2002). It is an X-linked disorder that was first discovered more than a century ago (Duchenne, 1861). Duchenne MD is characterized by progressive wasting of skeletal muscles with the first signs of weakness detectable in the limb girdle muscles. The first symptoms of the disease manifest as early as 5 years of age, followed by an inability to walk by the age of 8 to 12 years (Brooke *et al*., 1989; McDonald *et al*., 1995).

Duchenne muscular dystrophy is caused by the absence of the protein dystrophin, a 427 kilodalton (kDa) protein localised to the cytoplasmic surface of the plasma membrane of muscle fibers in skeletal and cardiac muscle (Lovering *et al*., 2005). Becker muscular dystrophy (BMD) is an allelic variant of DMD. Whereas DMD is caused by the essential absence of dystrophin, BMD is caused by abnormalities in the quality or quantity of dystrophin (Lovering *et al*., 2005). It is generally believed that a greater amount of dystrophin results in a less severe form of the myopathy (Kakulas, 1999). The onset of BMD is usually between the ages of 5 and 15 years, but can occur as late as the fourth decade of life (Lovering *et al*., 2005). The phenotypic presentation of BMD is similar to that of DMD, but is clinically milder and with more variability and a much slower progression. Patients with BMD do not have contractures or severe scoliosis, and many live well into adulthood, sometimes to a normal life span (Lovering *et al*., 2005).

The dystrophin protein is responsible for mechanical stability of the sarcolemma. It is likely involved in force transmission between the intracellular contractile apparatus and the extracellular matrix (ECM), which envelops the fiber and is connected to the tendon (Petrof *et al*., 1993). Without dystrophin the structural stability of the sarcolemma is compromised, leading to fragility and inability to withstand the stresses of normal muscle contractions (Petrof *et al*., 1993). The resulting membrane damage leads to increased intracellular Ca^{2+}, which activates proteases that ultimately result in fiber death or necrosis.

The regeneration of myofibers that normally occurs after damage to healthy skeletal muscle, also in the first few years of life in muscle of DMD patients, does not persist as these patients mature. The regenerative capacity of dystrophin-deficient muscle becomes inadequate to effectively replace lost muscle fibers (Blau *et al*., 1983; Webster and Blau, 1990; Bockhold *et al*., 1998). Necrotic fibers are replaced by fat and connective tissue, leading not only to muscle wasting and weakness, but also to an apparent 'pseudohypertrophy' (Lovering *et al*., 2005). This phenomenon is mostly observed in calves of boys suffering from Duchenne's. This muscle wasting and weakness is responsible for a clinical hallmark of the disease termed Gowers' sign that was first described in 1887. It is also referred to as Gowers' manoeuvre.

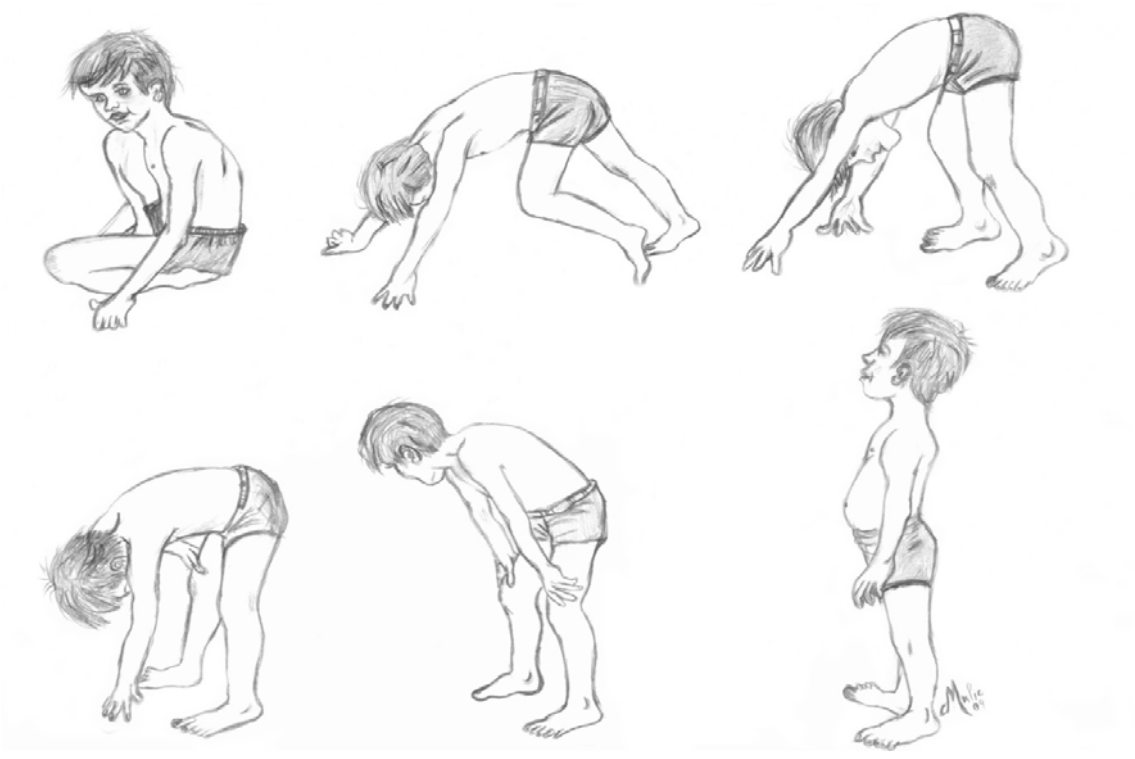

Figure 2.1: Schematic representation of Gower's sign in the muscular dystrophies.

Gowers' sign (Figure 2.1) was first illustrated by Sir William Richard Gowers (1845-1915). He described the characteristic peculiarity in which children with Duchenne dystrophy rise from a seated position. These children use their upper body strength by placing their hands on their knees, climbing up their thighs by pushing with their hands and arms in order to overcome weakness of the pelvic girdle muscles when attempting to rise from the floor (Figure 2.1)(Pearce, 2000; Hartman *et al*., 2007).

The clinical hallmark of a condition, then termed pseudo-hypertrophic muscular paralysis, known as Gowers' sign, was described with exceptional detail by Gowers (Gowers, 1886 in Pearce, 2000). As this detailed clinical illustration still holds diagnostic value in modern medicine, Sir Gowers' exact description is sketched in his own words in text box 2.1.

Text box 2.1

Gowers' sign

"The difficulty in going upstairs is especially due to the weakness of the extensors of the knee and hip. The defect of the extensors of the hip causes the gait to have a peculiar oscillating characters. The greatest defect, however, is in the power of rising from the floor, and the most characteristic peculiarity is the mode in which this is achieved, if it be still possible, and no objects near, by which the patient can aid himself. He commonly has not sufficient power to extend the knees when the weight of the trunk is on the upper extremity of the femur, which is then a lever in which power, applied between the fulcrum and the weight, acts at least advantage. He therefore places his hands on his knees, his arms thus bring much of the weight of the upper part of the trunk on the femur close to the fulcrum, between this and the power, which can then act at greater advantage. When the knees are extended, the power of the extensors of the hip may be sufficient to raise the body into the upright position, or the patient may aid them by an upward push with the hand as he takes it off. If, however, these extensors are weak, the hands are often moved higher and higher up the thighs, grasping alternately, and thus pushing up the trunk. To get the requisite support, the knees must not be quite extended, and if their extensors have no power, the device cannot be employed, and the patient is altogether unable to rise. In many cases, especially when extension of the hip is easy, the patient achieves the extension of the knees in another way; he puts the hands on the ground, stretches out the legs behind him far apart, and then, the chief weight of the trunk resting on the hands, by keeping the toes on the ground and pushing the body backwards, so as to bring a larger portion of the weight of the trunk over the legs. Then one hand is placed upon the knee, and a push with this, and with the other hand on the ground, is sufficient to enable the extensors of the hip to bring the trunk into the upright position." (Sir William R Gowers, 1887)

A great deal about the genetic basis of the dystrophin-deficient disease has been unravelled (Lovering *et al*., 2005), since the cloning of the mutated gene in the 1980s (Murray *et al*., 1982; Kunkel *et al*., 1985). The identification of its protein product, dystrophin, (Hoffman *et al*., 1987) the complex it forms in muscle, (Ehmsen *et al*., 2002) and the mapping of mutations linked several MDs and their associated proteins to dystrophin.

In skeletal muscle injuries, particularly those resulting from lengthening, or eccentric contractions, the membrane is damaged and the cytoskeleton is disrupted (Lovering and De Deyne, 2004), leading to a compromise in the structural stability of the muscle cell. The initial injury is followed by pain, inflammation, and weakness that usually results in necrosis, which is then followed by regeneration of muscle fibers (Lovering *et al*., 2005). As an effect of the disease, continuous cycles of active regeneration and degeneration follows until this sequence of events eventually falls out of equilibrium, inevitably resulting in muscle wasting.

Dystrophin binds indirectly or directly to a group of proteins at the sarcolemma, collectively known as the dystrophin-associated protein complex (DAPC or DPC) or the dystrophin-glycoprotein complex (DGC) (Straub *et al*., 1997; Allamand and Campbell, 2000; Ehmsen *et al*., 2002; Lovering *et al*., 2005). Dystrophin binds to this complex through the interaction of its WW domain. The W represents the letter code of tryptophan. The WW domain is a protein-binding module composed of 35 to 40 amino acids (aa) that include two conserved moieties of tryptophan (Bork and Sudol, 1994) and nearby sequences with the carboxyterminal (C-terminal) cytoplasmic sequence of β-dystroglycan (Jung *et al*., 1995), a transmembrane protein (Petrucci *et al*., 2001). The N-terminal and extracellular portion of β-dystroglycan associates with α-dystroglycan, which in turn connect the DGC to the ECM (Petrucci *et al*., 2001). The major ligand of α-dystroglycan in the ECM is likely laminin-2, a major component of the basement membrane surrounding the muscle fibers. Neurexin and agrin may also be significant binding partners (Michele *et al*., 2002).

Additional components of the DGC include several sarcoglycans, which also span the sarcolemmal membrane, and peripheral membrane proteins, including syntrophins and dystrobrevins that bind to the C-terminal region of dystrophin. Inside the muscle fiber, the N-terminus of dystrophin binds to F-actin (Norwood *et al*., 2000), connecting the DGC to the actin cytoskeleton and ultimately to the contractile apparatus. Therefore, dystrophin is the central component of the molecular link that connects the contractile apparatus inside the muscle fiber to the ECM outside the muscle fiber (Lovering *et al*., 2005). Dystrophin plays a crucial structural role in stabilizing the sarcolemma during

muscle contraction (Petrof *et al*., 1993), and is thought to transmit force laterally across the sarcolemma to the ECM (Tidball, 1991; Patel and Lieber, 1997). In contrast to DGC-linked muscular dystrophies, dysferlin-linked muscular dystrophies introduce a new class of the disease where the repair, and not the structure of the plasma membrane, is disrupted (Bansal and Campbell, 2004). This is a novel mechanism of muscle degeneration (Bansal and Campbell, 2004).

Table 2.1 The Muscular Dystrophies

Disease	*Protein Missing/Deficient*	*Age of onset*	*Muscles Affected*	*Complications*
DUCHENNE (DMD)	Dystrophin	Early childhood	Muscles of hips, legs, shoulders, and spine, and the heart	Severe muscle weakness and wasting, scoliosis, contractures, respiratory failure, pneumonia, and dilated cardiomyopathy. Death early 20s.
BECKER (BMD)	Dystrophin	Adolescence or adulthood	Similar to DMD	Muscle weakness as in DMD, but slower progress and much less severe. Cardiomyopathy
LIMB-GIRDLE (LGMD)				
LGMD 1A	Myotilin	Adolescence to early adulthood	Proximal shoulder/pelvic girdle musculature	Walking may not be possible within 20 years of onset
LGMD 1B	Lamin			
LGMD 1C	Caveolin			
LGMD 1D	Not identified			
LGMD 1E	Not identified			
LGMD 1F	Not identified			
LGMD 2A	Calpain-3	Infancy to early adulthood	Proximal shoulder/pelvic girdle musculature	Type 2 LGMD is much more severe than type 1 LGMD and some result in a DMD-like phenotype. Cardiac complications, sometimes occurring in later stages.
LGMD 2B	Dysferlin			
LGMD 2C	γ-sarcoglycan			
LGMD 2D	α-sarcoglycan			
LGMD 2E	β-sarcoglycan			
LGMD 2F	δ-sarcoglycan			
LGMD 2G	TCAP			
LGMD 2H	TRIM 32			
LGMD2I	FKRP			
LGMD 2J	Titin			
DISTAL MUSCULAR DYSTROPHIES				
Miyoshi myopathy	Dysferlin	Late adolescence	Posterior compartment of legs	Can eventually affect anterior compartment and distal arm muscles. Slow progression and able to maintain independent ambulation throughout life.
Tibial muscular dystrophy	Titin	Late adulthood	Anterior compartment of legs	Slowly progressive. Eventually can affect upper extremities and heart.
Welander myopathy	Unknown	Fifth decade	Distal muscles of upper limbs	Slowly progressive. Eventually affects lower limbs.
Nonakel myopathy (also known as distal myopathy with rimmed vacuoles) and inclusion body myopathy	Acetylglucosamine epimerase	Late adulthood	Anterior compartment of legs	Display red-rimmed autophagocytic vacuoles. Weakness can progress to proximal muscles, but quadriceps femoris muscles are spared.
Laing myopathy	Unknown	Ranges from infancy to adulthood	Anterior compartment of legs and neck flexors	Weakness can progress to proximal muscles.
Myofibrillary / desmin-related myopathy	Desmin		Initially distal lower extremities, but eventually proximally	Aggregation of desmin and other proteins inclusion bodies. Slow progress, eventual cardiomyopathy.

Disease	*Protein Missing/Deficien*	*Age of onset*	*Muscles Affected*	*Complications*
CONGENITAL MUSCULAR DYSTROPHIES (CMD)				
MDC 1A	Laminin α2 (merosin)	At birth	Proximal limb muscles	Joint contractures, cognitive and speech problems, seizures. Most do not learn to walk. White matter changes and structural abnormalities on magnetic resonance image.
MDC 1B	Not identified	At birth		
MDC 1C	FKRP	At birth		
MDC 1D	LARGE	At birth		
Fukuyama CMD	Fukutin	At birth	Proximal upper limbs, distal lower limbs, face and neck.	Cortex malformation and brainstem hypoplasia. Primarily in Japanese population.
α7 integrin congenital myopathy	α7 integrin	At birth	Mild myopathy	Generalized weakness.
Rigid spine CMD	Selenoprotein N1	At birth	Contractures of spinal extensors	Spine rigidity, early restrictive lung disease.
Muscle-eye-brain disease	POMGnT1 glycotransferase	At birth	Generalized	Retinal abnormality, myopia, cataracts, optic nerve atrophy, seizures.
Bethlem myopathy / Ullrich syndrome	Type VI collagen	At birth	Proximal limb muscles	Early contractures, flat feet. Rare and mild.
OTHER TYPES				
Emery-Dreifuss (EDMD)	Emerin/lamin	Childhood to early teens	Proximal upper extremity and distal lower extremities	Early contractures, cardiomyopathy.
Epidermolysis bullosa	Plectin	Childhood	Generalized	Skin blistering with range of severity, joint contractures, dysphagia.
Oculopharyngeal (OPMD)	Poly-A-binding protein 2	Age 40-60 years	Eyelids, throat	Ptosis of eyelids, dysphagia, aspiration pneumonia.
Facioscapulohumeral (FSHD)	Not identified	Childhood to early adolescence	Face, shoulders, proximal upper extremities	Cardiac conduction defects, mild hearing loss, retinal abnormalities.
Myotonic(DM)	Myotinin protein kinase, ZNF 9	Infancy (more severe) to adulthood	Distal extremity muscles first, then proximal as well	Myotonia, cataracts, hypogonadism, cardiac arrhythmias. Adult form is mild compared to early onset.

Key

TCAP	Telethonin, a protein that interacts with, or 'caps', another protein in muscle called titin
TRIM 32	One of 37 TRIM proteins containing a tripartite motif (TRIM)
FKRP	Fukutin-related protein
LARGE	The LARGE gene was so named because it covers over 660 kb of genomic DNA; the protein it encodes is a putative glycosyltransferase
POMT1	Protein O-linked mannose β-1,2-N-acetylglucosaminyltransferase
ZNF9	Zinc finger protein 9

Reproduced with permission of the authors (Lovering *et al.*, 2005)

2.3 LIMB-GIRDLE MUSCULAR DYSTROPHIES

Limb girdle muscular dystrophy is the generic name for a heterogenous group of neuromuscular disorders inherited either dominantly or recessively. They are characterized by muscle wasting and atrophy mostly in the shoulder and pelvic girdle but with a quite variable degree of severity and disease course (Urtizberea *et al*., 2008).

The diagnostic criteria for this subclass of MDs include raised serum creatine kinase (CK) activity, myopathic electromyography, muscle biopsy with features ranging from mildly myopathic to overt dystrophic changes and absence or reduction of a protein involved in the specific form of LGMD, on a Western blot (Borsato *et al*., 2006). Differential diagnosis of these disorders requires the careful application of a broad range of disciplines including, clinical assessment, immunohistochemistry and immunoblotting, using a panel of antibodies and extensive molecular genetic analysis (Laval and Bushby, 2004).

Within this subclass of MDs are the forms of limb-girdle muscular dystrophy caused by deficiencies of the sarcoglycan complex and by aberrant glycosylation of α-dystroglycan caused by mutations in the fukutin-related protein gene. However, other forms of this disease have distinct pathophysiological mechanisms (Laval and Bushby, 2004). Deficiency of dysferlin disrupts sarcolemmal membrane repair, whilst loss of calpain-3 may exert its pathological influence either by perturbation of the IκBα/NF-κB pathway or through calpain-dependent cytoskeletal remodelling (reviewed in Laval and Bushby, 2004). Implicated in numerous cell-signalling pathways (Shaul and Anderson, 1998), caveolin-3 is also involved in the biogenesis of the transverse tubule (T-tubule) system (Parton *et al*., 1997). Alterations to the nuclear lamina caused by mutations in lamin A or C, sarcomeric changes in titin, telethonin or myotilin at the Z-disc, and subtle changes in the extracellular matrix proteins laminin-α2 or collagen VI can all lead to limb-girdle muscular dystrophy phenotypes. However, the specific pathological mechanisms remain obscure (Laval and Bushby, 2004).

The muscle pathology is characterized by necrotic and regenerating fibers, increase in fiber size variation, fiber splitting and centrally located myonuclei. Chronic cycles of degeneration and regeneration of muscle fibers result in replacement of muscle with fatty and fibrous tissue (Borsato *et al*., 2006). The quest for order in the group of diseases designated 'limb-girdle' muscular dystrophy (LGMD) in the classifications of the 1950's has led in various directions over the past 50 years (Bushby, 1999 a). For most of this time, LGMD has been an unpopular and poorly defined

diagnostic term conveying little information for either the clinician or the patient. In the initial classifications, the description of LGMD emphasized heterogeneity. This include the potential for either autosomal recessive (a defect or mutation on the gene from the chromosome of each parent is involved) or autosomal dominant (single gene defect on a chromosome from either parent or one copy of a mutant gene and one normal gene) inheritance, onset of disease in either the pelvic girdle or the shoulder girdle musculature, and slow or more rapid progression. Even sporadic cases of LGMD have been reported (Stübgen and Stipp, 1997; Stübgen, 2008), emphasising the heterogeneity in this group of disorders.

Earlier on, exclusion of alternative diagnoses was the only diagnostic tool, and for a while the existence of a separate 'LGMD' category at all, was questioned (Bushby, 1999 a). When it became clear that the level of heterogeneity was likely to be great, with several independent loci identified, a locus-based classification was proposed by a consortium meeting under the auspices of the European Neuromuscular Centre. It was agreed to name the different LGMD loci based on chronological order and mode of inheritance; with the dominant LGMD loci designated LGMD 1A, B, C, *etc*., and the recessive forms as 2A, B, C, *etc*., in the order of their identification. The suffix '1' points out the dominant form, and the suffix '2', the recessive form (Bushby, 1999 a; Urtizberea *et al*., 2008).

The starting point for investigation of these patients is clinical examination, as many clues can be gained from the history and examination as to what type of LGMD might be present (Bushby, 2000 a). Just more than a decade ago, the protein involved in chromosome 2-linked LGMD, limb girdle muscular dystrophy type 2B (LGMD 2B), was identified (Bashir *et al*., 1998; Liu *et al*., 1998). Dysferlin is the product of a novel mammalian gene which shows homology to a nematode protein, ferlin-1 (FER-1), involved in spermatogenesis (Achanzar and Ward, 1997; Bashir *et al*., 1998). In 1999, Yasunaga and co-workers identified a second human gene, otoferlin, which shows high homology to both dysferlin and FER-1. Otoferlin was implicated in an autosomal recessive form of non-syndromic deafness. All three proteins were predicted to share a number of common characteristics: a C-terminal transmembrane domain and at least three C2 domains (Bushby, 1999, b). Davis and co-workers, 2000, described the identification and characterization of another member of the ferlin family, which they called myoferlin, a protein nearly identical in size to dysferlin. Myoferlin was found to associate with the plasma membrane fraction of skeletal muscle, but was also found in nuclei, and enriched in nuclear membrane fractions (Davis *et al*., 2000).

Dysferlin localizes to the muscle fiber membrane and is expressed from very early in human development (Anderson *et al*., 1999). Dysferlin was simultaneously shown to be involved in two forms MD; LGMD 2B and the predominantly distal muscular dystrophy, Miyoshi myopathy (MM) (Bashir *et al*., 1998; Liu *et al*., 1998), now collectively termed dysferlinopathy. The underlying means by which mutations in this gene are responsible for these different phenotypes is yet to be revealed. One possible factor is environmental influences, as genes are not sealed in a vacuum (Bermúdez-Crespo and López, 2007) they are susceptible to multi-factorial alteration. The environment plays a determining role in gene expression and, in many genes the expression is regulated by multiple promoters, which reflects the complexity behind gene expression (Bermúdez-Crespo and López, 2007).

Although the MDs are classified traditionally by their patterns of muscle involvement, this mode of classification is challenged by the involvement of a single gene in two phenotypically different forms of muscular dystrophy (Bushby, 1999 a). The same homozygous mutation has been described in association with a variable presentation in large chromosome 2-linked families. Different family members were found to present with either proximal (LGMD 2B-like) or distal (MM-like) phenotypes in the presence of a shared haplotype. This is suggestive of another factor, genetic or environmental, that may act to modify the phenotype (Bushby, 1999 b).

2.4 DYSFERLINOPATHY

Dysferlinopathy encompasses a large variety of neuromuscular diseases characterized by the absence of dysferlin in skeletal muscle and an autosomal recessive mode of inheritance. The term ‘dysferlinopathy’ was coined in 1999 by Bushby after MM and LGMD 2B were found to be allelic disorders. Nowadays, it corresponds to the various clinical phenotypes related to a complete or partial absence of dysferlin (Urtizberea *et al*., 2008).

Historically, the first phenotype of dysferlinopathy was described by a Japanese physician, Miyoshi, in 1967 and subsequently in 1986 (Miyoshi *et al*., 1967; Miyoshi *et al*., 1986). In Miyoshi’s original publication, four patients from two consanguineous families presented with recessively inherited late-onset distal myopathy, associated with clear-cut muscular dystrophy and significantly elevated CK levels. This phenotype was called Miyoshi myopathy. Long thought to be confined to Japan, the disease was later reported in Europe and elsewhere thereafter (Urtizberea *et al*., 2008).

To date, three main phenotypes have been reported: MM, LGMD 2B, and distal myopathy with anterior tibial onset (DMAT) (Illa *et al*., 2001). Although rare, dysferlinopathies can account for up to

30% of progressive recessive muscular dystrophies in certain geographical areas, notably in the Middle East and the Indian subcontinent (Urtizberea *et al*., 2008). Guglieri and Bushby, 2008, reported the population frequency of the LGMDs to be highly variable and the prevalence of different forms of LGMD to differ between populations, depending on geographical and ethnic factors. For many areas, including South Africa, there is a lack of demographic data, on the dysferlinopathy prevalence. This lack of demographic data may possibly be attributed to the lack of accurate diagnosis of the disease in clinical practice. Alternatively, since there is no treatment, and the disease is not life threatening, and does not result in early mortality; following diagnosis, many patients do not return to the clinic.

Shared features between the dysferlinopathies so far, are the autosomal recessive form of inheritance, age at onset, most commonly in the late teens or early 20's, high serum CK levels, and transient calf myalgia (Ueyama *et al*., 2002). The myopathological diagnosis of a primary dysferlinopathy is currently based on the presence of degenerative muscle alterations in conjunction with a marked reduction or absence of sarcolemmal anti-dysferlin immunoreactivity (Kesper *et al*., 2008). A variety of other muscular dystrophies such as BMD, LGMD 1C and LGMD 2A may also display altered dysferlin immunostaining (Tagawa *et al*., 2003). However, the final diagnosis of a primary dysferlinopathy can, to date, only be established by the absence of dysferlin staining on Western blotting and/or the presence of two mutated alleles in dysferlin gene analysis (Kesper *et al*., 2008).

Misdiagnosis is commonplace in patients with primary dysferlinopathy. Worse, it can lead to unnecessary and potential hazardous therapeutic interventions such as long-term oral administration of corticosteroids or immunosuppressors (Urtizberea *et al*., 2008). This group of patients are, in particular, likely to be misdiagnosed as myositis, which appears to be non-responsive to steroids (Guglieri and Bushby, 2008). In a study by Brunn and co-workers, 2006, clear differences between the cellular composition of inflammatory infiltrates and their cytokine expression pattern in dysferlinopathies and idiopathic inflammatory myopathies were revealed. The findings were indicative of a pathogenically relevant mechanism of muscle fiber injury in dysferlinopathies, distinct from idiopathic inflammatory myopathies. A pro-inflammatory milieu with expression of interferon-γ (IFN-γ) in the absence of interleukin-10 (IL-10) expression and membrane attack complex deposits were reasoned as possible contributors to progressive muscle damage in primary dysferlinopathies (Brunn *et al*., 2006). Bansal and co-workers, 2003, reported a functional DGC in dysferlin-null mice

and confirmed that the mechanism in LGMD 2B and MM patients is different from the DGC-linked muscular dystrophies.

2.4.1 Clinical Phenotypes

Limb girdle muscular dystrophy type 2B (LGMD 2B)

In LGMD 2B, the clinical phenotype shares a great deal of similarities with MM, making exact initial diagnosis very difficult. The age of onset is also in the late teens and progression is usually slow. Distribution of muscle weakness, although selective, is predominant in the proximal pelvic girdle muscles while the shoulder girdle is relatively spared until late in the disease. Distal involvement in the lower legs can occur, after years of progression, and can result in foot drop (Mahjneh *et al*., 2001). In some instances the initial presentation is a proximo-distal muscle weakness. This distal involvement happens to be a key clue in diagnosis (Urtizberea *et al*., 2008).

Miyoshi Myopathy (MM)

Miyoshi myopathy is the most common form of autosomal recessive distal myopathy. It has also been reported to be the most recognizable subtype of dysferlinopathies, at least in theory (Urtizberea *et al*., 2008). Muscle weakness, initially affecting the gastrocnemius muscle from late teens or early adulthood, characterizes MM. One of the most striking features on examination is the wasting of both calves. Muscle weakness can extend to the pelvic girdle muscles and to the upper limbs, more distally, over time.

Cardiac and respiratory complications are not part of the mainstream form of dysferlinopathy (Urtizberea *et al*., 2008). Serum levels of muscle enzymes (CK, lactic dehydrogenase (LDH), and aldolase) are massively elevated in the early stage of the disease, and the pattern of myopathic changes in muscle is clearly dystrophic with numerous inflammatory foci (Urtizberea *et al*., 2008). At first, patients complain of an inability to stand on tip-toe, therefore, corroborating the primary involvement of the gastrocnemius muscle. Other distal symptoms include difficulties such as going down stairs, Gowers' sign, episodes of ankle subluxation and even foot drop when the leg anterior compartment of the lower extremities becomes affected. Patients occasionally complain of painful legs, sometimes unilaterally, with concomitant calf swelling but without any myoglobinuria. Disease progression is generally slow, over decades, but 10-20% of MM patients become wheelchair dependent (Urtizberea *et al*., 2008).

Distal Myopathy with onset in Tibialis anterior

Distal myopathy with onset in tibialis anterior (DMAT), also referred to as distal anterior compartment myopathy (DACM), comprises a new entity of the dysferlinopathy phenotype found by Illa and co-workers, in 2001. An extended Spanish consanguineous family was shown to carry one homozygous mutation in the dysferlin gene (*DYSF)* but with an atypical clinical presentation. If age of onset, CK levels and histological changes were indeed comparable to MM, the muscle weakness distribution was found to be significantly different. The anterior tibial muscles being the first muscle group involved. As disease progresses, muscle weakness also extend to the posterior compartment (Illa *et al*., 2001).

Other Clinical Variants and novel cases

Other clinical variants with mutations in the dysferlin gene have been described lately (Nagashima *et al*., 2004; Diers *et al*., 2007; Nguyen *et al*., 2007; Klinge *et al*., 2008; Okahashi *et al*., 2008; Paradas *et al*., 2009). These cases included an intermediate form with proximal and distal weakness from onset, patients with rigid spine and leg muscle stiffness, onset after the seventh decade of life, and a novel case resembling congenital muscular dystrophies with onset in the first decade of life. While the clinical symptoms in dysferlinopathies may be distinct at onset, the patterns of muscle involvement often become less specific as the disease progresses with the consequence that phenotypes may overlap in the later stages of the disease.

Recently, an intermediate 'proximodistal phenotype' (PD) has been described with weakness of the proximal lower limbs and calf atrophy as presenting symptoms (Nguyen *et al*., 2007). It appears that there is no genotype-phenotype correlation as mutations can lead to different phenotypes even within the same family (Illarioshkin *et al*., 2000).

Nagashima and co-workers, 2004, reported dysferlinopathy and rigid spine syndrome occurring in a 50-year-old male patient. The patient presented with not only the LGMD type of muscle involvement, but also generalized joint contractures, and rigid spine syndrome. Muscular weakness and wasting of the lower extremities had developed since age 40-years, accompanied by a limitation of anterior bending of the spine. Gene analysis of the dysferlin gene disclosed compound heterozygotes for frameshift and missense mutations. The authors concluded that although it might be by chance that the patient has both dysferlinopathy and rigid spine syndrome. A possibility remains that some mutations in the dysferlin gene might be related to rigid spine syndrome (Nagashima *et al*., 2004).

Diers and co-workers, 2007, reported on an adolescent female with a severe and rapidly progressing clinical course of LGMD 2B which has been suggested by the muscle histopathology and western blot and proven by mutation analysis in the dysferlin gene. The Caucasian girl presented with painful enlargement and mild contractures of calf muscles. A novel compound heterozygous mutation of which one affects the extracellular part of the protein was detected. This report was the first on a mutation in this region of dysferlin and might explain the unusual phenotype of the patient (Diers *et al*., 2007).

Klinge and co-workers, 2008, reported on a patient with disease onset at 73 years, the eldest age of onset of dysferlinopathy reported to date. The presenting symptom was exercise-induced stiffness of the trunk and proximal leg muscles without major progression over a period of 12 years. Gastrocnemius muscle biopsy revealed dystrophic morphology and biochemical depletion of dysferlin. Sequence analysis revealed two novel compound heterozygous splicing mutations of the dysferlin gene. Both mutations were located outside the coding region for C2 domains but the functional significance of this remains to be elucidated (Klinge *et al*., 2007).

Spuler and co-workers, 2008, reported a novel finding that mutations in the dysferlin gene can cause amyloidosis. Amyloid is the abnormal deposition of autologous proteins and peptides in fibrillar aggregates. It was found that mutations located between exons 7 and 16, corresponding to the predicted second and third C2 domain of dysferlin, were amyoloidogenic. In this study, Hamlet antibodies (against dysferlin protein) failed to stain the amyloid deposits, and in contrast, a peptide antibody directed against the second C2 domain of dysferlin, readily stained the amyloid deposits. These findings suggested that the amyloid protein is a proteolytic cleavage product of dysferlin (Spuler *et al*., 2008).

In 2009, Paradas and co-workers, described a new phenotype of dysferlinopathy resembling congenital muscular dystrophies (CMD) caused by a mutation in the dysferlin gene. The two patients, aged 2 years and 5 years, showed weakness in proximal lower limbs and neck flexor muscles at birth. The presence of normal CK levels during the first years of life was noted. Initial magnetic resonance imaging (MRI) showed no abnormalities, but short-time-inversion-recovery (STIR) sequences revealed myoedema in gastrocnemius and hamstring muscles at the age of 5 years. No inflammation and no specific structural muscle alterations were observed except for mild dystrophic changes. The group suggested that these features probably reflect that muscle degeneration in dysferlinopathies become significant several years after birth with increasing

muscular activity, especially after walk acquisition. This explains the normal CK level at birth in the reported case (Paradas *et al*., 2009). The dysferlin mutation reported, was in a homozygous state and has previously been described and associated with different phenotypes, including asymptomatic hyperCKemia at second decade. This report was the first on congenital onset in dysferlinopathies. The authors suggested that it could be attributed to genetic modifier factors that may be responsible for the phenotype variability of this muscular dystrophy (Paradas *et al*., 2009).

2.4.2 Clinical Features

Many patients usually participated actively in sports during adolescence, before disease onset. The first symptoms usually appear during the second or third decade of life as 'clumsiness when running', 'fatigue when walking long distances' and 'difficulty in climbing stairs' (Borsato *et al*., 2006). All of these difficulties are related to proximal lower limb weakness, and are characteristic of patients with the LGMD phenotype whereas the 'incapacity to walk on tiptoes' is characteristic of the distal phenotype. Calf hypertrophy and tendon contractures are rare. Hyperlordosis and waddling gait are also present, and patients can remain asymptomatic for many years with only hyperCKaemia before showing the first clinical signs of disease (Laval and Bushby, 2004; Borsato *et al*., 2006).

Probably the most insightful and astute research study on the disease progression in the field of dysferlinopathy is the study by Mahjneh and co-workers, in 2001. The study reported on a 23-year follow-up of a family where 10 members, age 17 to 76 years, homozygous for the same frameshift dysferlin mutation, were evaluated. A 23 base pair (bp) insertion which has resulted from tandem duplication, presumably as a result of replication slippage, occurred. The mutation was predicted to introduce premature termination of the protein 41 aa downstream.

The detailed clinical results of the study represent a comprehensive review of the clinical features of dysferlinopathy in the family, and allow comparison with other forms of LGMD. Progression of muscle weakness in patients with LGMD 2B on the lower limbs were measured with the functional scale according to the method by Walton (1981), and modified by the group of Mahjneh, 2001. This detailed evaluation not only provides insight to the clinical manifestation and progression of the disease, but also offers a standard that can be used to assess the stage of dysferlinopathy in clinical practice. The different stages of progression in dysferlinopathies, clinically present as the loss of ambulation are summarized in text box 2.2.

Text box 2.2

Different stages of progression in dysferlinopathy

Grade 1	A patient walks normally, but is unable to run freely.
Grade 2	A detectable defect in posture or gait occurs, and the patient is almost unable to run. Climbing stairs take place with slight difficulty. A patient can rise from the floor with a slight Gowers' sign.
Grade 3	The patient is unable to run. Dysferlin gait is observed, and the patient is able to walk at least 2 km. When climbing stairs the patient needs support of one hand on the thigh. A patient can rise from floor with slight Gowers' sign.
Grade 4	Slight dysferlin gait is observed, and the patient is able to walk more than 500 m. Climbing stairs require support of both hands on the thigh. The patient rises from a chair supporting on both thighs, and rises from the floor with moderate Gowers' sign.
Grade 5	Slight dysferlin gait is observed while the patient is able to walk more than 500 m. Climbing stairs requires support with both hands the on thigh. The patient rises from the floor with a severe Gowers' sign.
Grade 6	Moderate dysferlin gait is observed while the patient can only walk more than 200 m. Climbing stairs take place in an upright position with one hand supporting on the railing. The patient rises from a chair supporting on the arms of the chair, and rising from floor requires support on objects.
Grade 7	Severe dysferlin gait is observed, while the patient can only walk more than 100 m. Climbing stairs requires clinging to the railings with both hands. The patient needs to support on a table to rise from a chair, and supporting on objects to rise from the floor.
Grade 8	Severe dysferlin gait is observed, and the patient walks with aid of a cane. Only a few steps can be climbed, while clinging to the railings with both hands. The patient needs to support on a table to rise from a chair, and supporting on objects to rise from the floor.
Grade 9	The patient needs to use a wheelchair outside. The patient has lost the ability to climb stairs or rise from the floor, and can rise from a chair only with assistance from a person.
Grade 10	A patient becomes wheelchair-confined.

(Mahjneh *et al*., 2001)

It was reported on the standing posture of dysferlinopathy patients that signs of abnormality in begin to be apparent only about seven years after disease onset, when a slight degree of hyperlordosis begins to show (Mahjneh *et al*., 2001). "Lower limbs are abducted and externally rotated, usually with a wide base support, due to weakness in the hip muscles. Hyperextension of the lower limbs is present due to the weakness of the quadriceps and gastrocnemius muscles. This results in the phenomenon of back-kneeing in order to avoid sudden flexion of the knee and consequent falls. Bilateral gastrocnemius weakness produces ankle plantar flexion.

The upper limbs are limp and hang along the sides with internal rotated arms and hands facing backwards. This posture abnormality becomes more evident after 10 years, when patients start presenting with balance problems. A patient has difficulty in keeping his/her position for a prolonged period, as there is a prevalence of inversion rather than eversion of the feet. The patient tries to compensate for this with toe flexion in order to keep the feet fixed firmly on the ground. Some degree of rotation of the lower edge of the scapulae may be evident at this stage, although scapular winging never sets in. The deltoid has a characteristic appearance in the intermediate stages as a step at the scapulohumeral level, due to the wasting of the proximal part and hypertrophy of the distal part of the muscle."

In gait analysis Mahjneh and co-workers found that in the early stages (clinical grades/stages 1-2, described above), a patient may have some minor gait abnormalities. "Due to weakness of the quadriceps muscle, the acceleration of the lower limbs forward, during rapid walking, is deficient and the knee extension during the heel strike phase is weak. Patients tend to compensate for weakness of the quadriceps muscle by externally or internally rotating the thigh, leg and foot during the gait phases. This allows a decreased effect of gravity. Furthermore, the calf muscle weakness leads to an inefficient push off movement phase during the gait. Step length is normal but stride width is wider due to hip adductor and quadriceps weakness.

Marked and evident gait abnormalities are present after 10 years of disease (around clinical stage 4). The abnormalities are due to diffuse pelvic girdle- and lower limb muscle weakness. The gait becomes less complex and the stance phase is constituted by only the 'foot flat' period. There is a loss of heel strike and push off thereafter the foot leaves the ground with a slight double flexion of the knee and hip. With the knee in a bent position that falls heavily to the ground with a flat foot. At this stage there is a double support phase which is not stable due to deficient knee extension, and the other leg leaves the ground. The swing phase is greatly reduced due to the marked knee flexion deficiency. There is slight hip tilting due to the weakness in hip and back extensor muscles. Severe deficiency of accelerating the lower limbs forward during rapid walking is noted. At this stage the patients have mild hyperlordosis. Upper limb swing is deficient; the arms are thrown backwards, internally rotated and the forearms and hands externally rotated. There is a wide base of support, and step length becomes shorter with a wide asymmetrical stride width." (Mahjneh *et al*., 2001)

Careful clinical analysis of the distribution of the muscle weakness combined with gait analysis in LGMD 2B patients allowed the characterization of a distinct type of gait which have been termed

'dysferlin gait' by the group of Mahjneh, 2001. Dysferlin gait is clearly different from the gait observed in dystrophinopathies and sarcoglycanopathies (Ben Hamida *et al*., 1983; Eymard *et al*., 1997), who show a typical waddling gait. Mahjneh and co-workers stated that dysferlin gait is pathognomonic for dysferlinopathy patients. Making use of the selective involvement of specific muscles in the muscular dystrophies, researchers has described particular appearances in different muscular dystrophies, such as the 'valley sign' in DMD and BMD, the 'poly-hill sign' in facioscapulohumeral dystrophy, and the 'shank sign' in myotonic dystrophy (Pradhan, 2006). These signs were found to make use of the fact that some muscles show relative enlargement of preserved bulk, whereas others show wasting in the same region (Pradhan, 2006).

The involvement of the shoulder girdle is believed to be a much later event in the dysferlinopathies (Straub and Bushby, 2008). Pradhan, 2006 has observed a particular appearance in muscles of the shoulder girdle in MM-type dysferlinopathy that appeared to be specific to this phenotype. When patients were asked to raise their arms with shoulders abducted and elbows flexed to 90°, an appearance, described as 'calf heads on a trophy sign', was perceived. The sign was marked by six specific features.

- First, a prominent deltoid muscle looking like a calf's head with the mouth at the muscle's insertion and one of the several linear depressions appearing like a half-closed eye was observed. The prominence of the calf's head was found to be further enhanced at its lower border by slight wasting of the long head of the triceps muscle laterally, and the lateral part of the infraspinatus muscle medially.
- The second specific feature was found to be a cordlike upper border of the trapezius muscle appearing like a horn on the calf's head. The horn appeared more prominent because of wasting of the supraspinatus muscle and the overlying trapezius muscle below it.
- The third feature that marked the sign was found to be a prominent upper medial part of the infraspinatus muscle. The sharp demarcated wasting of the lower and lateral part looked like a downward directed ear of a calf.
- The fourth feature was the spinous process of the scapula. This was found to become prominent because of the wasted supraspinatus above it, appearing like the upper border of a calf's neck. A medial continuation as a subnuchal dorsal hump caused by the levator scapulae and rhomboid minor muscles shwoed a lump-like prominence at the insertion over the upper medial border of the scapula.

- The fifth feature that marked the sign was a ventral frill of a calf's neck formed by enlarged latissimus dorsi and teres major muscles.
- The last feature was the overall appearance of the upper back that created the impression of a trophy with superolateral concave arches formed by 'calf heads', and lower lateral convex arches formed by the ventral frill of a calf's neck. The prominent upper borders of the latissimus dorsi muscles were found to form the inferior border of the trophy on either side. The prominent lower borders of the trapezius muscles, which meet in the middle, formed the medial border. The hollowing of the interscapular region, owing to wasting of the rhomboid major muscle and the overlying trapezius muscle were found to be responsible for the prominent appearance of the sign (Pradhan, 2006).

In addition to the calf head sign, Pradhan, 2008, reported the 'diamonds on quadriceps sign' in MM and LGMD 2B phenotypes, which indicated selectivity of the dystrophic process not only among different muscles but also within a muscle. Patients showed asymmetric diamond shaped bulges with wasting of muscles above and below. The sign was suggested to be specific to the dysferlinopathies (Pradhan, 2008). Collectively these findings provide a platform for studying affected muscles in the dysferlinopathies. Together with the clinical picture described by the team of Mahjneh, 2001, this information is not only valuable for diagnostic purposes but may be very valuable in the application of cell-based therapies, as they stipulated the exact muscle involvement of the shoulder girdle, and the extent to which muscles are affected.

2.4.3 Muscle Pathology

Fanin and Angelini, 2002, assessed several parameters in muscle biopsies from dysferlinopathy patients, in order to evaluate their role in the development and progression of the disease. The assessed parameters included the extent and localization of inflammatory response, the amount and type of cellular infiltrate, the extent of muscle fiber degeneration and regeneration, the fiber type composition and the severity of histopathological changes. The series of muscle biopsies were scored in four different categories, according to the characteristics and severity of the pathology picture. Mild myopathy, moderate dystrophy, active dystrophy and advanced-stage dystrophy, were described. The latter categories were characterized by increased fiber size variability, fibro-fatty replacement, and advanced-stage dystrophy that showed many lobulated fibers.

Most biopsies that showed active dystrophy were found in patients younger than 30 years, and no definite correlation between the severity of the pathological picture and the duration of disease or

type of muscle biopsied, was found. An evident increase in the percentage of type 1 fibers in patients with an advanced stage of dystrophic process was observed. The highest rate of degeneration and regeneration in muscle biopsies showing acute dystrophy was observed, mostly from young patients.

An increased inflammatory response was observed in the majority of muscle biopsies, where macrophages were the most abundant cell types, either surrounding or invading muscle fibers or localized in the endomysium. T lymphocytes were localized both in the perimysium and in the perivascular region, and in the endomysium or invading fibers in phagocytosis. The authors reported an increased myosin heavy chain class I (MHC-1) positive reaction in association with the presence of macrophages that was localized to the cytoplasm of regenerating fibers. This reaction was occasionally found on the surface of non-necrotic and non-regenerating fibers suggesting that the inflammatory response might precede necrosis. Occasional MHC-1 positive fibers that were in different planes of sectioning were surrounded or invaded by phagocytes, and showed disruption of cellular integrity. The finding of expression of MHC class I molecules on muscle fibers is indicative of muscle fibers that were immunologically activated.

The extent of muscle fiber degeneration and regeneration was related to the stage of the dystrophic process. Severe muscle changes were observed either in the active phase of a necrotizing myopathy or in the advanced stage of a long-term dystrophy. Fanin and Angelini further observed that the normal fiber type distribution was shifted towards a predominance of type 1 fibers in an advanced stage of dysferlinopathy. The percentage of type 1 fibers was inversely correlated with the amount of degenerating and regenerating fibers, supporting their notion that type 1 fiber predominance, is a feature of advanced-stage dysferlinopathy. This observation was possibly due to a preferential type 2 fiber loss or a fiber type conversion. De Palma and co-workers, 2006, reported a remodelling of fiber type in dysferlinopathy quadriceps muscles. An increased proportion of slow fibers, in addition to a shift towards oxidative metabolism were observed.

Fanin and Angelini found inflammatory reactions to occur in the majority of biopsies, where it appeared secondary to necrosis, as demonstrated by the predominance of macrophage infiltrates. Positive labelling for the membrane attack complex (MAC) was observed on the surface of isolated non-necrotic fibers. This observation suggested that both muscle inflammation and complement cascade activation precede necrosis, and might be triggered by the presence of a structurally altered membrane (Fanin and Angelini, 2002).

2.4.4 Muscle Involvement

Computed tomography (CT) has established that in the early stages of dysferlinopathy, weakness is detected only in the posterior compartment muscles of the lower limbs; hamstrings, adductors, gastrocnemius and soleus and to a lesser degree in the quadriceps and gluteus (Mahjneh *et al*., 2001).

The anterior tibial (TA) and posterior tibial (PT) muscles are involved later, around clinical stage 4. However, long flexor and extensor muscles of the toes (extensor digitorum longus (EDL), and brevis (EDB) and extensor hallucis longus (EHL)), and intrinsic foot muscles are seen to be involved only at clinical stage 9, with mild degree (Weiler *et al*., 1996; Mahjneh *et al*., 2001).

Later on, weakness becomes detectable in the upper limbs and is most pronounced in the biceps, less so in the triceps, pectoralis, rhomboid, infraspinatus and supraspinatus muscles (Bejaoui *et al*., 1995; Weiler *et al*., 1996; Mahjneh *et al*., 2001). The deltoid as well as the trapezius muscles becomes affected very late (Weiler *et al*., 1996). The latissimus dorsi, and small muscles of the hand are relatively spared. Early contractures due to iliotibial band tightness may be present to a slight degree. Slight contractures become more widespread following loss of ambulation. Winging of the scapulae has not been reported in early stages, but Mahjneh and co-workers found that in the late stages it was observed as deficient abduction of the lower edge of the scapulae in six of their patients. The involvement of the proximal muscles of the thigh is much more prominent in LGMD 2B patients than in MM (Mahjneh *et al*., 2001).

The muscle CT in the LGMD 2B patients provided evidence of the presence of some degree of hypodensity on spinal muscles, whereas these aspects were not present in the muscle CT of the MM patients (Linssen *et al*., 1997; Mahjneh *et al*., 2001). Patients with the MM-type show early involvement of gluteus minimus in muscle CT scans, while this muscle is almost normal in LGMD 2B patients. In upper limbs, distal involvement of the forearm muscles is present in patients with MM but not in LGMD 2B patients (Miyoshi *et al*., 1986).

Beyond diagnostic implications, MRI techniques help to detect selectivity of skeletal muscle affection in inherited muscular dystrophies (Kesper *et al*., 2008). The MRI technique has been described as a sensitive method for detecting the earliest changes in dysferlinopathy (Okahashi *et al*., 2008). Whole-body high-field MRI is a non-invasive method to demonstrate various degrees of skeletal muscle alterations and disease progression in MDs (Kesper *et al*., 2008).

High-field MRI is becoming increasingly available in the clinical setting (Schick, 2005), and it shows a high diagnostic accuracy in the detection of early fatty replacement in muscles (Kesper *et al*., 2008). Fat suppressed T2-weighted images also allow the detection of edema as another possible early feature of muscle involvement (Mercuri *et al*, 2007).

In the first detailed whole-body high-field MRI analysis in patients with primary dysferlinopathies, Kesper and co-workers, 2008, found a characteristic pattern of skeletal muscle abnormalities. Evaluation with MRI was found to be sensitive in detecting subclinical muscle involvement in symptomatic patients. In addition, this evaluation gave normal results in LGMD 2B patients when studying muscles of the shoulder girdle. Patients with MM showed moderate to severe degeneration of the subscapularis and teres major as well as mild to moderate involvement of latissimus dorsi muscles. Moderate fatty degeneration of the erector spinae muscle mainly affecting its caudal and lateral parts was observed in both LGMD 2B and MM patients. Pectoralis muscles showed atrophy in all MM patients, while obliquus externus muscles showed atrophy or at least moderate degeneration in all MM patients.

All MM patients and one LGMD 2B patient showed a mild degree of fatty degeneration of the gluteus maximus muscles following investigation of the pelvic musculature Signs of focal edema of gluteus maximus muscles were additionally observed in all MM patients. One LGMD 2B patient and all MM patients in Kesper's study presented with a severe degeneration of the gluteus minimus. All MM patients displayed mild fatty degeneration of the gluteus medius muscles.

All symptomatic patients showed an involvement of thigh muscles with a characteristic sparing of sartorius and gracilis muscles. The anterior thigh compartment (quadriceps femoris), the internal hamstring (semi-membranosus) and external hamstring (biceps femoris) muscles were found to be severely affected. The adductor magnus showed a moderate fatty degeneration in all symptomatic patients. All MM patients further showed a moderate involvement of adductor longus and brevis muscles. Evaluation of lower legs, revealed an involvement mainly affecting the gastrocnemius in all symptomatic patients. When compared with the lateral heads, the medial heads of gastrocnemius muscles were found to be relatively mildly affected. The TA muscles and the peroneal group in the anterior compartment of the lower legs were affected in four and five patients, respectively (Kesper *et al*., 2008).

Okahashi and co-workers, 2008, reported a case where typical distribution of muscle involvement was demonstrated by MRI but not by CT, which contributed to facilitating diagnoses in the earliest

stage of preclinical dysferlinopathy, presenting with asymptomatic elevation of serum CK (Okahashi *et al*., 2008). The work of Kesper's group provides new diagnostic potential that may have value superior to current invasive diagnostic techniques. It also provides a viable technique for identification of muscle involvement and the extent to which muscles are affected in a patient-specific manner. This application will become increasingly useful in cell-based therapeutic strategies for direct identification of affected muscles.

2.4.5 Mutations

In the late 1990's, the gene mutation responsible for the pathology in dysferlinopathy has been identified (Bashir *et al*., 1998; Liu *et al*., 1998). Dysferlinopathies can manifest either as LGMD 2B, MM or DMAT. Moreover, the same mutation in the dysferlin gene has been shown to lead to both LGMD 2B and MM phenotypes within a single family (Weiler *et al*., 1999; Illarioshkin *et al*., 2000) or lead to overlapping in phenotypes in a single patient (Nguyen K *et al*., 2005). Such clinical heterogeneity has previously been reported in other human genetic disorder and is of particular importance in muscular dystrophies (Nguyen K *et al*., 2005). It is expected that additional factors such as genetic-, functional-, or environmental-, might play a role in the phenotypic expression of the clinical and morphological heterogeneity.

The dysferlin gene (*DYSF)* is located on chromosome 2p13, contains 55 coding exons and spans 150 kb of genomic DNA. The transcript is 6.3 kb large and is mainly expressed in skeletal muscle. The dysferlin gene is large, and the 55 exons spanning at least 150 kb of genomic DNA, predict a cDNA of around 7 kb and a protein of 2 088 amino acids (Aoki *et al*., 2001). All mutations in *DYSF* found to date include point mutations or small deletions or insertions distributed all over the entire coding sequence (Nguyen K *et al*., 2005). No hotspot has been identified (Nguyen K *et al*., 2005). Missense as well as nonsense or frameshift mutations have been reported (Aoki *et al*., 2001; Takahashi *et al*., 2003). Nguyen K and co-workers, 2005, reported a series of 54 sequence variations in *DYSF,* 34 of which were novel, in a large group of patients with various ethnic origins. The study highlighted the large number of non-pathogenic polymorphisms disseminated along *DYSF*, which could, in some instances, lead to misdiagnosis in patients in whom the levels of expression of dysferlin have not been evaluated (Nguyen K *et al*., 2005).

2.4.6 Pathogenic Mechanism of Dysferlinopathy

The muscle fiber plasma membrane (sarcolemma), is a highly structured and very specialized cellular structure. It is the physical boundary and limit to the cell, acting as the surface through which the

cell interacts with its environment. The sarcolemma has a very close and highly organized association with the ECM and requires a highly efficient means of self-repair. These specialized features are necessitated by the stresses involved in repeated rounds of muscle contraction and relaxation (Laval and Bushby, 2004).

In normal muscle, sarcolemmal injuries lead to accumulation of dysferlin-enriched membrane patches and resealing of the membrane in the presence of Ca^{2+} (Wenzel *et al*., 2005). Disruption of the plasma membrane is a common event in various normal mammalian cells, and membrane-repair machinery is essential to prevent disruption-induced cell death. In skeletal muscle membrane disruptions are most often observed under physiological conditions, because muscle fibers contract repeatedly and are often susceptible to varying degrees of mechanical stress. The fragility of the sarcolemma makes it unable to withstand these mechanical stresses, and a membrane-repair defect will more easily results in necrosis of the muscle fibers (Hayashi, 2003).

Vesicles must accumulate and fuse with the plasma membrane to afford rapid repair of a disrupted membrane (Hayashi, 2003). Membrane-repair machinery is thought to be involved in Ca^{2+}-dependent exocytosis of lysosomes, which are mainly predocked at the plasma membrane in non-secretory cells (Jaiswal *et al*., 2002). Due to its homology to a nematode gene that mediates vesicle fusion to the plasma membrane in spermatids, dysferlin has been suggested to be involved in membrane fusion (Hayashi, 2003). Further studies reported abnormal accumulation of subsarcolemmal vesicles in dysferlin-deficient muscle to be indicative of a defective membrane-fusion process (Selcen *et al*., 2001; Bansal *et al*., 2003; Cenacchi *et al*., 2005).

In 2003, Bansal and co-workers investigated dysfunction in the membrane-repair machinery in dysferlinopathy. They were able to show that dysferlin accumulates at sites of membrane disruption in normal muscle, although other sarcolemmal proteins, including caveolin-3, and δ-sarcoglycan were lost at the site of injury. At direct assessment of resealing efficiency, laser-damaged membrane of wild-type mouse muscle resealed within a minute in the presence of Ca^{2+}. This Ca^{2+}-dependent resealing of injured sarcolemma was defective in dysferlin-null muscle fibers, suggesting a direct role for dysferlin in the Ca^{2+}-dependent membrane-repair process (Bansal *et al*., 2003). These findings lead to the hypothesis that failure to repair sarcolemmal damage following injury causes loss of cell homeostasis, resulting in cell death (Chiu *et al*., 2009).

2.5 DYSFERLIN

Dysferlin is an ubiquitously expressed 230 kDa molecule that is localized to the periphery of muscle fibers (Anderson *et al*., 1999). The protein is found in a variety of tissues including skeletal and cardiac muscle, kidney, placenta, lung, and brain, and it is most highly expressed in skeletal and cardiac muscle (Bashir *et al*., 1998; Han and Campbell, 2007). Dysferlin was identified through a positional cloning strategy aimed at determining the gene involved in LGMD 2B and MM (Bashir *et al*., 1998; Liu *et al*., 1998). It was named according to the only sequence homology detected at the time of its cloning, to the *Caenorhabditis elegans* (*C.elegans*) protein FER-1 (Bushby, 2000 b).

The predicted cytoplasmic components of dysferlin contains Ca^{2+}-binding motifs homologous to C2 domains (Liu *et al*., 1998), which are believed to trigger Ca^{2+}-signalled membrane fusion (Rizo and Sudhof, 1998). It was later reported that dysferlin contains seven C2 domains (some authors still report only six C2 domains) and a single transmembrane domain located at its C-terminus (Han and Campell, 2007; Glover and Brown, 2007). A single missense mutation in any of five dysferlin C2 domains (C2A, B, C, D, E and G) has been reported to cause muscular dystrophy (Therrien *et al*., 2006), again suggesting non-redundancy among individual C2 domains (Han and Campbell, 2007). Mutations in these C2 domains may also lead to dysferlin misfolding and thus degradation (Therrien *et al*., 2006; Fujita *et al*., 2007). The dysferlin C2A domain binds phospholipids in a Ca^{2+}-dependent manner (Davis *et al*., 2002), consistent with its role in skeletal muscle membrane repair (Lennon *et al*., 2003; Bansal *et al*., 2003; Han and Campbell, 2007).

Also supported by this novel function is the ultrastructural observation of prominent subsarcolemmal small vesicle aggregations of unknown origin (Selcen *et al*., 2001; Bansal *et al*., 2003; Cenacchi *et al*., 2005) in dysferlin-deficient skeletal muscle. Furthermore, the sarcolemma shows many gaps and microvilli-like projections rather than being continuous and smooth (Bansal *et al*., 2003; Cenacchi *et al*., 2005), and the basal lamina is multilayered in some regions (Cenacchi *et al*., 2005; Han and Campbell, 2007). Dysferlin is a type II transmembrane protein with a membrane topology suggesting that it anchors to the plasma membrane by its C-terminal transmembrane domain, whereas the N-terminal part of the protein resides in the cytoplasm of the muscle fiber (Bansal and Campbell, 2004).

Dysferlin can be detected at Carnegie stage 15 or 16 (embryonic age 5-6 weeks) and is therefore present at a stage of development when the limbs start to show regional differentiation (Anderson *et al*., 1999). Lack of dysferlin at this critical time may contribute to the pattern of muscle

involvement that develops later with the onset of muscular dystrophy primarily affecting proximal or distal muscles (Anderson *et al*., 1999). Studies performed using the C2C12 mouse cell line showed that dysferlin was expressed at low levels in myoblasts and at high levels in mature myotubes (Davis *et al*., 2002). In normal primary human muscle cultures, both dysferlin mRNA and protein expression were found to be higher in multinucleated myotubes than at the myoblast stage. This is suggesting a role for dysferlin in muscle differentiation (De Luna *et al*., 2004). Dysferlin deficiency delays myoblast fusion/maturation *in vitro* (De Luna *et al*., 2006), suggesting that dysferlin may also participate in muscle differentiation and/or regeneration (Han and Campbell, 2007).

As discussed above, Bansal and co-workers, 2003, have identified a role for dysferlin during the membrane fusion step of the repair process in muscle fibers. Such a role is consistent with the presence of several C2 domains in dysferlin and with its homology to several known proteins with a role in vesicle fusion. It has been proposed that dysferlin, present on the vesicles, facilitate vesicle docking and fusion with the plasma membrane either by interacting with the other dysferlin molecules or with some other unknown protein-binding partner(s) at the plasma membrane (Bansal *et al*., 2003).

Chiu and co-workers, 2009, have identified a role of dysferlin in chemotactic signalling from internal vesicles in order to facilitate the attraction of neutrophils to a site of injury. The team suggested an extension to the muscle membrane repair model as they revealed a novel molecular pathomechanism affecting muscle regeneration and maintenance in dysferlinopathy. Emphasis was also laid on the content of vesicles which fuse with the cell membrane after muscle injury, which include neutrophil chemotactic factors. Together with the function of dysferlin in vesicle fusion (Bansal *et al*., 2003; Lennon *et al*., 2003), the observation of reduced cytokine release by dysferlin deficient cells provides an alternative explanation, that part of the function of dysferlin is to release cytokines from internal vesicles in order to attract neutrophils to the site of injury (Chiu *et al*., 2009).

2.5.1 Other Members of the Ferlin-Protein Family

After the identification of dysferlin, several novel genes showing protein structure and sequence homology to dysferlin were identified (Yasunaga *et al*., 1999; Britton *et al*., 2000). Consequently, a new family of mammalian proteins named ‘ferlin-1 like proteins’ was predicted on the basis of structural similarity and sequence homology (Han and Campbell, 2007). These include dysferlin or FER1L1 (Bashir *et al*., 1998; Liu *et al*., 1998), otoferlin or Fer1L2 (Yasunaga *et al*., 1999; Yasunaga *et al*., 2000), myoferlin or Fer1L3 (Britton *et al*., 2000; Davis *et al*., 2000), FER1L4, FER1L5 and FER1L6.

Each protein contains multiple C2 domains, which anchors to the membrane via a single C-terminal transmembrane domain, and shows sequence homology to the *C. elegans* ferlin-1 (*FER-1*) gene (Han and Campbell, 2007).

High conservation between homologous C2 domains of dysferlin and myoferlin has been reported (an average of 74% homology), which implicate that the C2A of dysferlin is more related to C2A of myoferlin than it is to the other C2 domains in dysferlin (an average of 15%) (Davis *et al*., 2002). A phylogenetic tree constructed from the alignment of individual mammalian ferlin C2 domain sequences showed that in all ferlins, a given C2 domain is more similar to other C2 domains at similar positions in the other proteins than to C2 domains in different positions of the same protein (Washington and Ward, 2006). This observation suggests that the multiple C2 domains may be required for protein activity (Han and Campbell, 2007), as was shown by Klinge and co-workers, 2007, where all the C2 domains were required to function in membrane fusion and repair.

FER-1

The spermatogenesis factor, FER-1, is specifically expressed in primary spermatocytes of *C.elegans*. In spermatids, mutations in FER-1 cause infertility by impairing the fusion of large vesicle with the plasma membrane (Ward *et al*., 1981; Achanzar and Ward, 1997). The fusion of these vesicles with the plasma membrane adds extra membrane to the plasma membrane at the fusion site. Mutations in FER-1 have been found to lead to immobile spermatids and consequently sterility in *C.elegans* (Bansal and Campbell, 2004).

Otoferlin

Mutations in otoferlin are responsible for DFNB9, a specific type of autosomal recessive deafness in humans (Yasunaga *et al*., 1999). Sequence and northern blot analysis on the RNA isolated from human tissues suggests that otoferlin is smaller than dysferlin. It shows 64% similarity and 31% identity to dysferlin at the level of amino acid sequence (Bansal and Campbell, 2004). Otoferlin encodes a 1230 aa protein with a molecular mass of 140 kDa, and has three predicted C2 domains and a transmembrane domain at its C terminus (Yasunaga *et al*., 1999). Dysferlin shows homology to otoferlin mainly at its C-terminal region, and the C2 domains of otoferlin correspond to the last three C2 domains of dysferlin.

In addition to the 140 kDa isoform, a longer isoform of otoferlin was detected in human and mouse tissues which encode a protein composed of 1997 amino acid residues, with a molecular mass of

≈227 kDa (Yasunaga *et al*., 2000). Similar to dysferlin, this longer isoform possesses seven C2 domains and a single transmembrane domain (Bansal and Campbell, 2004; Han and Campbell, 2007). The transcripts for the long isoform of otoferlin could be detected in both humans and in mice while the transcripts for the shorter isoforms (three C2 domains) could only be detected in human tissues (Yusanaga *et al*., 2000).

Mouse otoferlin shows expression in the cochlea, vestibule and brain. A basal level of expression could also be detected in several other tissues, including lung, kidney, skeletal muscle and heart (Yusanaga *et al*., 1999). Otoferlin has been shown to be essential for a late step of synaptic vesicle exocytosis and may act as the major Ca^{2+} sensor, triggering synaptic vesicle-plasma membrane fusion at the inner hair cell ribbon synapse (Roux *et al*., 2006).

Myoferlin

Following the identification and characterization of myoferlin it was named according to its high homology to dysferlin and its high expression in cardiac and skeletal muscle. Myoferlin was found to be nearly identical in size to dysferlin; ≈230 kDa in molecular weight (Davis *et al*., 2000). The sequence of myoferlin has been reported to be highly homologous to that of dysferlin, whereas Fer1L4 has been found most homologous to that of otoferlin (Bansal and Campbell, 2004).

Myoferlin is predicted to be a type II transmembrane protein, with a large cytoplasmic domain containing seven C2 domains and a C-terminal membrane spanning domain. Databases do not agree on the number of C2 domains. There are probably seven C2 domains in both myoferlin and dysferlin, but both the fifth and the seventh domains are only weakly predicted by two databases with expect values (E values) > 0.001 (Patel *et al*., 2008), and therefore, many authors only report six C2 domains.

Immunohistochemical analysis suggested that, similar to dysferlin, myoferlin is present on the plasma membrane but, in contrast to dysferlin, it is also present in the nucleus of the muscle fibers (Bansal and Campbell, 2004; Han and Campbell, 2007). This localization suggests a function unique to that of dysferlin and may explain the need for two highly homologous proteins in the same tissues (Davis *et al*., 2000). In contrast to dysferlin, myoferlin has been shown to function in myoblast fusion during muscle differentiation/maturation and myoferlin-null mice show muscle atrophy (Doherty *et al*., 2005). Immunoelectron microscopic analysis using an anti-myoferlin antibody revealed that most of the signals of myoferlin were found localized to the inside surface of the normal skeletal myofiber (Inoue *et al*., 2006).

Unlike dysferlin, myoferlin has an SH3 domain that may mediate interactions with other proteins. Myoferlin is upregulated at the plasma membrane of muscle fibers in dystrophin-deficient mdx mice, the murine model for DMD (Sicinski *et al*., 1989; Durbeej and Campbell, 2002), and is hypothesized to play a role in muscle regeneration and, potentially, muscle repair (Davis *et al*., 2000). Because of its high homology to dysferlin, myoferlin has been suggested as a possible compensator for the absence of dysferlin (Inoue *et al*., 2006). Although the myoferlin gene seems to be a candidate gene for the modifier, the compensatory overexpression of myoferlin was not detected in dysferlin-deficient muscles (Inoue *et al*., 2006). The gene for myoferlin (*MYOF*) mapped to chromosome 10q24, and is reported to be a novel candidate gene for muscular dystrophy or cardiomyopathy (Davis *et al*., 2000).

Fer1L4, 5, and 6

The Fer1L4, Fer1L5, and Fer1L6 proteins are predicted from the human and mouse genomic sequences but have not yet been characterized (Han and Campbell, 2007). The open reading frame of Fer1L4 predicts a 1952 aa protein with five C2 domains (Doherty and McNally, 2003). Research is in progress investigating a possible link between mutations in the genes encoding these proteins and human disease (Bansal and Campbell, 2004).

2.5.2 C2 Domains

Crystallographic studies have shown that the C2 domain is an independently folding domain composed of eight β strands forming a β sandwich structure (Sutton *et al*., 1995; Shao *et al*., 1996). At one end of the β sandwich structure, Ca^{2+}-binding loops reside, and Ca^{2+} binding is mediated through a conserved group of aspartic acid residues (Davis *et al*., 2002). The Ca^{2+}-binding sites of topology II C2 domains, similar to dysferlin and myoferlin, have been noted to often lack one or more of the five conserved aspartic acid or glutamic acid residues and to contain alternative residues capable of coordination (Nalefski and Falke, 1996).

Proteins directly implicated in membrane fusion such as the synaptotagmins contain two C2 domains (Davis *et al*., 2002). The first C2 domain of synaptotagmin binds Ca^{2+} and anionic phospholipids (Davletov and Sudhof, 1993; Chapman and Jahn, 1994). The second synaptotagmin C2 domain aids in protein-protein interactions and homo-oligomerization (Chapman *et al*., 1995) and was shown to bind phospholipids (Fernandez *et al*., 2001; Bai *et al*., 2002). Data has emerged supporting the role of synaptotagmins as Ca^{2+} sensor regulating the process of fast exocytosis (Sugita

et al., 2001; Fernandez-Chacon *et al*., 2001). In synaptotagmins, up to three Ca^{2+} ions are known to bind at three loops at the end of the β sandwich structure (Davis *et al*., 2002).

Davis and co-workers, 2002, tested the suggested six C2 domains of moyferlin and found that only C2A demonstrated the binding to phospholipids under the experimental conditions. They reported the role of the remaining ferlin C2 domains to be unknown, but suggested that, similar to other C2 domain-containing proteins, these domains may be involved in protein-protein interactions. The study also found the first C2 domain of dysferlin to demonstrate similar Ca^{2+} and phopholipid binding properties to myoferlin C2A. The cooperative binding of these two C2 domains is consistent with binding multiple Ca^{2+} ions. The C2A domains are found at the extreme amino termini of dysferlin and myoferlin, most remote from the transmembrane domain at the C-terminus. It is speculated that this placement may indicate a role for the C2A domain in localizing the amino terminus to the plasma membrane or possibly in the attraction of ferlin-containing vesicles to the plasma membrane (Davis *et al*., 2002). To function in membrane fusion and repair, all the C2 domains of dysferlin are required (Klinge *et al*., 2007), most likely mediating interactions with other proteins, known to interact with dysferlin, as described in section 2.4.5 below.

It is worth mentioning that the two novel compound heterozygous splicing mutations of the dysferlin gene, found in a 73 year-old patient, were located outside the coding region for C2 domains (Klinge *et al*., 2007). The authors stated that the implication of the finding is unknown. However, it is tempting to suggest that the patient-specific mutation in dysferlinopathy plays a particular role in the disease onset, and progression. Klinge and co-workers, reported a case only affected at a very late age, in conjunction with unaffected C2 domains. This observation may provide the first evidence that the severity, onset and progression of the dysferlinopathies might be directly attributable to the coding region affected by the mutation. More specific, the unaffected region coding for C2 domains, might result in a milder phenotype.

2.5.3 Dysferlin-Mediated Membrane Repair: Response to Membrane Wounding

Progress towards elucidating the mechanisms involved in Ca^{2+}-dependent membrane repair has led to the proposal of two mechanisms: the lipid flow promotion hypothesis and the patch hypothesis (Han and Campbell, 2007). It has recently been shown that a minor portion of dysferlin is also associated with the T-tubule system in skeletal muscle (Ampong *et al*., 2005; Huang *et al*., 2007), whereas the sarcolemmal labelling is not attributed to peripheral T-tubule profiles or caveolae (Anderson *et al*., 1999; Ampong *et al*., 2005). In numerous types of MD, a secondary displacement of

dysferlin to the cytoplasm has been observed (Piccolo *et al*., 2000). Subsarcolemmal accumulation of vesicles is uniquely found in dysferlin deficient skeletal muscle (Selcen *et al*., 2001).

Klinge and co-workers, 2007, examined the subcellular localization of dysferlin in untreated and wounded C2C12 myotubes to study its role in early myogenesis. It was found that although dysferlin is mainly expressed in the T-tubular network in developing muscle, it is able to translocate to the site of injury at the plasma membrane as an immediate and specific response to membrane wounding. The results demonstrated that in the early stages of C2C12 myotube maturation dysferlin does not localize to the sarcolemma but is expressed at the T-tubule system and at sites of cell fusion. The C2C12 myotubes were found to be capable of resealing membrane ruptures in a Ca^{2+}-dependent fashion involving translocation of dysferlin to the site of membrane injury (Klinge *et al*., 2007). The study by Klinge's group showed that in differentiated C2C12 myotubes dysferlin accumulates at the site of myoblasts fusing to myotubes. At this stage of muscle development, dysferlin is predominantly expressed in the T-tubule system of multinucleated myotubes, and the full-length protein is required for its correct localization (Klinge *et al*., 2007).

T-tubules form an intracellular membrane system that penetrates the myofiber allowing the action potential to reach the muscle fiber interior and to facilitate excitation contraction coupling (Flucher *et al*., 1993). T-tubules develop from beaded tubular invaginations of the plasma membrane and partly from longitudinal, cytoplasmic profiles, also termed beaded tubules, which are formed of strings of caveolae (Ishikawa, 1968; Schiaffino *et al*., 1977; Flucher *et al*., 1991). The results of Klinge's group strengthen the hypothesis of synaptic vesicle fusion machinery, a process analogous to the patch hypothesis for membrane repair. They have shown for the first time the focal accumulation of dysferlin positive structures in a Ca^{2+}-dependent manner, at and around the sites of injury as a consequence of membrane wounding. While in mature skeletal muscle the source of dysferlin accumulation at the wounding site is unknown, the group of Klinge have shown that in early myogenesis, dysferlin accumulation at the wounding sites is derived from a T-tubule localization. This response requires the full-length dysferlin protein, and this mechanism is in place in an early stage of development, as T-tubules have not yet orientated into the typical transverse pattern (Takekura *et al*., 2001).

2.5.4 Proteins that Interact with Dysferlin

2.5.4.1 Caveolin-3

Caveolae are vesicular invaginations of the plasma membrane, measuring 50-100nm in diameter (Engelman *et al*., 1998), and function as 'message centres' for regulating signal transduction events (Galbiati *et al*., 2001 a). Caveolin, a 21 to 24 kDa integral membrane protein, has been shown to be a principal component of caveolar membranes *in vivo* (Glenny, 1989; Glenny and Soppet, 1992; Rothberg *et al*., 1992). It has been proposed that caveolin family members participate in vesicular trafficking events, and signal transduction processes, by acting as scaffolding proteins to organize and concentrate specific lipids and lipid-modified signalling molecules within caveolar membranes (Galbiati *et al*., 2001 b). The expression of Caveolin-3 is muscle-specific, and it is the principal structural protein of caveolar membrane domains in striated and smooth muscle cells (Galbiati *et al*., 2001 a). Its expression is induced during the differentiation of skeletal myoblasts, and caveolin-3 is localized to the sarcolemma where it forms a complex with dystrophin and its associated glycoproteins (Song *et al*., 1996).

The importance of caveolin-3 is emphasized by the observation that mutations in the *CAV3* gene cause a dominantly inherited LGMD (LGMD 1C) (Minetti *et al*., 1998). These mutations apparently behave in a dominant negative manner, forcing aggregation of both mutant and wild-type caveolin-3 proteins in the golgi apparatus (Galbiati *et al*., 1999). Matsuda and co-workers, 2001, proposed the first description of a possible dysferlin interacting protein. The team suggested that one function of dysferlin may be to interact with caveolin-3 to subserve signalling functions of caveolae. In addition, caveolin-3 has been implicated in T-tubule system biogenesis (Parton *et al*., 1997), and when caveolin-3 expression is defective, dysferlin localization has been reported to be abnormal (Matsuda *et al*., 2001; Tateyama *et al*., 2002; Fisher *et al*., 2003; Yabe *et al*., 2003).

Ampong and co-workers, 2005, have found Dysferlin and caveolin-3 to coprecipitate with the dihydropyridine receptor (DHPR), a protein complex localized to T-tubules. Dysferlin and DHPR were observed to partially co-localize by double immunofluorescent staining in skeletal muscle fibers. The findings suggested that dysferlin might be involved in the fusion of caveolin-3-containing vesicles with T-tubules (Ampong *et al*., 2005). The team of Hernández-Daviez, 2006, described the cellular distribution of dysferlin with respect to caveolin-3 and showed that muscle disease-associated caveolin-3 mutants affects dysferlin traffic to the plasma membrane. It was demonstrated that co-expression of epitope-tagged dysferlin and mutated caveolin-3 or caveolin-1 caused a dramatic accumulation of dysferlin in the golgi complex in both muscle and non-muscle cells. Dysferlin traffic

to the cell surface was found to be impaired in the absence of caveolin-1 and caveolin-3, suggesting that caveolins are necessary for plasma membrane localization of dysferlin (Hernández-Daviez *et al.*, 2006).

2.5.4.2 CALPAIN 3

Calpain 3 is a skeletal muscle-specific member of the calpain superfamily of non-lysosomal, Ca^{2+}-dependent cysteine proteases (Goll *et al.*, 2003). Several cytoskeletal components have been identified as partners and substrates for calpain 3, linking its function to the regulation of cytoskeleton structure and cytoskeleton-membrane interactions (Guyon *et al.*, 2003; Taveau *et al.*, 2003). This protein has been shown to predominantly localize in several regions of the sarcomere, associated with the protein, titin (Sorimachi *et al.*, 1995).

Duguez and co-workers, 2006, found a deregulation of sarcomere remodelling due to a lack of proteolysis of substrates by calpain 3, to be a possible mechanism of LGMD 2A pathogenesis. A secondary reduction for calpain 3 was reported for a subset of patients with dysferlinopathy (Anderson *et al.*, 2000). The reciprocal has been observed by the team of Chrobáková, 2004, in a subset of LGMD 2A calpain-deficient patients. In co-immunoprecipitation experiments, using llama-derived antibody fragments, Huang and co-workers, 2005, have shown that calpain interacts with dysferlin. Inhibition of calpain activity has been shown to prevent the Ca^{2+}-dependent plasmalemmal resealing of crayfish giant axons (Godell *et al.*, 1997).

Like dysferlin, calpain 3 was suggested to be implicated in the patch fusion repair of the muscle membrane through its interaction with the annexins A1 and A2, as calpain 3 cleavage of annexins A1 and A2 might be critical for patch formation and/or membrane insertion (Lennon *et al.*, 2003). Glover and Brown, 2007 reported annexins A1 and A2 to be likely targets for calpain cleavage in the context of the putative muscle repair protein complex, because both proteins harbour a putative recognition sequence for calpain in their amino termini (Barnes and Gomes, 2002). In addition, annexin A1 has been shown to undergo proteolysis by calpain *in vitro*, a process that enhances the Ca^{2+} sensitivity of annexin A1 for phospholipid binding (Ando *et al.*, 1989).

Calpain 3 and AHNAK were found to be in complex with dysferlin (Huang *et al.*, 2007). Huang and co-workers, 2007, demonstrated that AHNAK can interact with calpain 3 and serves as a direct substrate of calpain 3 in cell culture. The interaction of both these proteins and the cleavage of AHNAK by calpain 3 were supported by their colocalization in skeletal muscle (Huang *et al.*, 2007).

Calpain 3 cleavage caused a loss of AHNAK in cell culture, and AHNAK was found to be increased at the sarcolemma in patients with calpainopathy (Huang *et al*., 2007). Calpain 3-mediated proteolysis of AHNAK prevents interaction of AHNAK with dysferlin and myoferlin. This provided new mechanistic insight for the physiological function of calpain 3 in the dysferlin protein complex in skeletal muscle (Huang *et al*., 2008). The regulatory role of calpain 3 in the dysferlin protein complex may implicate an intimate relationship between muscle membrane repair and remodelling of the sarcomere and subsarcolemmal cytoskeleton architecture (Huang *et al*., 2008).

2.5.4.3 Annexins A1 and A2

Annexins are widely expressed Ca^{2+}- and phospholipid-binding proteins that are implicated in membrane trafficking, transmembrane channel activity, inhibition of phopholipase A2 and cell-matrix interactions (Raynal and Pollard, 1994). The functions of many of the annexins are not clear (Lennon *et al*., 2003). However, annexins A1 and A2 have been shown to aggregate intracellular vesicles and lipid rafts in a Ca^{2+}-dependent manner at the cytosolic surface of plasma membranes in many cells (Babiychuk and Draeger, 2000; Lambert *et al*., 1997). Annexin A1 mediates this aggregation by forming a heterotetramer with the protein S100A11, and annexin A2 has been postulated to have a similar relationship with the protein S100A10 (Gerke and Moss, 2002).

A Ca^{2+}-dependant interaction between dysferlin and annexins A1 and A2, expected to play a role in the aggregation and fusion of intracellular vesicles in response to membrane injury, were described by the team of Lennon, 2003. After membrane injury, a disruption of dysferlin binding to annexin A1, Ca^{2+}-dependent vesicle aggregation, and fusion with the surface membrane were observed (Lennon *et al.*, 2003). It was shown that this membrane repair process is severely upset in dysferlinopathic myotubes (Lennon *et al*., 2003). In addition, microarray analysis of expression patterns in dysferlinopathic biopsies indicated an over-expression of annexin A2, compared to normal subjects (Campanaro, 2002).

Cagliani and co-workers, 2005, investigated annexins A1 and A2 expression levels in dysferlinopathic patients and in subjects suffering from different muscle pathologies. All patients displayed increased annexin levels and a significant positive correlation was evidenced between protein expression and clinical severity. Annexin levels were also found to parallel dystrophic alterations as assessed by histological examination of muscle sections. The findings indicated that increased annexin levels are not a specific marker for dysferlinopathies. They rather represent a secondary phenomenon in the

development of muscle disease, which is largely independent from the underlying pathogenic mechanism (Cagliani *et al*., 2005).

McNeil and co-workers, 2006, demonstrated a requirement for annexin A1 in resealing responses, as the inactivity of annexin A2 were found to inhibit resealing. It was proposed that Ca^{2+} entering through a plasma membrane disruption causes cytosolic annexin A1 to bind to membranes surrounding the disruption site. It thereby initiates the homotypic and exocytotic membrane fusion events of resealing. This event initiates emergency fusion events wherever and whenever required (McNeil *et al*., 2006). Due to the correlation of annexin expression levels with disease severity in dysferlinopathy, irrespective of the clinical phenotype variability, annexins cannot be regarded as good candidates for modifier factors in this disease (Cagliani *et al*., 2005).

2.5.4.4 AHNAK

AHNAK, also called desmoyokin and is located on human chromosome 11q12-13 (Kudoh *et al*., 1995). This protein contains three main structural regions; the N-terminal, 498 aa; a large central region of ≈4300 aa with multiple repeated units, most of which are 128 amino acids in length, and the C-terminal of 1002 aa (Shtivelman *et al*., 1992). A second AHNAK nucleoprotein-like protein, AHNAK nucleoprotein 2, located on chromosome 14q32, was recently identified in a search for homologous sequences in the human genome (Komuro *et al*., 2004).

AHNAK is a family of two proteins of exceptionally large size, ≈600-700 kDa, characterized by common amino acid sequences and structural features (Komuro *et al*., 2004). Like dysferlin, high expression levels of AHNAK are observed in all muscle cells, including cardiomyocytes and skeletal muscle cells (Gentil *et al*., 2003). The exact biological function of AHNAK is largely unknown (Huang *et al*., 2008). However, the C-terminal region of AHNAK binds to G-actin and cosediments with F-actin *in vitro*, suggesting a role for AHNAK in the maintenance of the structural and functional organization of the subsarcolemmal cytoarchitecture in cardiomyocytes (Hohaus *et al*., 2002).

Huang and co-workers, 2007, described a novel interaction of AHNAK with dysferlin. The interaction sites have been identified as the C-terminal, 500 aa of both AHNAK variants and the C2A domain of dsyferlin and its homologue myoferlin (Huang *et al*., 2007). The functional significance of the interaction between dysferlin and AHNAK comes from the observation that AHNAK is, like dysferlin, primarily localized at the sarcolemma. AHNAK is also secondarily reduced in muscle from patients

with genetically confirmed dysferlinopathy, generally comparable to the loss of dysferlin (Huang *et al*., 2007).

In LGMD 1C, dysferlin and AHNAK showed a secondary overall reduction to the primary loss of caveolin-3. In contrast, in unrelated muscular dystrophies, dysferlin and AHNAK showed normal muscle staining (Huang *et al*., 2007). Evidence has been provided for a functional cooperation between dysferlin and AHNAK during muscle regeneration. Dysferlin and AHNAK show a marked increase and cytoplasmic localization during regeneration. This is consistent with the direct interaction between them and mobilization of the AHNAK-dysferlin complex during repair and regeneration (Huang *et al*., 2007).

In 2008, Huang and co-workers have demonstrated that AHNAK can interact with, calpain 3, and that AHNAK serves as a direct substrate of calpain 3 in cell culture. The interaction of both proteins and the cleavage of AHNAK by calpain 3 were supported by their colocalization in skeletal muscle (Huang *et al*., 2008). Calpain 3-mediated proteolysis of AHNAK prevents the interaction of AHNAK with dysferlin and myoferlin (Huang *et al*., 2008). In agreement with the proposed membrane repair function for AHNAK, it was demonstrated that AHNAK is also an integral component of a newly discovered Ca^{2+}-regulated vesicle capable of rapid exocytosis, called enlargosome. Enlargosome exocytosis is induced by plasma membrane disruption and is thought to be involved in both plasma membrane differentiation and repair (Borgonovo *et al*., 2002).

2.5.4.5 Affixin (β-Parvin)

Affixin is a novel focal adhesion (FA) protein that contains two tandem calponin homology (CH) domains (Matsuda *et al*., 2005). While ubiquitously expressed, the expression levels of affixin were found to be highest in the heart and skeletal muscles of humans (Matsuda *et al*., 2005). Affixin co-localizes with integrin-linked kinase (ILK) at focal adhesions of well-spread cultured cells and is suggested to be involved in integrin-ILK signalling (Matsuda *et al*., 2005). In human skeletal muscle, affixin and integrin-linked kinase co-localize at the sarcolemma (Yamaji *et al*., 2001). The biological significance of this interaction is not yet fully understood (Matsuda *et al*., 2005).

Affixin was found to be a dysferlin-binding protein by Matsuda and co-workers, 2005. The team showed that a deficiency of dysferlin caused a secondary reduction of affixin at the sarcolemma of MM and LGMD 2B muscles even though the total protein content did not change. The results suggested that affixin is closely associated with dysferlin at the sarcolemma of normal human muscle. The affixin-binding domain identified in dysferlin was the C-terminal intracellular region,

which does not show homology to any known protein motifs, while the CH1 domain of affixin was identified as a dysferlin-binding region (Matsuda *et al*., 2005).

Affixin plays an essential role in the formation of FA and actin stress fibers (Yamaji *et al*., 2001). It has also been shown to interact with α-actinin and participate in reorganization of F-actin (Yamaji *et al*., 2004). F-actin is depolymerised in response to membrane disruption and plays an important role in wound healing (McNeil, 2002). Although the physiological function of the dysferlin-affixin protein interaction is not yet fully understood, there is a possibility that dysferlin and affixin play some role in membrane repair through the organization of F-actin (Matsuda *et al*., 2005).

2.5.4.6 MYOGENIN

Myogenin or myogenic factor 4 is a member of the basic helix-loop-helix gene family which is essential for muscle development. In adult skeletal muscle myogenin expression is concurrent with satellite cell differentiation and fusion (Cooper *et al*., 1999). It is essential for terminal muscle differentiation downstream of myognesis and is upregulated in differentiating myoblasts in a pattern, similar to dysferlin (Glover and Brown, 2007).

Null mutations in the myogenin gene cause a severe reduction of skeletal muscle mass, showing that myogenin is essential for muscle development i*n vivo* (Hasty *et al*., 1993). In a study by De Luna and co-workers, 2006, human skeletal muscle primary cultures from dysferlinopathy patients showed that the absence of dysferlin remarkably alters the process of muscle differentiation *in vitro*. This finding indicated a signalling pathway that would involve dysferlin and myogenin. Severe reduction of myogenin in dysferlin-null myotubes suggested that myogenin could be involved in the defective muscle differentiation observed in dysferlin-null cell cultures (De Luna *et al*., 2006). The study supported the role of dysferlin in human muscle fusion and differentiation *in vitro*. Furthermore, it provided evidence of a link between dysferlin and myogenin and suggested they share a signalling pathway involved in differentiation of skeletal muscle *in vitro* (De Luna *et al*., 2006).

2.5.4.7 BIN 1

Bin 1 is a conserved member of the BAR family of genes and has been implicated in myoblast differentiation and membrane deformation (Lee *et al*., 2002). Caveolin-3 and Bin 1 have been shown to be involved in T-tubulogenesis (Parton *et al*., 1997; McNally *et al*., 1998; Lee *et al*., 2002). In mice lacking either caveolin-3 or Bin 1, T-tubules are abnormal but not absent (Galbiati *et al*., 2001 a;

Muller *et al*., 2003), suggesting that additional factors are likely to contribute to T-tubule development (Lee *et al*., 2002).

Klinge and co-workers, 2007, found that dysferlin co-localizes with Bin 1 in C2C12 myotubes. Bin 1 was found to be highly abundant at fusion sites of myotubes, co-localizing with full-length dysferlin. The authors suggested that this finding supports a possible joint role of Bin 1 and dysferlin in membrane fusion processes in developing muscle. Since dysferlin and Bin 1 expression both start at similar time points and fusion already takes place before this point, their role in fusion appears to be important in the later stages of differentiation (Klinge *et al*., 2007). This is reflected by the fact that Bin 1 and dysferlin deficient myotubes display impairment but not absence of fusion and differentiation (Lee *et al*., 2002; De Luna *et al*., 2006). The T-tubule localization of dysferlin and Bin 1 has important implications in the view of the fact that the T-tubule system is involved in the generation of membrane for the elongation and repair purposes (Engel and Franzini-Armstrong, 2004). Furthermore, it serves as a membrane source for membrane bound vacuoles. Subsarcolemmal vacuoles contiguous with the T-tubules are one of the ultrastructural hallmarks in dysferlin-deficient skeletal muscle (Selcen *et al*., 2001; Klinge *et al*., 2007). This could be explained by an abnormal membrane fusion/budding mechanism in dysferlin deficient muscle. In normal muscle the T-tubule system initiates the formation of, and serves as a membrane source for autophagic vacuoles and vesicles (Engel and Franzini-Armstrong, 2004).

2.6 DIAGNOSIS AND THERAPY

Reduced or absent expression of dysferlin are the most relevant features leading to the diagnosis of dysferlinopathy and prompt molecular geneticists to search for mutations at the genomic or transcriptional level in *DYSF* (Nguyen K *et al*., 2005). This genetic screening is of particular interest for the accuracy of diagnoses and therefore for more reliable genetic counselling and appropriate medical care (Nguyen K *et al*., 2005). Kesper and coowrkers, 2008, reported that the final diagnosis of a primary dysferlinopathy can to date only be established by the absence of dysferlin staining on Western blotting and/or the presence of two mutated alleles in dysferlin gene analysis.

Ho and co-workers, 2002, developed a new protein-based diagnosis using non-muscle tissues and less invasive sampling techniques in order to avoid the painful and invasive procedure of muscle biopsy for dysferlinopathy screening. The group reported a novel finding that dysferlin is expressed in blood monocytes, and more importantly, it was shown that dysferlin expression in monocytes

correlates with its expression in muscle. The findings led to the development of a new protein-based diagnostic assay for LGMD 2B and MM, without the need for a muscle biopsy (Ho *et al*., 2002).

Before employment of this procedure as a routine diagnostic screening assay for the dysferlinopathies, it should be kept in mind that the expression of dysferlin in monocytes is restricted to the type II (non classical) monocyte population (Chiu *et al*., 2009), that is distinct from the monocyte population which initially invade muscle following injury (Arnold *et al*., 2007). However, Chiu and co-workers, found the monocyte expression of dysferlin unlikely to be involved in the defective regeneration of dysferlin-deficient muscle. The reason being that type II monocytes are not involved until after the resolution of the inflammatory phase. At this point the regeneration of dysferlinopathic muscle is already abnormal (Chiu *et al*., 2009).

In dysferlinopathy, muscle CT and MRI clearly show characteristic muscle involvement of the posterior compartment of the legs (Bruss *et al*., 2004). The hallmark can be seen in the earliest stages or even in the preclinical stage of disease (Argov *et al*., 2000; Bruss *et al*., 2004). Brummer and coworkers showed that MRI change precedes the CT change. The CT change was found to be replacement of muscle by fat tissues, while changes like edema, which was the most sensitive parameter to detect dystrophic alteration in skeletal muscle, were detected with MRI (Brummer *et al*., 2005). MRI appears to be the far superior diagnostic tool, to date, due to its non-invasive mode of operation, in accurate diagnosis of the dysferlinopathies.

It is expected that diagnosis based on clinical presentation specifically in the pelvic girdle, can effectively be evaluated following the criteria described by Mahjneh and co-workers, 2001, which was modified from the functional scale described by Walton (1981). The different stages (text box 2.2) of progression in dysferlinopathies may offer a useful tool in clinical practice.

There is currently no effective treatment for patients suffering from dysferlinopathy. The care of patients with LGMD2 mainly consists of symptomatic treatment strategies and supportive measures. These include physical therapy, assistive devices and monitoring of respiratory function and heart health (Bushby and Straub, 2005), as well as treatment of disease complications (Straub and Bushby, 2008). These strategies mainly aim at prolonging survival and improving quality of life (Bushby and Straub, 2005).

Of all treatment strategy approaches in the muscular dystrophies, the most viable seems to be cell-based therapy. Murphy and Kehrer, 1989, stated that the underlying biochemical defect of muscular

dystrophy, as with nearly all inherited diseases, can only be cured if techniques are developed to repair or replace the defective genetic material.

Case by case approaches are necessary (Danièle *et al*., 2007), as the diversity of proteins involved in the muscular dystrophies, and their diverse functions within the muscle cell, render it almost impossible to develop a universal treatment. Cell grafting offers the possibility of gene delivery into dystrophic muscle (Danièle *et al*., 2007), while reimplantation of genetically modified host myoblasts or healthy donor cells not only has the potential to correct the gene deficiency but also has the capability to remodel the dystrophic tissue (Danièle *et al*., 2007). This could be of particular importance when addressing progressed cases of muscular dystrophy.

When considering the diverse functions of dysferlin, discussed in the present chapter, and the possibility of even more unrevealed functions and interactions of this protein, dysferlinopathy appears to be a candidate for cell-based therapies. Such therapeutic strategies should aim at restoring the protein defect by grafting of normal healthy cells into the dystrophic host tissue.

The group of Kong, 2004, has shown some success in a cell-based approach. Human umbilical cord blood cells were injected into dysferlin-deficient SJL mice. Fibers expressing human dysferlin, although in very small numbers, were detected. The study found that muscle precursor cells are present in human umbilical cord blood and that they can fuse with host muscle fibers after systemic delivery (Kong *et al*., 2004). Vieira and co-workers, 2008, achieved even more success in the field with systemic delivery of human adipose stromal cells into SJL mice, without immunosuppression. The team showed for the first time that human adipose stromal cells were able to fuse with the host muscle, express significant amounts of human muscle proteins, and to improve motor ability of injected animals (Vieira *et al*., 2008).

2.7 Oxidative Stress

Free radicals are highly reactive molecules or chemical species containing unpaired electrons that cause oxidative stress. This state can be defined as an imbalance between antioxidants in favour of the oxidants, potentially leading to damage (Sies, 1997). They are formed during normal physiological metabolism or caused by toxins in the environment. Oxidative stress can damage lipids, proteins, enzymes, carbohydrates and DNA in cells and tissue. The result: damage to membranes, fragmentation or random cross linking of molecules like DNA, enzymes and structural proteins, and ultimately cell death induced by DNA fragmentation and lipid peroxidation (Beckman and Ames, 1998).

The basis of our life on earth is the oxygen present in the atmosphere. However, it can under a number of conditions, be a very toxic substance (Bentinger *et al.*, 2007). Derivatives such as hydroxyl (OH^-) and superoxide (O_2^-) radicals, hydrogen peroxide (H_2O_2) and singlet oxygen (O_3) may be formed and are called reactive oxygen species (ROS). ROS appear not only in diseases but also under normal physiological conditions and interact with basic tissue components with consequences of disturbed function (Bentinger *et al*., 2007).

Various types of antioxidant systems are available in all organisms for limitation and elimination of these unwanted species (Bentinger *et al*., 2007). The functional activity of the mitochondria greatly influences the extent of ROS formation. Low intracellular levels of adenosine diphosphate (ADP) and high mitochondrial membrane potential gives high levels of ROS, whereas high ADP levels and low membrane potential result in low production of ROS (Bentinger *et al*., 2007). Mitochondrial electron transport accounts for two-thirds of the cellular oxygen consumption, and the observed limited leakage of electrons, 1 to 2%, is the largest contribution to the cellular O_2^- and H_2O_2 production in healthy cells (Papa and Skulachev, 1997).

The imbalance between the generation of ROS and their removal by enzymatic and nonenzymatic cellular defence systems could arise from its overproduction. This event occurs under certain pathological conditions and in association with inflammation, or from an impairment of the defence mechanisms, as seen in certain genetic loss-of-function disorders and deficiency states (Halliwell and Gutteridge, 1989). Implicit in this definition is the notion that such an imbalance is sufficient to lead to the oxidation of various cellular constituents and to cause cellular dysfunction and injury (Rando, 2002). As such, oxidative stress may also be viewed as a condition in which the production of oxidative products exceeds their removal by cellular repair mechanisms, which may lead to acute cellular metabolic disturbances and even cell death, if such changes accumulate (Rando, 2002).

During normal cellular metabolism, the primary generation of ROS comes from the leakage of the superoxide anion, O_2^-, from the electron transport chain (Halliwell and Gutteridge, 1989). A series of linked enzymatic reactions are responsible for the detoxification of O_2^-, where it is converted to H_2O_2 by the action of superoxide dismutase (SOD). Most animal cells contain two forms of SOD, the cytoplasmic Cu,Zn-SOD and a mitochondrial Mn-SOD (Theate *et al*., 1985). The selenium-containing enzyme glutathione peroxidase (GPx), is responsible for metabolizing H_2O_2 to oxygen and water, a reaction in which glutathione (GSH) is used as a cofactor (Murphy and Kehrer, 1989). Glutathione peroxidase converts most of the H_2O_2 in the cytoplasm. At sites of relatively high concentrations of

H_2O_2, such as peroxisomes, catalase (CAT) is an important antioxidant enzyme that also converts H_2O_2 to water (Murphy and Kehrer, 1989).

Inside a cell, H_2O_2 can react with metal ions to produce the highly reactive hydroxyl radical, OH^- (Halliwell and Gutteridge, 1990). Superoxide can react with nitric oxide ($NO^\bullet$) to produce peroxynitrite ($ONOO^-$) (Beckman and Koppenol, 1996). The OH^- and $ONOO^-$ are among the most reactive species present in biological systems and are capable of oxidizing nucleic acids, proteins, lipids, and carbohydrate moieties in the cell (Rando, 2002).

2.7.1 Susceptibility of Skeletal Muscle to Oxidative Stress

There is a very high concentration of myoglobin in muscle, and such heme-containing proteins are known to confer greater sensitivity to free radical induced damage by conversion of H_2O_2 to more reactive species (Ostdal *et al*., 1997). Free radicals preferentially attack polyunsaturated fatty acids within membranes Therefore; requirement of skeletal muscle membrane for phospholipids containing large proportions of polyunsaturated fatty acids may render those membranes particularly susceptible to oxidative damage (Murphy and Kehrer, 1989). The specific patterns of cell and tissue injury produced by hereditary or induced GSH depletion, suggest specific susceptibilities to oxidative stress that depend on both age and species (Rando, 2002). The findings of necrotic degeneration in adult mice rendered deficient of GSH, highlights the importance of antioxidant defences in skeletal muscle during normal activity (Martensson and Meister, 1989).

2.7.2 Evidence of Oxidative Stress in Muscular Dystrophy

Disatnik and co-workers, 1998, presented evidence that is consistent with the hypothesis, that free radical mediated injury contributes to the pathogenesis of muscle necrosis in the muscular dystrophies (Murphy and Kehrer, 1989). The hypothesis was initially based on the similarities between the pathology in the dystrophies and the pathology of muscle exposed to oxidative stress in vitamin E deficiency (Murphy and Kehrer, 1989).

Lipid peroxidation is a common index of free radical mediated injury (Halliwell and Gutteridge, 1989). Previous measurements of lipid peroxidation in dystrophin-deficient muscles have indicated elevated levels in both humans and mice (Kar and Pearson, 1979; Jackson *et al*., 1984; Mechler *et al*., 1995; Ragusa *et al*., 1997). The team of Disatnik, 1998, investigated the role of oxidative injury in muscle necrosis in mdx mice. In order to avoid secondary consequences of muscle necrosis, all experiments were executed in the pre-necrotic phase. An induction of expression of genes encoding antioxidant enzymes, indicative of a cellular response to oxidative stress, was recorded. Greater

levels of lipid peroxidation were recorded in mdx muscle than in control muscles (Disatnik *et al*., 1998). No relationship with $NO^{\bullet}$-mediated toxicity was found, but evidence of increased oxidative stress preceding the onset of muscle cell death in dystrophin-deficient mice was detected (Disatnik *et al*., 1998).

The imbalance between free radical synthesis and the antioxidant capacity has been reported, almost four decades ago, to be a possible contributor to the necrotic process (Mendell *et al*., 1971). Although the significance and precise extent of the oxidative stress contribution in the degenerative process of dystrophic muscle is poorly understood, there is increasing evidence that the degenerative process may indeed be due to oxidative stress (Niebrój-Dobosz and Hausmanowa-Petrusewicz, 2005).

2.8 IMPLICATION FOR ANTIOXIDANTS

Antioxidants are substances, which counteract free radicals and prevent the damage caused by them (Venkat Ratnam *et al*., 2006). Antioxidants are enzymes and nonenzymatic agents that can provide a high stability to lipids (Marinova *et al*., 2002) and prevent the formation of, or remove ROS (Turunen *et al*., 2004). There are four major groups of naturally occurring lipid soluble antioxidants, carotenoids, tocopherols, estrogens and coenzyme Q/ubiquinol/CoQ10 (Betinger *et al*., 2007). Antioxidant enzymes include SOD and various peroxidases such as GPx, CAT, thioredoxin reductase and peroxiredoxin. Nonenzymatic agents include vitamins C and E, cartenoids, glutathione, α-lipoic acid, flavinoids and the reduced form of CoQ10, $CoQH_2$. All these agents all rely on a mechanism of regeneration in the cell (Turunen *et al*., 2004).

A new approach for using highly specific anti-cytokine therapies to treat DMD was reported by Grounds and Torrisi, 2004. The study tested the novel hypothesis that the initial sarcolemmal breakdown resulting from dystrophin deficiency is exacerbated by inflammatory cells and that cytokines, specifically tumor necrosis factor-α (TNFα), contribute to muscle necrosis. The antibody Remicade® was used to neutralize activity of the TNFα protein in mdx mice to assess whether blockade of TNFα in patients with DMD has therapeutic value. Remicade® does not cause generalized suppression of the immune system and has been used clinically to treat inflammatory disorders (Gabay, 2002). Remicade® was administered weekly from before the onset of necrosis and dystro-pathology, which set in around 21 days of age in the mdx model. Pharmacological blockade of TNFα activity with Remicade® were found to clearly delay and greatly reduce the breakdown of

dystrophic muscle, in marked contrast to the situation in mdx and mdx/TNFα(-/-) mice (Grounds and Torrisi, 2004).

Antioxidants were found to exert a beneficial effect in experimental models of chronic injury in diabetic animals (Aragno *et al*., 1999; Eriksson and Simán, 1996). Aragno and co-workers, 2004, showed that dehydroepiandosterone (DHEA) or vitamin E treatment in diabetic rats restored the oxidative balance and improved muscle gene transcription (Aragno *et al*., 2004). It has been shown that DHEA, a multifunctional steroid secreted by the adrenal gland and brain (Baulieu *et al*., 2000), possesses a multitargeted antioxidant effect and prevents tissue damage induced by acute and chronic hyperglycaemia (Aragno *et al*., 2002). Treatment with DHEA prevented the reduction of antioxidant compounds and the increase of oxidant species induced in other tissues by chronic hyperglycaemia (Aragno *et al*., 1999).

A study by Buck and Chojkier, 1996 showed that the decreased body weight, muscle wasting and skeletal muscle molecular abnormalities of cachexia were prevented by treatment of TNFα mice with the anitoxidants D-α-tocopherol or BW755c, or the nitric oxide synthase (NOS) inhibitor nitro-L-arginine. TNFα induces oxidative stress and NOS in skeletal muscle of these mice, leading to decreased myosin creatinine phosphokinase (MCK) expression and binding activities.

Kaczor and co-workers, 2007 determined the effect of low intensity training on markers of lipid and protein damage by ROS as well as antioxidant and mitochondrial enzyme activities in skeletal muscle of mdx mice. Significantly higher levels of lipid and protein peroxidation markers were detected in the muscle of mdx as compared to wild-type mice. The activities of antioxidant enzymes, SOD, MnSOD, and CAT were found to be higher in white and red gastrocnemius muscles of mdx mice than in wild-type mice. Elevated levels of the protein content for GPx in EDL muscle of mdx were reported to be higher than that in wild-type mice. Mitochondrial enzymes, oxoglutarate dehydrogenase (OGDH), and cyclooxygenase (COX) activity were only significantly elevated in white gastrocnemius fibers of mdx as compared to wild-type mice. The study found that low intensity exercise had a beneficial effect on skeletal muscle of mdx mice, resulting in decreasing lipid and protein oxidative damage (Kaczor *et al*., 2007). Low intensity exercise was found to induce 'pathophysiological adaptation' in skeletal muscle of mdx mice. The authors believed that in the first few weeks of low intensity exercise, ROS generation increased and markers of oxidative stress were elevated. However, adaptation were found to occur over the duration of training, resulting in a lower

generation of free radicals and decreased level of malondialdehyde (MDA) and protein carbonyls in mdx mice (Kaczor *et al*., 2007).

The generation of ROS which appears to play an important role in DMD motivated the study of Buetler and co-workers, 2002, who tested whether the antioxidant effect of green tea extract could diminish muscle necrosis in mdx mice. The study provided evidence that dietary supplementation with green tea extract preferentially protected the EDL muscle of mdx mice from necrosis. The mechanism for green tea extract protection is not clear but was expected to be mediated by its antioxidant activity. In addition, green tea extract dose-dependently protected C2C12 myotubes from tert-butylhydroperoxide- (BHP) induced oxidative stress (Buetler *et al*., 2002). Furthermore, the levels of protection afforded by green tea extract supplementation were found to be similar to results described for creatine (Pulido *et al*., 1998; Passaquin *et al*., 2002).

Together, these studies suggest that the reduction of oxidative stress, by different methodologies, whether inhibitory- (Grounds and Torrisi, 2004; Buck and Chojkier, 1996), inductive-(Aragno *et al*., 2002; Kaczor *et al*., 2007), or other (Buetler *et al*., 2002), lead to a reduction in the adverse events in the concerned pathologies. These findings motivated the present application of antioxidant supplementation in dysferlin-deficient mice. The present investigation followed a similar approach but employed a different strategy. It was argued that if elevated levels of oxidative stress, responsible for the adverse effects in numerous pathologies, are also present in dysferlin-deficient mouse muscle; these adverse changes will be detectable at the cellular level by morphological analysis. If these changes were found to be present, what will the effect of a direct free radical scavenging approach be?

Further review of the literature provided informative guidelines for the selection of an appropriate single antioxidant, and a combination of antioxidants. The selection criteria were simple: ideally there should be evidence for potent antioxidant potential of a supplement to be applied in a study like the present. In addition, evidence of beneficial application in other disease conditions, preferably in animals and man, with a high dose tolerance and low side effect profile in subjects is desirable. Two antioxidant substances that complied with the criteria, in addition to its numerous other beneficial effects, were CoQ10 and resveratrol.

2.9 PROSPECTIVE ANTIOXIDANTS

2.9.1 COENZYME Q10

Coenzyme Q (CoQ) is a naturally occuring compound with properties similar to those of vitamins. Because of its ubiquitous distribution in nature, it is also known as ubiquinone (Bhakgavan and Chopra, 2006). CoQ belongs to a homologous series of compounds that share a common benzoquinone ring structure but differ in length of the isoprenoid side chain (Bhakgavan and Chopra, 2006). In humans and a few other mammalian species, the side chain is comprised of ten isoprenoid units; hence it is called Coenzyme Q10 (CoQ10) (Bhakgavan and Chopra, 2006).

CoQ10 is similar in chemical structure to vitamin K, but it is not considered a vitamin because of its *de novo* synthesis in the body (Bhakgavan and Chopra, 2006). It is a lipid-soluble component of virtually all cell membranes, and is located in the hydrophobic domain of the phospholipid bilayer of cellular membranes (Quinzii *et al*., 2007; Sohal and Forster, 2007). CoQ10 is the only endogenously synthesized lipid with a redox function in mammals and exhibits a broad tissue as well as intracellular distribution (Dallner and Sindelar, 2000). It is also the only known lipid-soluble antioxidant that animal cells can synthesize *de novo*, and for which there exists enzymatic mechanisms which can regenerate it from its oxidized product formed in the course of its antioxidant function (Ernster and Dallner, 1995). It is a hydrophobic molecule and its properties are given by the 10-isoprenoid side chain (Crane, 2001).

In humans, CoQ10 is biosynthesized from tyrosine through a cascade of eight aromatic precursors, via the mevalonate pathway (Folkers, 1996) where cells rely on *de novo* synthesis for their supply of CoQ10. The levels of CoQ10 are subjected to regulation by physiological factors that are related to the oxidative activity of the organism (Ernster and Dallner, 1995; Tran and Clarke, 2007). CoQ10 is distributed among cellular membranes and it has a significant concentration in the plasma membrane (Gómez-Díaz *et al*., 2000). It is also present in the endomembranes of cells as well as in the mitochondria, where it serves as a central component of the transmembrane electron transport system (Sun *et al*., 1992).

The finding of CoQ10 in all membranes brought on a concept of CoQ10 as an important antioxidant (Kagan *et al*., 1990). Even greater significance became apparent when it was shown that reduced CoQ10 could restore antioxidant function to oxidized tocopherol (Crane, 2007). The first successful application of CoQ to a medical condition was Yamamura's treatment of congestive heart failure

(Crane, 2007). In addition to its central role in the mitochondrial respiratory chain, CoQ10 is now involved in a number of aspects of cellular metabolism (Turunen *et al*., 2004).

A number of medical conditions have shown to respond to supplementation with CoQ10: immune deficiency (Bliznakov, 1987), congestive heart failure (Langsjoen and Langsjoen, 1998), indication of therapeutic effects in diabetes(Hodgson *et al*., 2002), Parkinson's and Huntingtons disease (Shults, 2003; Beal, 2004; Ryu and Ferrante, 2005), relief of statin side effects (Littarru and Tiano, 2005), ataxia or encephalomyopathy (Quinzii *et al*., 2006; Gempel *et al*., 2007; Le Ber *et al*., 2007), and Cancer (Hodges *et al*., 1999; Brea-Calvo *et al*., 2006). CoQ10 deficiency has recently been shown to be an autosomal recessive disorder with heterogenous phenotypic manifestations and genetic background (Gempel *et al*., 2007).

In order for CoQ10 to maintain its physiological properties in biological systems, there is a constant need for optimum levels of the coenzyme in order to meet the metabolic demand. Literature is expanding with reports focusing on the deficiency of CoQ10 in the body. The focus of CoQ10 deficiency states in pathological conditions might further be attributable to a reduced mechanistic efficiency of one or more of the biochemical and/or physiological pathways where CoQ10 is directly or indirectly involved. This phenomenon raises the notion of whether supplementation of pathological conditions with CoQ10, might address the level of severity and progression of the symptoms of disease states where CoQ10 deficiency has been diagnosed.

Primary CoQ10 deficiency is considered to be the only treatable mitochondrial disorder, since patients have a response to oral CoQ10 supplementation (Montini *et al*., 2008). The disease usually manifests with nephropathy and endocephalomyopathy (Salviati *et al*., 2005). It has been shown that oral CoQ10 may stop the progression of encephalopathy, but no benefit has been noted with respect to the evolution of renal disease associated with this deficiency (Salviati *et al*., 2005; Rötig *et al*., 2007). This observation emphasizes the superior value of pre-symptomatic supplementation. Montini and co-workers recently described the outcome of long-term CoQ10 supplementation on CoQ10 deficiency caused by a homozygous missense mutation in the *COQ2* gene. The study found that early administration of CoQ10, before any symptoms have developed, was important for the resolution of renal symptoms and for preventing neurologic damage in a patient with CoQ10 deficiency (Montini *et al*., 2008).

There is no evidence of a CoQ10 deficiency state in the dysferlinopathies, only a few earlier reports on deficiency of CoQ in mice with hereditary muscular dystrophy (Littaru *et al*., 1970), and on dystrophic mice responding to Coenzyme Q4 therapy (Scholler *et al*., 1968) (CoQ10 was not readily available in those days). Furthermore, definitely improved physical performance was reported after two double-blind clinical trials, supplementing patients suffering from different muscular dystrophies, with CoQ10 (Folkers and Simonsen, 1995). Folkers and co-workers, 1985, reported that CoQ10 does not alter genetic defects but can benefit the sequelae of mitochondrial impairment from such defects.

Rötig and co-workers reported that CoQ10 administration to a large number of individuals with or without ubiquinone deficiency were found to be safe. This was attributed to the fact that CoQ10 is not taken up by the cells with normal ubiquinone content as there is no possibility to place more lipids into the limited space in the mitochondrial membrane (Rötig *et al*., 2000). When the lipid is missing, as is the case in ubiquinone synthesis defects, the inner mitochondrial membrane has the capacity to accept exogenous CoQ10 that can restore the electron flow (Turunen *et al*., 2004).

2.9.2 CoQ10 as an Antioxidant

Mitochondrial $CoQH_2$ is efficiently regenerated by the respiratory chain and is normally kept in a highly reduced state (Aberg *et al*., 1992). Early studies had shown that the CoQ hydroquinone is an excellent free radical scavenging antioxidant but its role was restricted to mitochondria until a general membrane distribution was shown by Ernster and Dallner, 1995 (Crane, 2007). Experiments on liposomes, mitochondria, microsomes, beef heart submitochondrial particles and lipoproteins of the blood, demonstrated that CoQ10 in reduced form, ubiquinol ($CoQH_2$), is an effective antioxidant and inhibits lipid peroxidation (Bentinger *et al*., 2007). Bentinger and co-workers reported that CoQ10 is our only endogenously synthesized lipid soluble antioxidant, and is mainly present in the activated (reduced) form.

CoQ10's effectiveness as lipid peroxidation inhibitor is based on its complex interaction during the process of peroxidation. The primary action is the prevention of lipid peroxyl radical ($LOO^{\bullet}$) production during the initiation process. This is the first phase of the process, where an abstraction of a hydrogen atom from a methylene group of a fatty acid occurs, presupposing that it has several double bonds. $CoQH_2$ reduces the initiating perferryl radical with the formation of ubisemiquinone and H_2O_2. It is also possible that $CoQH_2$ eliminates $LOO^{\bullet}$ directly.

The reduced lipid effectively regenerates vitamin E from the α-tocopheroxyl radical (Bentinger *al*., 2007). There are several mechanisms in protein oxidation and it appears that the most common is the direct oxidation of amino acid residues (Stadtman ER, Levine RL, 2000). Protein oxidation may also occur by lipid-derived free radicals and by breakdown products of phospholipid hyperperoxides. These compounds link covalently to basic amino acid residues and in the latter case also to sulfhydryl groups, causing intra- and intermolecular cross-linking (Bentinger *et al*., 2007). CoQ10 is effective in preventing protein oxidation by quenching the initiating perferryl radical and functioning as a chain-breaking antioxidant, thus preventing the process of propagation. This is the second phase in lipid peroxidation, where $LOO^{\bullet}$ abstracts a hydrogen atom from an additional unsaturated fatty acid, leading to formation of a carbon-centered radical ($L^{\bullet}$) and lipid hyperoxide (LOOH), which can be reoxidized to $LOO^{\bullet}$. This will result in reinitiation of lipid peroxidation (Bentinger *et al*., 2007).

The sensitivity of proteins to oxidative stress depends on their structure, composition and localization. The close spatial relationship of CoQ10 to the neighbouring membrane proteins is the main factor for its protective effect against protein oxidation (Bentinger *et al*., 2007). CoQ10 also protects DNA against oxidative damage, which is of particular interest for mitochondrial DNA, since damage is not easily reparable (Bentinger *et al*., 2007). Oxidative stress may damage DNA by initiating a series of metabolic reactions in the cell leading to activation of nuclease enzymes that cleave the DNA backbone. A more common event is the interaction of H_2O_2 with metal ions bound to DNA, which leads to the generation of hydroxyl radicals. DNA oxidation in isolated mitochondria takes place in the presence of ADP-Fe^{3+} and ascorbate, resulting in elevated content of 8-hydroxy-deoxyguanosine (8-OH-dG) (Ernster and Dallner, 1995). Incubation in the presence of succinate and antimycin, which maximize the endogenous ubiquinol pool, eliminated the oxidative damage and decrease the increased strand breaks caused by ADP-Fe^{3+} (Bentinger *et al*., 2007).

In mitochondria, ubisemiquinone radical is formed during respiration which is effectively reduced to ubiquinol by the 'protonmotive Q cycle' described by Mitchell in 1975 (Mitchell, 1975). The large reducing capacity of the cell, which is able to regenerate CoQ10 by reduction at all locations of the cell, is a very important property, contributing to the effectiveness of CoQ10 as an antioxidant (Bentinger *et al*., 2007). Available evidence indicates that, owing to its metabolic roles, CoQ10 could positively influence the natural course of disease and potentially enhance the effect of other treatments by correcting some metabolic derangements (Littarru and Tiano, 2005). Metabolic derangements are often not causative; they are known to be the consequences of secondary aspects of diseases (Littarru and Tiano, 2005). Emily Bliznakov stated that: 'Treatment of patients with

various forms of cardiovascular diseases by a combination of CoQ10 and other antioxidants, concomitant with standard drug treatment, is justified and recommended" (Bliznakov, 1999).

2.9.3 RESVERATROL

Resveratrol (3,5,4'-trihydroxystilbene) was first isolated from the roots of *Veratrum grandiflorum O. Loes* (white hellebore) in 1940 (Takaoka, 1940), and later in 1963, from the roots of *Polygonum cuspidatum* (Japanese knotweed) (Baur and Sinclair, 2006). It is a polyphenolic phytoalexin found in many plants, nuts, and fruits and is abundant in grapes and red wine, and in the traditional Japanese medicine, Kojokon. Its function in nature is to protect the plant from injury, UV irradiation and fungal attack (Birell *et al*., 2005; Matsuoka *et al*., 2008).

Resveratrol has been reported to be along with flavonoids, at least partially, responsible for the health benefits of red wine (Frankel *et al*., 1993 a; Soleas *et al*., 1997). It has previously been reported that resveratrol is a rather weak antioxidant (Hu *et al*., 2007), and that its antioxidant effects may be due to its direct interaction with biomolecules that confer cellular stress resistance (Robb *et al*., 2008). Robb and co-workers have identified the endogenous antioxidant enzyme MnSOD as a specific target for resveratrol in human MRC-5 cells. A progressive and dramatic induction of MnSOD expression and activity elicited by the treatment of an untransformed human cell line with micromolar concentrations were reported (Robb *et al*., 2008). The overexpression of MnSOD has previously proven its sole capability of reducing intracellular oxidative stress and conferring stress resistance, in mouse cortical neurons subjected to chronic intermittent hypoxia-mediated oxidative damage (Shan *et al*., 2007).

Resveratrol attracted little interest until 1992 when this naturally occurring plant antibiotic, initially characterized as a phytoalexin, was postulated to explain some of the cardioprotective effects of red wine (Siemann and Creasy, 1992). This theory provides the basis for the observation that the incidence of cardiovascular diseases in France is lower than that expected for the French diet, which is rich in saturated fat. The so-called 'French Paradox' (Kopp, 1998; Cho *et al*., 2008). Resveratrol has shown to prevent or slow down the progression of cancer (Jang *et al*., 1997), cardiovascular disease (Bradamante *et al*., 2004), and ischaemic injuries (Wang *et al*., 2002 and Sinha *et al*., 2002), as well as enhancing stress resistance and extending the lifespan of various organisms, from yeasts to vertebrates (Howitz *et al*., 2003 and Valenzano *et al*., 2006).

Its free radical scavenging effects has been expanded by the finding that resveratrol decreases the traumatic effects of partial hepatectomy in rats, by reducing the levels of MDA, while increasing the

levels of the cofactor GSH. The authors recommended supplementation with resveratrol for the same application in donors and recipients undergoing living donor liver transplantations (Kirimlioglu *et al*., 2008). Resveratrol has shown the ability to reduce serum cholesterol in hamsters by down-regulating hepatic HMG-CoA reductase mRNA expression, following a high-fat diet (Cho *et al*., 2008). The cardiovascular benefits derived from resveratrol, have also been attributed to its estrogenic action, where resveratrol has been shown to be a phytoestrogen that exhibits variable degrees of estrogen receptor agonism in different test systems (Gehm *et al*., 1997).

Pharmokinetic studies have cast doubt on the physiological relevance of high concentrations of resveratrol, typically used in *in vitro* studies, since it is rapidly metabolized. It is unclear whether the benefits of resveratrol are merely the results of fortuitous interactions with dozens of mammalian proteins or is it acting through a specific genetic pathway that has evolved to increase disease- and stress resistance (Baur and Sinclair, 2006). Resveratrol has been suggested to be cardioprotective via various mechanisms such as its antioxidant activity (Fauconneau *et al*., 1997), inhibition of platelet aggregation (Pace-Asciak *et al*., 1996), induction of NO production (Hsieh *et al*., 1999), and modulation of the synthesis of hepatic apolipoprotein and lipids (Frankel *et al*., 1993 b).

Jang and co-workers, 1997, proposed a chemo-preventive property of resveratrol, as it was proposed to inhibit all three phases of tumour development: initiation, promotion, and propagation. Birell and co-workers, 2005, reported the ability of resveratrol to reduce lung tissue neutrophilia in an asthmatic rat model, to a similar magnitude as that achieved by treatment with budesonide. The results were associated with a reduction in the inflammatory mediators, by an NF-κB-independent mechanism. It was therefore suggested that resveratrol may possess anti-inflammatory properties via a novel mechanism. Resveratrol has been considered to be a caloric restriction mimetic in lower organisms, primarily on the basis of its activation of sirtuin proteins and its capacity to extend lifespan (Baur and Sinclair, 2006).

The maximum tolerated dose of resveratrol has not been thoroughly determined, but 300 mg/kg body weight showed no detrimental effects in rats (Crowell *et al*., 2004). Although the exact mechanism of resveratrol's action in mediating health benefits, is not yet fully understood, accumulating evidence suggest that resveratrol shows great potential in the treatment of the leading causes of morbidity and mortality. So far, little evidence suggests that these health benefits are coupled with deleterious side effects (Baur and Sinclair, 2006).

2.10 STUDY OBJECTIVES

It was the aim of the present study to determine, on a cellular level, how the morphology and ultrastructure in dysferlin-deficient SJL/J mouse muscle, whether subjected to oxidative stress or not, will be affected by antioxidant supplementation. CoQ10 and resveratrol, singly and in combination were used as the antioxidants of choice. The present study was directed by the following research objectives:

1. Implementation of the SJL/J mouse model for investigation of the cellular response to the administration of the antioxidants CoQ10 and resveratrol over a 90-day period, as articulated through the muscle morphology. Distribution of animals into different experimental groups, and calculation of antioxidant doses, comparable to human physiological levels, by a body surface area (BSA) normalization formula.

2. Assessment of non-specific parameters in SJL/J mice:
   a. Animal weight as a parameter of animal well-being during the course of the trial.

   b. Tensile strength as a parameter of disease progression as well as the effect of antioxidant supplementation on the physical strength of SJL/J mice, during week 7 to 11 of the 90 day trial.B

   c. Blood levels of the enzymes creatine kinase (CK) and lactate dehydrogenase (LDH).

   d. Quantitative analysis of white blood cell counts.

3. Assessment of histopathology in the quadriceps muscle as a qualitative parameter for the disease characteristics and the effect of antioxidant supplementation thereof.
   Evaluation will be done at:

   a. light microscopic level; the qualitative state of histopathological characteristics, as well as quantitative morphometric significance of fiber diameter variation in control and treated groups, as determined by the minimal Feret's diameter. In addition, the quantification of fibers with nuclei in the central position will be done.

   b. ultrastructural level, as determined by TEM and SEM, to study the ultrastructural hallmarks of the disease and any variation thereof, as a result of antioxidant supplementation. The ultrastructural analysis will also pay attention to non-specific

alterations and how they could be related to the disease processes in dysferlin-deficient muscle.

4. Assessment of the oxidative stress index (OSI) in the quadriceps muscles as a parameter of the degree of oxidative stress in the muscle tissue of the SJL/J mouse.

    a. Assessment of the malondialdehyde (MDA) levels and the effect of antioxidant supplementation over a 90 day period.

    b. Assessment of the antioxidant activity in quadriceps muscle, expressed as total antioxidant status (TAS), and the variation afforded by antioxidant supplementation over a 90 day period.

    c. Calculation of the OSI as a measure of the relationship between lipid peroxidation and antioxidant activity in quadriceps muscle.

Chapter 3

A 90 day antioxidant supplementation trail in the SJL/J mouse model for dysferlinopathy

3.1 INTRODUCTION

An ideal animal model for a disease has been described as one in which all animals of a strain develops the disease spontaneously (Weller *et al.*, 1997). The natural induction process of the disease can be studied and an optimally reproducible environment exists in which to test treatments. Many of these models have been painstakingly developed; others have been discovered by chance (Weller *et al*., 1997). Considering that the SJL mouse has been widely used as a model for different human diseases, and for experimental research on muscle regeneration and transplantation for more than 40 years, it was not without irony, a decade ago, that the SJL mouse was found to have a genetically determined degenerative muscle disease of its own (Bittner *et al*., 1999). The spontaneous onset and 100% incidence of myopathy in the SJL/J mouse rendered this strain a useful model for idiopathic myopathy (Weller *et al*., 1997) and now also for dysferlinopathy.

3.2 ANIMAL MODELS IN SCIENTIFIC PRACTICE

A major focus of modern biological research is to elucidate the molecular and cellular mechanisms that underlie human health and disease. Over the last few decades, both naturally occurring and genetically engineered animal models of human diseases have been employed for evaluating new therapeutic options and for elucidating pathological pathways (Doran *et al*., 2007). Doran and co-workers, 2007, stated that biological studies of animal models in conjunction with findings from clinical investigations can be extremely helpful for the initial evaluation of alternative treatment strategies. Animal models further offer a valuable tool, as they provide crucial information on genetic manipulations via transgenic or gene knockout technology as well as in cell transplantation studies in the development of therapeutic approaches for addressing human disorders. A variety of animal species are currently being used for detailed cell biological, physiological and biochemical analysis of numerous human diseases. These models are also applied in essential toxicological investigations for the development and testing of potential side effects of treatment regimes (Doran *et al*., 2007).

A good animal model should ideally exhibit specific characteristics. These should include (Doran *et al*., 2007):

i. resemblance of the etiology of the human disease in complexity and severity, onset, and progression,

ii. development of most or all of the multifactorial aspects usually observed in end-stage human pathology,

iii. imitation of basic mechanisms of the human pathology and metabolism that are important for disease progression or drug treatment,

iv. demonstration of similar primary genetic abnormalities in the case of inherited disorders, *eg.* have a genetic mutation causing absence of the same protein absent in the human condition,

v. illustration of comparable susceptibility to infectious or pharmacological agents in the case of infectious or pharmacogenetic diseases,

vi. being suitable for cell based treatment strategies and genetic manipulations, and

vii. being of adequate size to facilitate physiological and surgical procedures or to yield sufficient amounts of biological samples for extended biochemical analyses.

It is also important to keep the limitations of animal experiments in mind. The extrapolation of animal data to the human situation is sometimes very difficult due to species-specific differences. Small rodents commonly used in biological research may exhibit fundamental physiological differences as compared to humans. This includes differences in development, cellular differentiation, potential for tissue regeneration, mechanisms of cell regeneration, immune responses, susceptibility to infections, and patterns of detoxification of xenobiotics, metabolism and bioenergetics (Doran *et al*. 2007). Variations in basic biological mechanisms such as the maintenance of ion homeostasis, cell signalling, hormonal regulation or metabolic integration may exist between cellular systems in animal models *versus* human patients. Differences in compensatory mechanisms or redundant pathways between different species may complicate the interpretation of results from animal experiments (Doran *et al*., 2007).

Another important consideration, of which the importance might often be overlooked in studies testing substances other than anticancer drugs, is the dose calculation. In the development and testing of therapeutic agents, whether pharmaceutical or nutraceutical in nature, it is essential to appropriately translate the drug dosage from one animal species to another (Reagan-Shaw *et al*.,

2008). Confusion and concern may emanate from incorrect dose translations across species. Direct translation of animal doses to human doses may result in misleading interpretations (Reagan-Shaw *et al*., 2008; Halliwell, 2009). The importance of determining the appropriate dose of anticancer agents has been emphasized by the fact that individuals might have varying abilities to metabolize and eliminate drugs. The same dose of anticancer agents might show different pharmacokinetics and pharmacodynamics in different individuals (Kouno *et al*., 2003). For drugs that produce therapeutic effects at doses far less than those that cause toxicity, the incentive for precise dosing is far less than for drugs with a narrower therapeutic index (Hahn, 2005). The narrow therapeutic index of most antineoplastic agents has provided great impetus to deliver doses as precisely as possible (Hahn, 2005). Halliwell, 2009, reasoned that one explanation for the lack of demonstrating the benefits of antioxidant therapy in humans might be the utilization of wrong doses. One of the practices embedded in dosing of antitumor drugs is dosing by body surface area (BSA). More commonly, milligrams per square meter (mg/m^2). Body surface area is reported to be equivalent to the two-dimensional surface area of the skin (Hahn, 2005). Drug ineffectiveness has been argued to be associated with inappropriate translation of drug doses from one animal species to another (Reagan-Shaw *et al*., 2008).

3.3 SJL/J Mice

3.3.1 Origin of the SJL/J Model

The SJL mouse model was developed by James Lambert at The Jackson Laboratory in 1955 from three different sources of Swiss Webster mice. Dr ED Murphy of the Jackson Laboratory, Bar Harbor, Maine, reported in 1962 the development of spontaneous lymphomas resembling Hodgkin's disease in an inbred strain of SJL/J mice (Murphy, 1963). In 1967, Yumoto and Dmochowski described the strain as follows: "The SJL/J strain is a new inbred strain, derived from non-inbred Swiss Webster stock by brother-to-sister matings for over 46 generations. Spontaneous lymphomas occur in over 90% of the mice at an average age of 13 months". Murphy also observed lesions which he described as 'of striking histologic similarity' to human Hodgkin's disease in the SJL/J strain (Murphy, 1963).

The SJL mouse strain has been reported to be susceptible to many induced autoimmune diseases such as experimental autoimmune encephalitis (EAE) and inflammatory muscle disease (Bernard and Carnegie, 1975; Rosenberg *et al*., 1987). In addition, skeletal muscle of the SJL mice has been shown to have an increased regenerative capacity (Grounds and McGeachie, 1989; Mitchell *et al*., 1992), and to demonstrate a spontaneous occurrence of what has been designated an 'inflammatory

myopathy, accompanied by loss of strength' (Hohlfeld *et al*., 1988; Weller *et al*., 1997). Only about a decade later, Bittner and co-workers, 1999, identified a reduction in dysferlin protein in SJL/J mice, consistent with the dysferlin reduction in dysferlinopathy patients with a missense mutation. This novel spontaneous mutation in the dysferlin gene in the SJL/J mice strain, results in a reduction of dysferlin to approximately 15% of levels detected in dysferlin-competent animals and human samples (Bittner *et al*., 1999). Therefore this model is ideal for research in the field of dysferlinopathy.

3.3.2 General Information on the SJL/J Strain

The SJL model has been found to display a very high incidence of reticulum cell sarcomas resembling Hodgkin's disease by approximately one year of age (www.jax.org/jaxmice). Sarcomas first appear in the Peyer's patches and mesenteric lymph nodes and later in the spleen, liver, thymus and other lymph nodes. Most of the tumors are mixed-cell types classified as type B reticulum cell neoplasms, but a few are type A histiocytomas. This strain is also characterized by extreme aggression in males and its susceptibility to experimental autoimmune encephalomyelitis (EAE) for multiple sclerosis research. The SJL/J strain develops a spontaneous myopathy resulting from a splice-site mutation in the dysferlin gene (Bittner *et al*., 1999). This *Dysf*^{jm} allele has been shown to result in decreased levels of dysferlin protein in SJL/J mice and makes this mouse a good model for the dysferlinopathies (www.jax.org/jaxmice).

The spontaneous myopathy is characterized by a progressive loss of muscle mass and strength corresponding with an increase in muscle pathology. Pathological changes include muscle fibers with central nuclei, size variation, splitting, inflammatory infiltrate, necrosis and eventual replacement of muscle fiber with fat (Weller *et al*., 1997; Bittner *et al*., 1999; Suzuki *et al*., 2005). While muscle weakness can be detected as early as three weeks of age, the greatest pathology occurs after 6 months of age (Bittner *et al*., 1999; Fox, 2007; www.jax.org/jaxmice). A 171 bp in-frame deletion in the encoded mRNA of the SJL/J mouse is predicted to remove 57 amino acids from the corresponding protein (www.jax.org/jaxmice). The region corresponds to most of the fourth C2 domain of the protein, and the deletion has been reported likely to results in instability of the protein (www.jax.org/jaxmice). The molecular basis for the mutation is the result of a splicing mutation in the gene, resulting from a deletion of a small tandem repeat (www.jax.org/jaxmice). While western blotting was found to show a reduction of dysferlin protein in SJL mice, microarray data was found to show an upregulation of dysferlin mRNA (Suzuki *et al*., 2005).

3.3.3 Justification of the Model for Dysferlinopathy Studies

Histopathological examinations of muscles in SJL mice of different ages and different sources (SJL/J, SJL/Olac) by Bittner and co-workers, 1999, disclosed features compatible with a progressive muscular dystrophy. These features included degenerative and regenerative changes of muscle fibers and a progressive fibrosis. Proximal muscle groups were found to be primarily affected by these changes, whereas the distal muscles remained less affected (Bittner *et al*., 1999). The first histological changes could be observed as early as three weeks of age. By seven months, the dystrophic changes included inflammatory foci, as well as the appearance of fatty and fibrotic tissue (Bittner *et al*., 1999). The team of Bittner associated morphological alterations with signs of slowly progressive muscle weakness, which was detected as early as three weeks after birth, when mice were suspended by their tails. Subsequent breeding experiments revealed this muscular dystrophy phenotype to be inherited as an autosomal recessive trait (Bittner *et al*., 1999). Following genetic analysis, it came to light that the mutation mapped to the region syntenic with chromosome 2p13 in humans; the region where the gene mutated in human dysferlinopathy has been mapped (Bashir *et al*., 1998; Liu *et al*., 1998; Bittner *et al*., 1999). Immunoblot analysis with the NCL-hamlet antibody, displayed a reduction of dysferlin-specific bands of muscle samples from different sources of SJL mice. The reduction corresponds to that found in humans with a missense mutation in the dysferlin gene. The team of Bittner suggested that this mouse will become a useful animal model for studying the pathomechanisms of dysferlin deficiency and, moreover, for applying therapeutic rescue strategies.

Since SJL descends from a wild derived strain of Swiss mice which are genetically distinct from the common laboratory mouse, there is not an appropriate control strain available (Von der Haag *et al*., 2005), Therefore the SWR/J strain were found most suitable to use as a negative control in the present study. The SWR inbred strain was developed by Clara J Lynch at the Rockefeller institute who obtained Swiss mice from A de Coulon of Lausanne, Switzerland and began inbreeding around 1929. The strain was transferred to Raymond Parker at the University of Toronto who supplied them to The Jackson Laboratory in 1947 at F28+. The SWR/J mice are widely used in research as a general purpose strain (www.jax.org/jaxmice).

3.3.4 Histological Characteristics of the SJL/J Model

Muscle disease has been found to develop spontaneously in every member of the SJL/J mouse strain (Weller *et al*., 1997). Weller and co-workers, 1997, described that the disease has a very predictable

course and onset, and can be divided into three distinct phases (Weller *et al*., 1997). In young adult SJL/J mice (age 2 to 4 months), muscle functions normally and pathologic abnormalities are minimal although present. At age 6 to 8 months, the active phase begins, and all mice develop extensive muscle necrosis accompanied by the presence of immune cells and myophagocytosis. Strength is decreased, although muscular atrophy is still not present. In the final, degenerative phase of the disease, at age 10 to 16 months, muscle necrosis continues, strength loss accelerates, and muscle mass is progressively lost. By 16 months of age, SJL/J mice have lost half of their young adult muscle mass and strength (Weller *et al*., 1997). Weller and co-workers found that by 6 months of age, muscle from most SJL/J mice exhibited active myopathy, defined as 10 or more necrotic fibers per quadriceps, containing mononuclear cells.

Between different groups of 6 month old SJL/J mice, the percentage of individual animals with active disease varied from 60% to 100%, averaging 78% of mice overall. The typical pattern consisted of scattered single involved fibers, and as many as 100 such fibers per quadriceps cross section were counted. Involved fibers consisted of relatively intact muscle fibers with mononuclear cells beginning to enter the membrane, necrotic fibers completely filled with cells, and fiber remnants still containing a few cells (Weller *et al*., 1997). An increase in muscle fiber size variation was also found and areas of more widespread endomysial involvement typical of later disease stages were sometimes present and reported to appear especially near perimysial fascia (Weller *et al*., 1997). Mild perivascular inflammation was commonly observed, although not found to be predominant, while the histological pattern of fiber involvement at the age of 6 months appeared to be identical to autoimmune myositis (EAM) in this mouse strain, and like EAM the inflammatory infiltrate consisted primarily of macrophages (Weller *et al*., 1997). This evidence provided a platform for decision making of the age at which animals in the present study should be entered into the program. Considering evidence of full disease onset in the SJL/J model at six months of age, and the belief that 90 days of antioxidant supplementation will be best to determine the cellular effect brought about by the supplementation, it was decided to enter 14 week-old SJL/J mice into a 90 day program.

3.3.5 Muscle Regenerative Capacity

The muscle of young SJL/J mice has been found to be capable of vigorous regeneration (Grounds and McGeachie, 1989; Mitchell *et al*., 1992). Two-month-old SJL/J muscle regenerates almost completely *in vivo* after a crush injury, whereas injured Balb/c muscle forms scar tissue and few myotubes (Grounds and McGeachie, 1989). Weller and co-workers, 1997, found that young SJL/J mice are also

stronger than young Balb/c mice, suggesting a correlation with the higher muscle regenerative capacity. The inference was made that faster and better myotube formation compensates for early muscle damage in young mice, but eventually falls behind as more and more muscle fibers are destroyed (Weller *et al*., 1997). Mitchell and co-workers, 1992, found the formation of new myotubes in SJL/J muscle after crush injury to be associated with efficient clearance of muscle debris by macrophages. These cells were later reported to play the major clearance role in spontaneous myopathy in this strain (Weller *et al*., 1997). The superior regeneration of SJL/J muscles were found to be due to a faster and more extensive inflammatory response combined with a greater capacity for myotube formation (Mitchell *et al*., 1992). Intrinsic muscle factors were suggested to play a central role rather than the genotype of the bone marrow-derived macrophages (Mitchell *et al*., 1995).

3.4 The Animal Study

3.4.1 Design and Layout

This chapter provides a detailed outline of the animal study and study design that preceded the outcome of the research objectives concerned in the present study.

Sixty female animals with a mean weight of ≈20g were imported from the Jackson Laboratory, Bar Harbor, USA for the present study. An import permit was obtained from the Department of Veterinary Services, Ministry of Agriculture, and the conditions stipulated therein were strictly adhered to. Sample size was determined in collaboration with a biostatistician (Medical Research Council (MRC), South Africa), following convention in ANOVA studies that error degrees of freedom be at least 30. Ten of these animals were of the SWR/J strain and served as the negative control in the study, while the other 50 animals were SJL/J mice. On the date of shipment the SWR/J mice were nine weeks old and the SJL/J mice were eight weeks old. Forty days were allowed for acclimatization before commencement of the study.

Animals were housed at the laboratory animal facility of the University of Pretoria's Biomedical Research Centre (UPBRC) at Onderstepoort (Pretoria, South Africa). The barrier unit was free of all major pathogens as serology, bacteriology and parasitology tests, performed around the same time as the present study, all conformed to the facility's quality assurance policy. Animals were maintained in the facility's barrier unit in Tecniplast IVC cages (Figure 3.1), (Eurostandard type II L) with individual air supply, equipped with a pre-filter and HEPA filter system.

Sterile Agrebe basic 55cm^2, cotton sheet laboratory animal cloth bedding (for boxes Type II/III Ll) were used as bedding and changed once weekly. The main air supply system consisted of a 50% Fresh Air Primary filter and a Secondary Bag filter with 10 to 15 air changes per hour. A constant temperature of 23 to 24°C, a relative humidity of 40 to 60%, and a 12-hour dark-light cycle were maintained. The animals were allowed free access to JL Rat and Mouse 6F-IRRAD food (PMI Nutrition International, LLC) and water *ad libitum*.

Figure 3.1: Tecniplast IVC cage with individual air supply (top removed, lying on the left).

When a decrease and slowing in the mobility of the animals was observed, as a result of disease progression, it was decided to supplement the animals' diet by addition of Nestlé Cerelac sterile baby cereal on the floor of each cage, from day 50 until termination. The food supplementation did not contain any of the two products tested in the present study and were not expected to influence the results. All experimental protocols complied with the requirements of the University of Pretoria's Animal Use and Care Committee.

On day 0 of the 90 day trial, the animals were marked by means of earclipping according to the German identification system for laboratory animals. Accurate identification is of utmost importance when a large number of animals are used and housed collectively in order to avoid replicate procedures in the same animal. Identification is also important for the documentation of clinical observations and condition assessment of the animals, as each animal was assessed individually, and observations documented for each individual. At the age of 14 weeks and 15 weeks for SJL/J and SWR/J mice, respectively, the animals entered a 90 day experimental study. On this day, six SJL/J animals were terminated (as discussed in termination procedures below), for comparison of age-related changes with muscle tissue of 27 week-old SJL/J mice. The six animals were all 14 weeks of age, and represented the age control group.

The 54 animals that entered the study on day one of the 90 day trial were divided into the following groups, and caged communally in group order (Table 3.1). Ten SWR/J mice received a placebo for 90 days in the same volume as the antioxidants tested in the study, and represented the negative

control group. Eight SJL/J mice received a placebo for 90 days in the same volume as the antioxidants tested in the study, and represented the positive control group. Nine SJL/J mice received 60mg/kg resveratrol per day, and represented the resveratrol group. Nine SJL/J mice received 40mg/kg CoQ10 per day, and represented the low CoQ10 group. Nine SJL/J mice received 120mg/kg CoQ10 per day, and represented the high CoQ10 group, and nine SJL/J mice received a combination of 40mg/kg CoQ10 plus 60mg/kg resveratrol per day, simultaneously administered by oral dosing, and represented the resveratrol/CoQ10 combination group. Oral dosing was performed for all substances in all groups, using a 1000µl syringe with a mouse oral gavage needle nr. 20*g*. All animals were weighed on day one, and thereafter twice weekly.

Table 3.1 Summary of subject classification in group order

Group	Strain	Treatment	Concentration (mg/kg/day)	Age at Termination (in weeks)
Negative control	SWR/J	None	-	**28**
Positive control	SJL/J	None	-	**27**
Resveratrol	SJL/J	**Resveratrol**	60	**27**
CoQ10 (low)	SJL/J	**Low CoQ10**	40	**27**
CoQ10 (high)	SJL/J	**High CoQ10**	120	**27**
Resveratrol/CoQ10 combination	SJL/J	**Resveratrol/CoQ10**	60/40	**27**
Age control	SJL/J	None	-	**14**

Doses were calculated according to the BSA normalization method (Formula 3.1) for more appropriate conversion of drug doses from animal studies to human studies (Reagan-Shaw *et al*., 2008). Body surface area correlates well with parameters of mammalian biology, which makes BSA normalization logical for allometric scaling of drug doses between species, given that the activity of most drugs corresponds to the relationship between the drug and some physiological processes or functions (Reagan-Shaw *et al*., 2008). It was therefore decided to use the formula for dose translation based on BSA (formula 3.1), suggested by Reagan-Shaw and co-workers, 2008, to calculate the appropriate doses of CoQ10 and resveratrol to be administered in mice.

Formula 3.1: Dose translation based on BSA

$$\text{HED (mg/kg)} = \text{Animal dose (mg/kg)} \times \frac{\text{Animal } K_m}{\text{Human } K_m}$$

Where,

HED	Human equivalent dose in mg per kg
K_m	The K_m factor, body weight (kg) divided by BSA (m^2), is used to convert the mg/kg dose used in a study to an mg/m^2 dose
Animal K_m	3 (mouse)
Human K_m	37 (human weighing 60kg)

3.4.2 Dose Calculation, Dose Preparation, Supplements, and Solvents

The motivation behind the use of the BSA normalization method was that it has been justified as a reliable method for accurate dose translation from animal to human studies (Reagan-Shaw *et al*., 2008). In order to obtain doses high enough to provide a reliable indication of the antioxidant effectiveness in mice, comparable to a predicted effect in humans, BSA-based dose calculation was found to be the most appropriate method and has been reported to be far superior to the simple conversion based on body weight only (Reagan-Shaw *et al*., 2008).

To convert the dose used in a mouse to a dose based on surface area for humans, formula 3.1 multiply the mouse dose in mg/kg by the K_m factor for a mouse (3), divided by the K_m factor for a human (37). This calculation results in a human equivalent dose for a 60 kg person (Reagan-Shaw *et al*., 2008). The body weight approach has historically been the most common general approach to scaling in toxicology, particularly in regulatory toxicology testing, and the 'ideal' weight used in the BSA-based calculations (60kg), was presumably adopted from this system. There are several ways to perform a scaling operation on a body weight basis; the most often employed being to simply calculate a conversion factor (K). A difficulty with this approach is that the body weights of any population of animals or people change throughout life, and even a common age will present considerable variation. Custom is therefore, to use an 'ideal person' (70kg for men and 50kg for women, now set as a 'standard' of 60kg) or 'ideal' human weight (for which there is considerable less consensus) (Gad, 2006).

For the present study, it was decided to test two different concentrations of CoQ10, one relatively low, and the other three times higher, and one concentration of resveratrol. Two hundred mg per

day, as human physiological equivalent level, was decided on as the lower dose for CoQ10, and therefore the higher dose of 600mg/day. Resveratrol was administered at 300mg per day, as the human physiological equivalent level. Therefore, in order to obtain the animal equivalent dose (AED), formula 3.2 was derived from formula 3.1:

Formula 3.2: Dose translation from human to mouse doses

$$\text{AED (mg/kg)} = \text{HED (mg/kg)} \times \frac{K_m \text{ (human)}}{K_m \text{ (mouse)}}$$

Where,

AED	Animal equivalent dose in mg per kg
HED	Human equivalent dose in mg per kg
K_m	The K_m factor, body weight (kg) divided by BSA (m^2), is used to convert the mg/kg dose used in a study to an mg/m^2 dose.
Mouse K_m	3
Human K_m	37 (human weighing 60kg)

The concentrations incorporated in the study resulted in the following derived AEDs:

i. resveratrol group - 6omg/kg of resveratrol per day

ii. low CoQ10 group - 40mg/kg of CoQ10 per day

iii. high CoQ10 group - 120mg/kg of CoQ10 per day,

iv. resveratrol/CoQ10 combination group - 60mg/kg resveratrol plus 40mg/kg CoQ10 per day.

All supplement preparations were made up fresh every week in milliQ water, homogenized by ultrasonic treatment (as was done by Kettawan and co-workers, 2007), and stored at room temperature.

Resveratrol was obtained in a commercially available gel capsule at 50mg units, 98% pure, prepared from *Polygonum cuspidatum* (manufactured for CHM/RD Pty Ltd, and distributed by Blueskygreenearth Herbs Pty Ltd, Australia). The capsules were emptied, and powder was dissolved in appropriate volumes of milliQ water to obtain the desired concentration. No heat was added, the solution was activated by mild shaking. CoQ10 was obtained in the commercially available Q-Gel® formulation at 100mg per unit, in a softgel capsule. Each capsule contained 150 international units (IU) natural vitamin E (as d-alpha tocopheryl acetateUSP/NF) and 100mg CoQ10 (ubidecarenone

USP) (manufactured for Nutraceutical Sciences Institute; distributed by vitacost.com, USA). After addition of the CoQ10 to milliQ water, the container was placed in a waterbath at 60°C for 10 to 20 seconds and then removed to be mildly shaken. The procedure was repeated two to three times, until the solution was homogenous. In order to allow adaption to the strength of the antioxidants, half of the dose of each separate preparation was administered, however, the volume was maintained. These doses were administered for the first 14 days of the 90 day study, and thereafter, full doses were administered until the end of the study.

3.4.3 Routine Procedures and Observations During the Course of the 90 day Study

3.4.3.1 Dosing

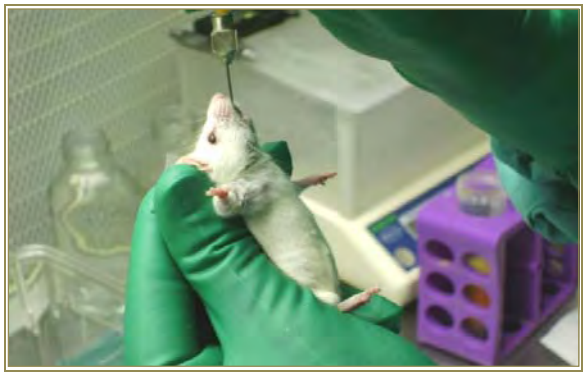

Figure 3.2: Oral dosing.

Administration (Figure 3.2) of specific concentrations was done at constant volume (200µl) (Figure 3.3) over all the groups, at different concentrations, once per day by oral dosing, for 90 days. The two control groups, (positive and negative), received 200µl of milliQ water as placebo.

Administration of supplements in all the groups was done in a single oral dose once daily. The same veterinary technologist performed the dosing procedure every day for the duration of the trial.

Figure 3.3: Syringe used for oral dosing at 200µl.

3.4.3.2 Weighing

Weights were measured twice weekly, mainly as indicative factor for overall well-being. Each animal was removed from the cage in a flow cabinet and placed on a balance. The animals were handled with care and allowed to adapt to the different environment (Figure 3.4). As soon as the animal sat still on the middle of the balance, the weight value in grams was recorded. Statistical analyses were done on weights recorded on the following days of the 90 day trial: day 1, as baseline weight; day 52, after additional supplementation with Nestlé Cerelac baby cereal was started; day 59, when definite weight gain in all groups was documented by the veterinary technologist; days 66, 73 and 80, as the days on which tensile strength was measured; day 90 as the last day of the 90 day trial. Statistic results are presented in section 4.3.1.

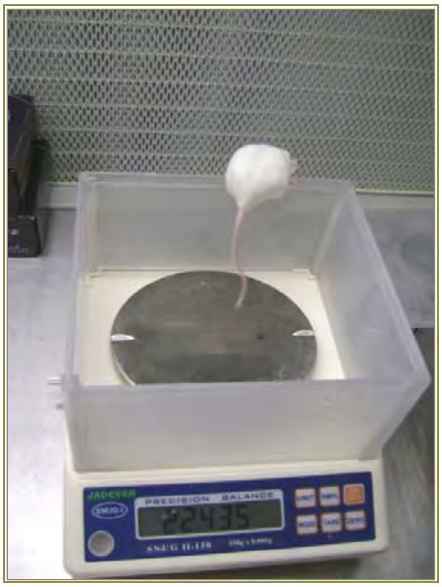

Figure 3.4: Weighing of an SJL/J mouse.

3.4.3.3 Tensile Strength Test

From week 7 to week 11, of the 90 day trail, the animals were assessed for total strength, by measuring the tensile strength on a custom built tensile strength meter (Figure 3.5). The tensile strength meter consisted of a load cell (from Emfuleni Scales, Vanderbijlpark, South Africa), allowing tensile force to be measured in grams. The system uses a smooth metal grid (custom made) (grid size 15 x 15 mm, wire diameter 2 mm) supported by a t-bar that is attached to the load cell at a 0° angle. The grid served as platform for the animal to grasp with the paws, while being pulled by the tail slowly backwards in the horizontal plane. The force applied to the bar the moment the grasp is released, represented the peak tension measured in grams. The load cell was connected to a

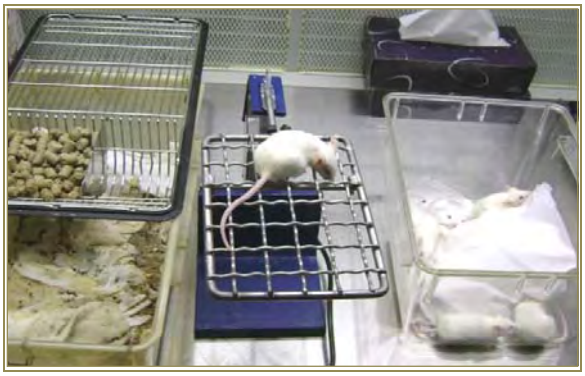

Figure 3.5: The tensile strength test meter.

computer with Digicator software which provided a peak hold function with an mv-RS 232 converter, that served as the sensor, recording the peak tensile strength afforded by each individual animal.

Maurissen and co-workers, 2003, recommended that grip performance data be collected using consistent techniques and with a thorough understanding of how the equipment of the test system functions. To ensure consistency in the present study, the procedure was done by the same veterinary technologist every time. The technologist was informed on the operational aspects and functions of system components upon installation of the tensile strength test meter. Calibration of the system was done upon installation, and every six months thereafter. For evaluation purposes every animal was taken from the cage, individually and put on the metal grid, then left to adapt (Figure 3.5).

As soon as the animal orientated itself in the correct position (tail orientated towards the direction in which the load cell affords a positive value), it was pulled slowly and steadily backwards by the tail, until the animal released the grasp (Figure 3.6).

Figure 3.6: Tensile strength test.

The value of strength in grams was recorded at the exact time point where the grasp broke. Animals were never forced to grasp the bars of the metal grid, nor were they forced to align in the position for strength measurement. For each animal the test procedure was repeated thrice, and values were recorded manually as displayed by the Digicator. The highest value of the three repetitions was recorded as the animal's grip strength for that session. And the final value was calculated as the mean strongest grip strength over the 5 week period for every group. Mice were not trained prior to testing and each mouse was tested once (3 consecutive times). If an animal showed no cooperation, by premature releasing of its grip or by walking backwards on the metal grid, as soon as force was exerted to the animal by pulling the tail, the animal was put back in the cage. No further assessments were attempted for that specific animal again on that specific day, in order to avoid any unnecessary exhaustion and stressing. Animals were allowed to grasp with all four paws simultaneously. The tensile strength meter was cleaned every week before and after every tensile strength test procedure, using 70% ethanol and

sterile tissue paper. The sensor was zeroed before and after every individual measurement taken. After each group was tested, the animals were assessed and scored for behaviour and activity.

3.4.3.4 Food Supplementation

As the animals served the imperative part of this study, and also in other research of this nature, apart from standard ethical consideration, all necessary measures were taken to ensure the comfort and maintenance of condition of all animals at all times. Therefore, when the veterinary technologist observed a decrease and slowing in the mobility of the animals (recorded on day 48), as a result of disease progression, it was expected that the animals might find it difficult to reach for their food, that was provided in the cage top (Figures 3.1 and 3.5). Condition assessment in the preceding two weeks revealed nothing other than progressive weakness, in addition to lethargy in some animals. Fighting between cage mates were often observed in this time and it appeared as if the animals were stressed. It was decided to supplement the animals' diet from day 50 of the 90 day trial by addition of Nestlé Cerelac, sterile baby cereal on the floor of each cage.

3.4.3.5 Observations

Routine observations were made every day at the same time, before and after oral dosing. Since the study did not include any invasive procedures, no pain or suffering was expected in the animals. However, due to the nature of the animal model itself, it was possible that episodes of discomfort could present. A pain score sheet was set up to evaluate the pain of the animals in order to ensure humane treatment at all times. If the pain score appeared to be altered above acceptable levels, euthanasia by cervical dislocation would have been performed, followed by an autopsy to determine the exact origin and cause of the detected condition. Scoring for diarrhoea was done on the following scale: 0 = normal; 1 = loose faeces on floor; 2 = pools of faeces on floor; 3 = running out on handling; +m = mucus; b = blood (in stools). The overall condition of animals were examined by assessing each individual daily for activity, scratching, anxiety, pinched face, ruffled coat, nose bleed, bite marks and diarrhoea. Overall condition were scored with limits being 1 = emaciated, and 4 = normal. A summary of key events during the course of the 90 day trial are provided in Table 3.2.

3.4.4 Findings, Difficulties and Limitations

All essential obligations for ensuring the well-being (freedom from discomfort, distress, and pain) were met at all times. With the exception of a few difficulties and the regretful, but unavoidable loss of four animals during the course of the animal study, all went according to plan, resulting in the

successful collection of the tissue of interest following termination. At termination all animals were still in a good condition.

One event that needed attention, was the resveratrol preparation used at the beginning of the study. The supplement was obtained in a commercially available vegetable capsules at 200mg *Polygonum cuspidatum* per unit, providing 50% (100mg) resveratrol (manufactured for Solgar Vitamin and Herb, UK, Herts). The product was a plant extraction preparation. After dissolving the capsules in milliQ water, the solution had a dark brown colour and a strong herbal smell. The animals treated with this preparation, showed resistance as aggression was observed in the concerned groups. On the 27th day nose bleeds were observed in these groups, mainly after dosing. On day 29 nose bleeds started as the veterinary technologist opened the container with the resveratrol before dosing, indicating a possible fear for the taste of the antioxidant. A new 98% pure formulation of resveratrol (a chemical preparation) was obtained and prepared in milliQ water. The colour of the preparation was milky-white, and it was tasteless and odourless. The behaviour of the animals changed to normal after administration of the new preparation, and no nose bleeds related to dosing were reported in these groups again.

The most common side-effects for CoQ10 has been reported to only involve the gastrointestinal system and included nausea, diarrhoea, appetite suppression, heartburn and epigastric discomfort (Rozen *et al*., 2002). In large studies the incidence of gastrointestinal side-effects is less than 1% (Rozen *et al*., 2002). No known side effects have been reported for resveratrol. To provide the animals with comfort at all times, it was decided to start the study with half the original doses, to prevent any gastrointestinal instability. Even at this concentration, diarrhoea was noticed in the groups treated with CoQ10. Time was allowed for the animals to adapt, and following toleration of the half concentrations, full doses were administered. No diarrhoea was reported after this change, and all the animals seemed to have tolerated the higher doses well. After day 9, no incidence of diarrhoea was reported for the CoQ10 group again.

Another common incident was fighting between cage mates. The fighting occurred in all antioxidant treated groups, and it became apparent that it was more frequent after the tensile strength test was performed. The strain of the procedure resulted in severe irritation and tension of the animals a short while after the procedure was performed. This resulted in cage mates biting each other. The reason why female animals were used in the present study is because they can be caged communally, while males are too aggressive. From the observations made in the present study, it

seems that although female SJL/J animals are more mildly tempered than what has been reported for males, they fight as a result of tension caused during a test procedure.

All four animals that died during the study were sent to the Golden Vetpath Laboratory (Pretoria, South Africa) for autopsy. Morphological diagnosis in animal 8 was found to be 'aspiration pneumonia'. The pathologist found the mouse to be in good body condition. The abdomen appeared distended and opening of the abdominal cavity, revealed severe gas accumulation within the intestine leading to the presence of dilated gas-filled intestinal loop. The finding was likely to be due to anorexia before death, since the stomach also did not contain notable amounts of food. The lungs appeared mildly congested with multifocal dark red areas that had a congested appearance with increased consistency. The areas were present all along the edges of the lobes and represented areas of suspected pneumonia. Mild sinusoidal congestion and leukostasis were found in liver histology. The most notable lesion was the multifocal necrogranulomatous bronchopneumonia.

In animal 33, moderate pulmonary congestion, with protein-rich lung edema was detected. Moderate congestion and blood pooling in hepatic sinusoids, with no presence of inflammation were found. Moderate autolysis in trachea and oesophagus were detected with thymic lymphoid tissue found to be well-populated with lymphocytic cells.

In animal 34, moderate congestion with blood pooling in the larger blood vessels as well as the capillary walls of the lungs were found. Mild extramedullary haemopoiesis in the spleen, but normal lymphoid tissue in the splenic white pulp was reported. Moderate congestion and blood pooling was observed in the liver, although no inflammation was detected.

In animal 42, histological evaluation was indicative of acute aspiration pneumonia with a purulent infiltrate affecting both lung lobes. No other specific lesions were observed. The carcass was found to be in good condition, the intestinal tract was gas-dilated and the stomach contained food. Moderate lymphoid hyperplasia was detected in histological assessment of the spleen. No findings in any of the autopsies could be related to any of the procedures or the antioxidant treatments used in the study.

Table 3.2 Important events and observations during the 90 day trail

Event	Day	Remark
Mice arrived from Jackson Laboratory, Bar Harbor, USA. Period of acclimatization started.	40 days before day 1	
Mice - earclipped and weighed.	*0*	
Termination of the age control group (at 14 weeks of age) First day of dosing. All doses are administered at half the concentration.	*1*	Half dose concentrations to allow adaptation.
The high CoQ10 and resveratrol/CoQ10 combination groups had diarrhoea; mucus present in faeces, faeces has an orange tint.	*3*	Faeces stick to bedding and to the side of the cage. No blood could be detected in the faeces.
Animals in all antioxidant supplemented groups drink more water than animals in the positive and negative control groups.	*4*	More water consumption (30–50 ml more) observed in antioxidant supplemented groups.
In the high CoQ10 and resveratrol/CoQ10 combination groups very soft faeces with a yellow-orange tint was observed.	*5*	Assessment for hydration, body weight, and body condition found animals to be in good condition.
In the high CoQ10 and resveratrol/CoQ10 combination groups – faeces were still soft, with yellow–orange tint	*6*	Animals maintain body condition. A slight decrease in activity was found in the concerned groups.
Faeces in both the high CoQ10 and resveratrol/CoQ10 combination groups were more formed, with the presence of a yellow-orange tint	*7*	Animals' bodies start to get use to the concentration of the antioxidants.
Faeces were more formed in the high CoQ10 and resveratrol/CoQ10 combination groups.	*8*	Overall condition of the concerned groups appeared improved. Animals' activity increased.
All groups had normal faeces.	*9*	
Animal 50 was not well; had an injury around anus; and seemed unsteady; weighed 19.97g	*12*	No weight loss in animal 50. No sign of dehydration detected.
Animal 42 died. Weight = 19.82g.	*14*	A 0.77g weight loss recorded for animal 42. Carcass sent for autopsy.
Full doses were administered in the resveratrol and low CoQ10 groups.	*15*	All animals displayed overall good condition.
Animal 30 had a swollen right eye. Resveratrol group presented with diarrhoea.	*16*	No dehydration or weight loss could be detected in any of the animals.
Animal 34 presented with a bitemark on abdomen; ±2mm upper right from vagina.	*17*	
Animal 30 still had a sore right eye. The eye was flushed with luke-warm water.	*19*	
Full doses were administered in the high CoQ10 and resveratrol/CoQ10 combination groups.	*22*	
Nose bleeds were observed in the resveratrol and resveratrol/CoQ10 combination groups. Animals 26, 27, 28, 30 & 52 presented with nose bleeds directly after dosing. Fighting was observed in the low CoQ10 group.	*27*	
Animals 33 & 34 were not well. They presented with pilo-erection and a hunched posture.	*28*	
Animals 33 & 34 were found dead in the cage. Resveratrol group-nose bleeds started directly before dosing. Resveratrol/CoQ10 combination group – only one nose bleed.	*29*	It is clear that the animals were being stressed by the dosing with resveratrol. The preparation smells and tastes bad. Carcasses sent for autopsy.
Started dosing a new preparation of resveratrol, prepared from a 98% pure form that was tasteless and odourless. Half doses of resveratrol were administered.	*30*	
New formulation of resveratrol was found to be handled well. No nose bleeds reported.	*31*	It is clear that the taste and smell of the previous resveratrol preparation caused severe stress in these groups.

Event	Day	Remark
Fighting occurred in the resveratrol and high CoQ10 groups.	32	
New resveratrol formulation administered at FULL doses.	36	Half doses of the new formulation of resveratrol seemed to be well-tolerated by all animals. Progress to full doses.
Fighting occurred in the resveratrol and resveratrol/CoQ10 combination groups.	38	
Animal 8 was not well. Presented with pilo-erection and a hunched posture. Erratic breathing was present.	39	
Animal 8 has recovered. Mice in the low CoQ10 group seemed to be fighting.	40	
Fighting amongst individuals in the low CoQ10 group continued.	41	
Animal 8 died. Animal 32 were badly bitten on hind-quarters.	42	Carcass of animal 8 sent for autopsy.
Animal 32 had a nose bleed.	43	
Animal 1 was slightly unstable after oral dosing.	44	
Progressive weakening over the past two weeks was noted in all SJL/J mice groups. Almost as if the animals drag their hind quarters. Animals appeared much more lethargic.	48	SJL/J mice were 21 weeks of age. Lethargy serves as an important clinical indicator of illness. In this case onset of muscular dystrophy. Food supplementation is considered.
Supplementation of all groups with Cerelac baby food on cage floors.	50	
First tensile strength test were performed in all groups. In all antioxidant supplemented groups, animals were fighting after tensile strength test procedures.	52	Aggression was noted amongst individuals of treated groups after tensile strength test was performed.
2nd Tensile strength test were performed. Less fighting in all the groups that were previously fighting. All groups showed weight gain.	59	
3rd Tensile strength test were performed. Fighting occurred in all antioxidant supplemented groups after testing.	66	Aggression was noted again after tensile strength test amongst individuals of treated groups.
4th Tensile strength test were performed. Fighting occurred in all antioxidant supplemented groups after testing.	73	
Final Tensile strength test were performed.	80	Final tensile strength test, in order to avoid possible influence with CK and LDH levels, as well as possible muscle injury.
Animals 32 & 38 were fighting. Bitemarks were present on their backs.	81	
Resveratrol group – mice seemed to look 'scruffy' (ruffled coat).	84	No sign of dehydration or body weight loss. Animals were closely monitored.
Resveratrol group – mice still looked unwell (ruffled coat). Animals 22 & 30 had heavy nose bleeds.	85	
Animal 30 had a nose bleed. Mice in the high CoQ10 group seemed to be fighting.	88	
Mice 43, 45 and 48 were fighting.	89	
Mice in the high CoQ10 group still seemed to be fighting. SWR/J mice were 28 weeks old. SJL/J mice were 27 weeks old.	90	
Termination	91	

3.4.5 HEALTH GUIDELINES

Health guidelines as described by Foltz and Ullman-Cullere, 1999 were followed and animals presenting with any of the obvious health problems were also assessed for the other. Subtle health problems (Foltz and Ullman-Cullere, 1999) that animals were examined for on a daily basis include:

i) *Activity/behaviour*: When opening a cage the behaviour of the mice was examined. Were the animals curious (demonstrating normal open-field activity), did any seem thin, runted, lethargic, or in pain (especially in comparison to cage mates)? Were any of the mice hunched up or having difficulty breathing? Were they grooming, over-grooming, scratching, licking or mutilating themselves? All these criteria were used as indications for closer examination and evaluation.

ii) *Dehydration*: Dehydrated mice will have eyes that appear recessed in their heads. Facial fur will appear fuzzier due to pilo-erection. Once one lifts the mouse's skin over the shoulder blades, it will not return quickly to its original shape, and will remain bunched. Euthanasia was indicated if any of the animals were positive for dehydration.

iii) *Diarrhoea*: mice with diarrhoea often don't have fluid faeces, but faeces might be moist and sticky. Bedding and sides of the cages were investigated daily. Faeces and the area around the anus were examined for the presence of blood in case of the presence of moist and sticky faeces. Diligent assessment of hydration, body weight and body condition was performed on all animals of a cage where diarrhoea was diagnosed.

Additional health observations (Foltz and Ullman-Cullere, 1999) were made under the following guidelines:

i) *Lethargy*: a lethargic mouse may exhibit sluggish behaviour, stupor, coma, hypoactivity, prostration, or a hunched posture. These were considered important clinical indicators of a serious illness. Supportive care or euthanasia was indicated.

ii) *Ruffled fur*: an unkempt and ungroomed appearance is indicative of a mouse that is not feeling well. If noticed along with other signs, such as dehydration or loss of body condition, this was considered an indication for euthanasia.

These guidelines were strictly adhered to during the course of the study and found to be very helpful in decision making in order to ensure that the well-being of all animals were maintained at all times. Fortunately, no incidence called for early intervention (euthanasia) in the present study and animals could be maintained optimally until termination.

3.5 TERMINATION PROCEDURES

The termination procedures (Figure 3.7) took place on day 91, the day after the 90 day trial ended. At this point animals from the SJL/J strain were 27 weeks old and animals from the SWR/J strain were 28 weeks old.

The animals were anaesthetized by isofluorane inhalation, and terminated by cardiac puncture (Figure 3.7 A). Blood was obtained from the cardiac puncture and blood smears were made, three microscopic slides for each individual animal. Blood was collected in 1ml Microtainer serum tubes (Figure 3.7 B), and transported within 2 hours after termination to the laboratory (Department of Companion Animal Clinical Studies, Section of Clinical Pathology, Faculty of Veterinary Science), for analysis of serum CK and LDH levels.

Quadriceps and gastrocnemius muscles (from the right limbs) were isolated by the laboratory veterinarian and washed once in phosphate buffered saline (PBS), and thereafter immediately snap frozen in liquid nitrogen (Figure 3.7 C), before the samples were stored in 2 ml cryotubes, in liquid nitrogen, until analysis.

Quadriceps and gastrocnemius muscles from the left limbs were isolated and samples (Figure 3.7 D) appropriately sized for chemical fixation (Figure 3.7 E) were dissected from the mid-belly region of the muscle. Three different samples from each muscle, approximately 2 x 3 mm in size, were isolated. From each animal, one sample was fixed in a 2.5% formaldehyde, 0.075 M phosphate buffered solution for light microscopy work, the other two samples for electron microscopy work were fixed in a 2.5% glutaraldehyde/2.5% formaldehyde, 0.075 M phosphate buffered solution. Chemical fixation was done overnight.

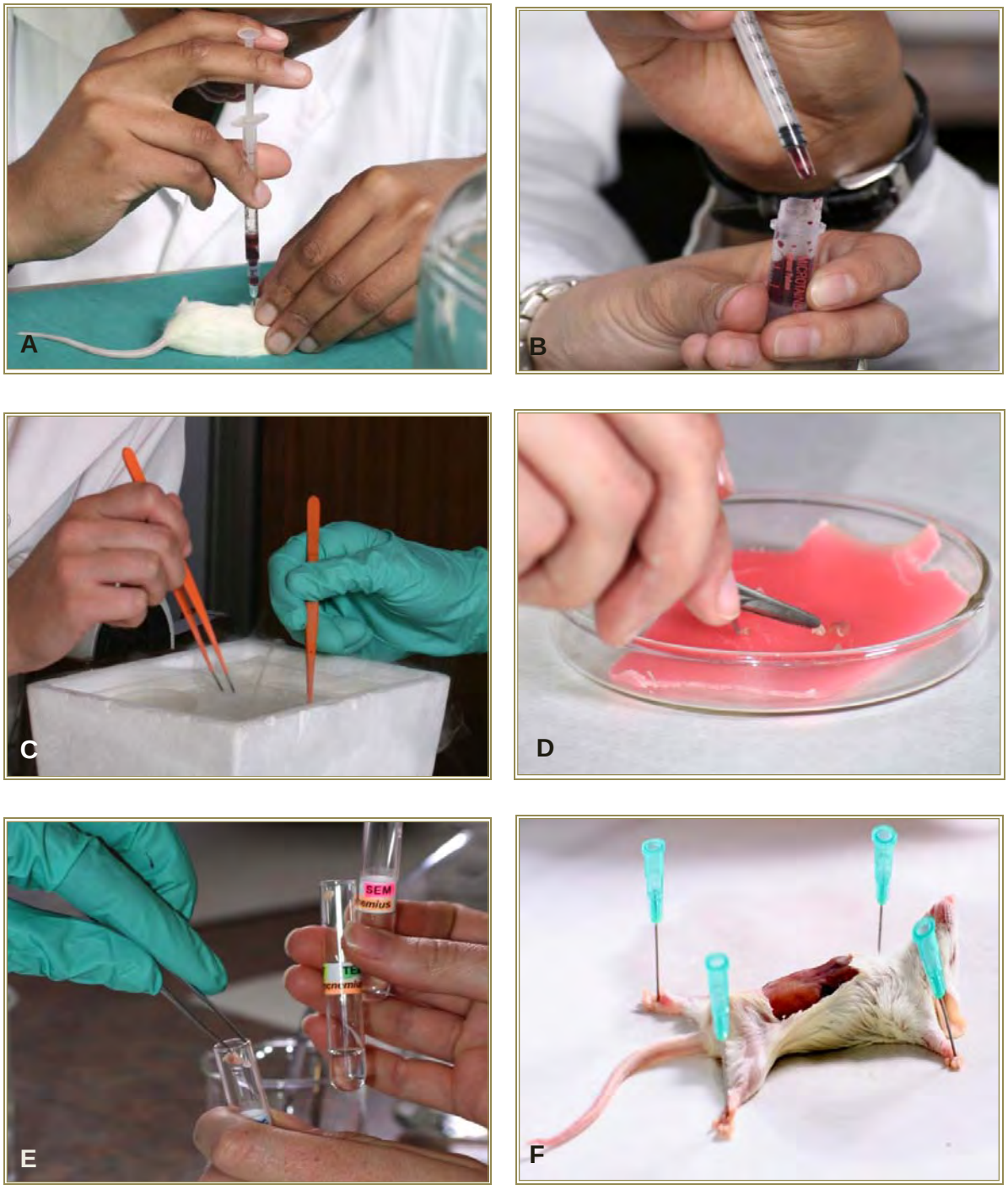

Figure 3.7: The termination procedure. A) Blood are collected from cardiac puncture; B) in a serum tube; C) Muscle tissue are snap-frozen in liquid nitrogen; D) Tissue sampling for microscopic analysis; E) Tissue collection in glass vials containing fixative; F) Mouse prior to dissection.

Chapter 4

Measuring non-specific parameters not directly related to muscle cell structure, and not directly affecting histopathology in dysferlin-deficient muscular dystrophy

4.1 INTRODUCTION

Weights and physical strength

The body weight of the mouse is a measure of muscle mass as well as of overall well-being (Li *et al*., 2005).It is usually monitored weekly or monthly throughout chronic experiments as an index of general health (Grounds *et al*., 2008). A weight loss of 10 to 15% within a few days or an overall weight loss of 20% is a decisive factor for euthanasia (Foltz and Ullman-Cullere, 1999).

Strength-assessing methods such as the length of time an animal can hang from a cage top or swim in a tank, are not very quantitative and can be very hard on the animal (Weller *et al*., 1997). Force transduction strength testing is a non-invasive procedure that can be used to test an animal frequently without great distress (Weller *et al*., 1997). It is a behavioural test that was eventually introduced into regulatory test batteries to screen for neurobehavioral toxicity (Maurissen *et al*., 2003). This extremely quantitative method allows for accurate assessment of treatment (Weller *et al*., 1997). Typically, a grip strength apparatus consists of a grasping device or platform that is connected to a strain gauge or load cell. In general, the test measurement is conducted by allowing the animal to grasp the device and then pulling it away until its grip is broken (Maurissen *et al*., 2003). Maurissen and coworkers, 2003, identified factors that can affect grip strength testing. These factors include parametric factors, peripheral sensory nervous system damage and diet restriction-induced changes in body weight and muscle mass. Changes in grip performance due to loss of body weight has been found to be reversible and positively correlate with changes in hind limb muscle mass (Maurissen *et al*., 2003).

Blood enzymes

The amount of ATP within the muscle fiber at any one time is sufficient for only about eight twitches (Silverthorn, 2004). As a backup energy source, muscles contain phosphocreatine. The high-energy phosphate bonds in this molecule are created from creatine and ATP when muscles are at rest (Silverthorn, 2004). When muscles become active, the high-energy phosphate group of

phosphocreatine is transferred to ADP, creating more ATP to power the muscles (Silverthorn, 2004). The enzyme responsible for transferring the phosphate group is creatine kinase (CK), also known as creatine phosphokinase (CPK) (Silverthorn, 2004). Muscle cells contain large amounts of this enzyme. Consequently, elevated blood levels of CK usually indicate damage to skeletal or cardiac muscle (Silverthorn, 2004).

Miyoshi, 1967, reported four patients from two consanguineous families that presented with recessively inherited late-onset distal myopathy associated with clear-cut muscular dystrophy and significantly elevated CK levels. Elevated CK levels are not specific in themselves (Urtizberea *et al*., 2008). In early stages of dysferlinopathy, they are usually markedly elevated, up to 50 to 100 times over normal values (Urtizberea *et al*., 2008). In the context of a patient presenting with distal motor symptoms, this massive increase is quite suggestive of Miyoshi myopathy (MM) and therefore of dysferlinopathy. Over time, CK levels tend to decline and lose their informative value (Urtizberea *et al*., 2008).

In a study by Nemoto and co-workers, 2007, serum CK levels of SJL/J mice were found to increase along with exacerbation of the inflammatory changes, when compared to B10 mice. In younger SJL/J mice (animals were approximately 14 weeks old) CK values were found to be already elevated (mean CK was 522.0 ± 219.1 IU), though there were a few inflammatory changes. As early as 1960, activities of the enzymes CK and lactic dehydrogenase (LDH) were found to be elevated in the blood of patients with Duchenne's muscular dystrophy (DMD) (Thomson *et al*., 1960; Cohen and Morgan, 1976). Reductions in increased levels of these enzymes had been used in earlier studies as an indicator of the efficacy of experimental drug treatments in DMD (Cohen *et al*., 1976; Chazot *et al*., 1972). Massively elevated serum levels of muscle enzymes, including CK, LDH, and aldolase, have also been reported in early stage dysferlinopathy (reviewed by Urtizberea *et al*., 2008).

Haematology

One of the most important functions of blood is transport of humoral agents and cells of the immune system that protect the body from pathogenic agents, foreign proteins, and transformed cells (Ross *et al*., 2003). Blood cells and their derivatives include: red blood cells (erythrocytes), white blood cells (leukocytes), and platelets (Ross *et al*., 2003). Leukocytes are subclassified into two general groups: granulocytes, including neutrophils, eosinophils, and basophils, and agranulocytes, including, lymphocytes and monocytes (Leeson *et al*., 1988; Ross *et al*., 2003). De Gruchy expressed a conviction of most haematologists when he stated that the examination of the blood smear is 'the most important single investigation in the anaemic patient' (De Gruchy, 1965). Hattersley and

Ragusa, 1965, added that the skilful examination of a well-prepared blood smear is one of the most important examinations in non-anaemic patients.

Cells of the innate immune system play a crucial role in the initiation and direction of adaptive immune responses, as well as subsequent removal of pathogens that have been targeted by an adaptive immune response (Janeway *et al., 2005*). Leukocytes are functional only to a small extent in the bloodstream, their greatest activity being exhibited in the tissues (Leeson *et al.,* 1988). These cells are capable of amyloid movement, enabling them to travel out of the circulatory system in order to elicit an immune response in the tissues where such response is needed. Increased demand for particular leukocytes in various sites is reflected by increased numbers in the circulation. The absolute and differential white cell count is therefore a useful pointer to diagnosis (Young *et al*., 2006).

The antioxidant properties of CoQ10 and resveratrol are of interest to the present study as this chapter aim to determine whether or not its administration will have any effect on non-specific parameters in SJL/J mice. Non-specific parameters are regarded as factors not directly related to muscle cell structure, and not directly affecting histopathology in dysferlin-deficient muscular dystrophy. These parameters include body weight, physical strength, the levels of inflammatory leukocytes at the haematopoietic level, and CK and LDH levels in blood. A quantitative analysis was performed on white blood cell counts, blood CK and LDH levels, as well as the weight change and tensile strength of animals.

4.2 Materials and Methods

4.2.1 Weights and Tensile Strength

The weight of each individual animal was recorded twice weekly, as described in section 3.4.3.2 throughout the course of the study. The average weights of the assessed mice, for each experimental group, are presented in Figure 4.1. The repeated weight measurements of each SJL/J mouse were compared between the six experimental groups via repeated measures ANOVA. A level of significance ($P \leq 0.05$) was utilized during the statistical analysis conducted. For physical strength analysis, the tensile strength of each individual animal was measured, as described in section 3.4.3.3, once per week for weeks 7 to 11 of the 90 day trial. For each mouse, the five tensile strength measurements acquired were utilized to determine the change in physical strength over time relative to the animals' starting physical strength, measured on day 52. The relative physical strengths, for each of the four occasions, were then compared separately between the six groups, (positive control, negative control, resveratrol, low CoQ10, high CoQ10 and resveratrol/CoQ10

combination groups) with the utilization of one-way ANOVA. A level of significance ($P \leq 0.05$) was utilized during the statistical analysis conducted. The recorded weights and tensile strengths of each SJL/J mouse measured during the course of the trial were assessed together, to determine if a relationship existed between the two factors. The assessment was conducted, for each group of mice over a 5 week period, via the calculation of the coefficient of determination.

4.2.2 Haematological Analysis

Three blood smears were prepared for each of the animals and allowed to air-dry. All slides were later stained with Wright's stain. A single blood smear was evaluated with a Nikon Optiphot transmitted light microscope equipped with a Nikon digital camera DXM 1200F, for each of five animals within all the groups under study (positive control, negative control, age control, resveratrol, low CoQ10, high CoQ10 and resveratrol/CoQ10 combination groups). The purpose of the evaluation was to manually quantify each cell of the leukocyte species (Figure 4.8); namely lymphocytes, monocytes, neutrophils, basophils and eosinophils; counting up to 100 leukocytes per slide in a total of three zones. Each slide was analyzed until 100 white blood cells were observed. Each white blood cell species was considered separately between the experimental groups via a one-way ANOVA or Kruskal-Wallis one-way ANOVA, depending upon whether the necessary assumptions for the parametric test were met or not.

4.2.3 Laboratory Tests

Blood samples, drawn at termination from each mouse, were evaluated for their serum CK and LDH levels. Analysis of serum CK and LDH levels were performed by Department of Companion Animal Clinical Studies, Section of Clinical Pathology, Faculty of Veterinary Science, University of Pretoria. Blood was collected in 1ml Microtainer serum tubes at termination and transported within 2 hours after termination to the laboratory. For determination of CK levels, the laboratory used a modification of the optimised standard method according to the recommendations of the IFCC. The Alfa Wassermann Creatine Kinase Reagent is intended for the quantitative determination of the Creatine Kinase activity in serum and plasma using the Alfa Wassermann Clinical Chemistry systems (ACE® and the NExCT™).

Principle of the Procedure:

$$\text{Creatine phosphate} + \text{ADP} \xrightarrow{CK} \text{Creatine} + \text{ATP}$$

$$\text{Glucose} + \text{ATP} \xrightarrow{HK} \text{Glucose-6-P} + \text{ADP}$$

$$\text{Glucose-6-P} + \text{NADP}^{+} \xrightarrow{\text{G-6-PDH}} \text{Gluconate-6-P} + \text{NADPH} + \text{H}^{+}$$

The reaction rate is measured at 340 nm.

For determinations of LDH levels the laboratory used a modification of the optimised standard method according to the recommendations of the Deutsche Gesellschaft Fur Klinische Chemie. The Alfa Wassermann Lactate Dehydrogenase Reagent is intended for the quantitative determination of Lactate Dehydrogenase (LDH) activity in serum and plasma using the Alfa Wassermann Clinical Chemistry systems (ACE® & NExCT™).

Principle of the Procedure: Pyruvate + NADH + H^+ ^{LDH} L-Lactate + NAD^+

The rate of the reaction is measured at 340 nm.

The levels of CK and LDH were expressed as units per liter (U/l). The quantified serum CK and LDH levels were compared between the six experimental groups via a one-way ANOVA and a non-parametric Kruskal-Wallis one-way ANOVA, respectively. A level of significance ($P \leq 0.05$) was utilized during the statistical analysis. The statistical program, NCSS, was utilized in order to perform statistical analysis.

4.3 Results and Discussion

Information regarding animal age at termination, and dosages of antioxidants supplemented in the respective groups, were summarized in Table 3.1.

4.3.1 Body Weight

Table 4.1 expresses the days chosen for weight assessment as well as the reason for its utilization. Through the use of the Anderson-Darling test for normality the data within each group was found to assume a normal distribution, allowing for the utilization of the parametric repeated measures ANOVA test. The repeated measures ANOVA test revealed that there was no statically significant difference between weights of the assessed groups over the entire study ($P = 0.74$) (Figure 4.1), although, there was a significant difference found to exist between the recorded weights on each of the assessed days (Table 4.1) within all the groups ($P < 0.00001$) (Figure 4.2). The subsequent use of the Tukey-Kramer Multiple-Comparison Test revealed that general weight alteration patterns existed within each of the groups. Weights increased significantly from day 1 to day 90 (Figure 4.2), although the weights recorded on days 66, 73 and 80 were all smaller than that of day 90 and larger than that of day 1. They were not significantly different from each other.

Table 4.1 Days chosen for weight assessment and the reason for its utilization

Day	Reason
1	Baseline weight; beginning of 90 day trial.
52	Food supplementation with Cerelac baby cereal. 1st tensile strength test.
59	Definite weight gain recorded for all the groups. 2nd tensile strength test.
66	3rd tensile strength test.
73	4th tensile strength test.
80	5th tensile strength test.
90	End-point weight. Last day of the study.

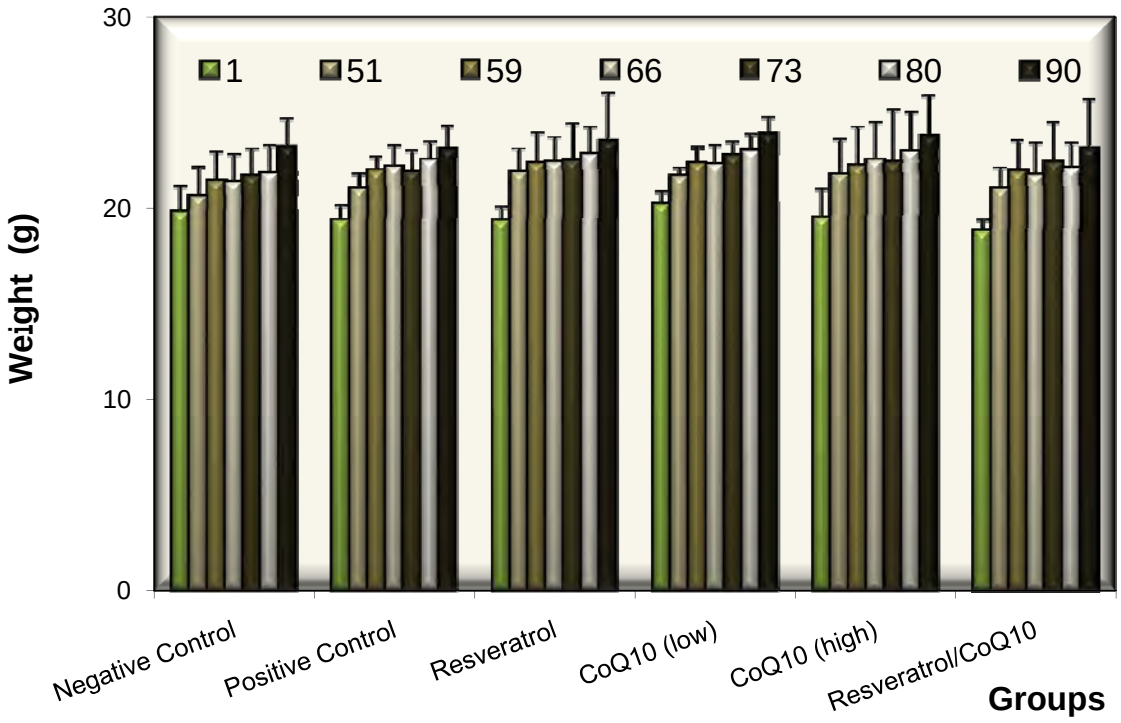

Figure 4.1: Average weights of experimental groups on specific dates as stipulated in Table 4.1 with error bars representing the standard deviation (SD).

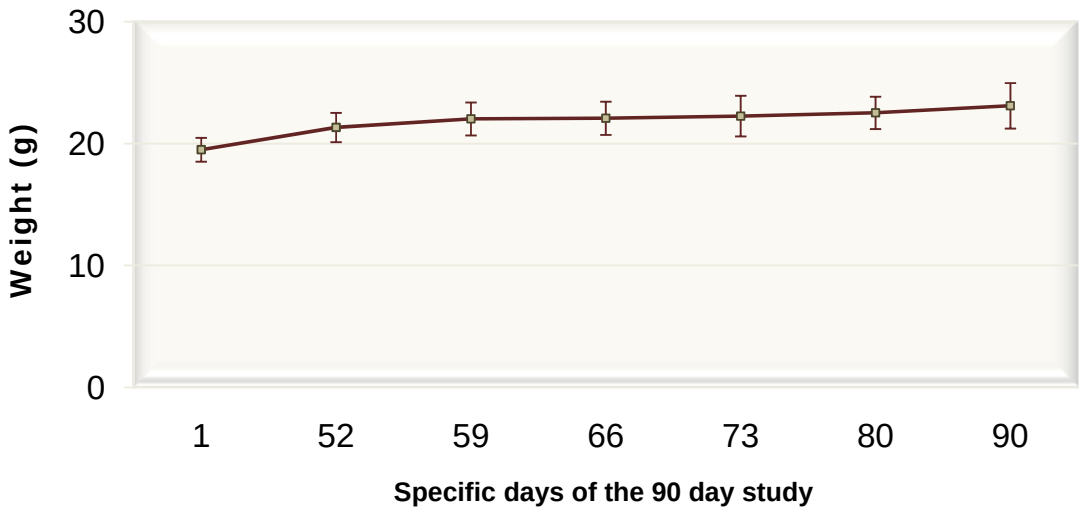

Figure 4.2: Animal weights increased significantly (P < 0.00001) in all groups from day 1 to day 90 with error bars representing the standard deviation (SD).

In establishing criteria for assessing health and endpoint determinations, a common descriptive ground for monitoring criteria were met in collaboration with the veterinary staff of the UPBRC. When an animal has lost 20% or more of its body weight, an experimental endpoint would be reached, allowing for early intervention, in this case euthanasia by cervical dislocation. The weight loss can be sudden or over a few days, while closely monitoring the condition of the concerned animal. If an animal presented with deteriorating condition in the form of ruffled coat, dehydration, excessive diarrhoea, decreased food or water consumption, and decreased activity, the weight of such an animal was closely monitored every day before dosing.

Weight change was used as the main indicative factor of the overall condition and well-being of the SJL/J and SWR/J mice in the present study. Food was initially provided in a container on the cage top (Figure 4.5, B) where mice had to reach on their hind limbs to feed. As weakness set in, nutritional health of the animals became a matter for concern. Supplementary food was provided from day 50 of the 90 day trial, until termination, on cage floors to ensure that the animals were well-fed. It was therefore expected that the added nutrition would result in a weight gain, as was recorded in all groups (Figure 4.2), 9 days after supplementation started.

Weights differ significantly between day 1 and day 90 in all assessed groups (P < 0.00001) (Figure 4.1), but no significant differences were found between groups (P = 0.74) (Figure 4.2). The significant increase in weights between day 1 and day 90 could be attributed to the supplementary food provided.

4.3.2 Physical Strength

The muscle tensile strength of each of the groups was measured on 5 separate occasions during week 7 to 11 of the 90-day trial. Up to three measurements were performed, if possible, on each occasion, with the largest of these utilized in subsequent statistical analysis as it was considered to be the maximum muscle tensile strength for that individual mouse at that particular point in time. Through the use of Shapiro-Wilk W test for normality the data within each group was found to assume a normal distribution, thus allowing for the utilization of the parametric repeated measures ANOVA test. The repeated measures ANOVA test revealed that there was no statically significant difference between the assessed days for the various groups (P = 0.89) (Figure 4.3) although over the entire 5 week period there was a statically significant difference between certain groups (Figure 4.4) in terms of their tensile strengths (P = 0.0036).

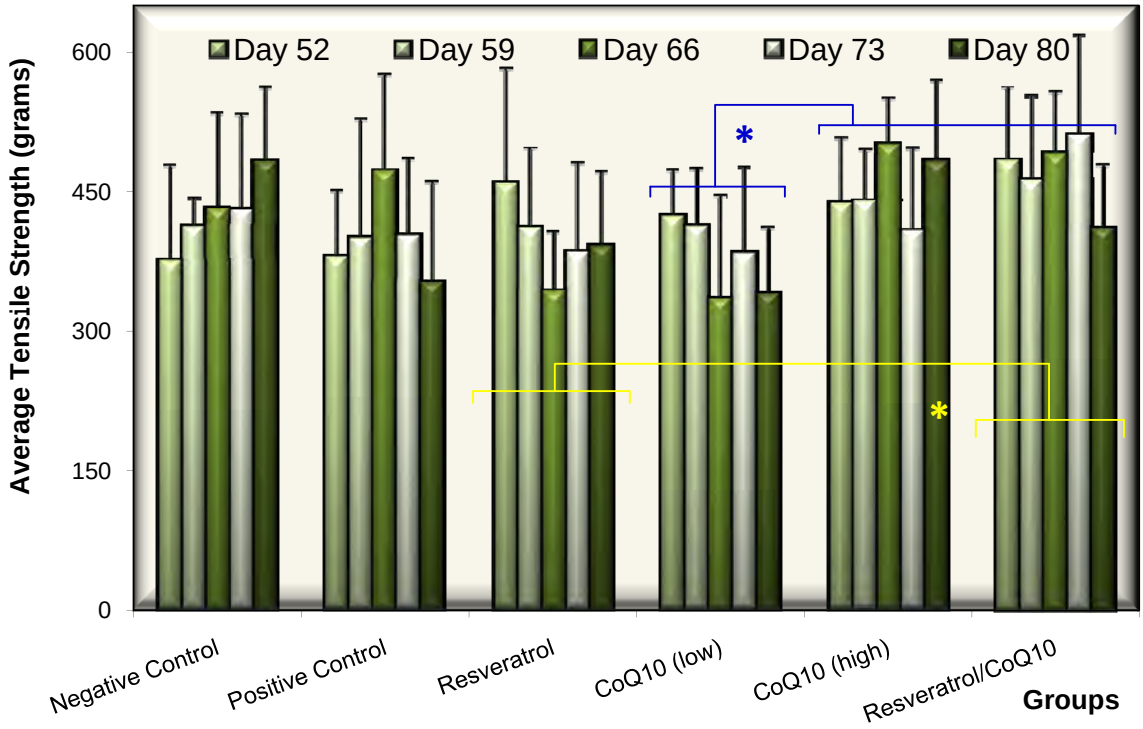

Figure 4.3: Average tensile strength of mice for five weeks in the 90-day trial. There was no statically significant difference between the assessed days for the various groups (P = 0.89). Standard deviation (SD) is represented by the error bars.

The use of the Tukey-Kramer Multiple-Comparison Test revealed that the low CoQ10 group (379.3 ± 40.6g) was physically significantly weaker than both the high CoQ10 (454.1 ± 37.1g) and resveratrol/CoQ10 combination (472.1 ± 38.3g) groups. The resveratrol group (398.8 ± 42g) was

significantly weaker than the resveratrol/CoQ10 combination group. The positive control group (402.13 ± 44.4g) displayed slightly higher values than both the low CoQ10 and the resveratrol groups, although not significant. The negative control group (427.47 ± 38.8g) displayed greater physical strength than what was observed in the positive control, low CoQ10 and resveratrol groups, although lower than that of the high CoQ10 and resveratrol/CoQ10 combination groups. Weller and co-workers, 1997, found that young SJL/J mice are also stronger than young Balb/c mice.

Within each experimental group no relationship could be determined between the assessed factors of weight and tensile strength when assessment was conducted for each group via the calculation of the coefficient of determination (r^2). It can therefore be concluded that these two factors appear to have no association, at least statistically, with each other. (Negative control r^2 = 0.0403; Positive control r^2 = 0.0304; Reveratrol r^2 = 0.0710; Low CoQ10 r^2 = 0.0356; High CoQ10 r^2 = $2x10^{-7}$; CoQ10 + Resveratrol r^2 = 0.0705).

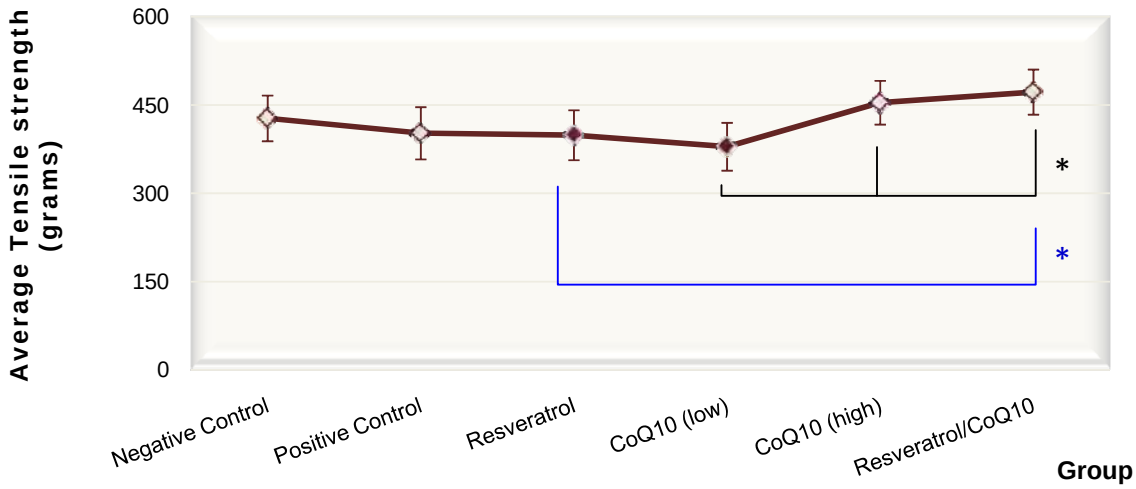

Figure 4.4: The trend in average tensile strength of experimental groups over the 5 week period, following supplementation with antioxidants. Statically significant differences (*) between certain groups in terms of their tensile strengths (P = 0.0036) occurred. The average strength of the low CoQ10 group was found to be significantly smaller than the high CoQ10 and resveratrol/CoQ10 combination groups. The resveratrol group was only found to be significantly smaller than the resveratrol/CoQ10 combination group. Error bars represent standard deviation (SD).

Strength loss can be due to multiple factors. Weller and co-workers, 1997 reported that the loss of strength can be attributed to the normal aging process. Weller's team found that this loss of strength appeared to be accounted for by loss of muscle mass relative to body weight, indicating a correlation between body weight and strength. Interpretation of grip performance data must critically consider

the fact that factors such as loss of body weight, changes in sensory function, and other non-motor (operational, systemic and behavioural) changes contribute to the overall grip performance measurement (Maurissen *et al*., 2003). It was expected that the supplementation of the animals' diet in the present study with Nestlé Cerelac sterile baby cereal, and the weight gain recorded as a result thereof, could have an effect on the strength measured. Calculation of the coefficient of determination showed that no association between these two parameters could be detected in the present study.

In SJL/J mice, Weller and co-workers found that strength in SJL/J mice does not decline steadily but in distinct drops which are correlated in time to specific pathological events. An early strength drop (at 6 and 8 months) was suggested to be attributed to the active process of early muscle disease, and is the only strength loss that could not be accounted for by loss of muscle tissue (Weller *et al*., 1997). One factor that could have contributed to the results obtained was the fact that animals from all groups in the present study showed adaptive behaviour (Figure 4.5), a non-motor change that may influence the grip performance test (Maurissen *et al*., 2003). Instead of pulling the grid bars with their paws, when force was exerted at the tail end, in the horizontal plane away from the grid, these animals started walking backwards. Sometimes they even turned around, to avoid the demanding task. Although this behaviour was observed in all groups in the present study, it is likely that some animals who showed adaptive behaviour found the task to hold on to the bar, until their grip was broken, too strenuous. Therefore an animal could release the grip prematurely and turned around. There was no way an animal would be forced to grip the grid bars, and usually if this behaviour occurred with the first pull, it continued, and for that specific day, that animal did not provide any data.

After the tensile strength test was performed, aggression and fighting occurred amongst individuals in most of the groups (chapter 3, table 3.1). Therefore, it was of the essence to cause the least amount of strain and distress on the animals during the procedure. Animals were not subjected to gripping more than three times on a given day, as this presumably might have been harmful to their stress levels. No strength testing was done in the last week before termination in order to rule out any possible muscle injury or trauma.

The results from the tensile strength test suggest that high dose antioxidant supplementation offered preservation of physical strength in 6 month-old SJL/J mice, to levels slightly higher than that measured in healthy SWR/J mice of the same age. These strengths were not dependent on the weight gain recorded in these groups.

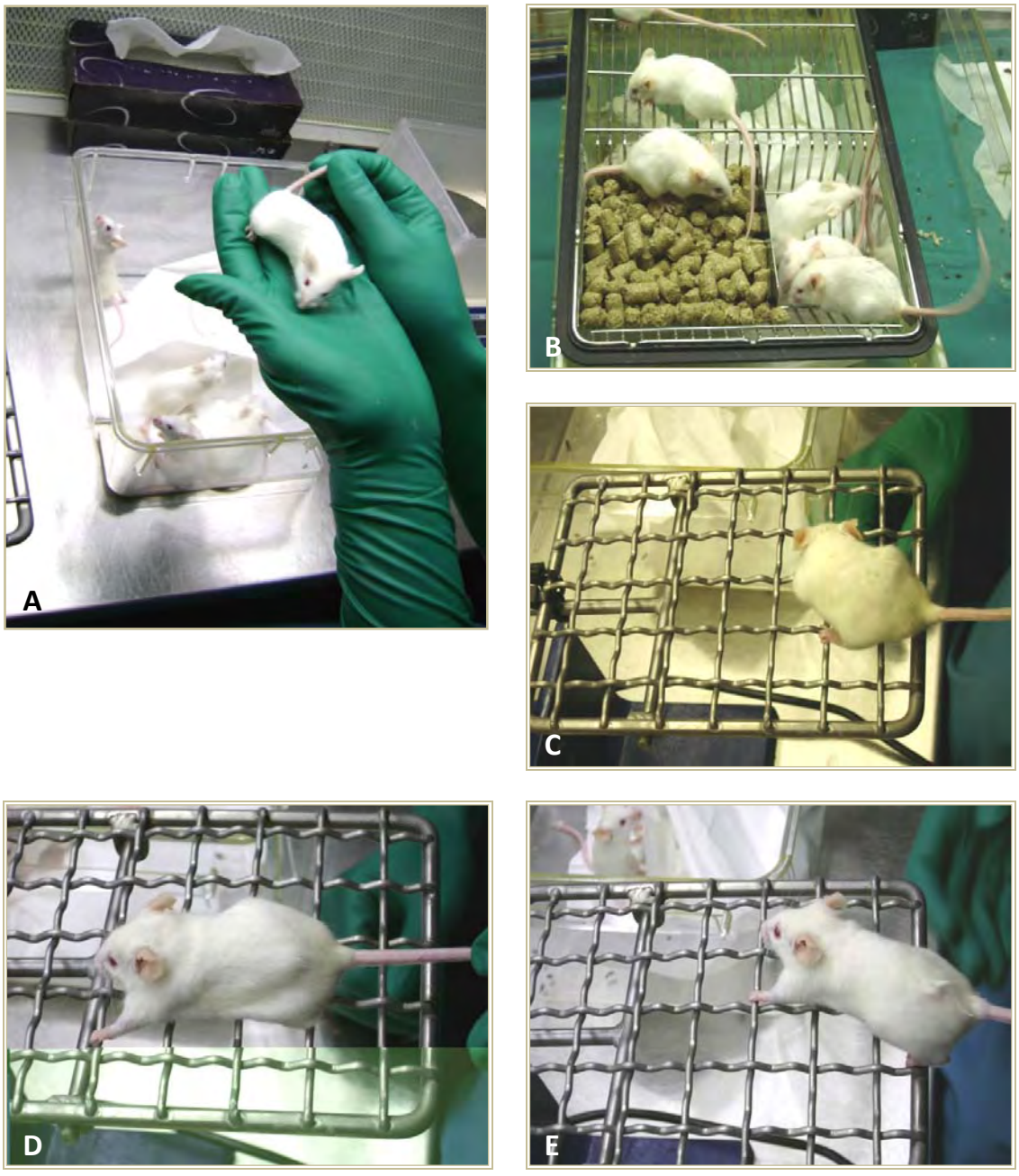

Figure 4.5: The condition of every animal was monitored before (A) and after (B) every tensile strength test. C) An animal whose grip broke, just after performing the tensile strength test. D) An animal with a firm grip during tensile strength testing. E) An animal showing adaptive behaviour. The animal prematurely released its grip every time force was exerted to the tail, and orientates its body in a side-ways direction on the grid.

4.3.3 Blood Enzyme Levels (CK & LDH)

As equal sample size existed in each of the experimental groups considered, as seen from the variance of the groups, it was considered to be equal for both enzymes. For the analysis of derived CK values a parametric one-way ANOVA could be utilized, as the random and independent data possessed a normal distribution. The results of this parametric test are presented in Table 4.2. The parametric one-way ANOVA test could only be utilized for the CK results, as the random and independent LDH observations did not meet a normal distribution pattern. In the case of the LDH analysis a non-parametric equivalent, the Kruskal-Wallis one-way ANOVA was run instead and the result is presented in Table 4.2. Both the CK and LDH levels were not significantly different between the six different groups, where significance was set at $P \leq 0.05$. The CK and LDH values of SJL/J mice at the age of 27 weeks (≈190 days) in the present study are given in table 4.3, as represented in Figure 4.6.

Table 4.2 Statistical comparison serum CK and LDH levels of the six experimental groups

Statistical Test	Enzyme	P value
One-Way ANOVA	**CK**	0.41
Kruskal-Wallis One-Way ANOVA	**LDH**	0.27

P-value = level of significance

Table 4.3 Mean CK and LDH levels ± standard deviation (SD), and standard error (SE) for CK and LDH data

Group	CK (U/l 37°C) ± SD	SE (CK)	LDH (U/l 37°C) ± SD	SE (LDH)
Negative control (n = 6)	5228.83 ± 4434.88	***2134.66***	2425.00 ± 1017.16	***990.00***
Positive control (n = 6)	1700.67 ± 1382.78	***694.30***	2000.83 ± 533.82	***816.84***
Resveratrol (n = 6)	2346.00 ± 2053.55	***957.75***	2220.17 ± 787.86	***906.38***
Low CoQ10 (n = 6)	2171.50 ± 2433.60	***886.51***	1972.00 ± 661.51	***805.07***
High CoQ10 (n = 6)	2308.67 ± 2467.74	***942.51***	2343.33 ± 682.76	***956.66***
Resveratrol/CoQ10 combination (n = 6)	3208.83 ± 2421.47	***1310.00***	3957.17 ± 2430.73	***1615.51***

SE = SD/√*n*, and *n* represent the sample size within the group

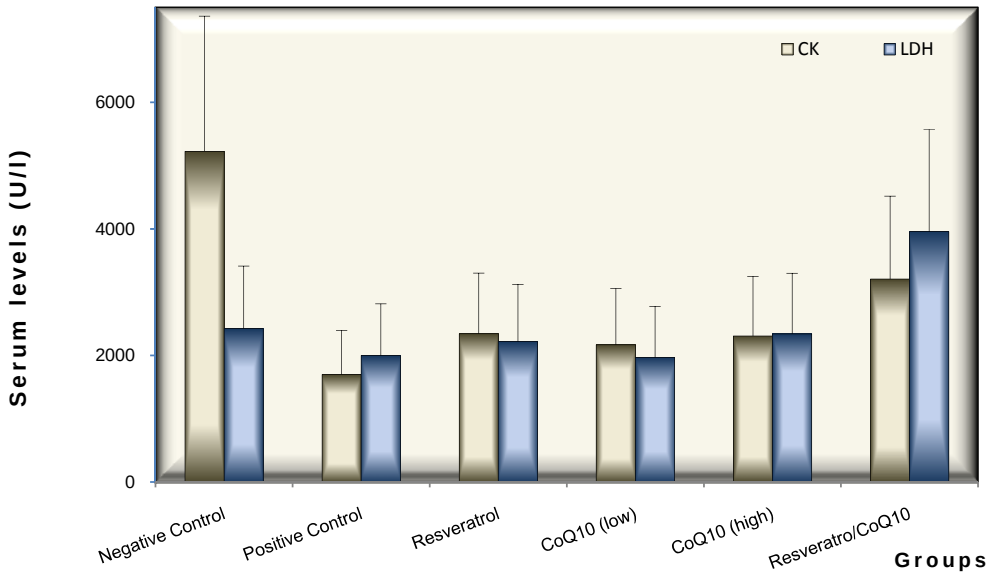

Figure 4.6: Mean serum CK and LDH levels (U/l 37°C) with error bars representing standard error (SE).

Nemoto and coworkers found an age related increase in CK levels of SJL/J mice. The current study revealed an increase in CK levels in all the groups treated with antioxidant therapy, when compared to the untreated positive control group. Also, all the CK values of the present study in SJL/J mice, treated and untreated, were found to be lower than that of the negative control SWR/J mice, in which values were not expected to be elevated. None of the differences between the groups, revealed any statistical significance for either CK or LDH level analysis. The LDH assay has previously been reported to be less satisfactory as a measure of blood muscle enzyme levels than CK. The reason being, any haemolysis that occurred during the preparation of the samples can cause elevated LDH (Morgan *et al*., 1981).

The results of laboratory CK and LDH levels from the present study displayed abnormally high values obtained in the negative control groups for both CK and LDH assays. The very large difference between the data points and their means are emphasized by the abnormally high SD's. To formulate an inference from the CK and LDH data, SE bars were utilized, to get an indication of the region where the mean of the whole possible set of results or the whole population can be expected to lie (Figure 4.6; Table 4.2). Standard error provides a measure of how variable the mean will be, if the study is repeated many times (Cumming *et al*., 2007). Even subsequent to calculation of the SE, the data points were found to be not constant enough to provide a reliable representation of the region where the mean could be expected for the whole possible set of results. Because of the very high serum CK value displayed by the negative control, no pattern of the elevation trend could be related

to the disease condition, or the antioxidant supplementation. Similar to the CK values, the serum LDH data was considered rather contentious and not reliably indicative of a significant tendency. The sample size and single assay procedures in the present study can be reasoned as cause for the inconclusive results. With a small sample size, any outliers in such a population will influence a mean to an extent where the results can be found inconclusive.

4.3.4 Differential White Blood Cell Count

Between each of the seven groups the comparison of monocyte-, lymphocyte- and neutrophil-counts were facilitated via one-way ANOVA, as all the necessary assumptions for these parametric tests were met. The comparisons of eosinophil and basophil counts from the seven groups were conducted with the aid of the non-parametric Kruskal-Wallis one-way ANOVA, as the data considered, did not assume a normal distribution. Table 4.4 expresses the statistical tests run for each white blood cell species and the outcomes thereof where significance was set at $p \leq 0.05$.

Table 4.4 Statistical comparison performed upon the various leukocyte cell species derived from the blood of the assessed groups

Leukocyte species	Test utilized	P value	Difference between compared groups determined, if applicable, with the aid of Tukey-Kramer Multiple-Comparison Test's
Monocytes	One-way ANOVA	0.961	No significant difference existed between any group's monocyte counts.
Lymphocyte	One-way ANOVA	0.857	No significant difference existed between any group's lymphocyte counts.
Eosinophil	Kruskal-Wallis one-way ANOVA	0.0104	The eosinophil count for the age control group was significantly higher than that of all the other groups assessed except for the negative control group.
Neutrophil	One-way ANOVA	0.0454	The neutrophil count for the age control group was significantly higher than that of the resveratrol/CoQ10 combination group.
Basophil	Kruskal-Wallis one-way ANOVA	0.0654	No significant difference existed between any group's basophil counts.

Table 4.5 Percentage leukocyte species per group

Group	*Lymphocytes*	*Monocytes*	*Neutrophils*	*Basophils*	*Eosinophils*
Negative control	47.8	44.6	2.6	0.8	4.2
Positive control	52	45.2	1.6	0	1.2
Resveratrol	57.4	40.6	0.8	0.4	0.8
CoQ10 (low)	54.6	43	1.2	0.4	0.8
CoQ10 (high)	49.4	46	2.8	0	1.8
Resveratrol/CoQ10 combination	63.6	34.8	0.6	0.2	0.8
Age control (14 weeks)	48.4	38.8	5.2	1	6.6

Table 4.5 gives the percentage of leukocyte species counted for each group. Eosinophil counts were significantly higher in the age control group than all other groups assessed except for the negative control group (P = 0.0104). Neutrophil counts of the age control group were significantly higher only when compared to the resveratrol/CoQ10 combination group (P = 0.0454). Both monocytes and macrophages circulating in the bloodstream were counted as monocytes.

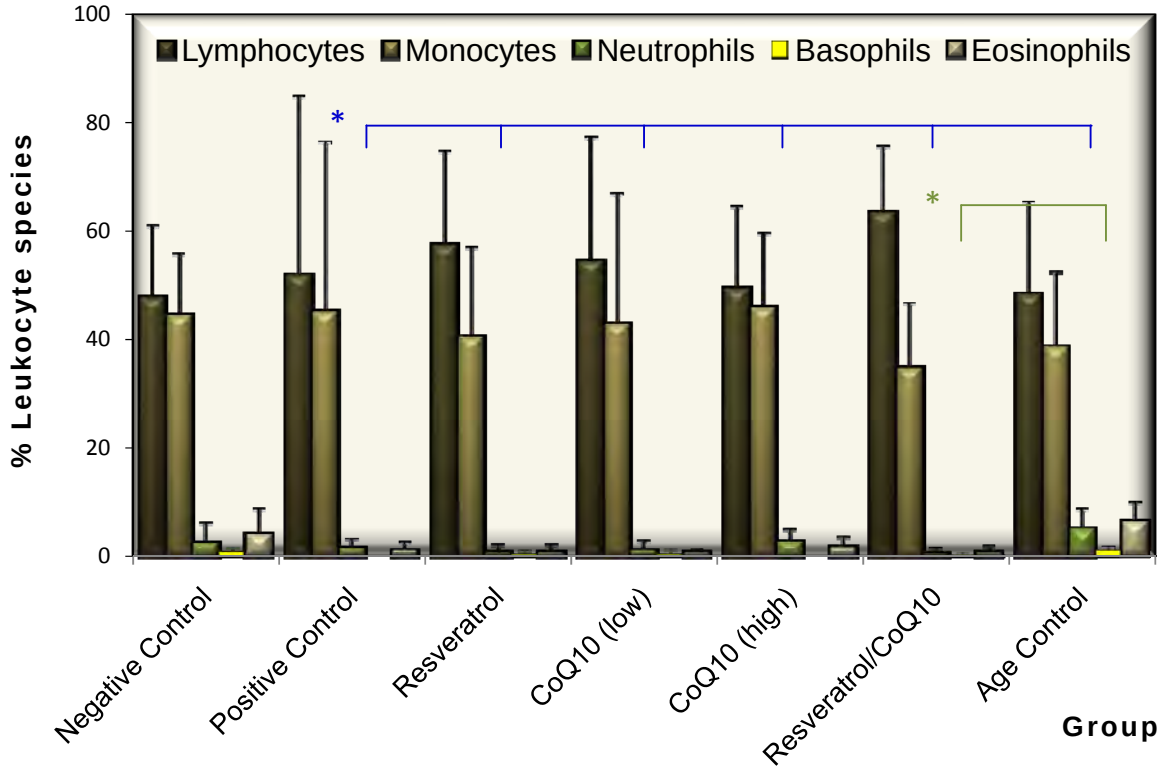

Figure 4.7: Average percentage of leukocyte species assessed per group. Statically significant differences (*) between certain groups in terms of their eosinophil counts (blue line) (P = 0.0104) and neutrophil counts (yellow line) (P = 0.0454) occurred. Standard deviation (SD) is given by the error bars.

From Figure 4.7, it can be seen that the resveratrol/CoQ10 combination group displayed the highest lymphocyte count. The lowest monocyte, neutrophil and eosinophil count, as well as the lowest non-zero basophil count were also detected in this group. In addition, this group displayed the highest lymphocyte count. It is therefore predicted that this group will display the least inflammation at the tissue level. The age control group displayed the highest neutrophil, eosinophil and basophil count. The high CoQ10 group displayed the lowest lymphocyte count, as well as the lowest (zero) basophil count, in conjunction with the positive control group. It is worth mentioning that the high CoQ10 and the positive control groups, with a basophil count of zero displayed the highest monocyte count

overall. Further, the high CoQ10 group had the smallest lymphocyte to monocyte ratio of the experimental groups, in conjunction with the negative control group.

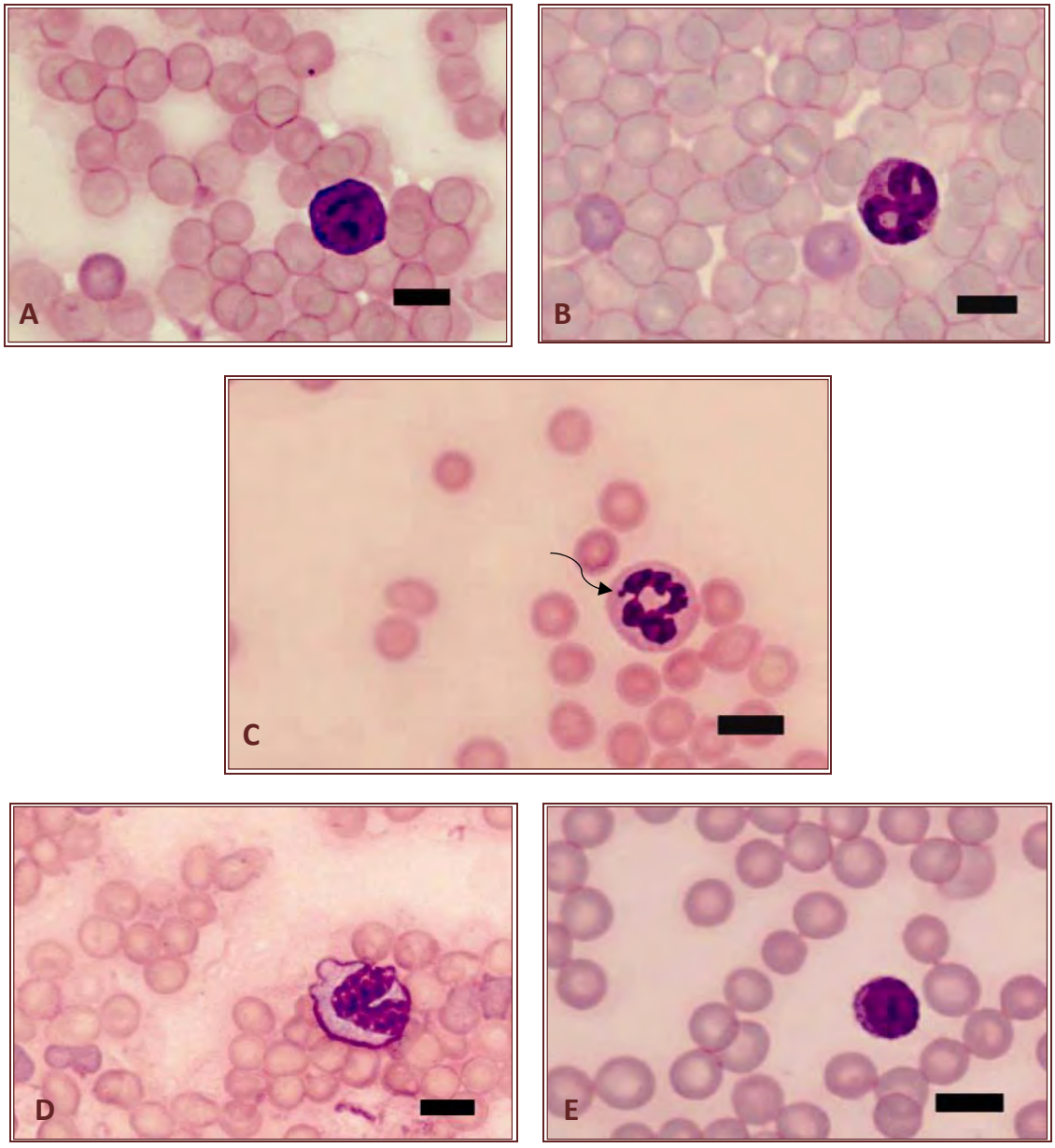

Figure 4.8: Blood smears stained with Wright's stain. Leukocytes from SJL/J mouse blood, **a**) Basophil; **b**) Eosinophil; **c**) Neutrophil; **d**) Monocyte; **e**) Lymphocyte. Scale bar = 10 µm

Neutrophils are attracted by chemotactic factors (chemotaxins) released from damaged tissue or generated by the interaction of antibodies with antigens on the surface of the microorganisms

(Young *et al*., 2006). They are amoeboid cells that squeeze through the capillary walls and enter the tissue fluid where they phagocytise foreign material (Ross *et al*., 2003).

Eosinophils are able to modulate inflammatory responses at several levels and have a central role in the induction and maintenance of inflammatory responses due to allergy (Young *et al*., 2006). Eosinophils can act as pro-inflammatory leukocytes and are able to modulate local immune responses. Mast cells and basophils act as effector cells in allergic disorders mediated by IgE and T helper lymphocytes as well as in the immune response to parasites (Young *et al*., 2006). Monocytes appear to have little function in circulating blood. These cells are motile phagocytic cells and are the precursors of macrophages found in peripheral tissues and organs (Young *et al*., 2006). They respond by chemotaxis to the presence of factors from damaged tissue, micro-organisms and inflammation by migration into the tissues and differentiation into macrophages. With their capacity for phagocytosis and content of hydrolytic enzymes, they engulf and destroy tissue debris and foreign material as part of the process of healing (Young *et al*., 2006).

Text box 4.1

The 'drumstick appearance'

The 'drumstick appearance' of the sex chromatin was found in a neutrophil from the present study (Figure 4.8 c, arrow). This appearance is observed in 3% of human female neutrophils, and represents the heterochromatin of one of the two X chromosomes of the female. Although presumably present in all neutrophils, it is often closely packed with one of the lobes of the nucleus in most cells and is therefore obscured (Kelly *et al*., 1984).

Macrophages and neutrophils are of the innate immune system. They are essential for the control of common infections and provide the first line of defence against many common microorganisms. Lymphocytes play the central role in all immunological defence mechanisms where they circulate between various lymphoid tissues and all other tissues of the body via the blood and lymphatic vessels (Young *et al*., 2006). There is a constant recirculation of lymphoid cells through tissues and back to the circulation as part of immune surveillance. Large lymphocytes represent either B and T lymphocytes (activated lymphocytes which possess surface receptors that interact with a specific antigen) or natural killer (NK) lymphocytes (programmed to kill certain types of transformed cells). They are *en route* to the tissues where they will become antibody-secreting plasma cells (Young *et al*., 2006; Ross *et al*., 2003).

Raised neutrophil counts are indicative of an acute inflammatory response and are especially seen in association with bacterial infections. Raised eosinophil counts are seen in response to allergy and in infections with certain parasites, as eosinophils are able to modulate inflammatory responses at several levels. The highest lymphocyte counts were observed in the resveratrol and resveratrol/CoQ10 combination groups, suggesting a possible mechanism of resveratrol in

modulating the immunological response. The lowest monocyte, neutrophil and eosinophil counts, as well as the lowest non-zero basophil count were observed in the resveratrol/CoQ10 group. This observation leads to the hypothesis that this group will display the least inflammation at the tissue level. On the contrary, the highest neutrophil, eosinophil and basophil counts observed in the age control group indicate an aggressive inflammatory response at the tissue level. Histopathological assessment in chapter 5 will shed more light on this observation. The high CoQ10 group displayed the lowest lymphocyte counts, with the smallest lymphocyte to monocyte ratio in conjunction with the negative control group. This group further displayed lymphocyte, monocyte and neutrophil counts, with the highest similarity to that observed in the negative control group. In addition, the highest eosinophil count, compared to other antioxidant supplemented groups and the positive control group were detected in the high CoQ10 group. This observation suggests a decreased inflammatory reaction in the high CoQ10 group.

4.4 Concluding Remarks

The good condition maintained in animals in the present study, suggest that supplementary food provided at a more convenient location, may be a good practice to employ as standard, when maintaining muscular dystrophy murine models beyond the point of full disease onset.

Significant stronger tensile strength tests were performed by mice from the high CoQ10 and resveratrol/CoQ10 groups, compared to low CoQ10 and resveratrol groups. Although stronger than the control groups, differences were not significant. The results suggest that the antioxidant supplementation in low CoQ10 and resveratrol groups were not sufficient in protecting muscle against pathological changes that lead to a strength loss. The results further suggest that a higher concentration antioxidant supplementation, as administered in the high CoQ10 and resveratrol/CoQ10 combination groups, increase the limb strength in SJL/J mice.

From the CK and LDH data, the degree of difference from the average CK value for the specific populations, represented by each group in the study, was very large. It is therefore concluded that the CK and LDH values in the present study might not be indicative or representative enough of the disease or the effect of antioxidant supplementation in the SJL/J mouse. It can be concluded that in order to obtain more informative values, the assays should be repeated more times, and preferably include a larger sample size/population.

At the earlier stages of dysferlinopathy at the age of 14 weeks, as represented by the age control group, the increase in eosinophil counts could very likely be a compensatory mechanism to decrease

initial inflammation in the muscle tissues of the dysferlinopathic mice. Considering no significant difference in number between the negative control group and the 14 week-old age control group, it is possible that as disease progressed, the production of eosinophils was down regulated in SJL/J mice in an age-dependent manner. In addition, as the inflammatory process increased with age, the initial possible compensatory mechanism offered by eosinophils is likely not to be able to keep up with the ever increasing inflammatory progression. Neutrophils are linked to early inflammatory responses and often sensitised in self-antigen recognition characteristic to autoimmune disease, a known complication in the SJL/J strain (www.jax.org/jaxmice). Thus the higher neutrophil count in the age control group is probably related to inflammation at disease onset, but may also be indicative of autoimmunity; whereas the eosinophil count may possibly play a more definite role in the pathogenesis of dysferlinopathy.

The hypothesis that the resveratrol/CoQ10 combination group will display the least inflammation at the tissue level, due to the lowest monocyte, neutrophil, basophil and eosinophil numbers measured in this group are further supported by the observation that this group also displayed the greatest physical strength. In addition to this observation, a similar decrease in tissue inflammation is expected in the high CoQ10 group, due to similar white blood cell counts to the negative control group. Histopathological studies in chapter 5 will provide more insight to these observations.

Chapter 5

Histological assessment of SJL/J mice treated with Coenzyme Q10 and Resveratrol

5.1 INTRODUCTION

The most abundant tissue in the body is represented by skeletal muscle, making up about 40% of the total body weight and is involved in many essential physiological and biochemical processes, which include heat homeostasis and metabolic integration, movement, and posture (Engel and Franzini-Armstrong, 1994; Silverthorn, 2004). The degeneration of skeletal muscle is the most common pathological feature of the muscular dystrophies (Bansal and Campbell, 2004). Muscular dystrophies characterized by dysferlin deficiency have been shown to be defective in repairing injuries to the plasma membrane (Bansal *et al*., 2003). Histopathological examinations of muscles in SJL/J mice of different ages and different sources (SJL/J, SJL/Olac) by Bittner and co-workers, disclosed features compatible with a progressive muscular dystrophy, including degenerative and regenerative changes of muscle fibers, together with a progressive fibrosis. These changes were found to primarily affect the proximal muscle groups, whereas the distal muscles remained less affected (Bittner *et al*., 1999).

Muscle morphology

Skeletal muscle is a highly specialized tissue with primary function being the generation of physical force. It is therefore more susceptible to plasma membrane damage and requires more efficient membrane repair machinery than perhaps any other tissue (Bansal and Campbell, 2004). The smallest independent cellular units of mature skeletal muscle are called fibers, also referred to as muscle cells (Kelly *et al*., 1984). Fibers are cylindrical, multinucleate, cellular structures which vary greatly in length. Fibers are grouped together into bundles called fasciculi. Within a given muscle the fibers conform to one of three modes of attachment (Kelly *et al*., 1984): *i*) those extending from one end of the fasciculus to the other; *ii*) those beginning at one or the other end of the fasciculus and terminating within the substance of the bundle; and *iii*) those having both ends within the muscular substance. Individual muscle fibers vary considerably in diameter from 10 to 100µm and may extend throughout the whole length of a muscle, reaching up to 35cm in length. In addition, the shortest fibers in small muscles are less than a millimetre in length (Kelly *et al*., 1984; Young *et al*., 2006). When viewed in cross section, the mature multinucleated muscle fiber reveals a polygonal shape (Ross *et al*., 2003). Although fibers of different thickness are intermingled in the same muscle, there

is more or less a typical size for each muscle, and some correlation has been found between the heaviness of the work a muscle performs and the thickness of its fibers (Kelly *et al*., 1984). The increase in size of a muscle which takes place during growth of an individual or which is brought about by exercise is due to an increase in the size of its fibers rather than an increase in their number (Kelly *et al*., 1984). The vast majority of the volume of each fiber is occupied by the massive cross-striated contractile organelles, the myofibrils (Kelly *et al*., 1984; Mader, 2001). Myofibrils are cylindrical in shape and run the length of the muscle fiber. With light microscopy it can be shown that the striations of myofibrils are formed by the placement of protein filaments within contractile units called sarcomeres (Mader, 2001).

The nuclei of a skeletal muscle fiber are located in the cytoplasm, immediately beneath the plasma membrane, known as the sarcolemma. They assume a position just inside the sarcolemma and usually vaguely align in rows or spirals, but occasional isolated central nuclei may be observed in histological normal muscle (Carpenter and Karpati, 1984). Peripheral nuclei are elongated parallel to the myofibrils, appearing in longitudinal sections as long ovals, 4 to 5µm in length and 1 to 2µm in width. Approximately 3.8% of nuclei in adult human muscle at the periphery of muscle fibers are those of satellite cells. These nuclei cannot be distinguished from the myonuclei in cryostat sections, but occasionally on resin sections, as they tend to have denser chromatin (Carpenter and Karpati, 1984). Also, they have a slightly more slender appearance, and a definite division between the nucleus and the sarcolemma can be observed at the ultrastrucutral level.

The sarcolemma represents the plasma membrane of the cell, its external lamina and the surrounding reticular lamina (Ross *et al*., 2003), now referred to as the sarcolemma and the basal lamina. The plasma membrane of muscle fibers is similar to that of other cells in the body in being a fluid mosaic sheath, composed of a lipid bilayer with embedded proteins (Carpenter and Karpati, 1984). The basal lamina or basement membrane of muscle fibers is attached to the outer leaflet of the plasma membrane and partly penetrated by the acidic glycoproteins of the cell coat (Carpenter and Karpati, 1984). The function of the basal lamina is believed to provide external mechanical support for the fiber and to facilitate muscle fiber regeneration (Carpenter and Karpati, 1984).

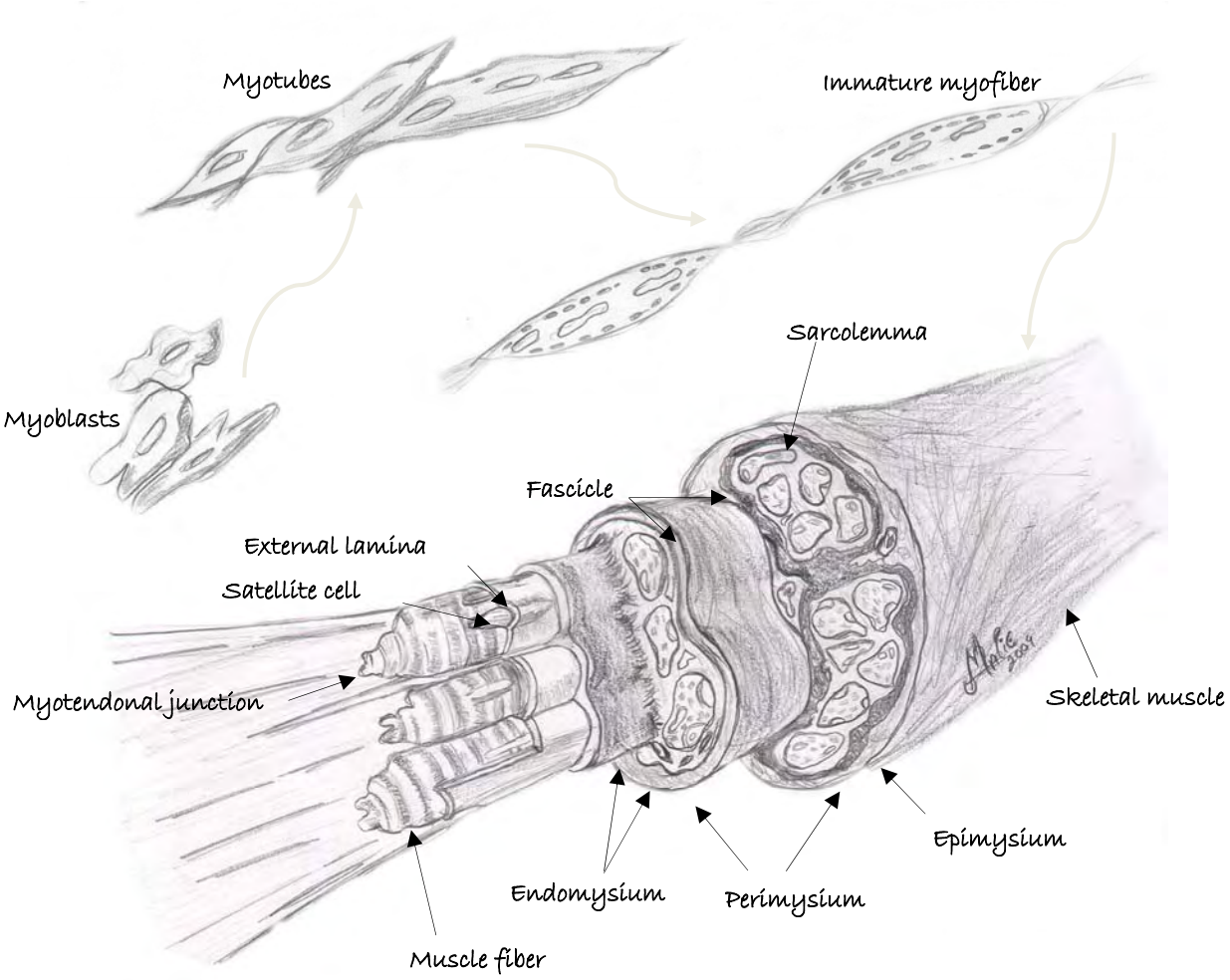

Figure 5.1: Schematic representation of skeletal muscle development and organization of muscle fibers and their connective tissue ensheathments. (Adapted from Kelly *et al*., 1984)

The connective tissue that surrounds both individual muscle fibers and bundles of muscle fibers is essential for force transduction (Ross *et al*., 2003). At the end of the muscle, the connective tissue continues as a tendon or some other arrangement of collagen fibers that attaches the muscle usually to bone. A rich supply of blood vessels and nerves travels in the connective tissue. The connective tissue associated with muscle is named according to its relationship with the muscle fibers (Figure 5.1). Endomysium is the delicate layer of reticular fibers that immediately surrounds individual muscle fibers. Only small-diameter capillaries and the finest neuronal branches are present within the endomysium, running parallel to the muscle fiber. The perimysium is a thicker connective tissue layer that surrounds a group of fibers to form a bundle or fascicle. Fascicles are functional units of muscle fibers that tend to work together to perform a specific function. Larger blood vessels and nerves travel in the perimysium. The epimysium represents the sheath of dense connective tissue

that surrounds a collection of fascicles that constitutes the muscle. The major vascular and nerve supply penetrates the epimysium (Ross *et al*., 2003).

Why histopathology assessment?

This chapter discusses skeletal muscle histopathology in the SJL/J mouse model for dysferlinopathy. Light microscopic investigation of the early pathological abnormalities in non-necrotic muscle fibers of dysferlin-deficient patients revealed that muscle specimens displayed abnormal variation of fiber size, fiber splitting, an increased number of internalized nuclei, scattered necrotic and regenerating fibers, and increased endomysial and perimysial connective tissue (Selcen *et al*., 2001). Other abnormalities consisted of small, irregularly circumscribed decreases of oxidative enzyme activity, few lobulated fibers, rare ring fibers, and sparse perivascular mononuclear cells (Selcen *et al*., 2001). Abnormal distribution of the muscle fiber size in muscle cross-section is a hallmark of the pathological changes in dystrophic muscle (Briguet *et al*., 2004). To allow for reliable quantitative assessment of fiber size variation in SJL/J quadriceps muscle, it is essential to select a method for determining the muscle fiber cross-sectional size which is not, or as little as possible influenced by the sectioning procedure. It was therefore decided to determine the variability of muscle fiber size in the SJL/J mouse model for dysferlinopathy in the current study with the minimal Feret's diameter parameter to allow for quantitative assessment of the influence of the dystrophic process on fiber size. The evaluation is based on 1µm thick resin sections since they offer by far the best morphological detail. They offer a view analogous to very-low-power electron microscopy with the advantage of a much larger sampling area (Carpenter, 2001 a), ideal for studying alterations at the cellular level.

The study of the form of structures seen with a microscope, with specific focus on the anomalies thereof, defines the purpose of the present chapter. Dysferlin deficient muscular dystrophy manifests as the result of, amongst others, a defective membrane repair mechanism. The cellular alterations, as observed with a light microscope, associated with this defect and the effect of antioxidant supplementation, are investigated. The effect of CoQ10 on cells and tissues has been proposed to be wide-ranging with the capacity to modulate diverse tissue activities and disease processes via small intrinsic cell metabolic perturbations (Linnane *et al*., 2002). In the present study the distribution of skeletal muscle lesions and the severity thereof were examined by histopathological examinations and morphometric comparison of the fiber diameter. The differences were compared between 14 and 27 week-old untreated SJL/J mice, the different 27 week-old antioxidant supplemented groups, and the 27 week-old SWR/J group, as the negative control.

5.2 Materials and Methods

5.2.1 Morphology

Quadriceps and gastrocnemius muscle samples were collected for histological investigation at termination. A small piece (± 2 x 3 mm) of muscle tissue was dissected from the belly area of the quadriceps and gastrocnemius muscles. Tissue samples were immediately fixed in 2.5% formaldehyde in 0.075 M phosphate buffer, pH 7.4 at room temperature overnight. The tissue was removed from the fixative, rinsed thrice, 10 min each, in 0.075 M phosphate buffer and serially dehydrated in 30%, 50%, 70% and 90% ethanol, followed by three changes of absolute ethanol for 15 min per dehydration step. Tissue was then infiltrated with 50% LR White Resin (SPI Supplies, West Chester, PA) in absolute ethanol for one hour, followed by infiltration with 100% LR White Resin for a minimum of four hours. Thereafter, tissue was orientated in order to produce transverse tissue sections, embedded in 100% LR White Resin and labelled accordingly. Samples were polymerized for 24 hours at 60°C. Ten to 20 serial sections of between 0.5µm to 1.5µm (optimal 1µm) were cut with a Reichert-Jung Ultra Cut E ultramicrotome (Vienna, Austria). Sections were collected onto droplets of water on Menzel glaser glass slides and dried on a slide warmer. Three slides were prepared for each tissue type of each animal. All samples were numbered with a four digit numbering system that was documented with the initial animal group, number and tissue isolated. Slides were numbered accordingly. Gill's Haematoxylin (Solulab, Johannesburg, South Africa), a general nuclear stain, together with 0.2% Toluidine Blue O (Electron Microscopy Sciences, Washington, PA) in a 0.5% Na_2CO_3 (Merck) solution (pH 11) were utilized to stain the tissue sections, in order to distinguish fibers with centrally located nuclei from fibers with peripherally located nuclei, and to determine the presence of inflammatory infiltrates and fiber size. Sections were stained with Haematoxylin for 1 hour, rinsed 10 times with water and then dehydrated on a slide warmer, followed by Toluidine Blue O staining for 30 sec, rinsed 10 times with water, followed by dehydration. Preparations were mounted with Entellan (Merck). Viewing and image capturing were done with a Nikon Optiphot transmitted light microscope (Nikon Instech Co., Kanagawa, Japan), equipped with a Nikon DXM 1200F digital camera. One to three slides from each and every sample were investigated at 20x, 40x and 100x objective lens magnification. Images from each sample were captured at 40x and 100x objective lens magnification for histological analyses. The resultant images were enhanced with Adobe Photoshop 7.0. In most instances the layers of the images were flattened and the colour from each image was removed as this produced a sharper image of the fiber periphery and other tissue components of interest. The severity of skeletal muscle lesions such as degeneration/necrosis, central nuclei and atrophy, cellular infiltration, and adipose tissue infiltration were evaluated

histopathologically and scored by a modified method of Kobayashi and co-workers. In short, histological lesions were assessed and scored as, none (0, not present), minimal (±, localized lesions), mild (+, scattered lesions), and moderate (+ +, multifocal lesions) (Kobayashi *et al*., 2009). A summary of the histological lesion assessment is given in Table 5.1.

5.2.2 Morphometry

For morphometric analyses six animals per group were randomly selected and between 10 and 20 microscopic fields for each group were captured at 20x objective lens magnification. At least 500 fibers per group were assessed for their minimal Feret's diameter (Briguet *et al*., 2004), utilizing Olympus analySIS software. All the fibers containing centrally located nuclei per microscopic field assessed, regardless of the number of centrally located nuclei (ranging from one to three), were counted. Only intact fibers were assessed for centrally located nuclei count and fiber diameter measurements, as nuclei present in cells undergoing necrosis, presumably represent those of phagocytic cells. Minimal Feret's diameter, for the assessed ≈500 cells in each experimental group, is presented in Table 5.2.

5.2.3 Statistical Analyses

For each muscle type the measured cells' diameters were then statistically compared between the various experimental groups, via Kruskal-Wallis one-way ANOVA. T-tests and Mann-Whitney U tests were also used to allow for the diameters of the gastrocnemius and quadriceps to be compared to each other within each experimental group. The statistical analyses were preformed with the use of the statistical program NCSS, with a level of significance of 0.05 being utilized during all the statistical analyses conducted.

5.3 Results and Discussion

5.3.1 Histological Findings

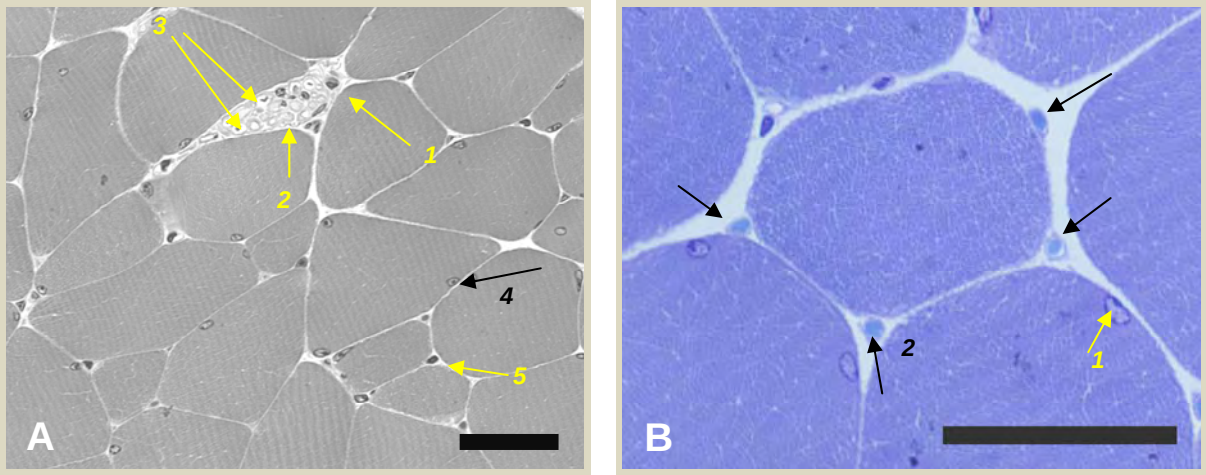

Figure 5.2: Quadriceps muscle sections from SWR/J mice at 27 weeks of age, representing the negative control group of the study. Sections were stained with Toluidine Blue O and Gill's Haematoxylin. A) A nerve bundle (1), with axons (2), and blood vessels (3) are present in this section. (B) Myonuclei (A, 4 & B, 1) and capillaries surrounding healthy myofibers (A, 5 & B, 2) are present. Scale bars = 50µm

Negative control group

Quadriceps muscle specimens analysed from all the 28 week-old SWR/J mice that represented the negative control group (Figure 5.2 A and B), displayed normal variation of fiber size. Neither inflammatory infiltrate nor active necrotic processes could be detected. Figure 5.2 A, 1 showed a nerve bundle in a transverse section. Axons (Figure 5.2 A, 2) and blood vessels (Figure 5.2 A, 3) was observed in this section. No occurrence of fiber splitting was detected while only ≈1.4% of fibers evaluated, displayed nuclei in the central position. Myonuclei (Figure 5.2 A, 4 and B, 1) were situated mostly in the peripheral position with a distribution of one to about five peripherally located nuclei per fiber. Many fibers were surrounded by a number of capillaries (Figure 5.2 A, 5 and B, 2), some displaying erythrocytes in the lumen (Figure 5.2 B, 2), while others appeared empty.

Age control group

Figures 5.3.1 and 5.3.2 display sections from the age control group, 14 week-old SJL/J mice that received no treatment. Mild (+) focal perimysial (Figure 5.3.1 A, arrow) and endomysial (Figure 5.3.1 B, arrow) inflammatory changes were observed in this group. Mononuclear cells were present between fibers (Figure 5.3.1 C, arrows). Mononuclear cells in the age control group were observed in smaller quantities, compared to that seen in the 27 week-old SJL/J groups treated with placebo.

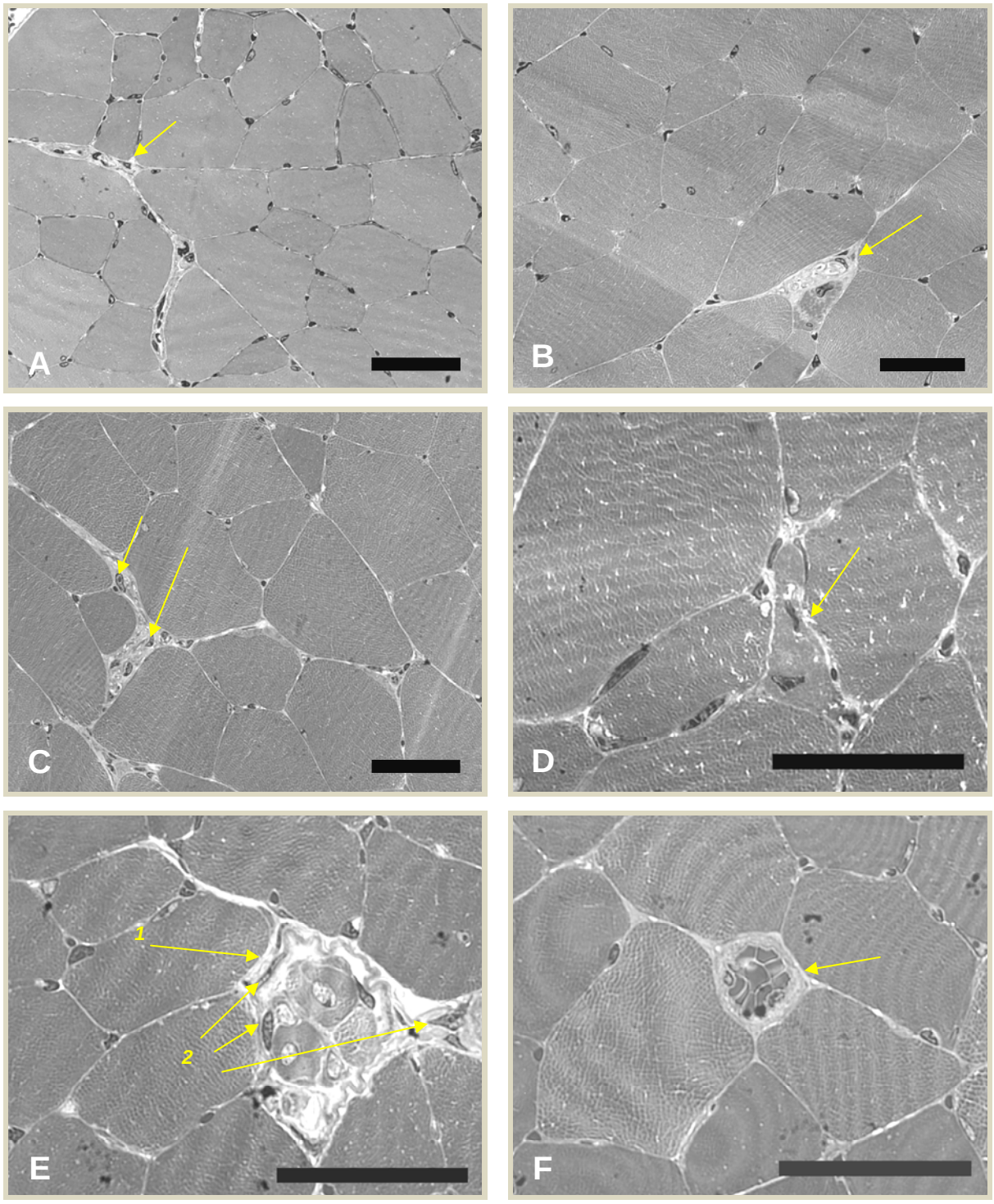

Figure 5.3.1: Quadriceps muscle sections from SJL/J mice at 14 weeks of age. Sections were stained with Toluidine Blue O and Gill's Haematoxylin. A) Perimysial and B) endomysial inflammatory changes are present (arrows). C) Mononuclear cells can be observed between fibers (arrow). D) Ongoing fiber necrosis was observed, where the degenerating fiber is invaded by mononuclear cells, presumably macrophages (arrow). E) Early stages of the necrotic process in a muscle fiber (1) with invasion by mononuclear phagocytic cells (2). F) A cluster of smooth muscle cells (arrow). Scale bars = 50µm

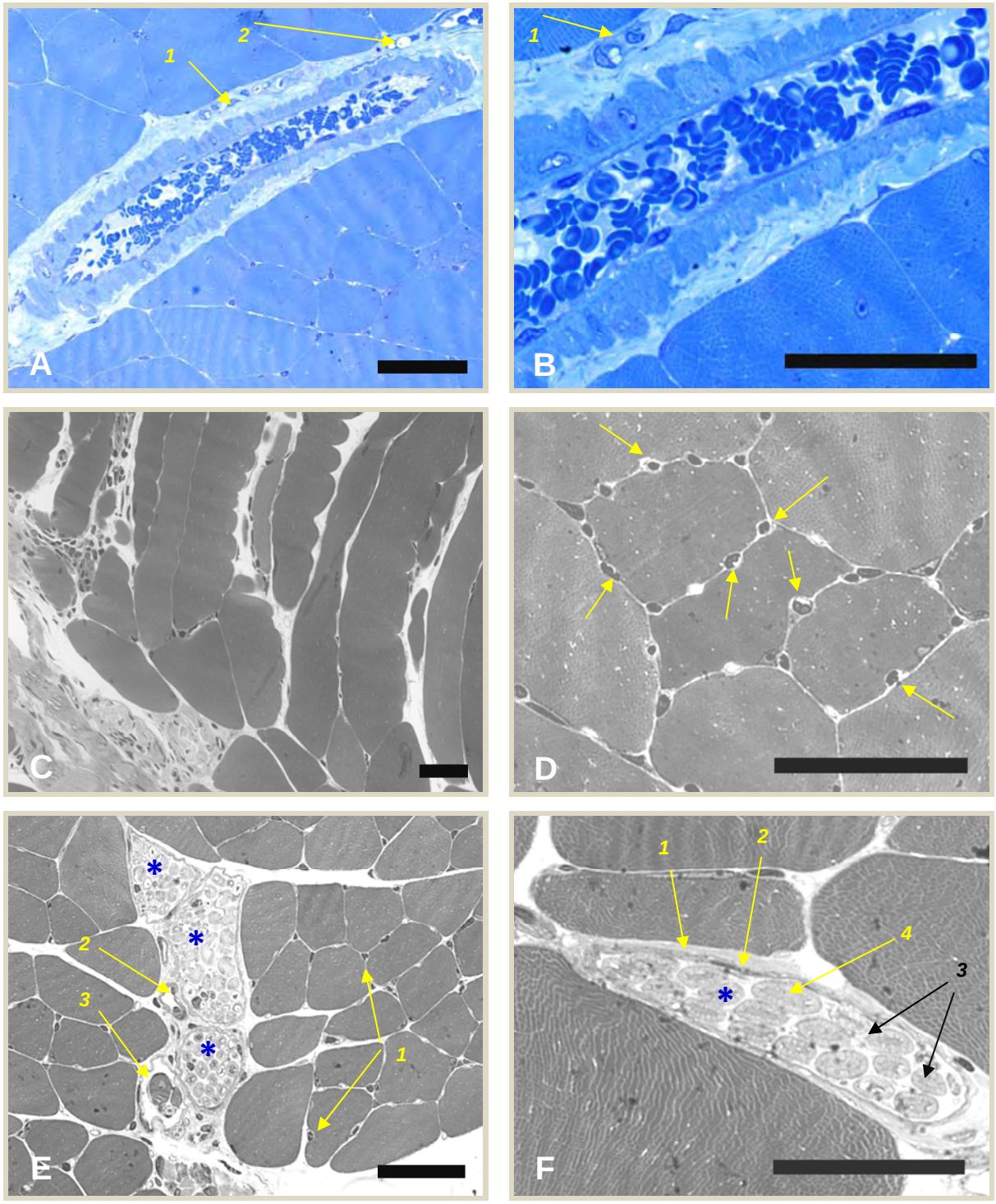

Figure 5.3.2: Quadriceps muscle sections from SJL/J mice at 14 weeks of age. Sections were stained with Toluidine Blue O and Gill's Haematoxylin. A & B) A relatively large blood vessel (arteriole) with the presence of a large number of erythrocytes in the lumen. Mononuclear cells are present in the extracellular space surrounding the arteriole (A & B, 1). Very small adipose cells are present in this region (A, 2). C) Longitudinal section of muscle fibers shows irregularly curved peripheries. D) Capillaries surrounding and indenting fibers (arrows & E, 1). E) Nerve bundles (asterisks), with blood vessels in the vicinity (2), and a muscle spindle (3) are present in the same region. F) This section display a nerve bundle with the perineurium (1), epineurium (2), individual neurons (3), and the nuclei of the perineurial cells (4) visible. Scale bars = 50µm

Necrotic fibers (Figure 5.3.1 D, arrow) were noted in regions where mononucleated cells were observed. In muscle samples from this group, mostly single fiber involvement was seen in necrotic events. These cells were often invaded by mononucleated cells presumably responsible for phagocytosis (Figure 5.3.1 D). Endomysial infiltrate (between the fibers) (Figure 5.3.1 C) was seen to a lesser extent (±) and was mostly noted around intact cells. Inflammatory infiltrate were found to be present to a lesser extent (±). 'Moth-eaten' appearance of fibers (Figure 5.3.1 D) was noted, although the overall appearance of the muscle fibers was good. Carpenter and Karpati, 1984, reported that many fibers in biopsies from limb girdle dystrophy patients show moth-eaten appearance in their centers and have prominent mitochondria along their periphery. Moth-eaten fibers have further been reported to be common in denervating conditions, though they may represent reinnervated fibers (Carpenter and Karpati, 1984).

Figure 5.3.1 E, 1, shows the early stages of an ongoing necrotic process in a muscle fiber. Invasion of the fiber by mononucleated phagocytic cells (Figure 5.3.1 E, 2) are characteristic of initial phases of the process, and these invading cells are presumably macrophages. A large number of fibers were angular in shape (Figure 5.3.1 A-F). Fiber diameter varied and ranged from 15.98 to 112.34µm, as determined by measuring the minimal Feret's diameter. Nuclei were mostly peripherally located and found in relative large numbers that vary among individuals in this group. In only 8.8% of fibers analysed, nuclei were found in the central position of the fibers.

A cluster of structures (Figure 5.3.1 F, arrow) surrounded by a multiple layered sheath was detected in one sample in this group. The smooth and shiny appearance of these structures differ markedly from the surrounding skeletal muscle fibers, and the nearest corresponding structure it could be correlated to, was smooth muscle (Carpenter and Karpati, 1984). In normal muscles smooth muscle cells are confined to the walls of veins and arteries. Carpenter and Karpati recorded a case in 1984 where there was marked independent proliferation of smooth muscle cells, accompanied by collagen in the endomysium of a limb girdle myopathy sample.

Relatively large blood vessels (Figure 5.3.2 A and B) were often observed in the age control group. Figure 5.3.2 A and B showed an arteriole, with the presence of a large number of erythrocytes in the lumen. Mononuclear cells were noted in the extracellular space surrounding the arteriole (Figure 5.3.2 A and B, 1). Very small adipose cells were also present in this region (Figure 5.3.2 A, 2). Occasional (±) fiber splitting was present in this group. On one longitudinal section, muscle fibers showed irregularly curved periphery (Figure 5.3.2 C). These indentations were of unknown cause, and remain to be further investigated at the ultrastructural level in chapter 6.

In a number of transverse sectioned samples, but not in all, numerous small circular objects were found to surround the muscle fibers (Figure 5.3.2 D, arrows, and 5.3.2, E, 1). These circular objects were compared to the work of Carpenter, 2001 a, who identified a similar occurrence as capillaries indenting a ragged-red fiber (Carpenter, 2001 a; Carpenter and Karpati, 1984). The lumens were mostly filled with erythrocytes, resulting in the dark appearance. Various nerve bundles of different sizes were observed in transverse sections from this group (Figure 5.3.2 E and F, blue asterisks). Blood vessels (Figure 5.3.2 E, 1) were often noted in these areas. A muscle spindle was identified in Figure 5.3.2 E, 3. A muscle spindle represents a specialization of certain skeletal muscle fibers and nerves to form a structure capable of giving elaborate feedback information to the nervous system on the muscle's state of activity. Muscle spindles are found relatively infrequently in routine muscle biopsies (Carpenter and Karpati, 1984). Figure 5.3.2 F, shows a larger magnification of a nerve bundle (blue asterisk). Peripheral nerves are composed of bundles of nerve fibers held together by connective tissue and a specialized layer(s) of cells, the perineurium (Figure 5.3.2 F, 1). The epineurium (Figure 5.3.2 F, 2) surrounds the bundles of nerve fibers, while the endoneurium is associated with individual neurons (Figure 5.3.2 F, 3). The nuclei of the perineurial cells (Figure 5.3.2 F, 4) appeared flat and elongated in a transverse section.

Positive control group

The quadriceps muscle specimens of 27 weeks old SJL/J mice treated with placebo (the positive control group) throughout the course of the trial, displayed abnormal variation of fiber size (Figures 5.4.1 and 5.4.2). Fiber diameter ranged between 11.82 and 99.01µm as determined by minimal Feret's diameter (Briguet *et al*., 2004). Mild (+) to moderate (+ +) perimysial inflammatory changes with endomysial involvement became predominant in this group (Figure 5.4.1). Quadriceps muscle exhibited active myopathic changes emphasized by the following findings; fiber splitting was prevalent (+) (Figure 5.4.1 A, 1 and F, 1) and its appearance was distinct in areas with more inflammatory infiltrate. Numerous necrotic fibers and fiber remnants (+ +) resultant of the ongoing necrotic processes ranging from mild (+) to moderate (+ +) were observed (Figure 5.4.1 B, 1 and D, 1). These fibers ranged from disrupted cells invaded by macrophage activity, to 'ghost' cells (Figure 5.4.1 C, 1 and E, 1), which is marked by a 'see-through' appearance of cell remnants representing the initial shape and size of the dead cell. Numerous mononucleated cells (+ +) (Figure 5.4.1 A, 2 and B, 2) were predominant in areas with inflammatory infiltrate. These cells were also found to invade fibers in the necrotic state (Figure 5.4.1 B, 3), and are presumably representative of macrophage activity.

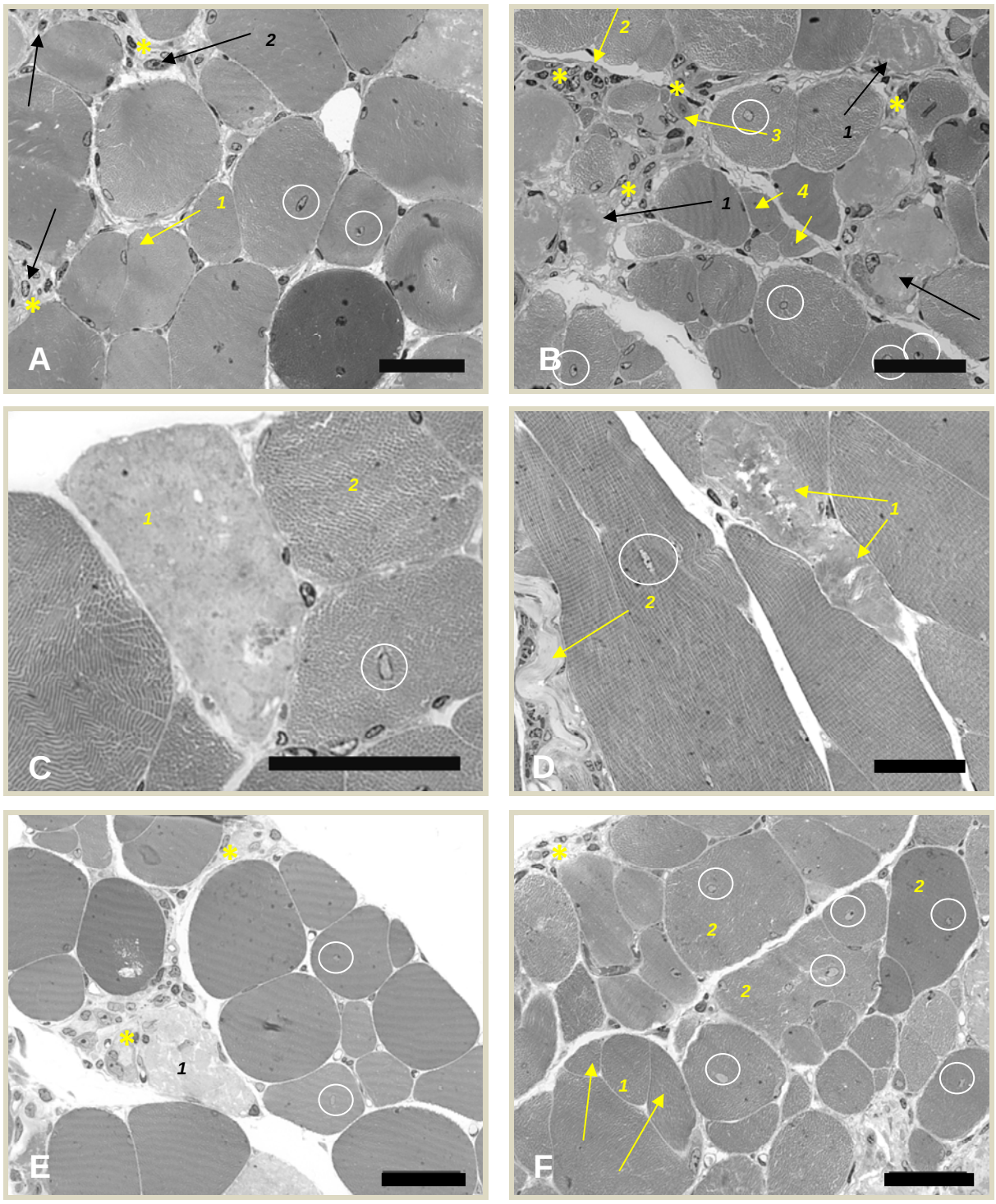

Figure 5.4.1: Quadriceps muscle sections from the positive control group; 27 week-old SJL/J mice treated with placebo. Sections were stained with Toluidine Blue O and Gill's Haematoxylin. Inflammatory infiltrate is prominent in this group (asterisks). Numerous fibers in this group display central nucleation (white circles). A) Fiber splitting is prevalent (1) and mononucleated cells are present in inflammatory regions (2). B) 'Ghost cells' (1) as a result of necrosis (asterisks) is observed. Mononucleated cells (2) are invading necrotic fibers (3). Small diameter fibers (4) are observed in nearby regions. C) Ghost cells (1) and moth-eaten appearance of cells is present. D) A necrotic fiber (1) and dense connective tissue (2) in extracellular space of fibers on a longitudinal section. E) The occurrence of ghost cells (1) in inflammatory regions (asterisk) is frequent. F) Fiber splitting (1) and hypertrophic fibers (2) are present. Scale bars = 50µm

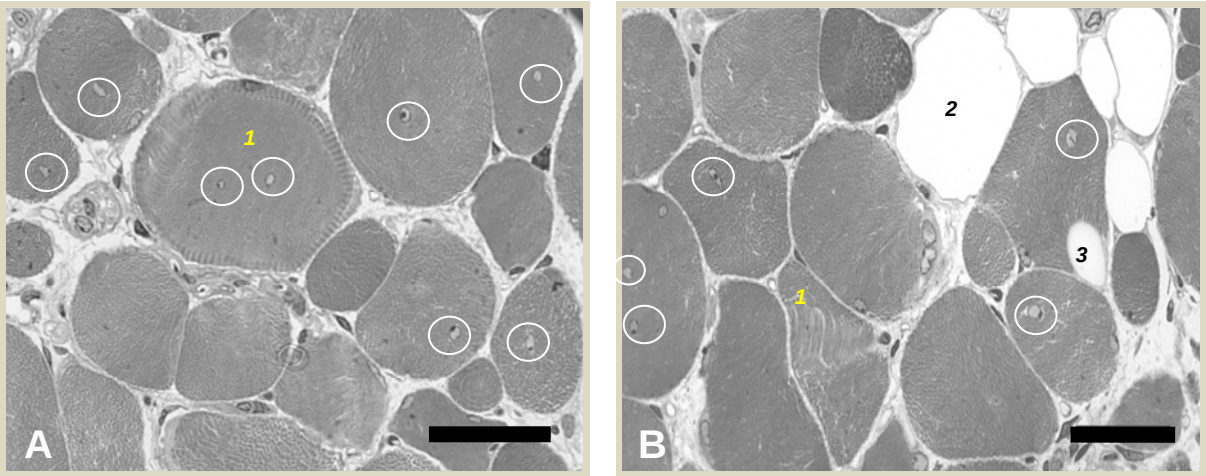

Figure 5.4.2: Quadriceps muscle sections from the positive control group; 27 week-old SJL/J mice treated with placebo (stained with Toluidine Blue O and Gill's Haematoxylin). A) Ring fibers are present (1). B) In some fibers myofibrils show a 'streaming' appearance (A, 1 & B, 1). B) Adipose cells (2) and vacuoles (3) are present. Scale bars = 50µm

The appearance of moth-eaten cells (Figure 5.4.1 C, 2) was frequent (+ +). Inflammatory infiltrate (Figure 5.4.1 A, B, E, and F, yellow asterisks) were present, ranging from mild dystrophic changes (+), characterized by numerous small diameter fibers (Figure 5.4.1 B, 4), intercepted by the occasional necrotic fibers, to moderate ongoing dystrophic processes (+ +), emphasized by large incidences of necrosis and much inflammatory infiltrate. In only one out of nine animals, no inflammatory infiltrate (0) could be detected in quadriceps muscle specimens examined, while seven out of nine showed mild (+) to moderate (+ +) dystrophic lesions and one animal showed lesions, more severe than what was classified as moderate in the present study, with up to zero intact cells in one microscopic field. This observation could possibly be explained by the possibility of inter-individual variation amongst animals, where onset of disease might have occurred later in the latter subject; or the dystrophic alterations were not affecting the muscle as a whole to the same extent. Therefore, a muscle sample showing no incidence of degeneration, might either represent an unaffected area of that specific muscle, or represent an individual likely to show full onset of the disease at a later stage.

Dense connective tissue (Figure 5.4.1 D, 2) was observed between fibers, where inflammatory infiltrate was distinctive, with a higher frequency in areas with higher necrotic incidence. Hypertrophic fibers were present and found usually together with very small fibers (Figure 5.4.1 F, 2). Ring fibers (Figure 5.4.2 A, 1) were detected in one sample from this group. Inflammatory infiltrate with mononuclear cells were present in the extracellular space surrounding this fiber. In the same sample, fibers of which the fibrils were 'streaming' (Figure 5.4.2 A and B, 2) were also seen.

In a sample from the same individual, adipose cells (Figure 5.4.2 B, 2) of which the size compared to that of the surrounding fibers, were observed. A large vacuole (Figure 5.4.2 B, 3) were noted in one of the fibers in this sample. Both angular as well as circular shaped intact fibers were present. The histological results from 6-month old, untreated, SJL/J mice were consistent with previous findings in SJL/J mice at a similar age (Weller *et al*., 1997; Ho *et al*., 2004; Suzuki *et al*., 2005; Nemoto *et al*., 2006;) and correlate with the histological findings in human dysferlinopathy patients (Gallardo *et al*., 2001; Selcen *et al*., 2001; Cenacchi *et al*., 2005).

Nuclei in the central position of fibers (white circles) were abundant and up to three central nuclei could be detected in a single fiber cross section. Nuclei in this position were found in 35.4% of fibers analysed. Peripheral nuclei were sparsely distributed along less- and unaffected fibers. The samples analysed from this group served as a baseline/reference for the experimental groups treated with the different concentrations of different antioxidants throughout the course of the trial.

Resveratrol group

A distinct variation in fiber size was apparent following qualitative histological assessment of 27 week-old SJL/J mice treated with resveratrol (60mg/kg/day). In quadriceps muscle samples analysed, minimal Feret's diameter ranged between 10.12 and 117.90µm. Angulated fibers were present although more fibers displayed a circular shape. Fiber splitting (+), was observed as groups of small nested fibers with complementary contours (Figure 5.5.1 A and B, 1). One or more of these fibers often displayed central nucleation. Mild (+) to moderate (+ +) degeneration and perimysial inflammatory changes with endomysial involvement (Figure 5.5.1 A and B, yellow asterisk) was present and underlined by the distinct presence of mononucleated cells (+) (Figure 5.5.1 A and B, 2).

The presence of necrotic fibers as 'ghost cells' (Figure 5.5.1 C, 1) as well as fiber remnants (Figure 5.5.1 A, 3), resultant of the ongoing dystrophic process was observed. Large numbers of mononucleated cells, as part of the inflammatory infiltrate were noted in areas of necrotic events. Ring fibers (Figure 5.5.1 D, 1) were detected in one sample from this group. Fibers of which the fibrils appeared to be 'streaming' (Figure 5.5.1 C, 2 and E, 1) were also seen. Mild (+) infiltration of adipose tissue ranged from very small single cell presence to colonies of more than ten adipose cells (Figure 5.5.1 E, 2) in one area of which the size compared to those of the muscle fibers. Intense vacuolation was observed in some fibers (Figure 5.5.1 F, 1). The infiltrate in perimysial spaces was mostly dense connective tissue (Figure 5.5.1 F, 2), presumably collagen. Fibroblasts (Figure 5.5.1 F, 3) with fine extending processes were found in conjunction with connective tissue infiltration.

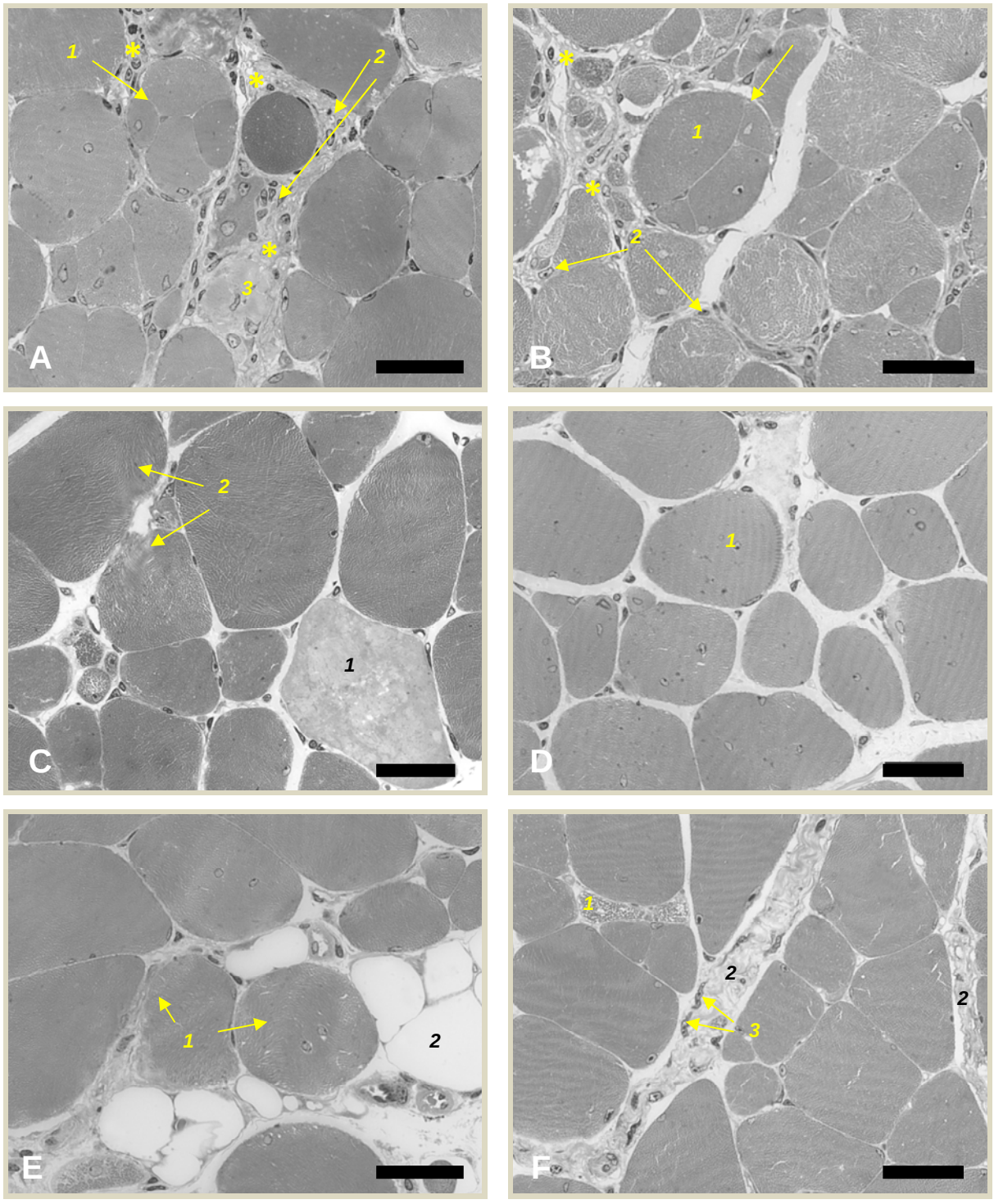

Figure 5.5.1: Quadriceps muscle sections from the 27 week-old SJL/J group treated with resveratrol. Sections were stained with Toluidine Blue O and Gill's Haematoxylin. A & B show fiber splitting as a group of nested fibers (1) in an area with moderate inflammatory infiltrate (asterisks), that contain numerous mononucleated cells (2), and fiber remnants (A, 3). C) Ghost cells (1) and fibers of which the fibrils are 'streaming' (2) can be observed. D) Ring fibers (1) are present. E) Fibers of which the myofibrils are streaming (1) in an area infiltrated by adipose cells (2). F) Vacuolation (1) occurs in fibers of this group. Connective tissue in the perimysial areas (2) are presumably collagen, with the presence of fibroblasts (3) with thin extending processes. Scale bars = 50µm

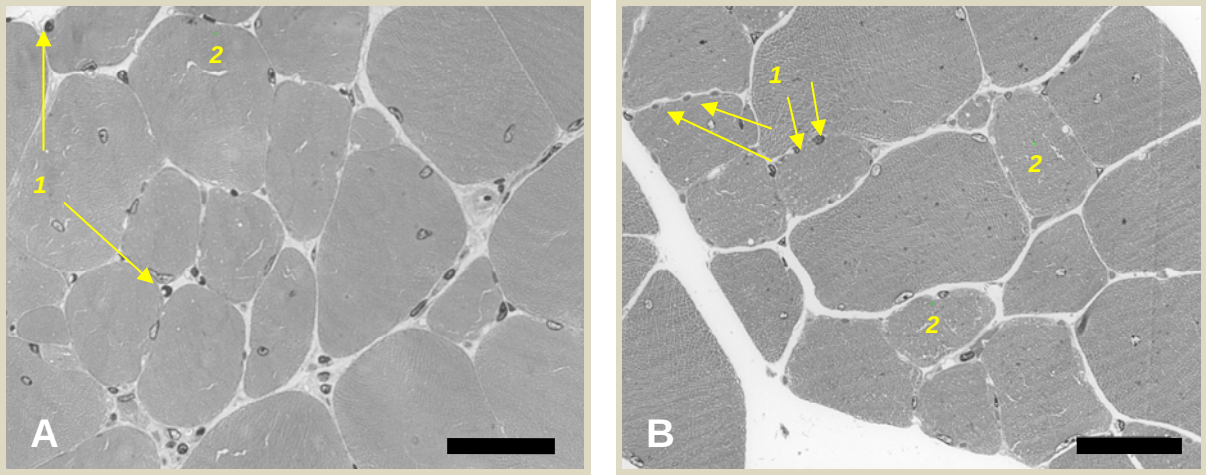

Figure 5.5.2: Quadriceps muscle sections from of the 27 week-old SJL/J group treated with resveratrol. Samples were stained with Toluidine Blue O and Gill's Haematoxylin, and display (A & B) capillaries surrounding and indenting fibers (1) and fibers which appear moth-eaten (2). Scale bars = 50µm

The presence of capillaries surrounding, and indenting fibers, (Figure 5.5.2 A and B, 1) was observed. A moderate (+ +) presence of fibers with a moth-eaten appearance (Figure 5.5.2 A and B, 2) was seen in this group. In general, fibers ranged from being intact (no incidence of dystrophic process in a specific microscopic field), healthy appearing cells with peripherally located nuclei to areas with multifocal lesions (+ +). Myonuclei in the central position of the fiber ranged from 1 to 3 nuclei per fiber with an occurrence of 31.6% in analysed quadriceps muscle samples. Evaluating from a qualitative point of view; more intact cells were detected in this group compared to the positive control group, who received only placebo.

Low CoQ10 group

A variation in fiber size was prominent, in the group of 27 week-old SJL/J mice, treated with a low concentration (40mg/kg/day) of CoQ10. Fiber diameter in this group ranged from 12.41 to 117.77µm as determined by minimal Feret's diameter. Groups of small fibers (Figure 5.6.1 A and B, 1) were frequently found. Dense connective tissue (Figure 5.6.1 A, 2) and mononucleated cells (+ +) (Figure 5.6.1 B, 2) were present in perimysial regions. Inflammatory incidence ranged from no inflammatory infiltrate (0) to mild (+) (Figure 5.6.1 A and B) and moderate (+ +) (Figure 5.6.1 C and D) changes in both perimysial and endomysial regions. Fibers ranged from being intact, healthy appearing cells with peripherally located nuclei to fibers undergoing necrosis (Figure 5.6.1 A, 3). Minimal infiltration of adipose cells (±) was observed (Figure 5.6.1 A, 4).

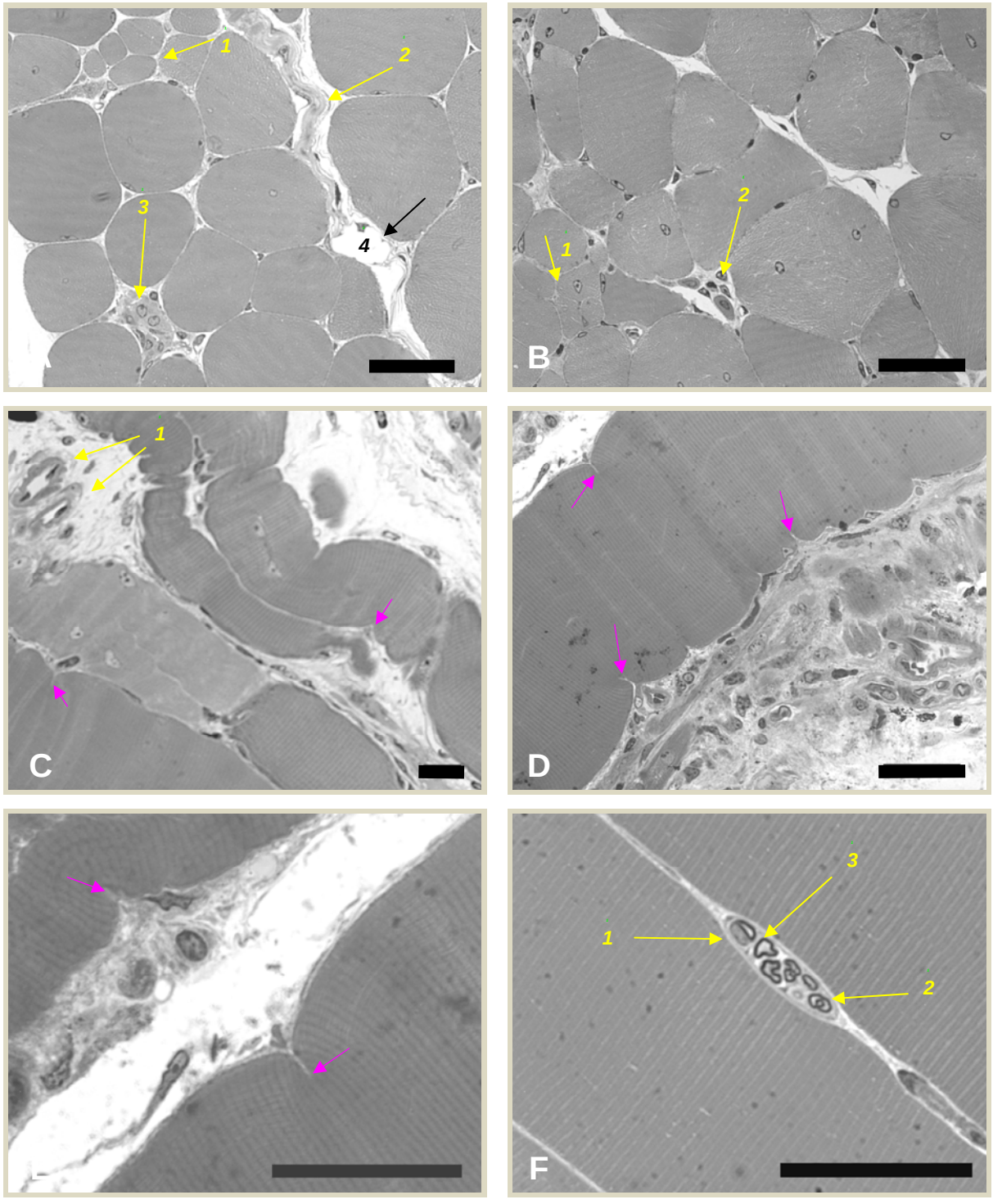

Figure 5.6.1: Quadriceps muscle sections from the 27 week-old SJL/J group treated with a low concentration of CoQ10. Sections were stained with Toluidine Blue O and Gill's Haematoxylin. A) Groups of small fibers (1) in a region with dense connective tissue (2) are present in perimysial areas. An ongoing necrotic process (3) and adipose infiltration (4) is present. B) A small group of two small fibers (1) are present with mononuclear cells (2) in the position where a fiber has undergone necrosis. C-E) Invaginations along the periphery of the fibers on a longitudinal section (pink arrows) are present. Blood vessels (C, 1) are present in the extracellular space. F) A nerve bundle (1) surrounded by a perineurium (2). Large meylinated fibers measuring up to 8µm in diameter probably represent proprioceptive afferents (3). Scale bars = 50µm

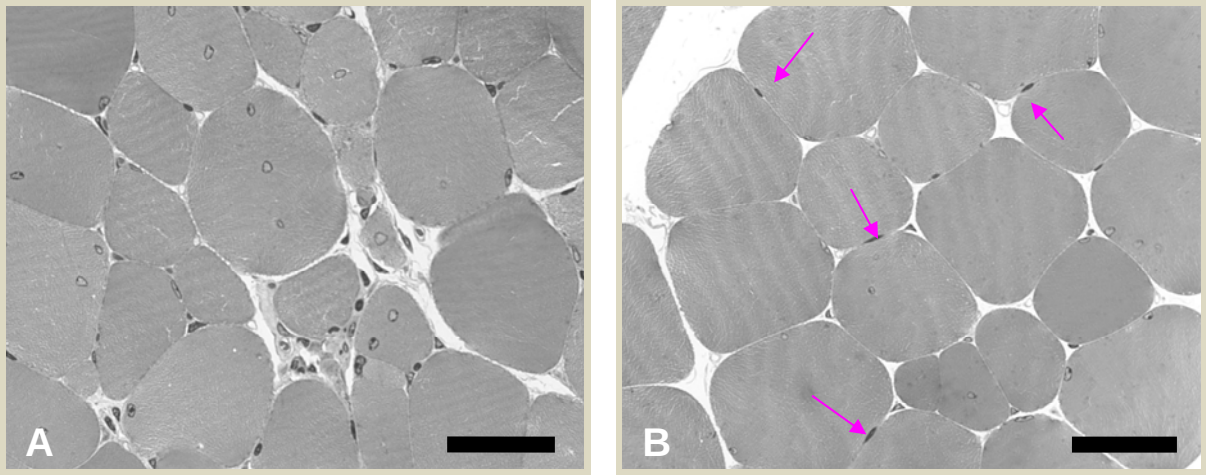

Figure 5.6.2: Quadriceps muscle sections from the 27 week-old SJL/J group treated with a low concentration of CoQ10. Sections were stained with Toluidine Blue O and Gill's Haematoxylin. A) Tissue from this group displays an incidence of 34.3% central nucleation. B) Nuclei, distinctly different in appearance from myonuclei, can be seen in this group, in intact fibers (pink arrows). The position of the nuclei fit that of satellite cells. Scale bars = 50µm

Longitudinal sections were mainly used as reference for orientation in the current study. Invaginations were observed along the periphery of the fibers (Figure 5.6.1 C, D and E, pink arrows) in some sections. These prominent indentations were of unknown origin, since no structure that could exert pressure to form the indentations could be detected in the vicinity. This incident was similar to that found in the 14 week-old group (Figure 5.3.2, C) and created the impression of fibers that are shrinking. Blood vessels (Figure 5.6.1 C, 1), dense connective tissue, and mononuclear cells were observed in the extracellular spaces of the endomysial regions in these sections. The specific incidence was observed in three different microscopic fields of one individual, while the other fibers appeared normal or necrotic in the longitudinal sections, but lacks these indentations. This observation remained to be further investigated on the ultrastructural level in chapter 6.

Nerve bundles (Figure 5.6.1 F, 1) with myelinated axons of Schwann cells were found quite frequently (+) in this group. Intramuscular nerves are seen in many muscle biopsies, but their presence as well as their orientation is a matter of chance. Intramuscular nerves are surrounded by a perineurium, a specialized structure made of flat cells with tight junctions (Figure 5.6.1 F, 2) (Carpenter and Karpati, 1984). Large myelinated fibers measuring up to 8µm in diameter probably represent proprioceptive afferents (Figure 5.6.1 F, 3) (Carpenter and Karpati, 1984).

Myonuclei in the central position of fibers (Figure 5.6.2 A) were found to be more abundant than in the resveratrol group, with an occurrence of 34.3%. Nuclei, distinctly different in appearance from myonuclei, were found in this group, in intact fibers (Figure 5.6.2 B, pink arrows). The position of the

nuclei fit that of satellite cells which are mononuclear cells found beneath the basal lamina of muscle fibers (Carpenter and Karpati, 1984). These cells are flat and somewhat elongated in the long axis of the muscle fiber. Their nuclei tend to contain darker clumped chromatin than myonuclei. When a muscle becomes necrotic, satellite cells are the source of the myoblasts (Figure 5.1) which regenerate the necrotic segment (Carpenter and Karpati, 1984). From a qualitative perspective; more intact cells were detected in this group compared to the positive control group samples (placebo), but less compared to the resveratrol group.

High CoQ10 group

Very little (±) (Figure 5.7 A) to mild (+) (Figure 5.7 B and C) and moderate (+ +) (Figure 5.7 D) degenerative and perimysial (Figure 5.7 B, C and E) inflammatory changes with endomysial involvement (Figure 5.7 A and D) were observed in animals treated with a high concentration (120mg/kg/day) CoQ10. As in the younger 14 week-old age control group, inflammatory changes, although more severe in this group, were found mostly in the perimysial regions where necrotic incidences (Figure 5.7 C and E, 1) could be detected.

A variation in fiber size was prominent, ranging from minimal Feret's diameter of 12.06 to 108.06µm (Figure 5.7 F). Nuclei in the central position of fibers were found in 22.9% of fibers analysed, which is distinctly lower than in the resveratrol and low CoQ10 groups. Markedly more myonuclei were detected in the peripheral position, and central nucleation was sparsely distributed in less and unaffected areas.

Numerous mononucleated cells (+) were present in infiltrate, indicating the presence of inflammatory incidence. Qualitative assessment indicated that fiber splitting (Figure 5.7 B and D, 1) occurred less frequently (±), compared to the resveratrol and low CoQ10 groups, and distinctly less frequently compared to the positive control group. Minimal adipose tissue infiltration (±) (Figure 5.7 D, 2) was seen in moderate (+ +) affected areas. Vacuolation (Figure 5.7 D, 3) were overall minimally (±) distributed in moderately (+ +) affected areas, while moth-eaten appearance (Figure 5.7 C, D and E, yellow asterisks) of cells was observed more frequently (+). No ring fibers were observed in the samples analysed from this group. A number of small capillaries were detected where they surrounded fibers, but did not indent them (Figure 5.7 A, B, C and E, white arrows). Nuclei, elongated, thin, and darkly stained, were also observed in the peripheral position in this group, in intact fibers (Figure 5.7 A, B, E and F, pink arrows). The position of the nuclei fit that of satellite cells. A number of nerve bundles located in the perimysial area were observed in some sections from this group (data not shown).

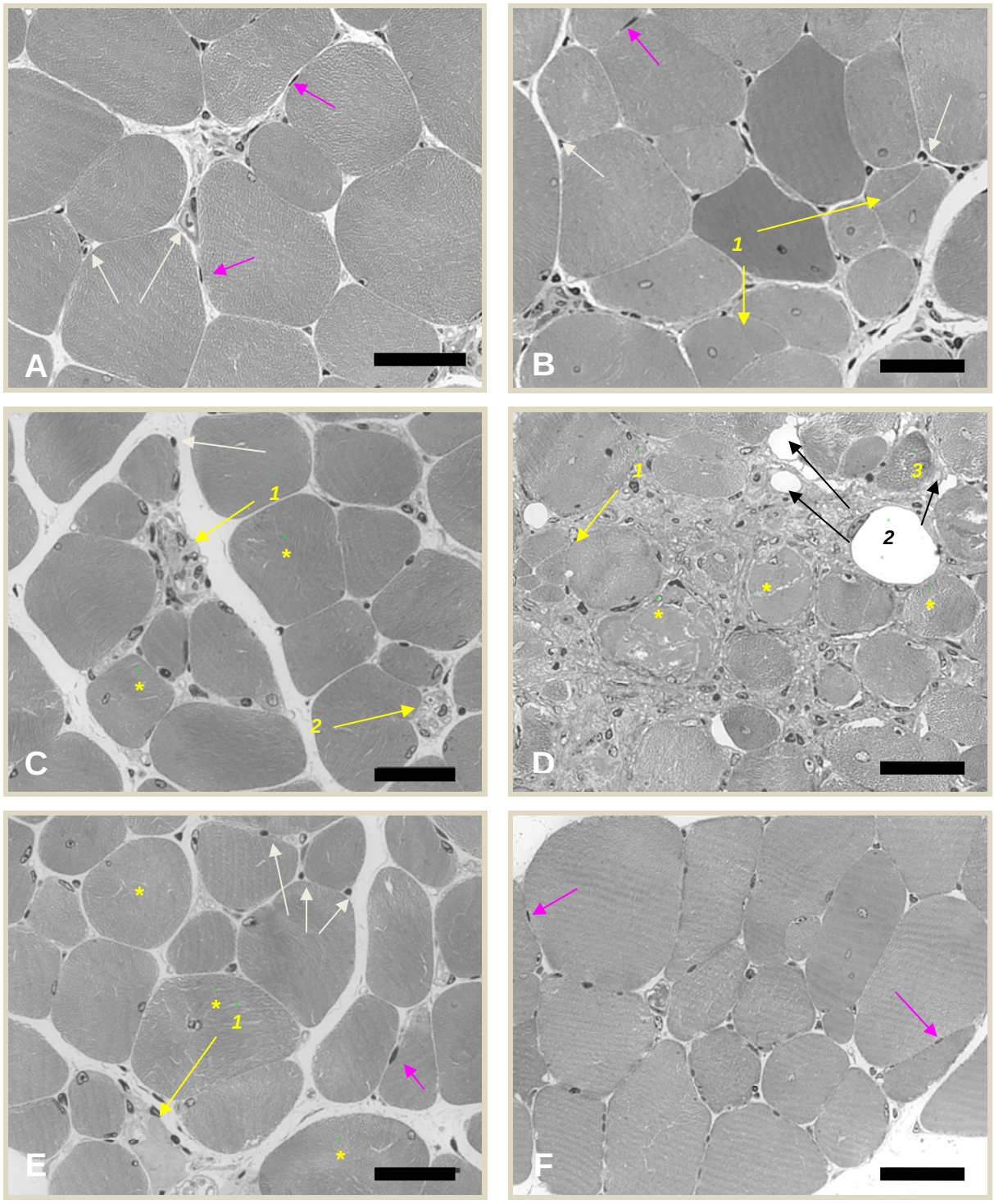

Figure 5.7: Quadriceps muscle sections from the 27 week-old SJL/J group treated with a high concentration of CoQ10. Sections were stained with Toluidine Blue O and Gill's Haematoxylin. Very little (A) to mild (B & C) and moderate (D) degeneration and perimysial (C & E, 1) inflammatory changes with endomysial involvement (A & D) are present. A number of small capillaries are present around fibers (white arrows). Fiber splitting (B & D, 1) is present, but less frequent. Mild adipose tissue infiltration (D, 2) is observed. Vacuolation (D, 3) is minimally distributed, while moth-eaten appearance (C, D & E, yellow asterisks) of cells is more frequent. F) Nuclei, distinctly different in appearance from myonuclei, are present (pink arrows; A, B, E & F). The position of the nuclei fit that of satellite cells Scale bars = 50µm

Resveratrol/CoQ10 combination group

Animals treated with a combination of resveratrol (60mg/kg/day) and CoQ10 (40mg/kg/day), showed minimal (±) (Figure 5.8 A and B) to mild (+) (Figure 5.7 C, D and E) degeneration and perimysial inflammatory changes with endomysial involvement (Figure 5.7 C, D and E). As in the high CoQ10 group, inflammatory changes were found mostly in the perimysial regions where necrotic incidences (± / +) (Figure 5.7 C and E, 1) could be detected extending into endomysial areas.

A variation in fiber size was prominent (Figure 5.8 A and B), ranging from minimal Feret's diameter of 13.17 to 108.10µm. Markedly more myonuclei were detected in the peripheral positions, and central nucleation was sparsely distributed (21.0% of all fibers analysed).

Numerous mononucleated cells (+) (Figure 5.8 C, D and E, yellow arrows) were present in affected areas. Fiber splitting (Figure 5.8 A, B and D, 1) occurred less frequently (±), compared to the positive control, resveratrol and low CoQ10 groups. Minimal adipose tissue infiltration (±) (Figure 5.8 D, 2) was observed. Ghost cells as a result of necrosis were detected (Figure 5.8 D, 3). Vacuolation (Figure 5.8 E, 1) was overall minimally distributed (±), while moth-eaten appearance (Figure 5.8 C and D, yellow asterisks) of cells was also markedly reduced compared to the findings in other groups. Ring fibers (Figure 5.8 E, 2) were observed in two samples of this group. The rings only affected part of the fibers, and did not form a complete ring. A few small capillaries were detected where they surrounded fibers. Elongated, thin, and darkly stained nuclei, that were possibly those of satellite cells were found in this group, in intact fibers (Figure 5.8 A and B, pink arrows), although in smaller numbers than in the high and low CoQ10 groups.

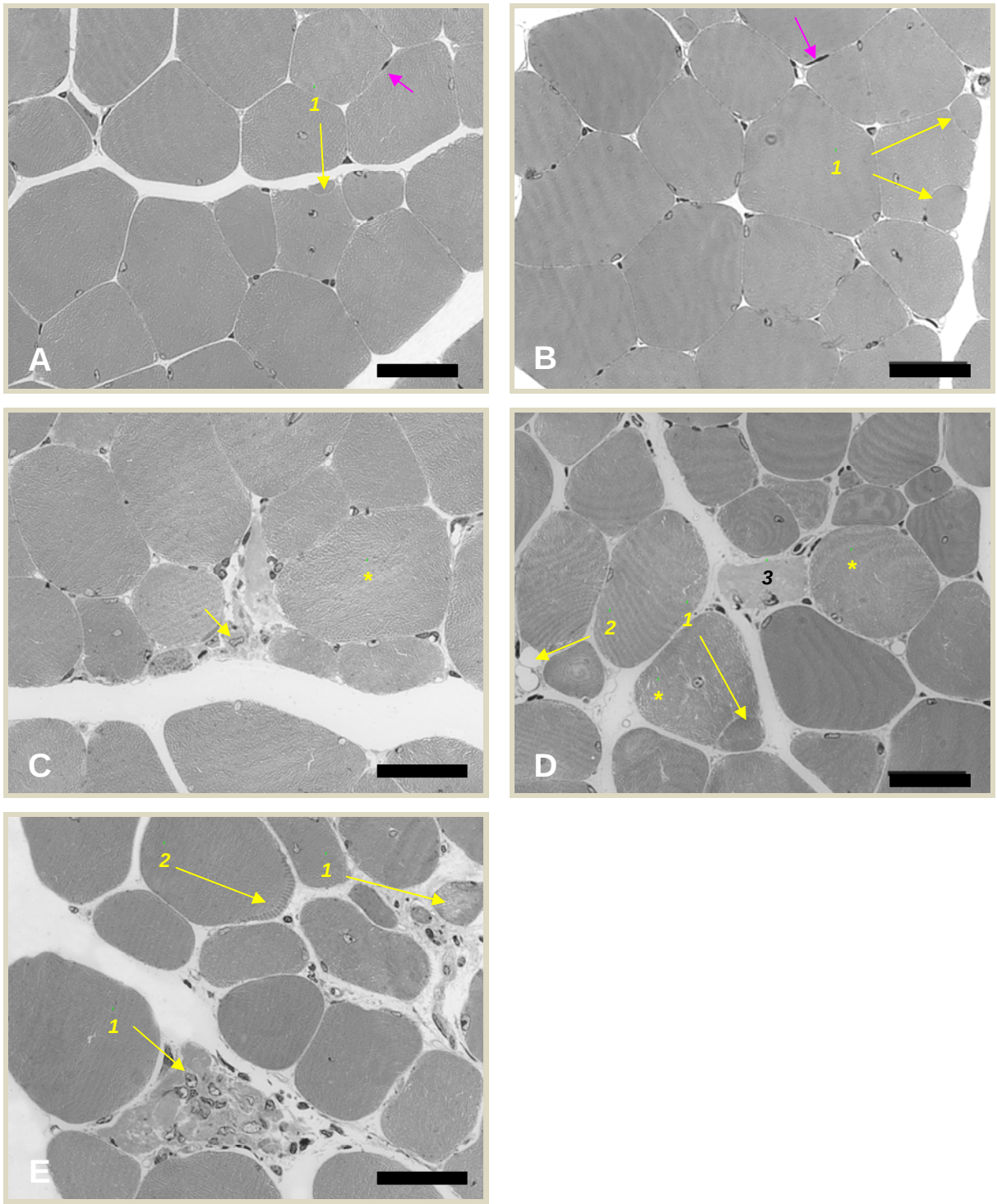

Figure 5.8: Quadriceps muscle sections from the 27 week-old SJL/J group treated with resveratrol/CoQ10 combination. Sections were stained with Toluidine Blue O and Gill's Haematoxylin. Minimal (A & B) to mild (C, D & E) degenerative and perimysial inflammatory changes with endomysial involvement (C, D & E) are observed in this group. Fiber splitting (A, B & D, 1) occurs less frequently. Minimal adipose tissue infiltration (D, 2) is present. Ghost cells as a result of necrosis (D, 3), vacuolation (E, 1), and moth-eaten appearance (C & D, yellow asterisks) of cells are minimally distributed. Mononucleated cells (C, D & E, yellow arrows) are present in affected areas. Ring fibers (E, 2) are observed, where it affected only part of the fiber. Nuclei, possibly belonging to satellite cells are observed in intact fibers (A & B, pink arrows). Scale bars = 50µm

Table 5.1 Summary and scoring of incidence of dystrophic processes in experimental groups

Age at termination (weeks)	27	27	27	27	27	14
Group / Changes	SJL/J Placebo	SJL/J Resveratrol	SJL/J (low) CoQ10	SJL/J (high) CoQ10	SJL/J Resveratrol + CoQ10	SJL/J No treatment
Fiber diameter range (µm)	11.82 – 99.01	10.12 – 117.90	12.41 – 117.77	12.06 – 108.06	13.17 – 108.10	15.98 – 112.34
% Central nuclei	35.4	31.6	34.3	22.9	21.0	8.8
Fiber splitting	+	+	±	±	±	±
Necrotic fibers / degeneration	+ +	+ / + +	+ / ++	+	± / +	±
Inflammatory infiltrate	+ +	+ / + +	+ / ++	0 / + / + +	+	±
Mononuclear cells (in extracellular spaces)	+ +	+	+ +	+	+	±
Ring fibers	Present	Present	Not detected	Not detected	Present	Not detected
Adipose infiltration	± / +	+	±	±	±	±
Vacuoles	+ / ++	+ / + +	+ / ++	±	±	±
Moth-eaten appearance	+ +	+ +	+ +	+	+	±
(**0**) = none; (**±**) = minimal; (**+**) = mild; (**+ +**) = moderate						

5.3.1.1 Necrosis

Necrosis was described by Carpenter, 2001 (a) as the death of a cell, where its inability to maintain homeostasis leads to its inevitable transition to debris. It is an irreversible phase during which the cell loses all function and viability (Carpenter and Karpati, 1984). Because of a muscle cell's multiplicity of nuclei, length and shape, it is possible for a segment of it to become necrotic while adjacent segments, termed stumps, survive (Carpenter and Karpati, 1984). Although a number of reports suggested that apoptosis can occur in skeletal muscle fibers, its status is not totally clear. At least in the cytoplasmic changes that accompany segmental death of a mature skeletal muscle cell, no distinction can be made between apoptosis and necrosis (Carpenter, 2001 a). Early stages of experimental necrosis, at the point where it begins, tend to show marked hypercontraction and tearing of myofibrils, resulting in a reticulated appearance (Figure 5.4.1, D).

Necrosis is often referred to as degeneration but this was thought to be an imprecise term that militates against exact pathological description (Carpenter and Karpati, 1984). Consistent with the literature (Kobayashi *et al.*, 2009), replacement of necrotic fibers by fatty (Figure 5.4.2, B) and fibrous (Figure 5.4.1, D) tissues was observed in the present study. Chiu and co-workers, 2009 have shown that reduced neutrophil recruitment in dysferlin-deficient muscle results in incomplete cycles

of regeneration. It was further reported that the inflammatory phase of muscle regeneration persisted beyond the stage where it was resolved in the control animals in their study. The team hypothesized that the persistent necrotic fibers provide foci for an ongoing inflammatory reaction, eventually directing cells towards a fibrotic fate.

The qualitative results of the present study suggest a reduction in necrotic incidence as well as in the amount of inflammatory foci in groups treated with the highest concentrations of antioxidants (high CoQ10 and resveratrol/CoQ10 combination groups) (Figures 5.7 and 5.8). These findings imply that the application of antioxidants interfere with the ongoing process responsible for initiation of necrosis, by an unidentified mechanism. It is nevertheless, tempting to speculate that the high dose antioxidants are most likely responsible for a reduction in metabolic disturbances, brought about by the ongoing inflammatory processes that were shown by Chiu's team. It is further suggested that these metabolic disturbances might also allow for accumulation of oxidative stress in the muscle, and that antioxidants scavenge these free radicals. This relief of oxidative stress insult will allow for the sufficient recruitment of anti-inflammatory cells, like neutrophils and macrophages. Thereby providing more effective clearance of necrotic fibers, and thus mediating more effective regeneration. The presence of oxidative stress in the SJL/J model will be further discussed in chapter 7 of the present study.

5.3.1.2 Inflammatory Infiltrate and the role of Macrophages

A study by Gallardo and co-workers, 2001, in patients with dysferlin-deficient dystrophy found that the predominant inflammatory cells were macrophages, which together with CD^{4+} T cells invaded degenerating fibers. True inflammatory cells are polymorphonuclear leucocytes, lymphocytes, plasma cells and monocytes (Carpenter and Karpati, 1984). Mononuclear cells seen in or around degenerative and/or necrotic muscle fibers of A/J and SJL/J mice was identified by Kobayashi and co-workers, 2009, as macrophages. Identification was based on their positive reaction for mouse F4/80 antigen, an antibody used to identify mouse macrophages.

Inflammatory cells which may be accompanied by increased fluid in the extracellular space (edema) may appear in muscle after various types of trauma or in inflammatory myopathies, (Carpenter and Karpati, 1984). Consistent with this statement, the findings of the present study revealed the presence of inflammatory cells surrounded by fluid, collectively termed inflammatory infiltrate in the present study, in and around fibers subjected to dystrophic changes Mitchell and co-workers, 1992, found the formation of new myotubes in SJL/J muscle after crush injury to be associated with efficient clearance of muscle debris by macrophages. Summan and co-workers, 2006, have shown

that clodronate liposome treatment, which targets mainly peripheral monocytes/macrophages result in a marked attenuation of the peak inflammatory response in injured muscle. Injured muscle was found to regenerate but the repair process was impaired by prolonged clearance of necrotic myofibers and a tendency for increased muscle fat accumulation (Summan *et al*., 2006).

Less inflammatory infiltrate was observed in muscle samples from the high CoQ10 and resveratrol/CoQ10 groups in the present study, compared to that observed in the positive control, resveratrol, and low CoQ10 groups.

5.3.1.3 Muscle Regeneration

Myogenesis involves the activation, proliferation and fusion (to form myotubes) of resident muscle precursor cells (myoblasts) that are normally quiescent on the surface of myofibres where they are termed satellite cells (Smythe *et al*., 2008). This process is tightly regulated by a complex interplay between various growth factors, and signalling and extracellular matrix molecules (Grounds, 2008). It involves a range of cell types including leukocytes, macrophages, and endothelial cells. Infiltration of damaged muscle by inflammatory cells is critical for the breakdown and removal of necrotic tissue, and when inflammation is prevented, the new muscle formation is impaired (Summan *et al*., 2006; Smythe *et al*., 2008; Chiu *et al*., 2009).

The ingrowth of new blood vessels (neovascularisation) is also required to support the process of new muscle formation (Smythe *et al*., 2008). The inflammatory and neovascular responses in injured skeletal muscle are dependent on changes in many components including the extracellular matrix (Grounds, 2008). The release of growth factors/cytokines from both muscle and non-muscle cell types (Smythe *et al*., 2008) promote these inflammatory and neovascular responses. A strong chemotactic response of leukocytes to skeletal muscle crush injury in SJL/J mice together with the weak response to uninjured muscle supported the concept that a local specific chemotactic factor is being generated at the site of injured muscle (Robertson *et al*., 1993).

Chiu and co-workers, 2009, identified a partial reduction in neutrophil recruitment associated with a reduction in macrophage recruitment in dysferlin-deficient muscle. This reduction in inflammatory response has been shown to cause a delay in clearance of necrotic fibers, leading to an ongoing inflammatory process, responsible for the dystrophic progression. In addition to its function in membrane repair, dysferlin has also been implicated in cytokine/chemokine release, following muscle injury (Chiu *et al*., 2009). Dysferlin deficiency is likely to be responsible for delayed regeneration of injured muscle fibers, resulting in the variation in fiber size observed in dysferlin-deficient muscle.

5.3.1.4 Small Fibers and Fiber Splitting

Small fibers may result from shrinkage or failure to grow, either primarily or after regeneration (Carpenter, 2001 a). Smallness refers to a reduced girth. An atrophic fiber can be regarded as a fiber measuring <20µm in diameter (Weller *et al.*, 1997), although not all fibers measuring <20µm are necessarily atrophic. The physiological, biochemical and molecular processes involved in storage and release of amino acids are collectively known as atrophy or wasting of muscle (Isfort, 2002). During atrophy, loss of a subset of proteins, including contractile proteins occurs (Isfort, 2002). Shrinkage is exemplified by the angular atrophic fibers of denervation, which tend to occur in groups (Carpenter, 2001 a). In diseases where necrosis is prevalent, as in the muscular dystrophies, small rounded fibers represent regenerants that have not been able to grow larger, because they do not have enough nuclei (Carpenter, 2001 a).

Fiber splitting refers to a group of small nested fibers with complementary contours (Figure 5.5.1, A 1) (Carpenter and Karpati, 1984). It might be debatable whether small fibers can result from longitudinal splitting of large fibers under normal conditions, but it is most probably the cause in the SJL/J mice, and more specifically dysferlinopathy (Figures 5.5.1, F; 5.6.1, A; 5.7.1, A). Split fibers are controversial. There is no consensus about their pathogenesis or even precise microscopic appearance. It has been suggested that hypertrophic fibers, due to a tendency towards structural abnormalities, might undergo fiber splitting (Carpenter and Karpati, 1984). Split fibers were frequently and without specific distribution, observed in all the groups in the present study. Carpenter and Karpati, 1984, described a split fiber as one which has a fissure extending from its periphery into its interior, consistent with what was seen on a transverse section in the present study (Figure 5.4.1, A, 1). Complete separation may result into what appear to be two distinct fibers whose contours are complementary to one another (Figure 5.7, B 1) (Carpenter and Karpati, 1984). The fissure may contain collagen and even a capillary. Some pathologists have been reported to use the term fiber splitting, as is the use in reporting the incidence in dysferlinopathy.

Four possible mechanisms have been suggested for fiber splitting or split fiber production (Carpenter and Karpati, 1984): Firstly, hypertrophied fibers under stress undergo actual cleavage, developing an invagination of the surface membrane which partially or completely divides them. A second possibility is the activation of satellite cells in the absence of muscle fiber necrosis. Thirdly, atrophic denervated fibers not only become angular but can present quite bizarre shapes. If such a fiber was reinnervated, and subsequently grew to a large size, it might assume a split appearance. A fourth mechanism appears to actually operate in producing small grouped nested fibers and forking. After necrosis the regenerating myotubes within a single basal lamina may fail to undergo lateral fusion

with one another, but they may fuse with the surviving stump, thus giving rise to a fiber with one or more forks (Carpenter and Karpati, 1984).

Totsuka and co-workers, 1998, suggested that splitting and/or fusion in dystrophic muscle may represent compensatory phenomena related to defective growth. From the current histopathology data it is more likely that the first mechanism proposed by Carpenter and Karpati, 1984, is involved in fiber splitting in dysferlinopathy. The large fiber size variation and a relative prominent shift towards fibers with a larger minimal Feret's diameter in SJL/J mice suggest that hypertrophied fibers under stress conditions may develop an invagination of the surface membrane. The invagination proceeds to complete separation, resulting in two or more small fibers. Totsuka and co-workers, 1998, showed that the summed area of post-splitting daughter fibers was almost the same as that of the parent fiber, indicating that the cross-sectional area is conserved after splitting. This statement is consistent with the split fibers observed in the present study. More than one mechanism might be involved. However, it has been shown that fiber splitting does not appear to be associated with loss of fiber content (Totsuka *et al*., 1998). Totsuka and co-workers therefore suggested that it may appear as a compensatory mechanism rather than a degenerative change. Discussion of the fiber size variation in SJL/J mice later in this chapter will provide more insight to this ambiguity.

5.3.1.5 Ring Fibers

A subset of the myofibrils, instead of extending parallel to the long axis of the muscle fiber, may be found circling or spiralling around the long axis (Carpenter and Karpati, 1984; Schotland *et al*., 1966). These structures have been termed ring myofibrils, spiral annulets, or ringbinden (Carpenter and Karpati, 1984), and they are not contraction band artefacts due to acid fixation or other cause (Schotland *et al*., 1966). Ring myofibrils are newly formed structures arising in muscle fibers which were normal, until their growth pattern was modified by the pathological process (Schotland *et al*., 1966).

The myofibrils in the center of such fibers tend to look normal. Sometimes the ring myofibrils may dip towards the center of the muscle and be sandwiched between normally oriented myofibrils. The fibers affected by the phenomenon are termed ring fibers (Carpenter and Karpati, 1984). The rings may be composed of a single myofibril, or more commonly can be 4 to 5 myofibrils thick. Occasionally much thicker rings may be found. Carpenter and Karpati, 1984, reported that elements of sarcoplasmic reticulum and T-tubules may be seen among the ring myofibrils and that mitochondria tend to be absent from them.

Affected myofibrils tend to be thinner than normal myofibrils (Carpenter and Karpati, 1984). Carpenter and Karpati, 1984 stated that ring fibers can be seen in the majority of myotonic dystrophy cases, and in over half of the cases of limb girdle dystrophy. It has been denoted conceivable that these structures are the result of disorderly myofibrillar protein synthesis or from a disorder of the cytoskeleton (Carpenter and Karpati, 1984). Bethlem and Van Wijngaarden, 1963 suggested that ring myofibrils may also branch from the ring, penetrate the muscle fiber and rejoin the aberrant myofibrils on the opposite side. This description correlates with what was termed snake coils, by Carpenter and Karpati, 1984. It was described to be represented by a braided appearance of the myofibrils on semithin resin sections and to occur in hypertrophied fibers in a variety of diseases, like denervation atrophy, and limb girdle dystrophy. A disorder of the cytoskeleton was suggested to be involved (Carpenter and Karpati, 1984).

Snake coils were found in the present study. Figures 5.4.2, A; 5.5.1 C, 2 and E, 1 showed that the myofibrils assume a streaming pattern, and appear distorted on semithin resin sections. This snake coil structures were also detected in fibers not displaying ring myofibrils on semithin resin sections (Figures 5.5.2 B,1 and 5.6.1 C2, and E1) in the present study. Schotland and co-workers, 1966, reported an electron microscopic study that confirmed the presence of peripheral circumferential ring myofibrils oriented in a plane at right angles to the muscle fiber. The presence of ring fibers in the dysferlinopathies has previously been described by others (Selcen *et al*., 2001; Comerlato *et al*., 2005; Pongpakdee *et al*., 2007; Liewluck *et al*., 2009). In the present study ring fibers have been identified, possibly for the first time, in the SJL/J mouse model (Figures 5.5.2 A, 1; 5.6.1 D, 1; 5.9 E, 2). Because of the rareness of these structures, it is impossible to draw any conclusions as to what role the administration of antioxidants in the present study could have or not have played in their formation and appearance.

5.3.1.6 Connective Tissue

Collagen is recognized to have several important functions as a structural component of all muscular tissues (Mayne, 1982). This connective tissue forms the linkages between the muscle and its associated connective tissues such as tendon or fascia. Collagen is the fibrillar component of the cell-to-cell connections which are present between individual muscle cells and between the muscle cells and neighbouring arteries, arterioles, veins, venules and capillaries (Figure 5.3.2 A and B) (Copenhaver *et al*., 1978).

Normally, so little collagen is present between muscle fibers that it is only visible by electron microscopy. An exception is in the region of neuromuscular junctions, where a small amount of

collagen tends to encircle muscle fibers (Carpenter, 2001 a). Muscle that has been severely damaged tends to show increased endomysial connective tissue (Figure 5.6.1 A, 2), usually in the form of tether, loose, randomly oriented collagen. In Duchenne and Becker dystrophy, the connective tissue proliferation, which begins to occur early, is distinctive, consisting of discrete dense bundles of collagen laid down parallel to the muscle fibers (Carpenter, 2001 a). This might be associated with irreversible joint contractures often observed in these patients (Carpenter, 2001 b). Carpenter, 2001 (a), reported that this pattern is also seen in some biopsies from patients with a limb girdle syndrome. In the present study, the finding of collagen parallel to muscle fibers (Figure 5.5.1 F,2) and in the endomysial (Figure 5.6.1 A, 2) regions in SJL/J mouse muscle, suggest the above findings by Carpenter, 2001 (a) are also true for the SJL/J dysferlinopathy animal model. The observation suggests that the excessive deposition of collagen in dysferlinopathies might also result in joint contractures seen in these patients at later stages of disease.

5.3.1.7 CAPILLARIES

Capillary density around some fibers has been shown to be increased in inclusion body myositis (Carpenter and Karpati, 1984). The number of capillaries in most cases of inclusion body myositis appears increased over normal. To some extent this increase reflects the atrophy and loss of muscle fibers. Other authors found fibers which appeared to have an excess of mitochondria to be indented by an unusually large number of capillaries (up to twelve) on cross section of inclusion body myositis samples (Carpenter and Karpati, 1984). The maintenance of higher vascularisation may be related to the frequent presence of ragged red fibers with abnormal mitochondria (Carpenter and Karpati, 1984).

Microvessel density has been shown to decrease with age in both, golden retriever muscular dystrophy (GRMD) dogs, and healthy control subjects (Nguyen F *et al*., 2005). Nguyen, F and co-workers, 2005 have demonstrated that fibrosis, the hallmark of muscle pathology in DMD boys and GRMD dogs, seems to be the major factor influencing mircrovascular architecture in skeletal muscles. The increasing extent of connective tissue correlated with lower microvessel density and longer intercappillary distance. This might create a physical barrier between the capillary contour and the myofiber membrane (Nguyen F *et al*., 2005). It is therefore a matter of concern that endomysial fibrosis might compromise intravascular therapeutic strategies performed in later stage muscular dystrophy.

In the present study, capillaries surrounding and indenting fibers that correlate with that found by Carpenter and Karpati, 1984, in inclusion body myopathy, were prominent in the 14 week-old SJL/J

mice (Figure 5.3.2 D). It was only minimally present in the resveratrol group (Figure 5.5.2 B, 1). Considering the prevalence of capillaries in the younger SJL/J mice, it is probably suggestive of higher vascularisation, associated with the increase in inflammatory incidence, and the higher demand of effective inflammatory cell transportation to the site of inflammation. It is furthermore possible, that as the inflammation starts to increase vascularisation is activated as compensatory mechanism in order to supply more immune cells to the site for more effective cleanup. The fact that fewer capillaries were observed in 27 week-old SJL/J mice suggest that this mechanism is less active after a certain age or disease stage. Smythe and co-workers, 2008, reported that the release of growth factors/cytokines from both muscle and non-muscle cell types are required for inflammatory and neovascular responses. It is therefore possible that older SJL/J mice lack sufficient chemotaxis for recruitment of these responses.

5.3.1.8 CENTRONUCLEATION

Displacement of nuclei from their normal subsarcolemmal position is the most common abnormality involving nuclei (Carpenter, 2001 a). Since semithin resin sections are so thin (1µm), they reveal far fewer nuclei than cryostat sections. Literature on histopathology in dysferlinopathy repetitively reports on nuclei detected in the central position of muscle fibers. While numerous reports suggested that nuclei in the central position of a fiber are indicative of regeneration, Totsuka and co-workers, 1998, reported that centronucleation is not a marker for regenerated fibers. Their team have demonstrated in dy/dy dystrophic mice that centronucleated fibers may otherwise be essentially normal.

Totsuka and co-workers, 1998, speculated that peripheral myonuclei may be restrained by the proximity of membranous structures in fibers. Central nuclei might therefore be more active than their peripheral counterparts, playing some important role in the growth and homeostasis of muscle. It is noteworthy that central nuclei (in general less than 1%) may also be observed in fibers of normal mammalian muscles (Totsuka *et al*., 1998).

In the present study, more than 35% of fibers analysed from the positive control group displayed nuclei in the central position of quadriceps muscle fibers, compared to the 0.8% of the negative control group, and 8.8% in the age control group (Figure 5.9). The numbers in the resveratrol and low CoQ10 groups compared with that of the positive control, at 31.6%, and 34.3%, respectively. The high CoQ10 and resveratrol/CoQ10 combination groups displayed markedly lower numbers compared to the positive control, resveratrol and low CoQ10 groups at 22.9% and 21%, respectively.

High levels of antioxidant supplementation in SJL/J mice have caused a decrease in the number of fibers with nuclei in the central position in quadriceps muscle.

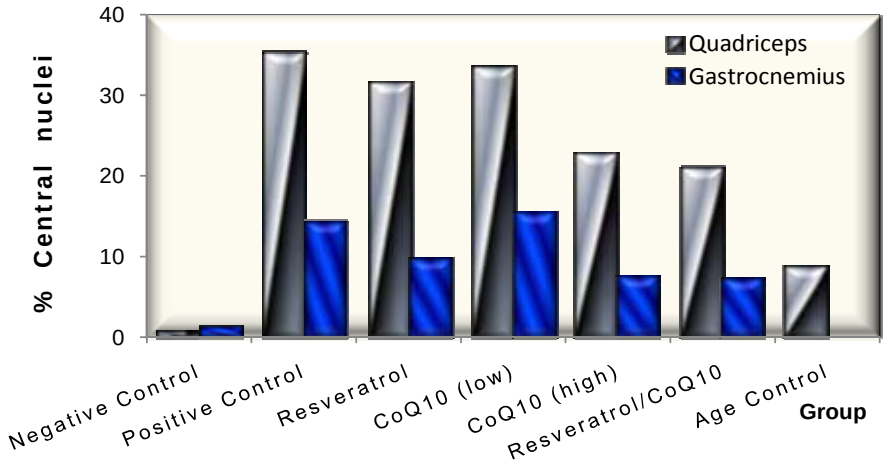

Figure 5.9: Percentage central nuclei in gastrocnemius and quadriceps muscle fibers.

Figure 5.9 shows the distinct lower number of nuclei in the central position of less affected gastrocnemius fibers from the same animals, compared to the quadriceps fibers. The highest numbers were found in the positive and low CoQ10 groups, at 14.4% and 15.5%, respectively. The resveratrol, high CoQ10 and resveratrol/CoQ10 combination groups displayed less than half this numbers.

From the present study, it can be suggested, that even if central nuclei is not a marker of regeneration, it is less frequent in muscle less affected by the ongoing dystrophic processes. It can be suggested that the mechanism responsible for centronucleation are affected by dysferlin-deficiency. From the results it is evident that high dose antioxidant supplementation in SJL/J mice, markedly reduces the manifestation of central nuclei in both quadriceps and gastrocnemius muscle fibers.

5.3.2 Morphometric Findings

Certain procedures such as measurement of the perimeter or the cross-sectional area of a fiber are mainly influenced by the plane of sectioning (Briguet *et al*., 2004). These authors described a method and provided reference values for the rapid, quantitative and reliable measurement of a relevant histological parameter of the dystrophic muscle in the mdx-mouse. The method relied on the determination of the muscle fiber size using the minimal Feret's diameter of a muscle fiber as seen in cross-section. The minimal Feret's diameter is a geometrical parameter that is frequently used for morphometric analysis (Nguyen F *et al*., 2005; Rouger *et al*., 2007; Grounds *et al*., 2008;

Steen *et al*., 2009), and is defined as the minimum distance between parallel tangents at opposing borders of the muscle fiber (Briguet *et al*., 2004).

Unlike other parameters to determine muscle fiber size, the minimal Feret's diameter parameter is very robust against experimental errors such as the orientation of sectioning angle (Briguet *et al*., 2004). Moreover, it reliably discriminates between dystrophic and normal phenotypes in a representative set of muscles.

The minimal Feret's diameter determined for all fibers of a specific muscle cross section were given as mean, minimum, and maximum, where the mean values were compared between groups for quadriceps (Figures 5.10 and 5.11) and gastrocnemius muscles (Figures 5.12 and 5.13), respectively. Measurements were also compared between the two muscles (Figure 5.14). Together with the percentage of fibers with centralized nuclei, this information is considered a reliable histological assessment of the pathology associated with dystrophin-deficiency (Briguet *et al*., 2004), and was therefore chosen for the quantitative component of the histological assessment of the pathology associated with dysferlin-deficiency in the SJL/J mouse model of the present study. A summary of the differences in fiber diameter is given in Table 5.3.

Comparison of Fiber Diameter in Quadriceps Muscle Fibers

An equal sample size of 500 measurements existed in each experimental group, therefore the assumption of equal variance was ignored. The parametric one-way ANOVA test could not be utilized to assess if there was any difference between the minimal Feret's diameters of experimental groups. The reason being the data did not assume a normal distribution. The fiber diameter of quadriceps muscle fibers was therefore compared via the non-parametric Kruskal-Wallis one-way test. This test revealed that a significant difference ($P < 0.000001$) existed between two or more of the compared six experimental groups (Figure 5.10). Tukey-Kramer Multiple Comparison tests were run, once again as *pos hoc* tests, in order to elucidate where this significant difference lay.

The age control group displayed a significant smaller mean minimal Feret's diameter compared to all the other groups. Fibers from the resveratrol group were significantly smaller in their diameter than that of the negative control group. The positive control and resveratrol groups' fibers displayed a significantly smaller mean minimal Feret's diameter compared to both CoQ10 groups. The diameter distribution (Figure 5.11) in both the CoQ10 groups displayed a peak size between 50 and 60µm, and thereafter a gradual extension of the skirt towards larger diameters, in contrast to the peak range observed in the positive control and resveratrol groups at 60 to 70µm and 40 to 50µm, respectively.

In the resveratrol group the percentage of fibers in the range larger than 50µm (≈56.1%) is proportional to the percentage of fibers smaller than 60µm (≈51.8%) in the positive control group. Although these two groups displayed very similar mean minimal diameters, the size tendency is towards different directions where the positive control fibers displayed a tendency towards a smaller fiber size, while the resveratrol group fibers displayed a tendency towards a larger fiber size. This might implicate that antioxidant supplementation with resveratrol facilitate the maturation of regenerated fibers.

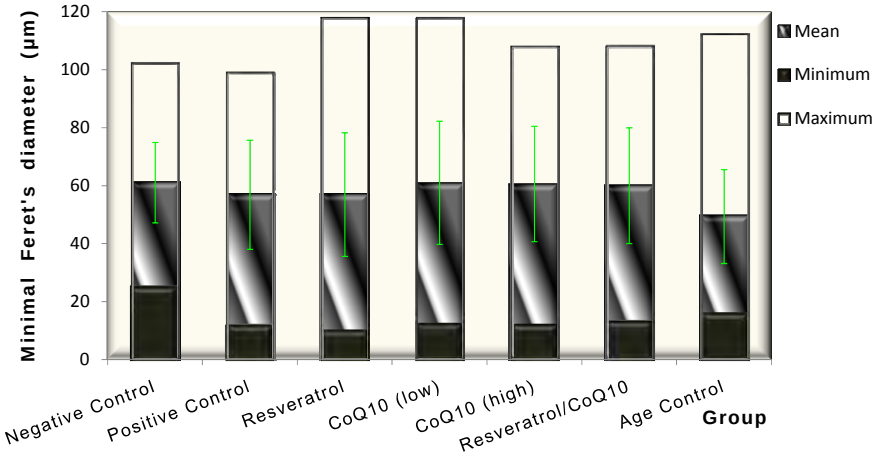

Figure 5.10: Minimum, mean (middle part of bars) and maximum minimal Feret's diameter of fibers measured in Quadriceps muscle tissue, with error bars representing the standard deviation (SD).

The resveratrol/CoQ10 combination group did not differ significantly in its mean minimal Feret's diameter to any other group, except the age control group. The data suggests a significant increase in mean minimal Feret's diameter of muscle fibers in quadriceps muscles of SJL/J mice from age 14 to 27 weeks. The small diameters in 14 week-old SJL/J mice is in relation to little disruption at the cellular level, as displayed by histopathology analysis (Figures 5.3.1 and 5.3.2), whereas the larger diameters in older SJL/J mice is in relation to a much disrupted phenotype at the cellular level of 27 week-old mice (Figures 5.4.1 and 5.4.2).

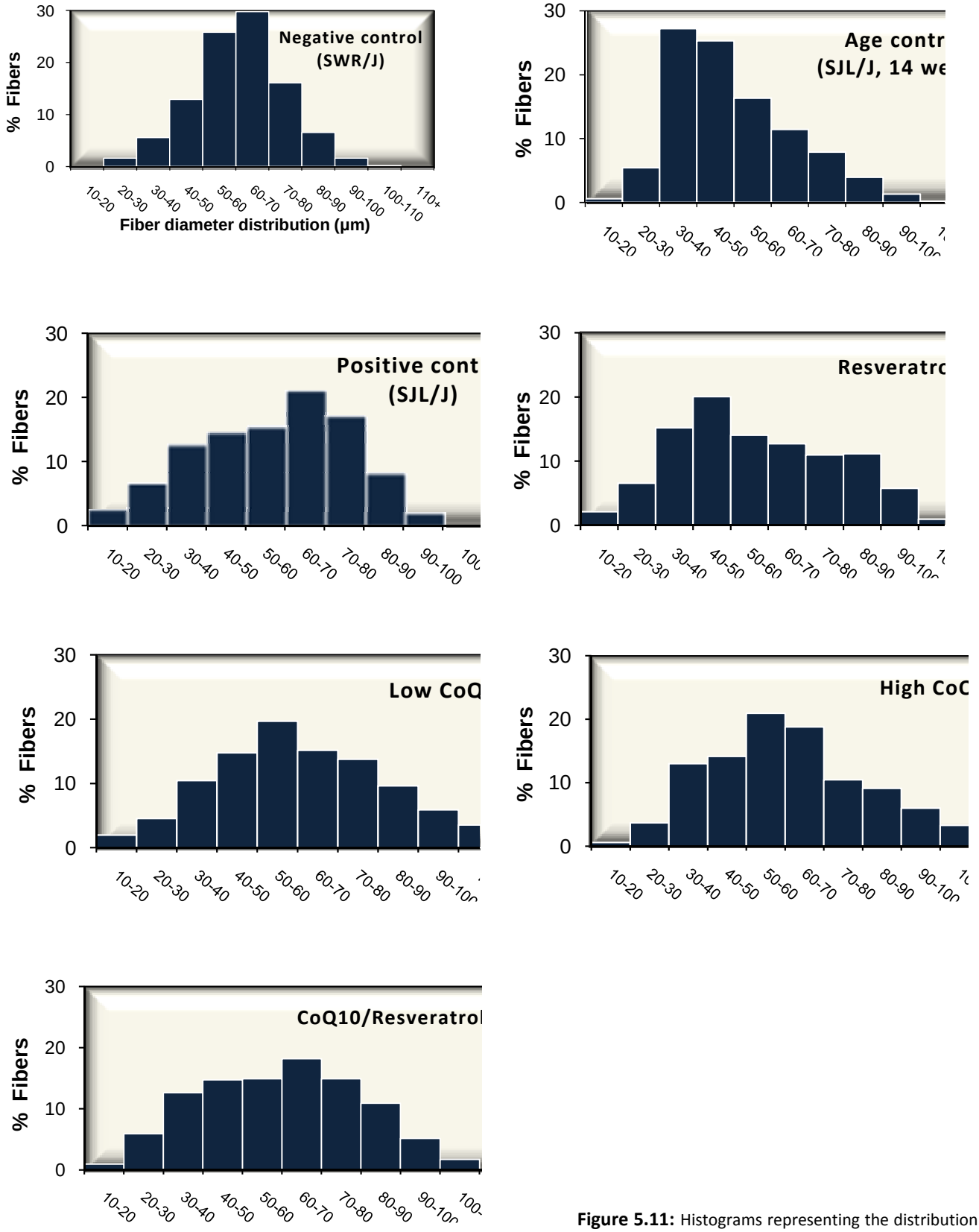

Figure 5.11: Histograms representing the distribution of mean fiber diameters in quadriceps muscles of experimental groups.

The data further suggests that the mean minimal Feret's diameter of all experimental groups treated with an antioxidant or combination thereof, did not differ significantly from that of the negative control group. However, in some groups (age control, resveratrol, low CoQ10 and high CoQ10) the fiber size distribution histograms (Figure 5.11) displayed a peak shift towards smaller fiber size, but with a larger number of fibers towards larger fiber sizes, compared to the positive control group. This observation strengthens the notion that antioxidant supplementation may afford maturation of regenerated fibers in older SJL/J mice.

Comparison of Fiber Diameter in Gastrocnemius Muscle Fibers

As equal sample size of 500 measurements, existed in each experimental group the assumption of equal variance was ignored. The parametric one-way ANOVA test could not be utilized to assess if there was any difference between the minimal Feret's diameters of experimental groups. The reason is the data did not assume a normal distribution. As a result, the gastrocnemius fiber diameters were compared via the non-parametric Kruskal-Wallis one-way test. This test revealed that a significant difference ($P < 0.000001$) existed between two or more of the six groups (negative control, positive control, resveratrol, low CoQ10, High CoQ10, and resveratrol/CoQ10 combination groups) compared (Figure 5.12). Tukey-Kramer Multiple Comparison tests were run in order to elucidate where this difference lay.

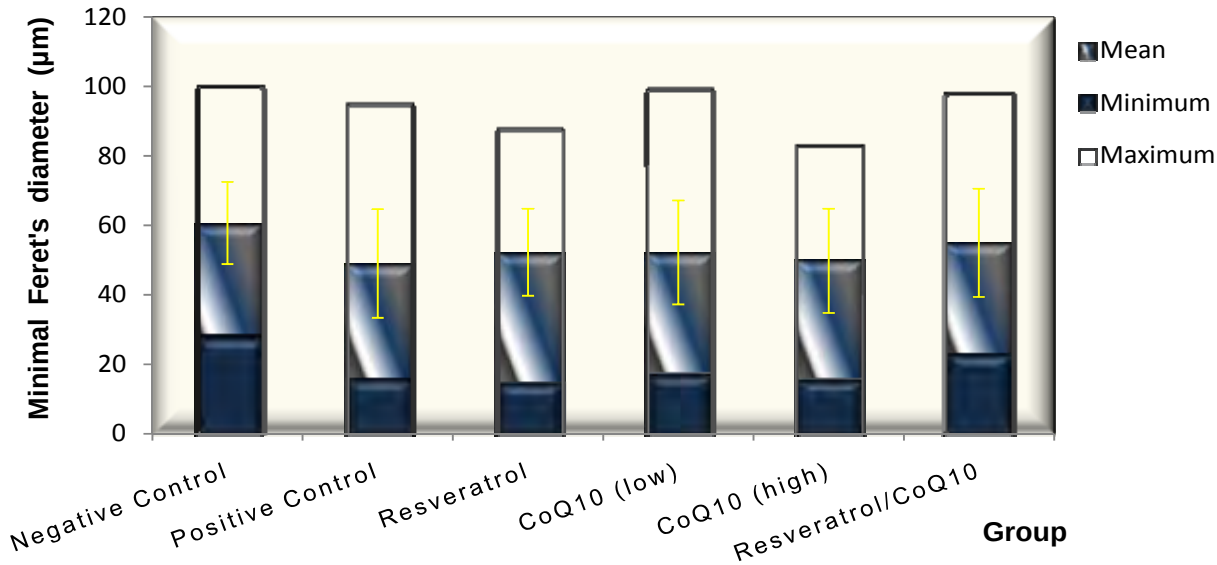

Figure 5.12: Minimum, mean (middle part of bars) and maximum minimal Feret's diameter of fibers measured in Gastrocnemius muscle tissue, with error bars representing the standard deviation (SD).

Mean minimal Feret's diameter in gastrocnemius fibers from the negative control group was significantly larger in comparison to all the other groups. When looking at the distribution of the data (Figure 5.13) in the negative control group, peak sizes occur at 60 to 70µm, with a rapid elevation of the skirt from smaller size towards the peak, followed by an even sharper drop towards larger diameters. The resveratrol group displayed the closest similarity in its fiber size distribution to the negative control group, with the exception of the peak shift towards 50 to 60µm.

The positive control group displayed a significantly smaller diameter to all groups except to the high CoQ10 group. Peak values in the positive control group were observed in the 40 to 50µm range, followed by a more gradual extension of the skirt towards larger diameters (Figure 5.13). The high CoQ10 group showed peak sizes in the 50 to 60µm range, followed by a very rapid and sharp drop towards a maximum of 80 to 90µm.

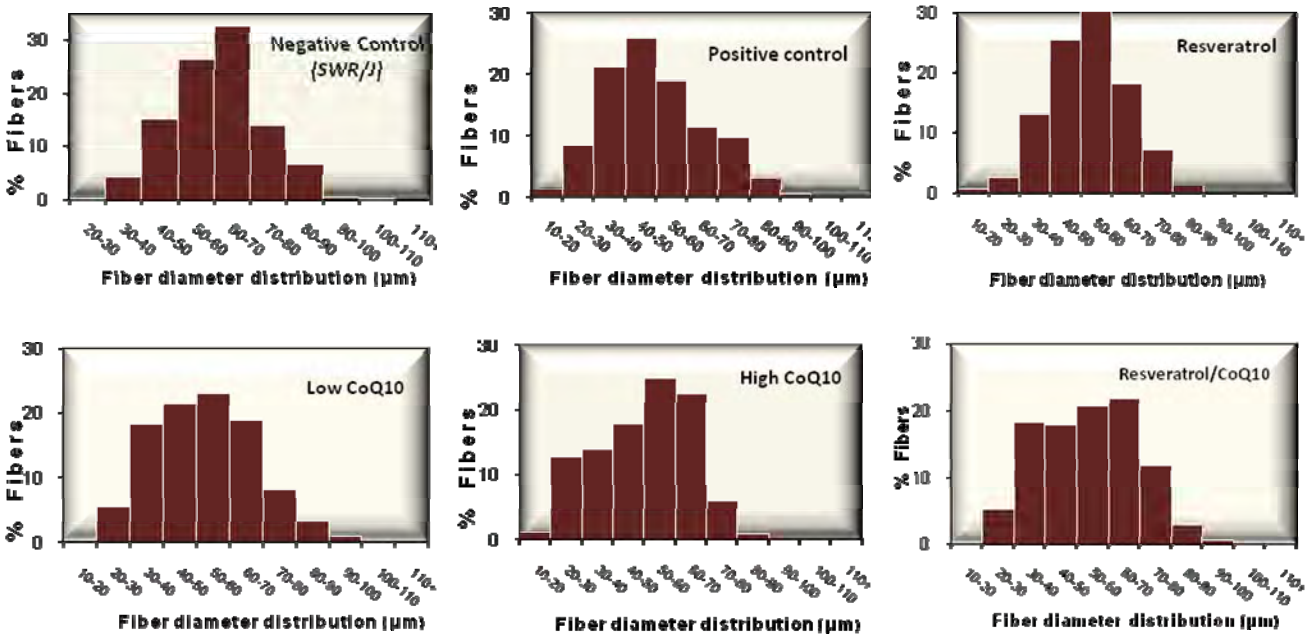

Figure 5.13: Histograms representing the distribution of mean fiber diameters of gastrocnemius muscles of experimental groups.

The increased proportion of fibers with diameters between 20 and 60µm in the high CoQ10 and resveratrol/CoQ10 combination groups were markedly different from that observed in other groups (Figure 5.13). The mean minimal Feret's diameter of the high CoQ10 group displayed significantly lower values than that observed in the resveratrol/CoQ10 combination group.

The values measured in the gastrocnemius muscle displayed closest similarity in mean minimal Feret's diameters to the age control group's quadriceps fibers. This observation suggests that the fiber condition in gastrocnemius muscle show similarity to that of quadriceps muscle in a younger phenotype.

Table 5.2 Summary of the mean minimal Feret's diameter of muscle fibers from gastrocnemius and quadriceps muscles, the diameter range, the amount of fibers analysed and the number of fibers that displayed central nucleation

Group	Quadriceps				Gastrocnemius			
	Mean minimal Feret's diameter ± SD (µm)	Number of cells measured	Number of central nuclei	Diameter range (µm)	Mean minimal Feret's diameter ± SD (µm)	Number of cells measured	Number of central nuclei	Diameter range (µm)
Negative control SWR/J mice	61.07 ± 13.85	504	4	24.81 – 102.19	60.65 ± 11.81	504	7	28.05 – 100.48
Positive control SJL/J, Placebo	56.90 ± 18.86	539	191	11.82 – 99.01	49.02 ± 15.64	514	74	15.68 – 95.21
Resveratrol	56.94 ± 21.31	519	164	10.12 – 117.90	52.25 ± 12.55	543	53	14.56 – 88.05
Low CoQ10	61.04 ± 21.21	508	174	12.41 – 117.77	52.20 ± 14.98	521	81	17.02 – 99.59
High CoQ10	60.63 ± 19.90	516	118	12.06 – 108.06	49.77 ± 15.03	500	38	15.5 – 83.47
Resveratrol/CoQ10 combination	60.02 ± 19.96	523	110	13.17 – 108.10	54.94 ± 15.57	574	42	22.81 – 97.87
Age control 14 week-old; SJL/J	49.38 ± 16.22	533	47	15.98 – 112.34				

Comparison of Fiber Diameter between Quadriceps and Gastrocnemius Fibers

The minimal Feret's diameter of gastrocnemius and quadriceps muscle fibers was compared within each group (Figure 5.14). The assumption of equal variance was ignored due to the comparison of equally sized samples. The parametric comparison test, the T-test, could only be utilized when comparing the different muscles' minimal Feret's fiber diameters in the negative control group as only in this situation did the assessed data assume a normal distribution pattern. In the case of all the other assessed groups, the data in one or both of the assessed muscle types did not assume a normal distribution and thus resulted in the non-parametric Mann-Whitney U test being utilized for comparison instead.

Table 5.3 Summary of the statistical comparison of fiber size between different groups and different muscles

Group		Morphometric findings (minimal Feret's diameter)				
		Quadriceps ($P < 0.000001$)		Gastrocnemius ($P < 0.000001$)		Quadriceps vs Gastrocnemius
		*Significantly **larger** than:*	*Significantly **smaller** than:*	*Significantly **larger** than:*	*Significantly **smaller** than:*	Quadriceps significantly larger than gastrocnemius in all groups, but the negative control
Control	**Negative Control (SWR/J)**	Age control, Positive control; Resveratrol	none	All groups	none	No significant difference ($P = 0.604177$)
Control	**Positive Control (SJL/J_27 weeks)**	Age control	Negative control; Low CoQ10; High CoQ10	none	Negative control; Resveratrol; Low CoQ10; Resveratrol/CoQ10	$P < 0.000001$
Control	**Age Control (SJL/J_14 weeks)**	none	All groups	none	Negative control	-
Experimental	**Resveratrol**	Age control	Negative control; Low CoQ10; High CoQ10	none	Negative control	$P = 0.006181$
Experimental	**Low CoQ10**	Age control; Positive control; Resveratrol	none	none	Negative control	$P < 0.000001$
Experimental	**High CoQ10**	Age control; Positive control; Resveratrol	none	none	Negative control; Resveratrol/CoQ10	$P < 0.000001$
Experimental	**Resveratrol/CoQ10 combination**	Age control	none	none	Negative control	$P = 0.000034$

For each of the other experimental groups the Mann-Whitney U test revealed that there was a significant difference between the two muscle types' fiber diameters (positive control group, $P < 0.000001$; resveratrol group, $P = 0.006181$; low CoQ10 group, $P < 0.000001$; high CoQ10 group, $P < 0.000001$; resveratrol/CoQ10 combination group, $P = 0.000034$)

The minimal Feret's diameters of quadriceps muscle fibers were in all instances found to be significantly greater than that of the gastrocnemius muscle fibers. This is consistent with the suggestion that gastrocnemius fibers are phenotypically similar to quadriceps fibers observed in the age control group.

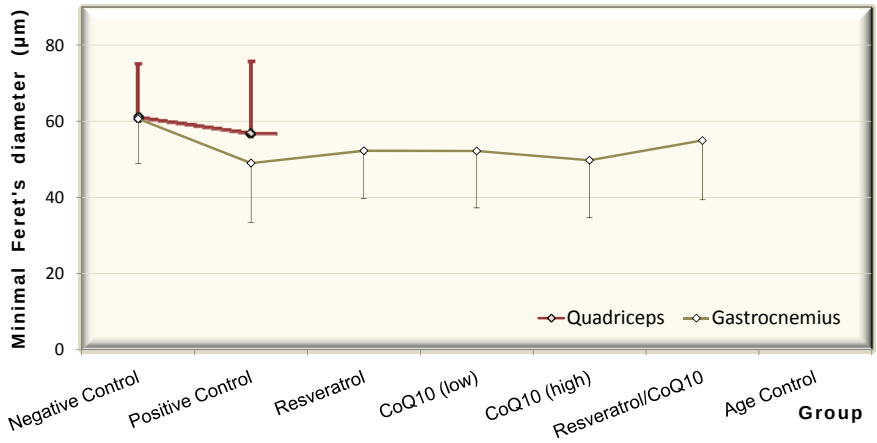

Figure 5.14: Relationship between mean minimal Feret's diameters measured in quadriceps muscle fibers and gastrocnemius muscle fibers. The error bars represent the standard deviation (SD).

5.3.3 Fiber Size

5.3.3.1 Variation in Quadriceps Muscle Fibers

The variation in fiber size was found to be the largest in the low CoQ10 and resveratrol groups, where variation is indicated by the range between minimum and maximum minimal Feret's diameter in a group (Table 5.2). A similar variation was observed in the age control group, although the minimum value was higher than that in older mice and the mean lower. The greatest number of fibers in the age control group displayed sizes smaller than 60µm (which is where fiber size in the negative control group peaked). The peak values occurred at smaller diameters in the age control group, while a very small number of fibers measured up to 110µm, and even larger. The reason for this could be that the active phase of the disease is setting in around this age, whereas muscle deterioration is not yet evident at cellular level. A low occurrence of fiber splitting was observed, and a large number of fibers were still in the process of maturation.

A stable fiber size distribution pattern was observed in the negative control group. The small variation in the negative control group indicates healthy, growing fibers. A larger proportion of fibers were found to be of intermediate size (peak values between 60 and 70µm), equally distributed between actively maturing fibers. The skirt of the histogram from the negative control group showed a firm but gradual increase towards the peak, and a slightly steeper, decline towards larger diameters (Figure 5.11). A very small number of fibers were larger than 100µm in diameter.

The small variation in the positive control group might indicate the disability of fibers to reach larger diameters because of the ongoing dystrophic process preventing maturation of myofibers. The continuous occurrence of fiber splitting observed from the histopathological picture in this group is contributing to this variation. From the histogram on fiber size distribution (Figure 5.11), it is clear that there is no tendency towards hypertrophy in this group, while a larger proportion of fibers displayed sizes smaller than the peak diameters. The tendency towards smaller diameter predominance in the positive control group can result from a combination of active regeneration with a lack of maturation, atrophy of fibers, and fiber splitting. When comparing the qualitative histopathology assessment of fiber splitting with the minimum minimal Feret's diameters over all the groups, it shows that the lower the incidence of fiber splitting, the higher the minimum diameter of fibers.

Fibers from both the resveratrol and low CoQ10 groups, showed a predominance towards larger fiber size compared to the positive and age control groups. The highest incidence of large fiber diameter, >110µm, was also recorded in these two groups. This data suggests that the application of antioxidant supplementation, afforded larger fiber diameters, suggesting that the antioxidants resveratrol and CoQ10 at low dose might afford fiber maturation after regeneration more effectively than in untreated groups. It is furthermore possible that the mechanism that is responsible for hypertrophying of fibers is stimulated by these concentrations of antioxidants.

The variation in fiber diameter in the high CoQ10 and resveratrol/CoQ10 combination groups showed a similar pattern to that of the negative control group. The proportion of fibers with diameters larger than peak values in these groups was larger than in the negative and positive control groups (Figure 5.11). This incidence is not indicative of a hypertrophic incidence as the maximum fiber diameters in the high CoQ10 and resveratrol/CoQ10 groups were found to be only slightly higher than that found in the negative control group (Figure 5.10), although in larger numbers. The observation suggests a more effective maturation of regenerated fibers, and perhaps a reduced occurrence of fiber splitting, consistent with the qualitative histopathology data.

The prevalence of maximum values is also slightly higher in the high CoQ10 and resveratrol/CoQ10 combination groups compared to the negative control group. These values were found to be still smaller than that in the resveratrol and low CoQ10 groups, indicating a lower hypertrophic tendency in the high CoQ10 and resveratrol/CoQ10 combination groups.

5.3.3.2 Hypertrophic Fibers

Paul and Rosenthal, 2002, formulated a definition for hypertrophy, where hypertrophy of skeletal muscle is defined as an increase in the size of fibers without an increase in their number, irrespective of any increase in the number of nuclei per fiber. Consistent with this definition, they have demonstrated that intrafascicularly terminating fibers are elongated in response to hypertrophic stimuli without an increase in fiber number (Paul and Rosenthal, 2002).

Fibers with large diameters (>110µm), although in small numbers, were observed, in addition to the age control group, also in the resveratrol, low CoQ10, high CoQ10 and resveratrol/CoQ10 combination groups. These values are indicative of the presence of a hypertrophic tendency. Hypertrophic skeletal muscle fibers are characterized by a cross-sectional area significantly increased above the normal range established for the age and sex of the individual (Carpenter and Carpati, 1984). Weller and coworkers, 1997, reported hypertrophied fiber in SJL/J mice to measure >100µm. Carpenter and Karpati, 1984, reported that hypertrophic fibres may be quite numerous in Duchenne dystrophy, even in areas where necrosis is not prevalent.

Maximum diameters in DMD may reach well over 100µm, and the mechanism of their production is likely to be analogous to that in experimental compensatory hypertrophy (Carpenter and Karpati, 1984). The primary stimulus to this hypertrophy is believed to be stretch exerted on the sarcomeres, rather than simple over activation of muscle fibers (Hall-Craggs, 1972, in Carpenter and Karpati, 1984). Carpenter and Karpati, 1984, stated that hypertrophic fibers have a tendency to exhibit architectural abnormalities, and that centrally situated nuclei are commonly seen in these fibers. Such fibers have also been found to reveal an increased incidence of apparent longitudinal splitting, and disorientation of myofibrils, like snake coil formations (Carpenter and Karpati, 1984). When a muscle fiber hypertrophies, the maintenance of the normal equilibrium between muscle volume to capillary ratio, requires a proportionate increase of perifiber capillary density (Carpenter and Karpati, 1984). If this adjustment of the capillary bed, required for normal metabolic functioning of the cell mass, is insufficient, it may lead to vulnerability of muscle fibers to ischemic damage (Carpenter and Karpati, 1984). Therefore, the incidence of moth-eaten appearance of fibers may occur especially in hypertrophic fibers due to the increased oxidative enzyme reactions (Carpenter and Karpati, 1984).

5.3.3.3 Variation in Gastrocnemius Muscle Fibers

A definite lower range of maximum diameters compared to that measured in the quadriceps muscle samples was recorded in gastrocnemius muscle samples (Table 5.2). Mean values were lower, while minimum values were higher than that measured in the quadriceps samples (Figure 5.14).

The resveratrol/CoQ10 combination group showed the highest similarity to the negative control group (Figure 5.12), with regard to the minimal, mean and maximum diameters measured. When comparing the distribution of size between these two groups (Figure 5.13), both showed peak values between 60 and 70µm, but the resveratrol/CoQ10 combination group showed an 'accumulation' of fibers (≈62.3% of fibers) sized between 20 and 60µm, while ≈45.8% of fibers were evenly distributed towards the peak size range in the negative control group. Although the variation (Figure 5.12) in the resveratrol/CoQ10 combination group showed high similarity to the unaffected group the size distribution histograms indicated that the fibers were affected by the disease.

Variation in fiber size of the positive control group's gastrocnemius muscles (Table 5.2) was similar to that of the age control group's quadriceps muscle, with the exception of larger maximum values in the age control's quadriceps. This indicates that gastrocnemius fibers show similarity to a younger phenotype, confirming that distal muscles in the SJL/J mice become affected later than the proximal muscles.

The antioxidant supplemented groups displayed a fiber size distribution where all peak values ranged between 50 and 60µm, with the larger proportion of fibers distributed towards smaller fiber size ranges. The resveratrol/CoQ10 combination displayed the same peak levels as the negative control group, with the exception of a larger proportion of fibers towards smaller diameters, following this combination of antioxidant supplementation.

5.3.3.4 From the Morphometeric Results

Collectively, the data suggests that antioxidant supplementation might direct muscle fibers' fate towards a more favorable state, whereas a larger number of fibers in supplemented groups displayed larger diameters than in the untreated groups. This might suggest that high dose antioxidant supplementation, by an undefined mechanism, is able to mediate fiber maturation after regeneration and perhaps the process of regeneration itself. A similar suggestion cannot be made for lower doses of antioxidants. The histopathology data from the resveratrol and low CoQ10 groups does not support the notion of more efficient regeneration or maturation, suggested by the fiber diameter distribution. In turn, fibers from these two groups displayed a hypertrophic tendency.

Collectively, these results suggest that the quadriceps muscles are more affected by the ongoing dystrophic process at the age of 27 weeks than the gastrocnemius muscles. Furthermore, it appears that supplementation with high levels of CoQ10 and resveratrol/CoQ10 in combination, afforded the least variation in quadriceps fiber size in SJL/J mice at 27 weeks of age.

5.4 Concluding Remarks

Bittner and co-workers found that the first histological changes could be observed as early as three weeks of age in the SJL/J mouse model. By seven months, the dystrophic changes include the appearance of fatty and fibrotic tissue, as well as inflammatory foci (Bittner *et al*., 1999). Proximal muscle groups were found to be primarily affected by these changes, whereas the distal muscles remained less affected (Bittner *et al*., 1999). It was therefore decided to analyse the quadriceps muscles of SJL/J mice for the cellular effect of antioxidant supplementation. Quadriceps was expected to represent the most reliable illustration of the condition. While muscle weakness can be detected as early as three weeks of age the greatest pathology occurs after 6 months of age (www.jax.org/jaxmice; Fox, 2007). Between different groups of 6 month old SJL/J mice, Weller and co-workers, 1997, found the percentage of individual animals with active disease to vary from 60% to 100%, averaging 78% of mice overall. It was therefore decided, in order to obtain a histological picture representative of full blown dysferlinopathy, to enter the animals in the present study into a 90-day trial at the age of 14 weeks, in order for them to display the greatest pathology by the termination date.

Histopathological data from the present study has confirmed that distal muscles are less affected and relatively spared in initial phases of the disease in SJL/J mice. The histological picture of the gastrocnemius muscle samples showed little to no dystrophic changes (data not shown), compared to samples from the quadriceps muscles (Figure 5.2 to 5.8). Fiber size variation in gastrocnemius fibers showed a shift towards that of a younger phenotype where all peak values ranged between 50 and 60µm, with the larger proportion of fibers distributed towards smaller fiber size ranges (Figure 5.14). A distinct lower number of nuclei in the central position were observed in gastrocnemius fibers (Figure 5.14).

Evident from the histopathological assessment of quadriceps fibers from 27 week-old SJL/J mice, is a constant influx of inflammatory infiltrate into tissue subjected to dystrophic changes. This finding is supported by the work of Chiu and co-workers, who reported an ongoing inflammatory reaction to be the result of attenuated muscle regeneration in dysferlin-deficient muscle that, together with a membrane repair defect, triggers dystrophic pathology. Consistent with this report, the present

study revealed a shift in fiber size predominance towards smaller fiber sizes in 27 week-old untreated SJL/J mice. The fiber size predominance accounted for a lack of fiber maturation in dysferlin-deficient muscle, resulting in incomplete regeneration in 27 week-old untreated SJL/J mice.

The minimal Feret's diameter parameter offers a useful tool for assessing fiber size variation in the muscle of SJL/J mice. In addition to this measurement, size distribution histograms provided more insight to the exact variation in the fiber size predominance than the mean minimal Feret's diameter alone.

A definite effect of antioxidant supplementation was observed when studying the histograms of quadriceps fiber size distribution (Figure 5.14). The findings provide evidence for the facilitation of fiber maturation in all antioxidant supplemented groups. Histopathological data showed that groups treated with the highest antioxidant concentrations (high CoQ10 and resveratrol/CoQ10 combination) displayed fewer split fibers, a factor influencing the fiber size variation. The fiber size distribution histograms for these two groups suggest that active regeneration occurred in these groups, followed by maturation of fibers towards larger fiber diameters.

In contrast to the untreated positive control group, muscle fibers of SJL/J mice supplemented with lower antioxidant concentrations tend to attain larger fiber sizes, with a tendency towards hypertrophy.

The number of nuclei found in the central position of muscle fibers, displayed a shift towards a lower percentage following supplementation with higher doses of antioxidants. This finding is supportive of an important role of central nuclei as a parameter for dystrophic progression in tissue analysis. Although it is yet to be discovered by what mechanism nuclei exchange their peripheral position for this central location in fibers of dystrophic muscle, it is nevertheless clear that high dose antioxidant supplementation, play a substantial role in altering this process.

Assessment of the histopathology showed, from a qualitative perspective, markedly reduced inflammatory insult in the more affected quadriceps muscles of animals treated with high doses of CoQ10 and a combination of resveratrol/CoQ10. An ongoing inflammatory reaction as the result of attenuated muscle regeneration in dysferlin-deficient muscle (Chiu *et al*., 2009), was markedly reduced. When taking the work of Chiu's team into account, collectively the findings of the present chapter allude to the ability of high doses of CoQ10 and resveratrol/CoQ10 in combination, to decrease the ongoing inflammatory process. The morphometeric analyses from these two groups

provide evidence strengthening the suggestion that a reduction in inflammatory processes resulted in more efficient muscle regeneration, followed by fiber maturation.

Investigation to the ultrastructural changes in SJL/J mice following antioxidant supplementation

6.1 INTRODUCTION

The assessment of muscle on the ultrastructural level has, according to Cenacchi and co-workers, 2007, a strategic position in improving the diagnostic accuracy of the histopathology not revealed by light microscopy. It gives insight into the pathophysiologic mechanisms and can guide molecular genetic analysis (Cenacchi *et al*., 2007). For effective analysis on the ultrastructural level, it is important to have a clear picture of the ultrastructural anatomy of mammalian skeletal muscle and the way the integrated components cooperate to produce function. It is moreover essential to have a sound understanding of the structure and functioning of healthy muscle in order to link alterations at the ultrastructural level to the pathology in a diagnostic approach. Therefore an overview of muscle ultrastructure and function are presented.

6.1.1 OVERVIEW OF SKELETAL MUSCLE ULTRASTRUCTURE

Myofibrils are the contractile structures of a muscle fiber (Figure 6.1). A sarcomere extends between two dark lines called the Z-discs. There are two types of protein filaments: the thick filaments, which are made up of myosin, and the thin filaments, which are made up of actin. The I-band is light coloured because it contains only actin filaments attached to a Z-line. The darker regions of the A-band contain overlapping actin and myosin filaments, while only myosin filaments are present in the H-zone (Mader, 2001). Surrounding the fibrils and accumulated near the nuclei are the remaining cytoplasmic components of the fiber, collectively called the sarcoplasm (Kelly *et al*., 1984). Each muscle contains a thousand or more myofibrils that occupy most of the intracellular volume, leaving little space for the sarcoplasm (Silverthorn, 2004).

Myofibrils

Each myofibril is composed of several types of proteins: the contractile proteins, myosin and actin, the regulatory proteins, tropomyosin and troponin, and the giant accessory proteins titin and nebulin (Silverthorn, 2004). Myosin is the protein that makes up the thick filaments of the myofibril. Each myosin molecule is composed of two heavy protein chains that intertwine to form a long coiled tail and a pair of heads. Two lightweight protein chains are associated with the heavy chain of each head (Silverthorn, 2004). In skeletal muscle about 250 myosin molecules join to create a thick

filament. The thick filament is arranged so that the myosin heads are clustered at the ends, and the central region of the filament forms a bundle of myosin tail.

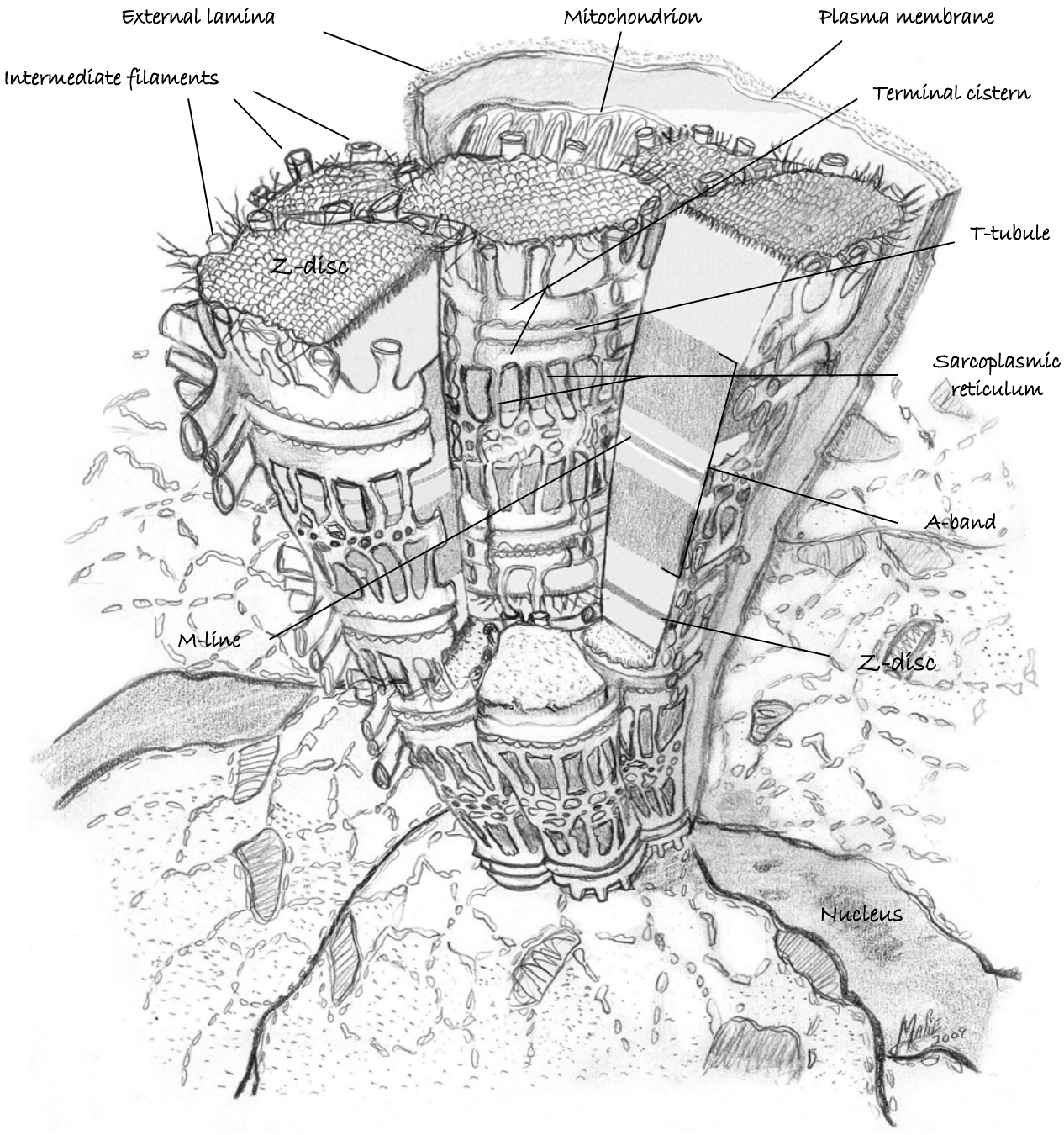

Figure 6.1: Schematic representation of the components in and around skeletal muscle myofibrils on an ultrastructural level. (Adapted from Kelly *et al*., 1984)

The rodlike portion of the thick filament is stiff, but the protruding myosin heads have an elastic hinge region where the heads join the rods. The hinge region allows the heads to swivel around their

point of attachment (Silverthorn, 2004). Actin is the protein that makes up the thin filaments of the muscle fiber. One actin molecule is a globular protein (G-actin). Multiple globular actin molecules polymerize to form long chains or filaments (F-actin). In skeletal muscle, two F-actin polymers twist together like a double strand of beads, creating the thin filaments of the myofibril (Silverthorn, 2004).

Myofibrils range from 1 to 2µm in diameter, but may be as small as 0.2µm (Kelly *et al*., 1984). In a cross section of a fiber the myofibrils are usually visible as punctuated densities with individual size and shape, separated from each other by narrow clear sarcoplasmic regions (Kelly *et al*., 1984). The arrangement of thick and thin filaments in a myofibril creates a repeating pattern of alternating light and dark bands (Silverthorn, 2004). One repeat of the pattern forms the sarcomere, which is the fundamental structural and functional unit of contraction in skeletal muscle (Kelly *et al*., 1984).

Sarcomeres

Each sarcomere is composed of smaller segments or 'bands' recognized by distinctive refractive differences (Kelly *et al*., 1984). The broad, darkly stained band is doubly reflective or anisotropic under polarized light, and is therefore known as the A-band (Kelly *et al*., 1984). At the outer edges of the A band, the thick and thin filaments overlap. The center of the A-band is occupied by thick filaments only (Silverthorn, 2004). The lightly stained band is relatively monorefringent or isotropic and is known as the I-band. Each of these bands is bisected by a narrow zone. It is dense in the I-bands and designated the Z-line or disc (from the German *Zwishenscheibe*, between disc) (Kelly *et al*., 1984). The portion of fibril between two successive Z-discs is a sarcomere. Its length in relaxed mammalian muscle is 2 to 3µm. It may be stretched to a greater length, and in greatly contracted fibers it may be reduced to about 1µm (Kelly *et al*., 1984). These zigzag structures are made up of proteins that serve as the attachment site for thin filaments (Silverthorn, 2004). The zone bisecting the A-band is pale and designated H (both from the German for light, *helles*, and the name of the discoverer, Hensen) (Kelly *et al*., 1984). The attachment site for the thick filaments, equivalent to the Z-disc for the thin filaments, is the M-line (from the German word for middle, *mittel*). An M-line divides one A-band in half (Silverthorn, 2004).

The sarcoplasm

The sarcoplasm is a complex assemblage of organelles which provides special structural and energetic support for the contractile apparatus, while also serving the general metabolic requirements of the living cellular system (Kelly *et al*., 1984). It includes an elaborate endoplasmic reticulum. This sarcoplasmic reticulum is a supportive framework of intermediate and finer filaments, microtubules, a golgi complex, variable amounts of mitochondria, few ribosomes,

glycogen and occasional lipid droplets (Kelly *et al*., 1984). The mitochondria of the muscle cell are found beneath the sarcolemma, around the nuclei, and in the sarcoplasm between the myofibrils. In this location, they are generally aligned with their long axis parallel to the direction of the myofibril. They may also be found encircling the myofibril transversely, particularly in the region overlying the Z-disc (Kelly *et al*., 1984).

The sarcoplasmic reticulum can be seen in electron micrographs as a network of cisterns or membranous tubules which run between and around the myofibrils (Kelly *et al*., 1984). It is an agranular reticulum because the relatively few ribosomes present are scattered through the cytoplasm and are not aligned on the membranes (Kelly *et al*., 1984). The cisterns run chiefly parallel to the myofibrils. Lateral anastomoses between the parallel or longitudinal cisterns form a perforated collar around the myofibrils at the level of the H-zone. In the vicinity of the I-band or Z-disc, the sarcoplasmic reticulum is expanded into terminal cisterns. These tend to be arranged into pairs which flank another, single membranous passage, the transverse tubule (T tubule) (Kelly *et al*., 1984).

T tubule system

The transverse tubular system or T system consists of numerous tubular invaginations of the plasma membrane (Ross *et al*., 2003). Each T tubule and its closely apposed two terminal cisterns constitute a triad. T tubules penetrate to all levels of the muscle fiber and show a triadic organization, accompanying terminal cisterns at the level of each A-I junction in mammalian skeletal muscle. T tubules provide two sets of tubules and terminal cisterns per sarcomere (Kelly *et al*., 1984; Ross *et al*., 2003). Their walls provide narrow tubular extensions of the cell membrane into the depths of the muscle fiber. Here they form complex membrane-to-membrane junctions with the membranes of terminal cisterns, within each triad. These are termed the triadic junctions or triadic couplings (Kelly *et al*., 1984). They contain voltage sensor proteins, depolarization-sensitive transmembrane channels, which are activated when the plasma membrane depolarizes. Conformational changes of these proteins affect gated Ca^{2+}-release channels located in the adjacent plasma membrane of the terminal cisternae (Ross *et al*., 2003). T tubules afford coordinated activity of all myofibrils as they serve for rapid transmission of impulses from the exterior to the deepest regions of the cell (Kelly *et al*., 1984).

Why an ultrastructural investigation?

Cenacchi and co-workers, 2007, described electron microscopy (EM) as an interesting tool for studying muscle pathologies. As a diagnostic tool, the main indication for EM is myopathies with

autophagic vacuoles, as it provides an understanding of pathological mechanisms of various muscular diseases and can even guide genetic analysis (Cenacchi *et al*., 2007). This chapter followed a qualitative investigation to the ultrastructure of SJL/J mice supplemented with the antioxidants CoQ10 and resveratrol for 90 days. Results are compared to that of the unaffected SWR/J strain as well as to that of 14 and 27 week-old SJL/J mice who received no antioxidant therapy. This chapter further elaborates on the light microscopic findings of chapter 5, as it focuses on the specific and non-specific ultrastructural changes that exemplify the dystrophic alterations in muscle tissue of the SJL/J mouse model. Electron micrographs were generated using transmission and scanning electron microscopy (TEM and SEM).

6.2 Materials and Methods

For ultrastructural analyses, quadriceps muscle samples (of all groups) were collected at termination. A small piece (± 1.5 x 2mm) of muscle tissue was dissected out from the belly area of the quadriceps muscles. Tissue samples were immediately fixed in 2.5% glutaraldehyde (SPI Supplies, West Chester, PA) and 2.5% formaldehyde (Merck) in 0.075 M phosphate buffer, pH 7.4 at room temperature, overnight. The tissue was removed from the fixative, rinsed thrice, 10 min each, in 0.075 M phosphate buffer. Tissue was then post-fixed in a 0.5% aqueous solution of osmium tetroxide (OsO_4) (SPI Supplies, West Chester, PA) for one hour. Thereafter, osmium tetroxide was removed and tissue was rinsed thrice, 10 min each, in 0.075 M phosphate buffer. Tissue was then serially dehydrated in 30%, 50%, 70% and 90% ethanol, followed by three changes of absolute ethanol for 15 min per dehydration step. For TEM analyses, tissue was then infiltrated with 30% Quetol (SPI Supplies, West Chester, PA) in ethanol for one hour, thereafter it was infiltrated with a 50% Quetol in ethanol solution for one hour. Finally tissue was infiltrated in 100% Quetol for a minimum of four hours. Immediately after infiltration, tissue was embedded in 100% Quetol epoxy resin (Van der Merwe and Coetzee, 1992) and polymerized for 39 hours at 60°C. Ultra thin serial sections (at an estimated thickness of 90nm each) were cut with a Reichert-Jung Ultra Cut E ultramicrotome (Vienna, Austria), and collected on copper grids. Tissue sections were contrasted for 10 min in 4% aqueous uranyl acetate in the dark and rinsed thrice in distilled water before it was contrasted for 5 min in Reynolds' lead citrate (Reynolds, 1963), thereafter it was rinsed again, three times in water. Samples were analysed with a JEOL JEM-2100F transmission electron microscope. All measurements were made with the aid of the Olympus iTEM analySIS software imaging system. Diameter was given as minimal Feret's diameter for any measured structure.

Muscle tissue samples from quadriceps belly area for SEM studies were dissected and fixed in the same way as for TEM analyses above. After the third dehydration step in absolute ethanol, samples

were stored in absolute ethanol until it was dried by critical point drying with liquid CO_2. Thereafter, samples were mounted and vaporized with ruthenium tetroxide (RuO_4) for one hour. Samples were analysed using a ZEISS ULTRA plus FEG SEM at 1kV.

Freeze-substitution

Small samples (0.2 x 1.2mm) were dissected from fresh tissue and mounted in hexadecene in a planchette. This was high pressure frozen using a Leica EM Pact II high pressure freezer. The samples were freeze substituted with acetone containing 1% OsO_4 using a Leica AFS2 freeze substitution unit. After substitution the samples were infiltrated and embedded with epoxy resin as for the chemically fixed material.

6.3 Results and Discussion

6.3.1 Ultrastructural Observations with TEM

The ultrastructure of quadriceps muscle from all the groups in the present study was assessed for specific and non-specific alterations. General morphology is shown in Figures 6.2 to 6.9, below. Different magnifications, as indicated by the scale bars, were utilized to visualize the structures of interest. SEM is a method for high-resolution imaging of surfaces that allow for very high magnification and greater depth of field (Denk and Horstman, 2004). Electron micrographs obtained with SEM analysis, provided insight on the surface structure of samples. Electron micrographs obtained by SEM analysis are presented in Figures 6.10 to 6.13, below.

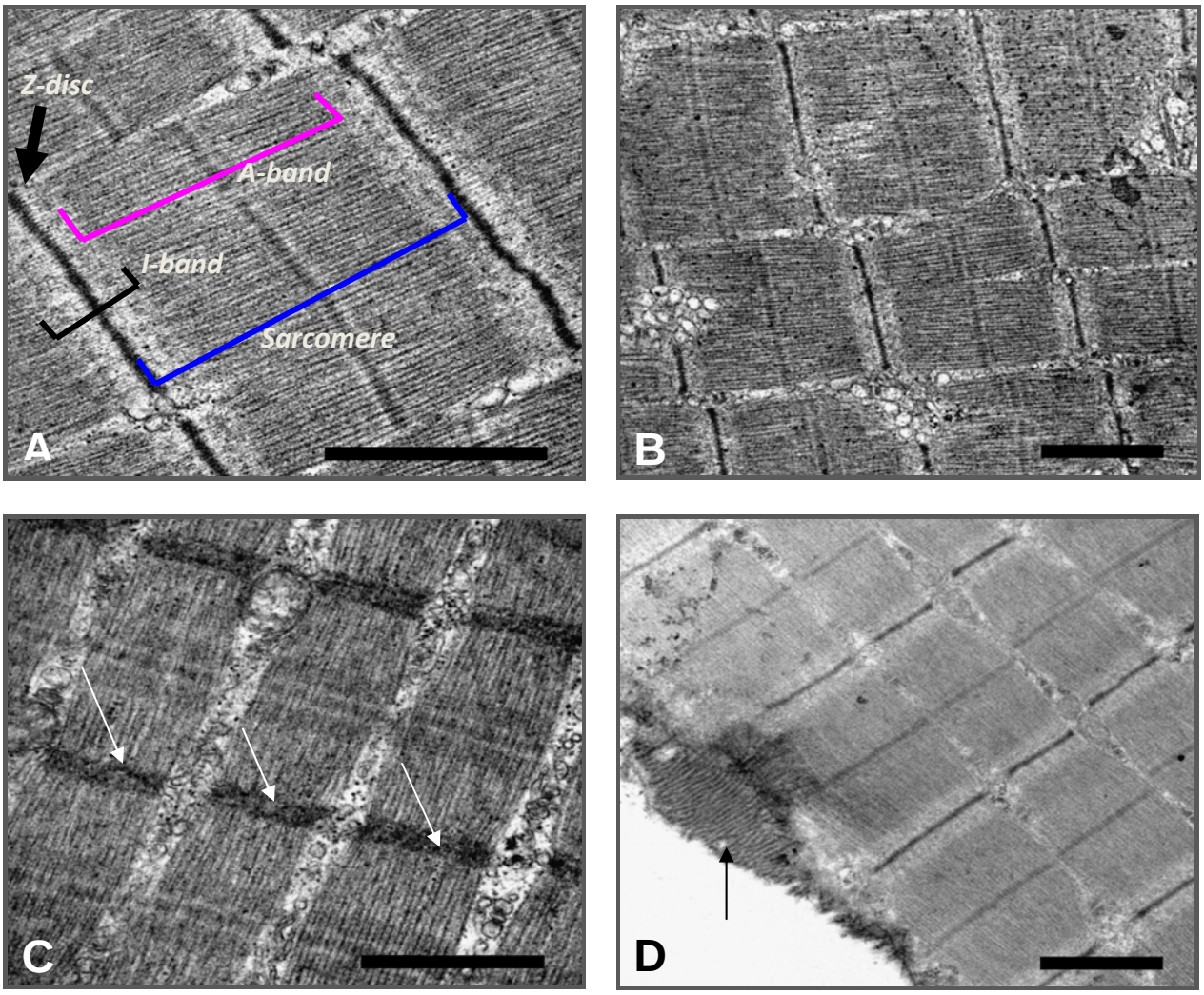

Figure 6.2: Electron micrographs from the negative control, SWR/J mice at 27 weeks of age that received placebo. A) Sarcomere and associated components. B) Small vacuoles between normal myofibers. C) Z-discs appeared thicker (arrows). D) Normal sarcomeres, with collagen fibers close to the periphery of the muscle fiber (arrow). Scale bars = 1µm

Negative control group

No structural abnormalities were observed in the 27 week-old SWR/J mice. Electron micrographs from this group (Figure 6.2) showed normal sarcomeres (A). Small bundles of vacuoles were seen in the Z-disk region. Generation of membranous structures are in response to normal membrane repair (Engel and Franzini-Armstrong, 2004). Mitochondria in this group displayed normal distribution between myofibrils at the level of the Z-disc, and in the subsarcolemmal position (B). Inner and outer mitochondrial membranes were found to be intact. Myofibrils in (C) displayed Z-discs that appeared slightly thicker than normal with no I-bands visible. It is expected that the muscle sample was possibly in contracting state upon fixation. Normal myofibrils (D) revealed normal sarcomeres with normal distribution of Z-discs, I-bands and A-bands. A small collagen bundle was observed on the periphery of the fiber in micrograph (D).

Figure 6.2 showed the distinct muscle tissue banding pattern corresponding to criteria for normal morphology. The Z-discs, A-bands, and I-bands are running at right angles to the long axis of the myofibrils. Sarcomeres were present in well defined units, and myofibrils aligned in an orderly manner. No abnormal distribution or dilatation was observed in the sarcoplasmic reticulum or the T-tubule systems. The plasma membranes appeared to be intact, with no vesicles observed in the subsarcolemmal position.

Age control group

Relatively large mitochondria were present in the subsarcolemmal position (A) of samples from the age control group, SJL/J mice at 14 weeks of age that received no treatment (Figure 6.3). Cristae were visible inside mitochondria, in addition to small spaces that appeared optically empty. This observation may be due to degenerative changes. In the same micrograph (A) small vacuoles, similar to that seen in the negative control group were seen. Vesicles accumulating under the sarcolemma were observed.

Any abnormal space or cavity in a muscle fiber may be considered a vacuole (Carpenter and Karpati, 1984). In Figure 6.3 (B), vacuoles that appeared optically empty were present. These vacuoles showed an irregular periphery, and they could be expected to be derived from mitochondrial vacuolation. Between these vacuoles, mitochondria with similar shapes as the vacuoles were observed. A tubular structure (B, arrow) was observed in the same area. Inside these mitochondria, dense cristae were visible (C). Cristae showed normal distribution, in relatively large mitochondria found in the intermyofibrillar position. Vacuole formation was observed in some mitochondria (D).

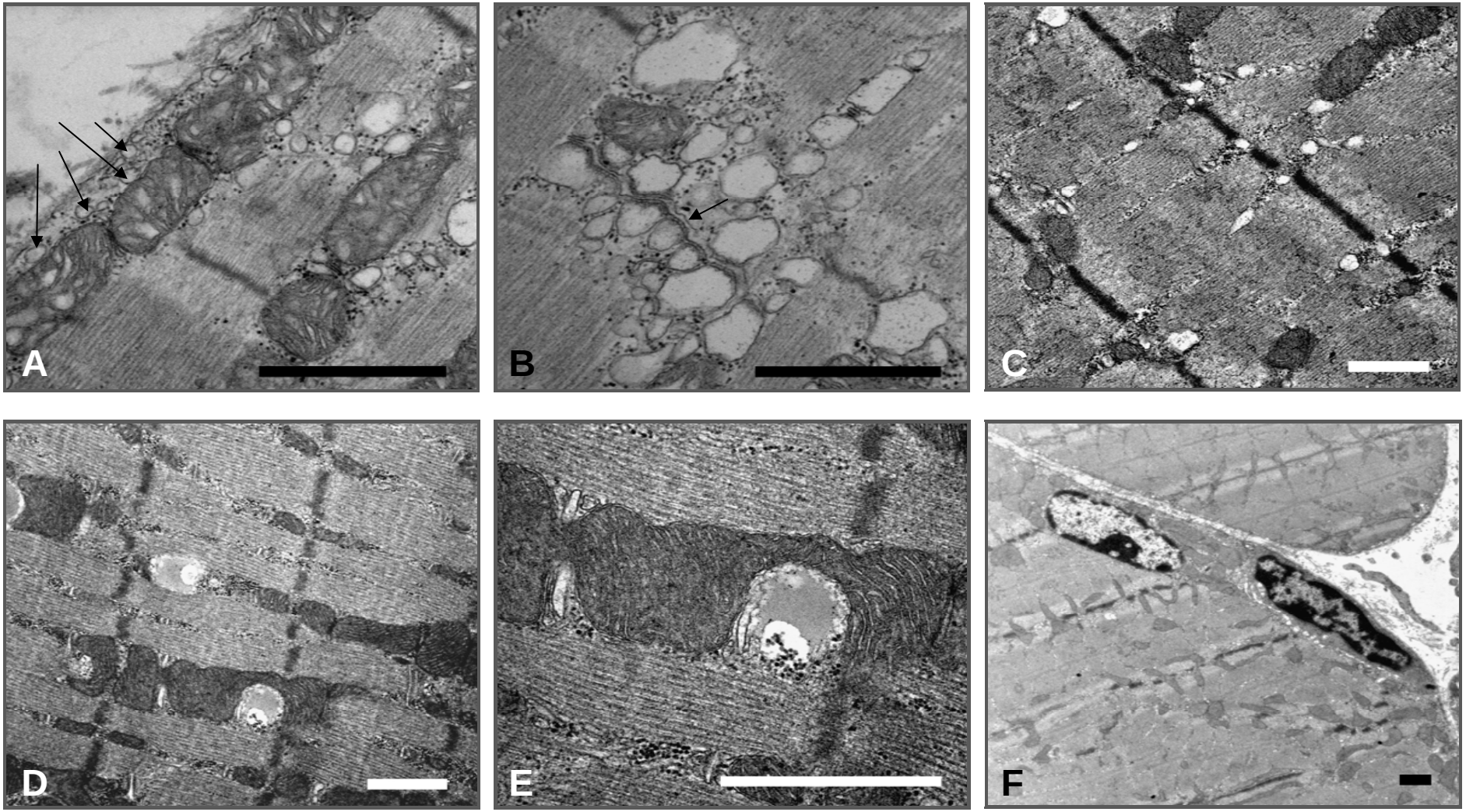

Figure 6.3: Electron micrographs from the age control group, SJL/J mice at 14 weeks of age that received no treatment. A) Mitochondria in the subsarcolemmal position and between myofibrils. The arrows point to vesicles accumulating under the sarcolemma. B) Empty vacuoles in a Z-disc position. The arrow point to a tubular structure in the region. C) Prominent Z-discs in healthy appearing myofibrils, intercepted by the presence of small vacuoles. D & E) Vacuoles between mitochondria. F) A myonucleus (left) and satellite cell (right). Scale bars = 1µm

At higher magnification (E) the vacuole in (D) appeared to have formed as a result of degeneration of a mitochondrion. On closer investigation it was established that the boundary of the vacuole was a double membrane structure, that of the mitochondrion. It was therefore evident that the mitochondrion was positioned around the vacuole and not invaded by it. In addition, no degenerative changes to the inner or outer membranes were visible in this mitochondrion either. The vacuole contained membranous structures, a lipid droplet, and glycogen particles. The cristae of the affected mitochondria were not dilated and showed normal distribution.

A satellite cell (F, right) was observed in the space between the plasmalemma and the basal lamina. These small, flattened cells are found in close proximity to the myofibril with an intervening space of ≈15nm between the plasmalemma and the satellite cell (Ovalle *et al*., 2008). This position enables the observer to differentiate between satellite cells and myonuclei (F, left). Satellite cells are the muscle's own population of stem cells and have the ability to repair or regenerate damaged segments of muscle fibers.

Positive control group

Figure 6.4 represents a series of electron micrographs from the positive control group, SJL/J mice at 27 weeks of age that received placebo. Myofibrils are bundles of thick and thin myofilaments in orderly arrangement with periodic Z-discs (Carpenter and Karpati, 1984). An interruption of this orderly arrangement was observed (A). Myofibrillar arrangement was intermittent with areas of myofibril loss (asterisk), suggestive of necrotic changes. Considering the low magnification of this micrograph, it is unlikely that the myofibrils simply left the plane of sectioning. It is more likely that they are affected by degeneration, as parts of the affected areas appear empty.

A longitudinal section through a muscle fiber (B) from this group displayed the tendency of thin filaments to bend (double bracket) in a muscle which is fixed in a relatively contracted state, in view of the length of the I-band. This bend that occurred in the middle of a myofibril caused the myofibril to split. From micrograph (B), it is evident that the split was initiated by an alteration to the tubular system, presumably dilatation of the sarcoplasmic reticulum or T tubules.

Myofibrils from this group showed smallness and in some instances the myofibrils were contracted, resulting in the appearance of a thickened Z-disc (C). It is possible that this muscle sample was in a contracting state upon fixation. Degenerative changes were observed in this group between myofibrils (D), characterized by large open spaces, dilated tubules, and mitochondrial remnants.

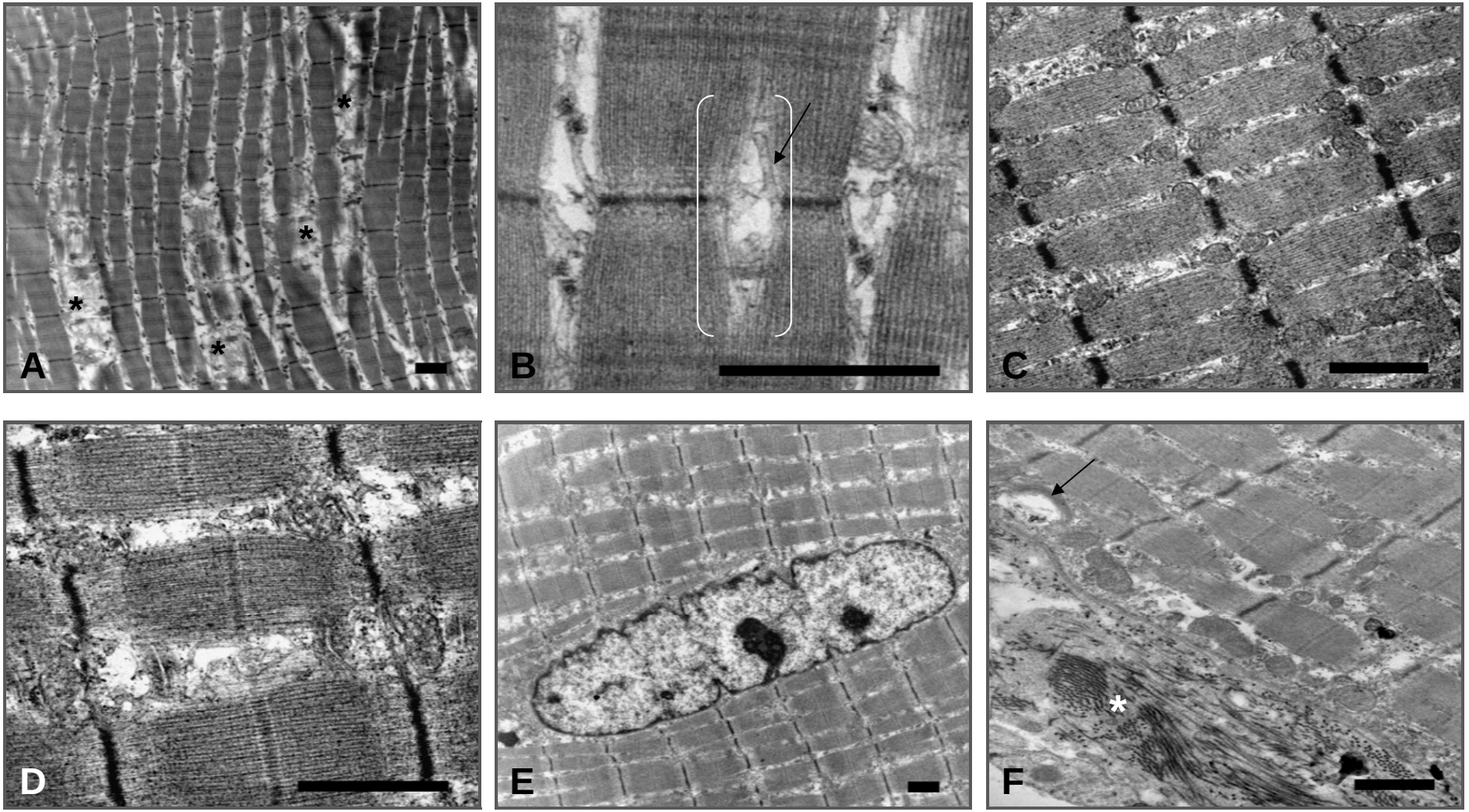

Figure 6.4: Electron micrographs from the positive control group, SJL/J mice at 27 weeks of age that received placebo. (A) Myofibrillar disruption that leads to myofibrillar loss due to necrosis (asterisks). (B) A bent in the myofibril at the level of thin filaments (double bracket) with dilated tubules (arrow) visible. (C) Small myofibrils in a state of hypercontraction. (D) Degenerative changes characterized by large open spaces, dilated tubules and mitochondrial remnants between myofibrils. (E) A myonucleus in the central position of a fiber. (F) Subsarcolemmal vacuoles (black arrow) are present. Collagen fibers (asterisk) can be seen in the extracellular spaces. Scale bars = 1µm

Light microscopy (in chapter 5) revealed that myonuclei situated in the central position of myofibers were quite common in this group, with the highest prevalence, compared to all other groups. Cytoplasmic invaginations were observed to the nucleus in Figure 6.4 (E) that is situated in a central position of the fiber. This incidence points to the difference seen between nuclei in this group, compared to nuclei from the age control group (Figure 6.3, F), which lack invaginations into nuclei, but is consistent with nuclei found in the negative control samples (data not shown). The mechanism behind this structural alteration is not known. Subsarcolemmal vacuoles (F, black arrow) were present in samples from this group. Collagen fibers (F, asterisk) were present in the extracellular spaces.

Resveratrol group

Electron micrographs taken from muscle samples of animals treated with resveratrol (Figure 6.5), revealed myofibrils that showed more consistency in size and less disruption of whole myofibrils (A) compared to the positive control group. Mitochondria detected in samples that were freeze-substituted displayed a relative normal distribution (B). Higher magnification (C) showed larger numbers of mitochondria in subsarcolemmal regions. These mitochondria displayed a variation in shapes ranging from oval to round. Cristae were not clearly visible in freeze-substituted samples.

Micrograph (C) showed a sarcolemmal gap (*) measuring 0.63µm, as well as thickening of the basal lamina measuring up to 0.5µm. Glycogen particles were visible in the sarcoplasm. Vacuolation was observed (B and D) that differs from that seen in the age control and negative control groups. They were slightly bigger, mostly empty, and were found scattered between myofibrils in conjunction with mitochondria. Myofibrils in this group revealed a more orderly arrangement of thick and thin filaments.

Micrograph (E) revealed that mitochondria in this group were severely challenged, and that the vacuoles observed in (D) could possibly be derived from mitochondrial degeneration. The centres of these vacuoles appeared optically empty and bounded by a membranous structure. The affected mitochondrion (E and F) displayed large open optically empty spaces, indicative of degenerative changes. Some of the vacuoles were empty while others showed remnants of what used to be the cristae (E). There were membranous whorls with a few glycogen particles present in the centre of the degenerating mitochondrion (F).

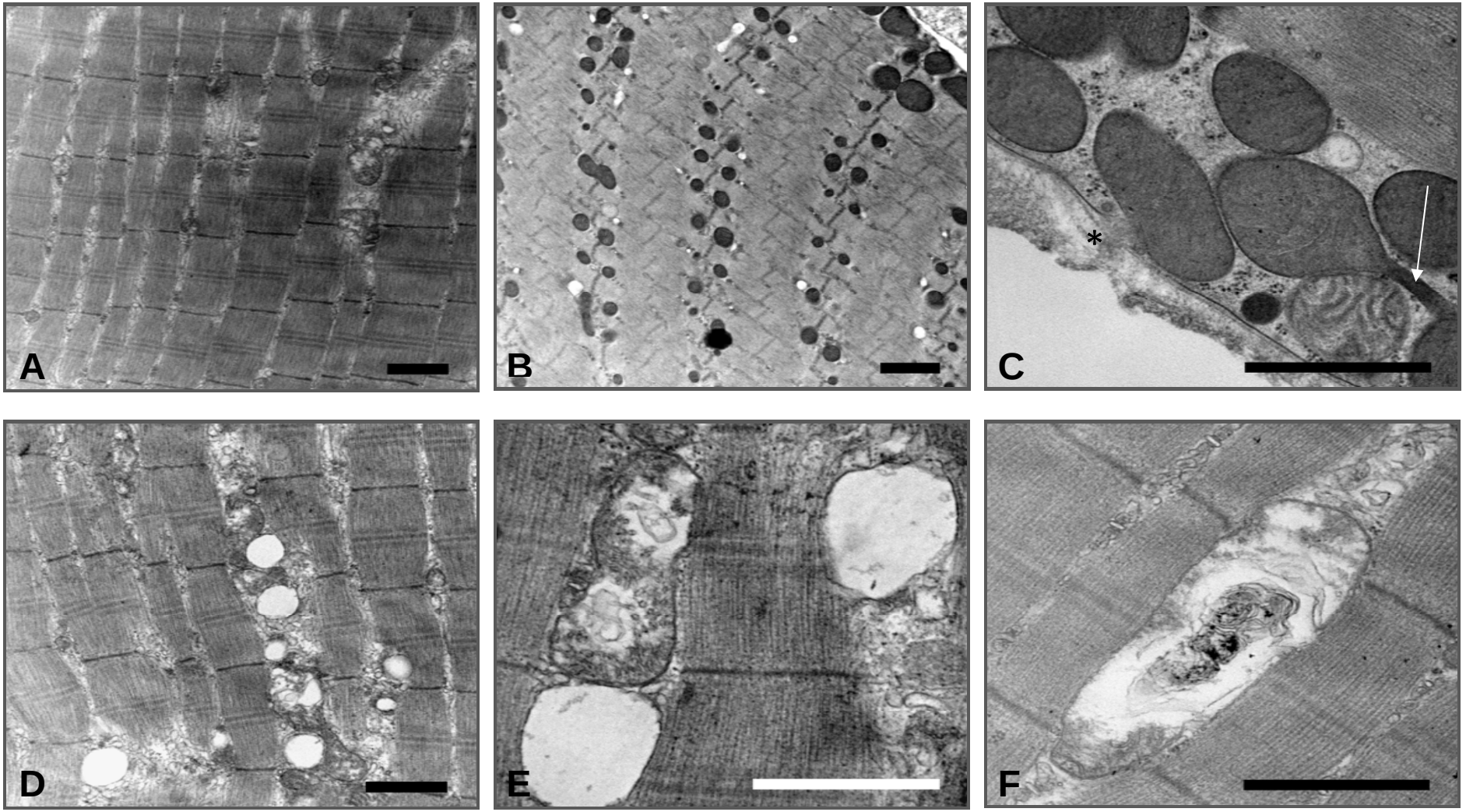

Figure 6.5: Electron micrographs from the resveratrol group. (A) Occasional myofibrillar degeneration. (B) Mitochondria show normal distribution, with large numbers found in the subsarcolemmal position (C). A plasmalemmal gap and basal lamina thickening is present on this freeze-substituted sample (C). A disruption in the plasma membrane is present (*)A strange connection (C, arrow) of unknown origin between two mitochondria. Vacuoles (D) can be observed between myofibrils, presumably resultant from mitochondrial degeneration. (E & F) Degeneration of a mitochondrion. Scale bars = 1µm

Low CoQ10 group

Figure 6.6 showed electron micrographs taken from samples representing the low CoQ10 group. Myofibrillar disruption (A and B) lead to unorderly arrangement of myofibrils in this group. Larger magnification (B) showed disruption of the Z-disc stability. In some instances the Z-disc disappeared (black arrow) in some myofibrils. Thick filament instability resulted in myofibrillar splitting (white arrow).

Micrograph (C) revealed that the thin filaments were also affected, resulting in splitting of part of a myofibril at the level of the I-band (black arrow). Plasmalemmal discontinuities, characteristic of dystrophic changes in muscle, were observed and included subsarcolemmal vesicles, membrane bound vesicles, and subsarcolemmal glycogen particle accumulation (C, white arrows).

Indentations into the membrane that was first observed by light microscopic analysis in this group and others, in chapter 5 (Figures 5.7.1, C and D), was now observed at the ultrastructural level (D and E). Ultrastructural analysis (D) revealed that these indentations might be the result of inflammatory infiltration by inflammatory cells and processes, and the pressure exerted on the fiber by these processes. Ultrastructure of this incident revealed an almost orderly spherical arrangement of myofibrils around the affected area (E).

In order to afford this arrangement of myofibrils, there has to exist a certain degree of structural adjustment in the myofiber. Micrograph (E) showed that this suggestion could hold truth, as there is a severe disruption of the normal myofibrillar structure, including Z-disc loss, and thick and thin filament disruption. Carpenter and Karpati, 1984, reported that Z-disc loss may occur in the early events of necrosis, and that this loss might be caused by activation of enzymes like proteases. It is also possible, due to the orientation of the fibrils around the indentation, that they simply leave the plane of sectioning, and appear disrupted. Investigation of the surface morphology by SEM will bring this finding to a close (Section 6.4; Figure 6.13).

Collagen bundles (F, asterisk) were also detected around fibers in this group.

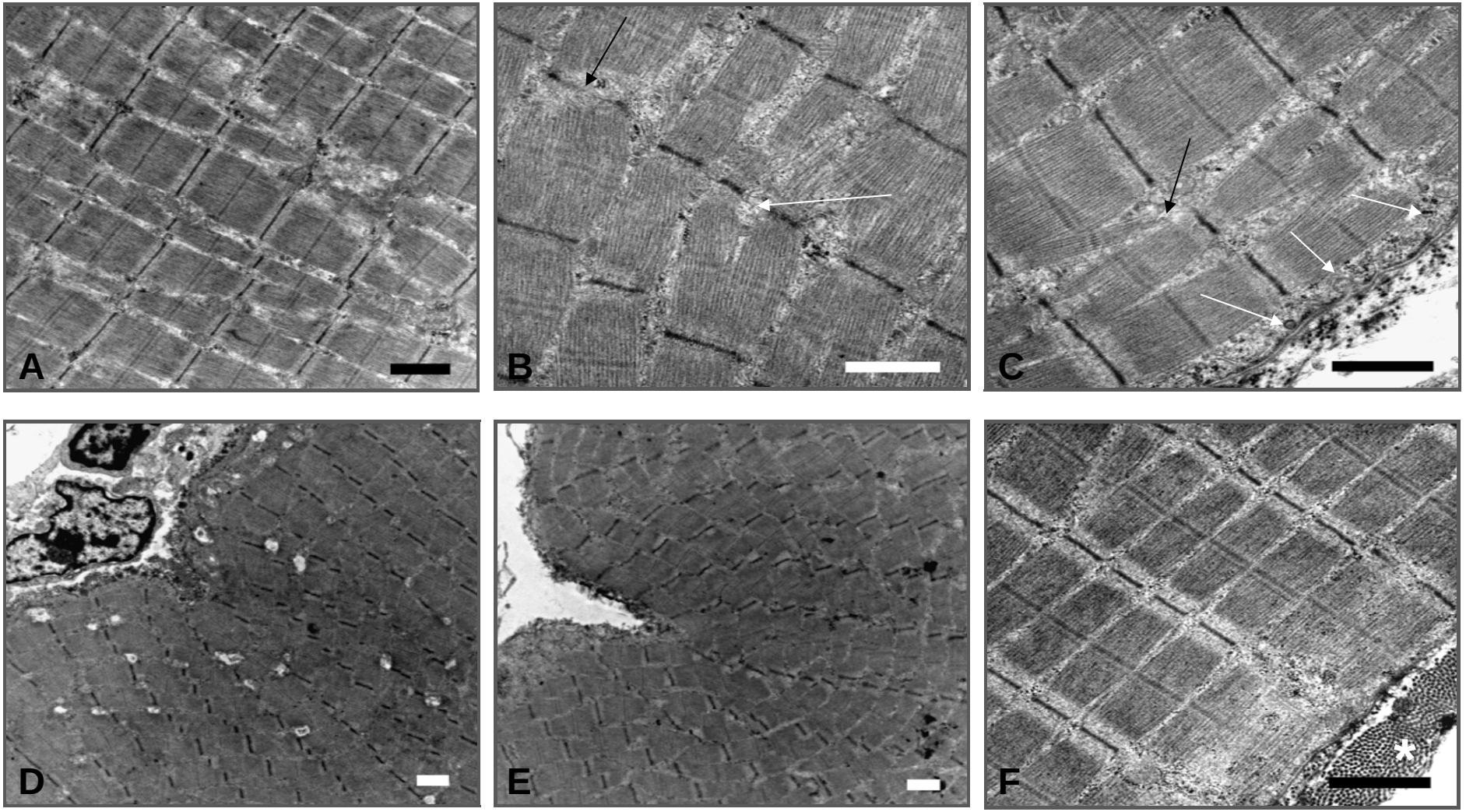

Figure 6.6: Electron micrographs from the low CoQ10 group. (A & B) Myofibrillar disruption leads to unorderly arrangement of myofibrils in this group. Larger magnification (B) shows Z-disc loss (black arrow) in some myofibrils as well as thick filament disorientation that resulted from myofibrillar splitting (whit arrow). (D) Myofibrillar arrangement around indentations in myofibers. Inflammatory cells, presumably macrophages, are present at the indent. (E) Thick and thin filament disorientation and probable Z-disc loss in myofibrils arranged around a fiber indent. (F) Collagen bundles (asterisk) were present around fibers in this group. Scale bars = 1µm

High CoQ10 group

Qualitative ultrastructural analysis of quadriceps muscle samples from the group treated with a high dose of CoQ10 (Figure 6.7) revealed intact membranes (A, black arrow) and overall less occurrence of membrane discontinuities, on a transverse section (A). The sarcoplasmic reticulum was observed in the perimyofibrillar position with no dilatation observed in the present micrograph. On the contrary, the basal lamina appeared thickened (A, white arrow) and presumably represents duplication. This is a known characteristic of dysferlin-deficient muscle membranes, observed by Selcen and co-workers (2001) and Cenacchi and co-workers (2005).

Freeze-substituted samples (B) showed membrane discontinuities, including small gaps, ranging from 0.08 to 0.2µm, and vesicles in the subsarcolemmal position. This electron micrograph also showed multiple, small globules of dense material embedded in a thickened basal lamina.

Numerous vacuoles were present in some regions, usually surrounding mitochondria (C) and between myofibrils (D). The mitochondrion in micrograph (C) appeared normal. The vacuoles in micrograph (C) were not optically empty; tiny particles were scattered throughout the visible centers. Mitochondria were found between myofibrils (C and D) and under the sarcolemma. Cristae were observed in most instances, although some mitochondria displayed tiny areas that appeared optically empty (D, white arrows).

Z-disc streaming, a common lesion, seen in numerous conditions and situations, was observed in one sample from this group (D, white arrow). Carpenter, 2001 (b) explained that it combines a mild focal loss of myofilaments and loss of the Z-disc lattice with streaming of the material of the Z-disc along either thin or remaining thick filaments. Micrograph (D) clearly showed that the streaming extends from one Z-disc to the neighbouring Z-disc, with the parts of Z-discs on the periphery of the myofibril, spared. The target fibers in denervating conditions, has shown that this phenomenon manifests in areas lacking mitochondria, but may actually be a manifestation of reinnervation (Carpenter, 2001 b). Since mitochondria were observed in the surroundings of the myofibril affected by Z-disc streaming, this finding might be suggestive of reinnervation. Numerous small spherical structures, presumably vacuoles, were visible around the affected myofibril. The myofilaments of the affected myofibril appeared optically transparent, compared to the other myofibrils.

Bending of myofibrils around an indentation (E) was observed in the present group.

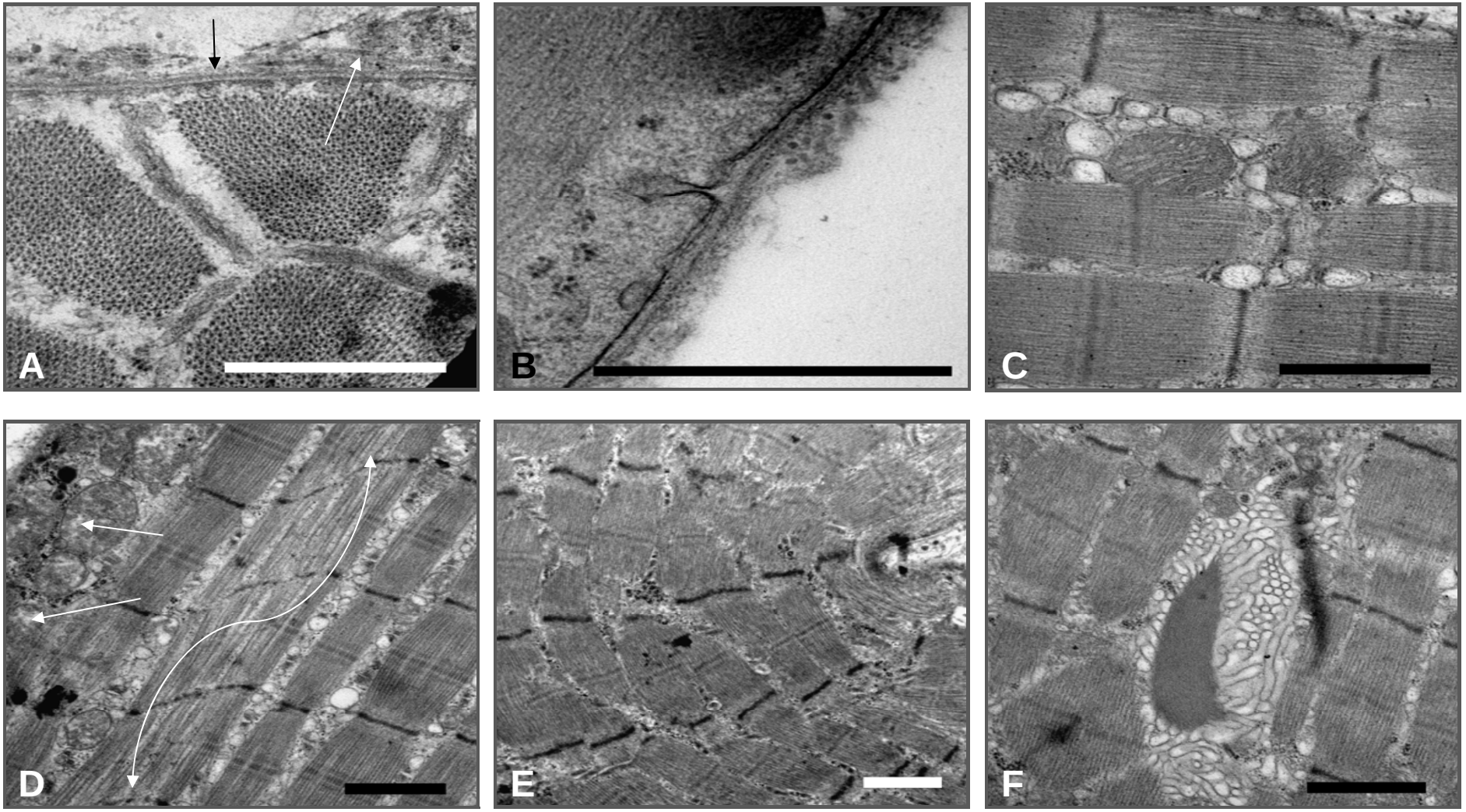

Figure 6.7: Electron micrographs from the high CoQ10 group. (A) An intact membrane (black arrow) on a transverse electron micrograph with a thickened basal lamina (white arrow). (B) Plasmalemmal discontinuities are present in some areas. (C) Small vacuoles can be seen between myofibrils. (D) A fiber in which Z-disc streaming (arrow) occurred. Some mitochondrial displayed areas that appeared optically empty (white areas). (E) Myofibrils bend around an indentation in a myofiber. (F) An area of focal accumulation of tubular structures surrounding a myofibril-like segment. Scale bars = 1µm

Another strange occurrence observed in this group was a focal dense area of tubular structures aggregated around a myofibrillar-like segment (F). The well defined tubular structures (F) were found to surround a part of what appeared morphologically similar to a myofibril that lacks any characteristic banding, but showed a similar surface structure to thick filaments. The structure was found between other myofilaments and the tubular structures that surrounded it. The tubular structures were found to be orientated in longitudinal and transverse positions and are supposedly derived from either one or all of the following; the T-tubule-, golgi-, and/or sarcoplasmic reticulum systems. This phenomenon was not observed in any of the other groups in the present study.

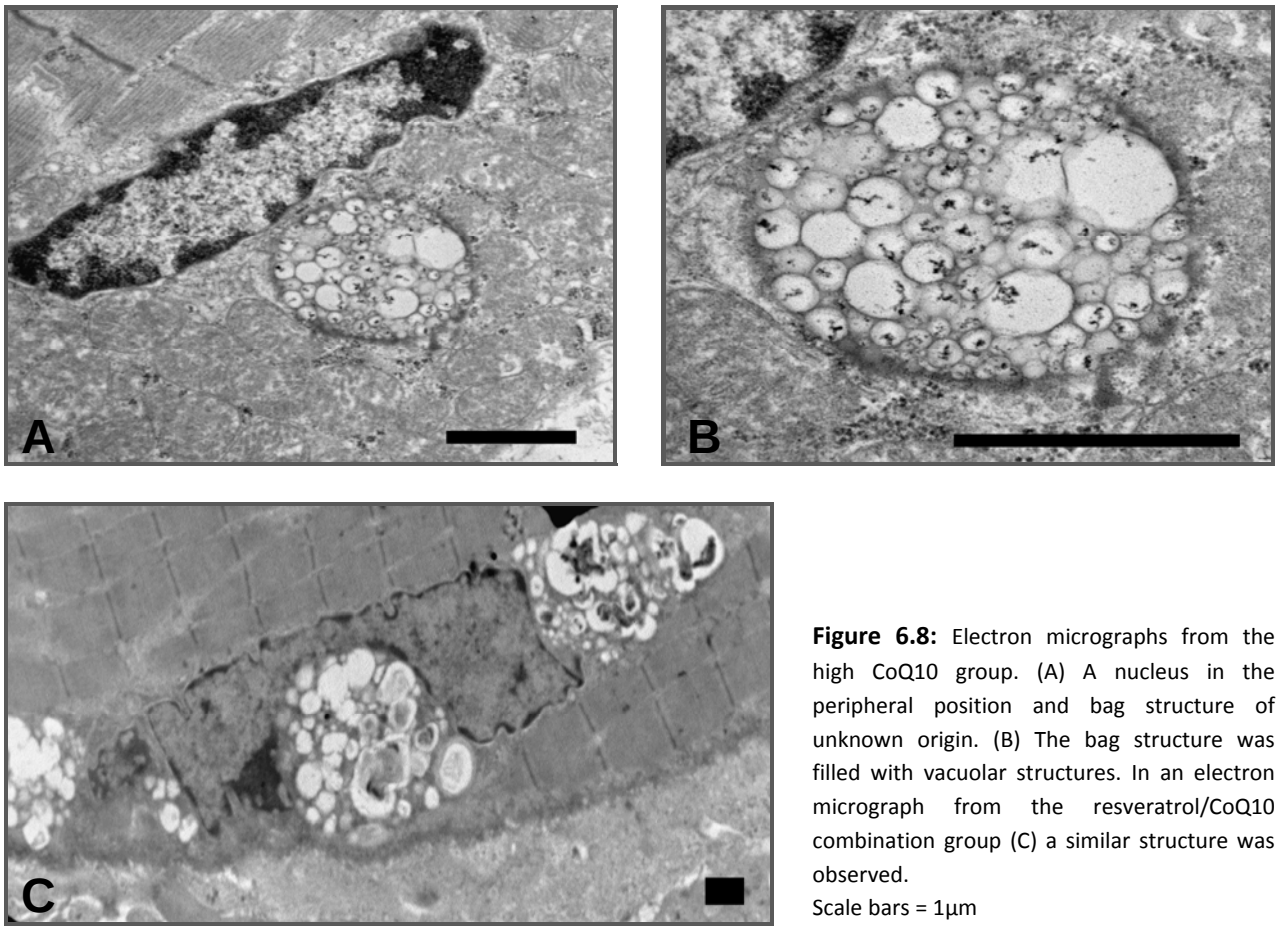

Figure 6.8: Electron micrographs from the high CoQ10 group. (A) A nucleus in the peripheral position and bag structure of unknown origin. (B) The bag structure was filled with vacuolar structures. In an electron micrograph from the resveratrol/CoQ10 combination group (C) a similar structure was observed.
Scale bars = 1µm

A nucleus (Figure 6.8, A) located near the periphery of a fiber from the same group, was found to be surrounded by a very large number of mitochondria (A), which is not uncommon. A strange bag structure bound by an optically dense structure (A and B), and filled with small membrane bound vacuolar organelles, was observed in close proximity to the nucleus. The structure was of unknown origin. A similar occurrence was observed near a peripherally located nucleus in the resveratrol/CoQ10 combination group (C). The structure was invading a degenerating nucleus and lacked a clearly defined boundary.

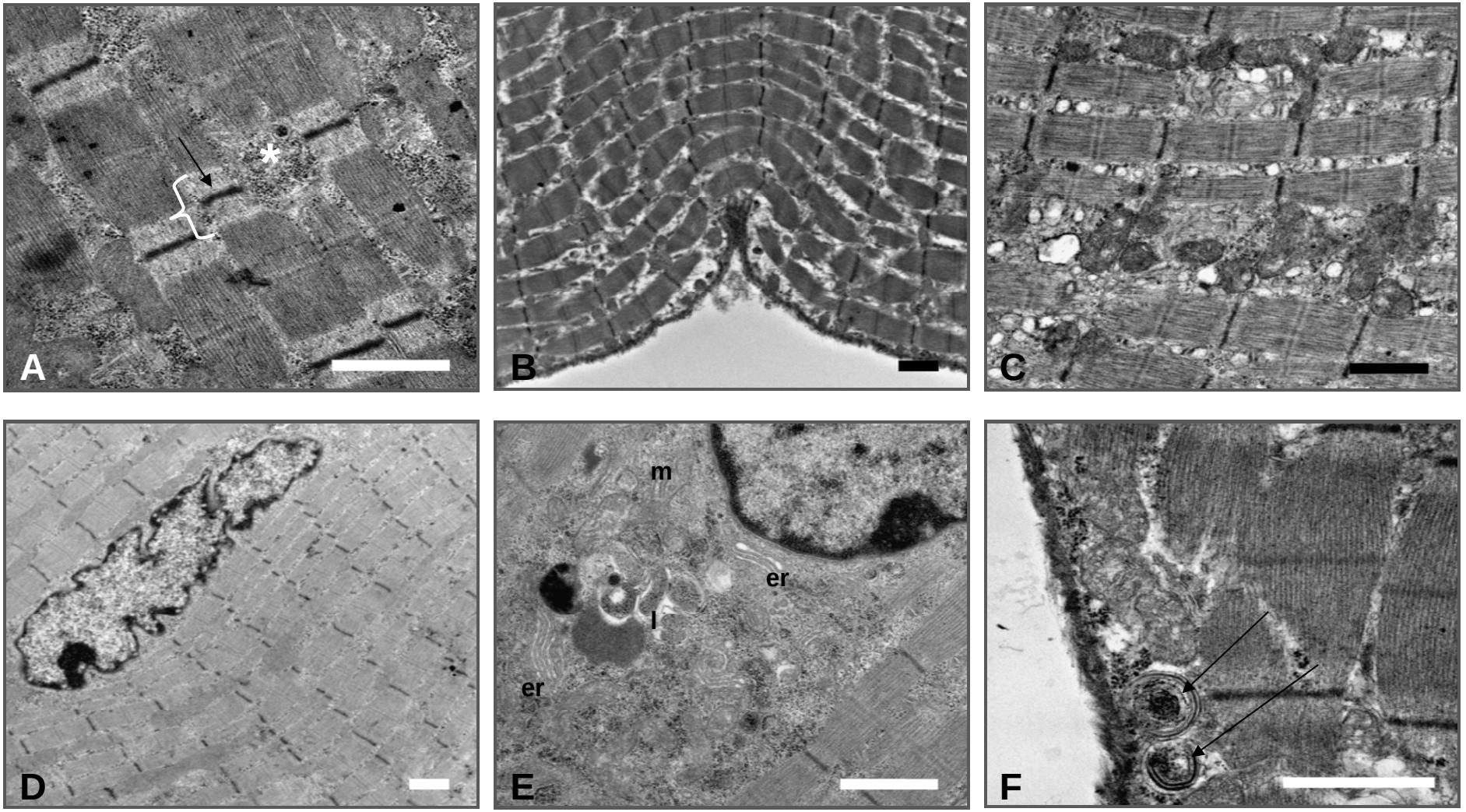

Figure 6.9: Electron micrographs from the resveratrol/CoQ10 combination group. (A) Myofibrils show 'missing' I-bands (asterisk), this does not represent myofibrillar loss or breakdown, and is just an effect of sectioning. The I-bands appear distinctly long in size (white brace). (B) Myofibrils bend around an indentation in a myofiber. (C) Mitochondrial and vacuole accumulation in areas of myofibrillar disruption. (D) A centrally located myonucleus. (E) The area around a central nucleus. Endoplasmic reticulum (er), mitochondria (m), round spaces, presumably lysosomal (l) which contained dense debris and glycogen particles are visible. (F) Membranous whorls (arrows) beneath the sarcolemma. Scale bars = 1µm

Resveratrol/CoQ10 combination group

Electron micrographs from the resveratrol/CoQ10 combination group are represented by Figure 6.9. Micrograph (A) revealed myofibrils that showed 'missing' I-bands from the myofibrils, that otherwise appeared to be in good condition (A, asterisk). These regions were focally dense with glycogen particle accumulation. Glycogen particles were also found between myofibrils.

Carpenter, 2001 (b), reported that they have seen selective I-band loss only rarely, focally in a few fibers, and only in denervating conditions. I-band loss has been demonstrated by Carpenter and Karpati, 1984, where it was shown that when the I-bands in myofibrils are lost, it result in blocks of thick filaments that became disorientated, and the orderly appearance seen in micrograph (A) is unavoidably lost. Carpenter and Karpati, 1984, reported that far too many micrographs of longitudinal sections have been interpreted as showing myofibrillar loss, or lysis, where the myofibrils simply leave the plane of sectioning. The myofibrils seen in (A) were in good order, yet the I-bands appeared missing. This observation has been shown by Carpenter and Karpati, 1984, to be purely an effect of sectioning. Therefore, the finding in (A) did not correspond to myofibrillar loss or breakdown.

Myofibrils in samples from this group were also found to bend around indentations in myofibers (B). Myofibrils were subjected to disruption, and mitochondria and vacuoles, accumulated at affected areas(C). Vacuoles were small but numerous.

A myonucleus found in the central position between myofibrils (D) showed deep invaginations, where it almost lead to a split in the nucleus. Nuclei that were divided into two separate parts were also observed in the present group. These nuclei were always found in a central position. The area around a central nucleus (E) displayed numerous mitochondria (m), endoplasmic reticulum (er), and round spaces, presumably lysosomal (l) which contained dense debris and glycogen particles.

Membranous whorls (F) were observed in one sample from this group. These two structures in micrograph (F) measured 0.41 and 0.54µm respectively, and are also known as myelin figures and/or myeloid bodies. Membranous whorls are often associated with a vesicular space whose walls they line (Carpenter and Karpati, 1984). Electron microscopy studies by Carpenter and Karpati, 1984, revealed that they are formed from cytomembranes, in a circumferential arrangement with a variable periodicity. Similar to the membranous whorls in inclusion body myositis (Carpenter and Karpati, 1984), the centers of the whorls found in the present study in SJL/J mice, were also occupied by glycogen particles.

6.3.2 Unravelling the Ultrastructural Findings

The main ultrastructural alterations in the sarcoplasmic compartment were found to be non-specific architectural changes. These include mild or severe loss of myofilaments (Figure 6.11), dilated sarcoplasmic reticulum and T system profiles, and degenerative changes of the mitochondria. In addition, large vacuoles containing myelin-like lamellae, and myofibrils orientated around indentations into the fiber, were observed. Central nuclei were often observed, in addition to many lipid vacuoles and mitochondrial aggregates, in both the intermyofibrillar and subsarcolemmal regions. These changes occur in all SJL/J animals. They were found to be more pronounced in the positive control group. Since ultrastructural analysis makes use of ultrathin resin sections (≈90nm), the field investigated is limited, and the findings are therefore discriminating within the same strain, between treated and untreated groups.

Specific alterations of muscle fibers from molecularly diagnosed dysferlinopathy samples were identified by Cenacchi and co-workers, 2005. They found that the ultrastructure of the surface cell layer at the level of the sarcolemma and basal lamina showed few sarcolemmal gaps and many elongated microvilli-like projections. The basal lamina was also found to be thickened or multilayered, and seemed to include some globular aggregates of amorphous electron dense material.

Similar observations were made in the present study, where the basal lamina measured up to 0.5µm (Figure 6.5, C). On investigation of the subsarcolemmal region it was found to be characterized by the presence of several aggregates of small vesicles, which presumably derived from the golgi apparatus. Most membrane defects were found to be small gaps, ranging from 0.08 to 0.63µm. Extensive plasmalemmal defects were typically found in necrotic fibers that were denuded of most of their surface membrane. These extensive membrane discontinuities were mostly detected in the positive control group of the present study. Plasma membrane defects were also present on non-necrotic fibers in all groups of SJL/J mice. In addition sarcolemmal replacement by one to multiple layers of small vesicles, were observed in most groups.

The investigations of the present study also paid attention to non-specific alterations on ultrastructural level; a sparsely described subject in the literature on dysferlinopathies. These changes included vacuolation, unorderly myofibrillar arrangement, and mitochondrial localization and structure.

Vacuoles

Vacuoles in skeletal muscle can be of many sorts (Carpenter, 2001 a). The contents of a vacuole may be stainable or appear optically empty, because the contents have dissolved or diffused out in processing (Carpenter and Karpati, 1984).Material such as glycogen can be carried artefactitiously into otherwise clear vacuoles (Carpenter, 2001 a). A vacuole can arise from various pre-existing organelles.

Small subsarcolemmal and intermyofibrillar vacuoles were detected in all groups analysed, including the SWR/J mice that served the negative control. Vacuoles described by Selcen and coworkers, 2001, were found either close to or abutted on the sarcolemma. The present study revealed numerous vacuoles in the subsarcolemmal position, but also in the intermyofibrillar position, often at the level of the I-band, and often associated with the presence of mitochondria nearby. They appeared singly or in clusters, and were either empty or contained degraded membrane fragments. Occasionally small, optically dense material was observed in their centers. Some vacuoles were found abutted on membranous networks of the T tubule system and/or sarcoplasmic reticulum.

The T-tubule system serve as membrane source for membrane bound vacuoles and vesicles in muscle (Klinge *et al*., 2007) and is involved in the generation of membrane for elongation and repair purposes of the sarcolemma, and to 'react' in regenerating muscle fibers (Engel and Franzini-Armstrong, 2004). Selcen and co-workers, 2001, have shown that subsarcolemmal vacuoles contiguous with the T-tubule system are one of the ultrastructural hallmarks of dysferlinopathy muscle. Klinge and co-workers, 2007, have shown that dysferlin accumulation at wounding sites in early myogenesis, are derived from a T-tubule localization. The T-tubule system appears to serve as a pool of dysferlin positive endomembrane in the process of membrane repair (Klinge *et al*., 2007). It is therefore possible that in areas of larger membrane disruptions where the fiber is challenged by large sarcolemmal degeneration, more vacuoles and vesicles will be present in the affected fiber, to provide a membrane source for repair (Figure 6.3, A and B).

As vacuoles have been detected in many muscle pathologies, it created the idea that vacuolation occurs in response to necrosis. Taking into consideration the work of others (Selcen *et al*., 2001; Klinge *et al*., 2007), it became apparent that vacuolation occurred in response to membrane damage as a first line attempt to repair the membrane injury. The present study found vacuoles in SJL/J quadriceps muscle of all groups, treated and untreated. The largest vacuoles, in the present study, as a result of mitochondrial vacuolation, were found in the resveratrol group (Figure 6.5 E and F).

Numerous smaller vacuoles and vesicles were detected in groups treated with a high dose of CoQ10 and resveratrol/CoQ10 in combination.

Mitochondria

The β-oxidation of fatty acids, the Krebs cycle, the respiratory chain and ATP synthase are located in the mitochondria, where a large proportion of the energy used by muscle cells is made available (Carpenter, 2001 b). In muscle cells, mitochondria are usually concentrated in four locations, between myofibrils at the I-band level, under the sarcolemma, at the motor endplate and at the poles of myonuclei (Carpenter, 2001 b).

The functional activity of the mitochondria greatly influences the extent of reactive oxygen species (ROS) formation. Low levels of ADP and high mitochondrial membrane potential give high levels of ROS. In turn high ADP levels and low membrane potential result in low levels of ROS production (Bentinger *et al*., 2007).

In the present study, numerous mitochondria of different shapes and sizes were observed in all groups under investigation. Some mitochondria in the age control group (14 week old SJL/J mice), displayed small empty spaces between cristae (Figure 6.3, A), while others showed dense distribution of cristae and were found to be larger in size (Figure 6.3, D). Mitochondria in the intermyofibrillar position of the positive control group, were found to be smaller in size (Figure 6.4, C), and in some samples appeared to undergo degenerative changes (Figure 6.4, D and F).

Large mitochondria were observed in the group supplemented with resveratrol. Some mitochondria in this group showed a normal distribution pattern under the sarcolemma and between myofibrils (Figure 6.5, B). In other samples from the same group mitochondria had undergone degenerative changes (Figure 6.5, A and D), leading to the formation of large vacuoles (Figure 6.5, E and F). Mitochondria were present in both CoQ10 groups and the resveratrol/CoQ10 combination groups, with little to no pronounced alterations observed.

Studying the morphology of mitochondria on an ultrastructural level, gives a good indication of the size, distribution and shape of the mitochondria. It is nevertheless difficult to make any conclusions on how dysferlin-deficiency exactly affects the mitochondria. It is also not possible to derive an exact conclusion on the effect of antioxidant supplementation on the mitochondria, as their alteration by the disease itself is not yet fully understood. It can be expected that, if the supplementation of antioxidants does affect the mitochondria *per se*, it will need to be confirmed by molecular analysis.

An apparent random distribution of alterations in mitochondria included swelling, considerable variation in size, and disintegration of the characteristic shape of the cristae, with general disorganisation of the inner membrane being evident usually in swollen mitochondria. The outer membrane appeared to be intact, almost in all instances. In some mitochondria from the positive control, low CoQ10 and resveratrol groups, the inner membrane was completely disrupted, resulting in the formation of intramitochondrial vacuoles. In some instances, open spaces occurred in regions, presumably once occupied by mitochondria. Smaller mitochondria were observed in the high CoQ10 and resveratrol/CoQ10 groups. These findings imply that the ongoing dystrophic changes in the SJL/J mouse are affecting the mitochondria, and that the alterations are less pronounced in the high CoQ10 and resveratrol/CoQ10 groups.

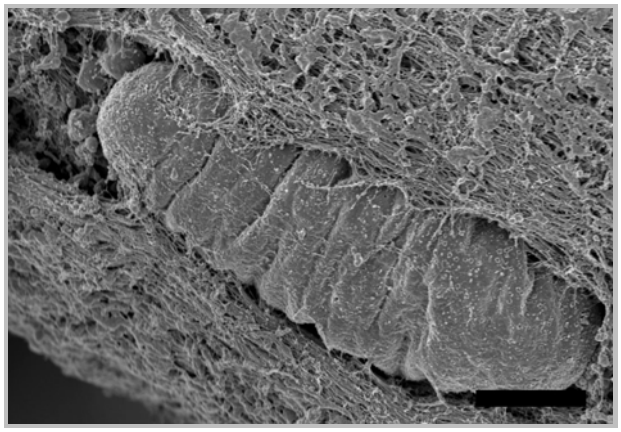

Figure 6.10: A scanning electron micrograph of a mitochondrion in the subsarcolemmal position from the age control group. The mitochondrion appears normal, but the sarcolemma is disrupted.
Scale bar = 2µm

The mitochondrial ultrastructural changes observed in SJL/J mice are consistent with the findings of Haycock and co-workers, 1996. Their team showed that mitochondrial ultrastructural alterations, similar to what was found in the present chapter, were the result of ROS-induced oxidative damage. A novel experimental approach by Haycock's group was employed to quantify the relative susceptibility of membrane-associated, contractile and mitochondrial proteins in normal human muscle tissue sections, to oxidative damage by ROS. The authors found that different proteins, differing in structure, function or intracellular localization, showed different susceptibility to oxidative damage. They found certain mitochondrial proteins (succinate dehydrogenase, cytochrome oxidase) to show particular susceptibility. In addition, ultrastructural analysis of subcellular organelle damage, revealed particular susceptibility of mitochondria to ROS-induced oxidative damage (Haycock *et al*., 1996). Haycock and co-workers, 1996, reported the possibility that mitochondria can tolerate a critical maximum volume of ROS induction, thereafter oxidative stress insult will result in bursting of the outer membrane, leading to the formation of small vacuolar spaces.

The finding of numerous small vacuolar spaces is consistent with this theory, further strengthening the possibility that the disruption to mitochondria in SJL/J muscle are the result of oxidative stress insult. Of further interest, was the observation of severely altered mitochondria in the resveratrol group but not in other antioxidant supplemented groups. This observation might suggest that resveratrol alone cannot protect mitochondria from the critical maximum volume of ROS that can be tolerated, but the higher dose antioxidant supplementations, afforded protection against these mitochondrial alterations.

It is therefore possible that higher concentrations of antioxidants reduced the level of ROS in the cell, thereby reducing the maximum volume of ROS 'attacking' the mitochondria. This action will result in less damage to mitochondrial ultrastructure, as was seen in the high CoQ10 and resveratrol/CoQ10 combination groups. To support this theory, further investigation on the effect of antioxidant supplementation on lipid peroxidation levels in the present model was done and reported in chapter 7.

6.3.3 Ultrastructure on the Surface

SEM has previously been found to provide a powerful tool for qualitative ultrastructural analysis when focussing on the surface integrity of tissue (Potgieter *et al*., 2009). SEM was utilized to shed more light on the surface integrity of muscle tissue in the present study (Figures 6.10 to 6.13). Although electron micrographs obtained by this analysis greatly lacked information specific to the pathology, it provided interesting information on the surface structure of the tissues examined by TEM. Figure 6.11 revealed how myofibrillar arrangement is distorted in the 27 week-old untreated SJL/J mice, compared to that of the negative control SWR/J mice.

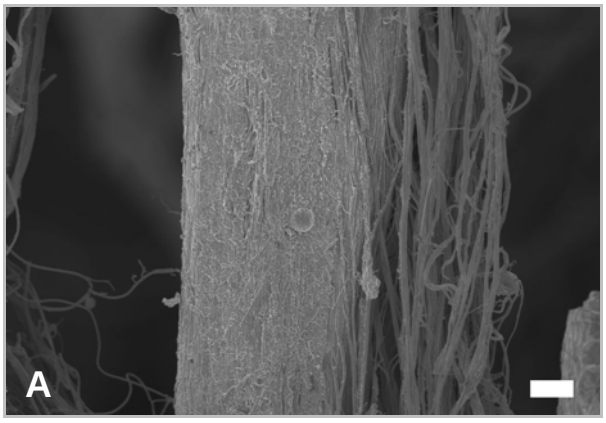

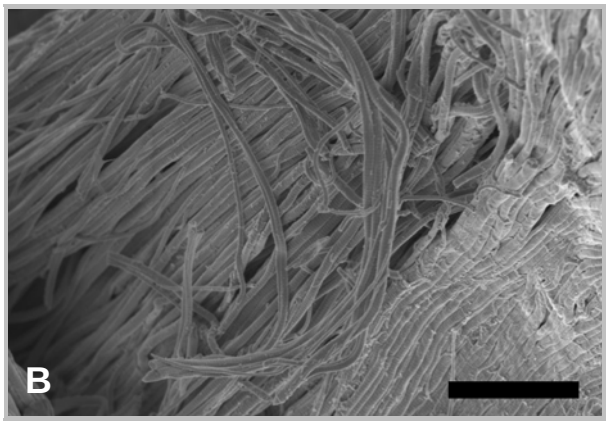

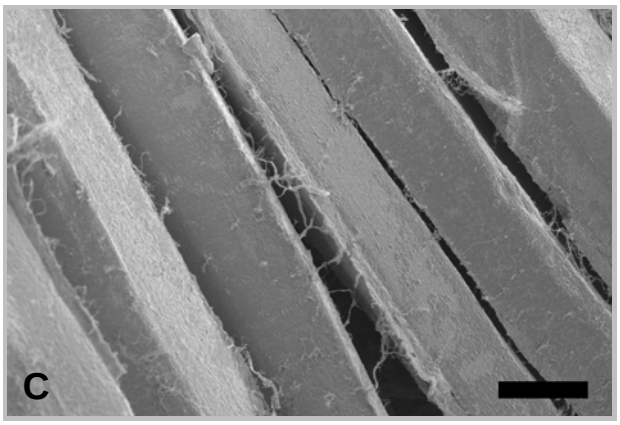

Figure 6.11: Scanning electron micrographs showing myofibrillar disruption and loss in the placebo treated positive control group (A & B), and solid fibers (C) from the negative control group. Scale bar = 2µm

Figure 6.12 displayed electron micrographs taken on the surface of muscle fibers, revealing the shape and size of vesicles accumulating under the membrane.

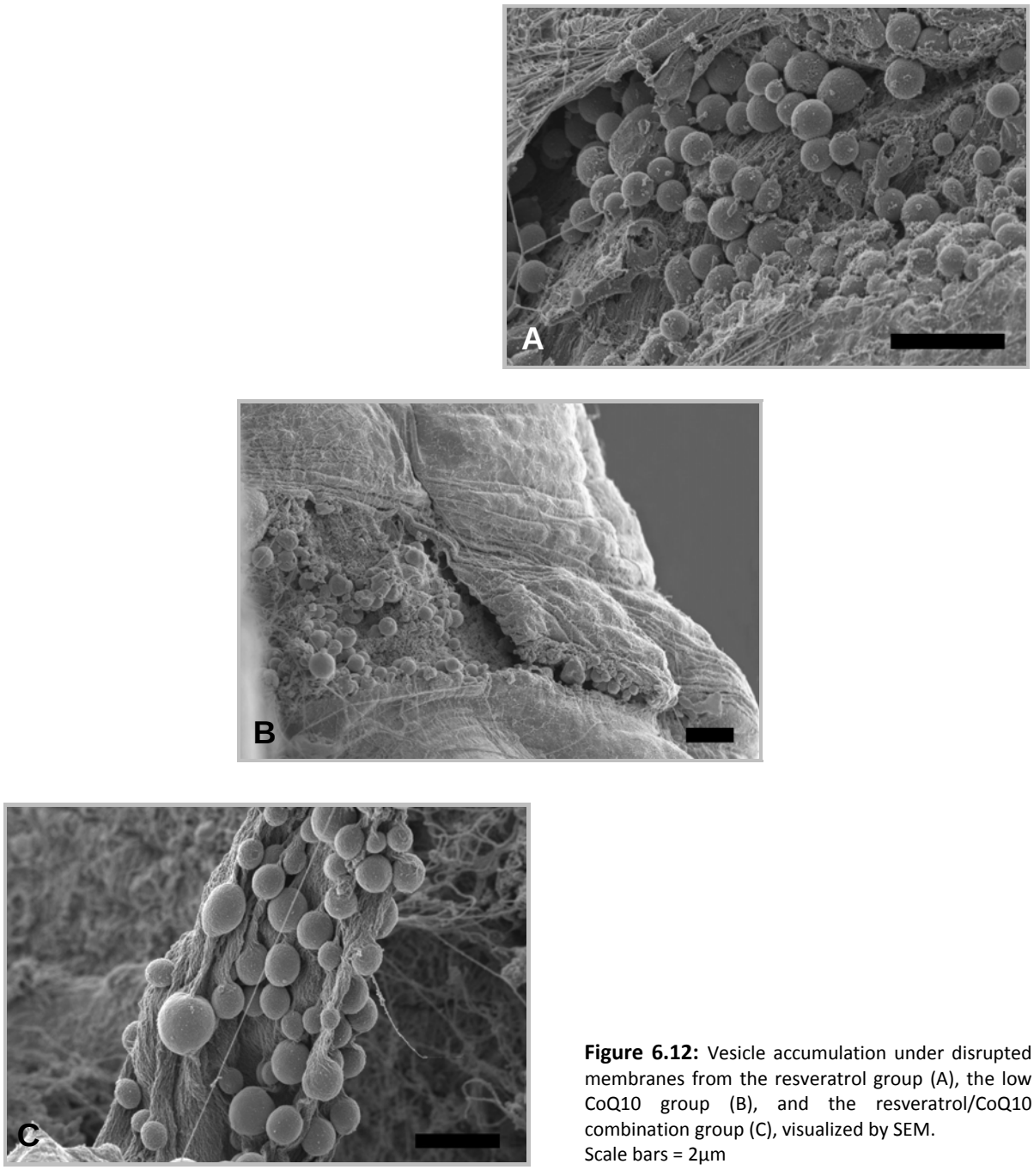

Figure 6.12: Vesicle accumulation under disrupted membranes from the resveratrol group (A), the low CoQ10 group (B), and the resveratrol/CoQ10 combination group (C), visualized by SEM.
Scale bars = 2µm

Other non-specific changes in the ultrastructure of SJL/J mice in the present study included, myofibrillar bending around an indentation in a muscle fiber (Figures 6.6, D and E; 6.7, E and 6.9 B), Z-disc streaming (Figure 6.7, D), and the formation of membranous whorls (Figure 6.9, F). The bending of the myofibrils around indentations in a muscle fiber created the impression of pressure exerted on the fiber *in vivo*. If this happens to be the reason, it is still not clear what caused the

pressure to the fiber, although one possibility might have been the invasion of fibers by inflammatory cells and their phagocytic activity (Figure 6.6 D). Alternatively and more likely, the muscles were in a contracting state when the animal was terminated and therefore, the sample was fixed in this state. SEM micrographs revealed a rippling effect in many fibers, in all groups, including muscle fibers from the negative control SWR/J mice. This proves that the event was not specific to the SJL/J mice, and thus not an alteration caused by the dystrophic process. In addition to the rippled fibers, normal fibers were also observed. Figure 6.11, C represents a micrograph of muscle fibers from the negative control group that did not display the rippling effect. It can therefore be suggested that the indentations observed in light microscopic images in chapter 5 and transmission electron micrographs in the present chapter, were present in the muscle before fixation.

Figure 6.13: Scanning electron micrographs of the indentations seen in transmission electron micrographs (present chapter) and light microscopy images (chapter 5). Micrograph (A) represents fibers from the negative control group, (B) represents fibers from the positive control group, and (C) represents a fiber from the high CoQ10 group. SEM clarified the uncertainty about the indentations; their formation occurred before fixation. Scale bars = 20µm

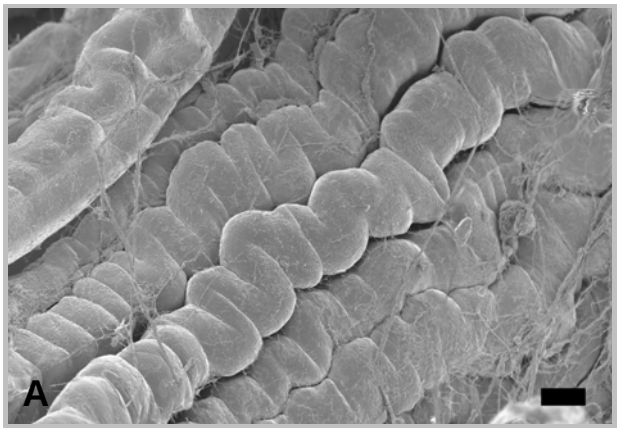

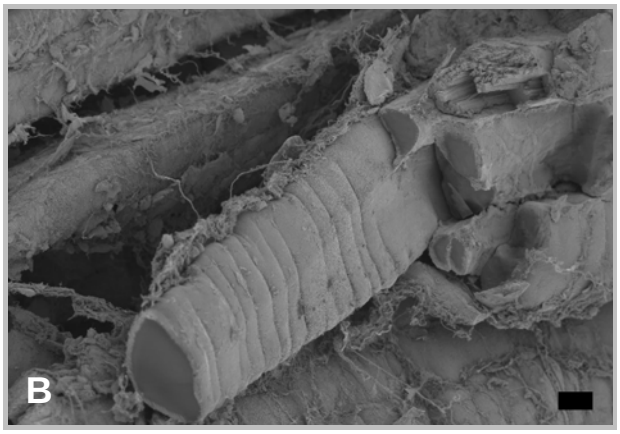

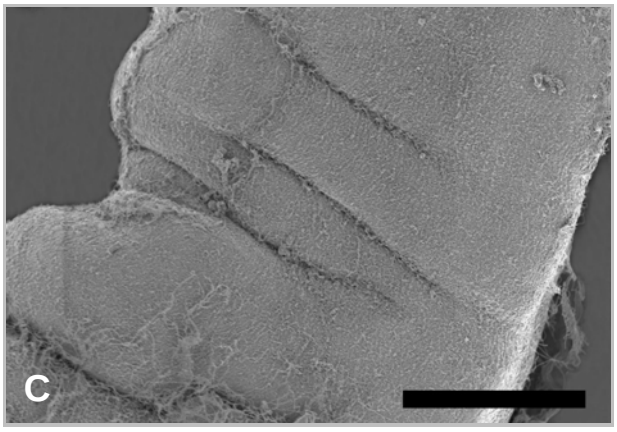

6.4 Concluding Remarks

Membrane repair requires efficient membrane fusion, a process that has been suggested by various lines of evidence, to involve dysferlin (Bansal *et al*., 2003; Selcen *et al*., 2001; De Luna *et al*., 2006; Klinge *et al*., 2007). Subsarcolemmal vesicle accumulation and vacuoles contiguous with the T-tubule system are two of the ultrastructural hallmarks of dysferlinopathy (Selcen *et al*., 2001; Cenacchi *et al*., 2005). The results from the qualitative ultrastructural analysis of quadriceps muscle from SJL/J dysferlin-deficient mice showed that vacuole formation occurred in muscle tissue of all groups of SJL/J mice as well as in the SWR/J mice. The results revealed that larger vacuoles were derived from mitochondrial degeneration. Also, large numbers of smaller vacuoles and vesicles presumably derived from the T-tubule system were observed in SJL/J mice, and vary in antioxidant supplemented groups.

Other non-specific changes observed, included Z-disc streaming, and the formation of membranous whorls. Although not attributable to the antioxidant supplementation or the lack thereof, this data provides concrete evidence for alternative non-specific changes in dysferlin-deficient muscle on the ultrastructural level in SJL/J mouse muscle.

Micrographs from the untreated positive control group in the present study revealed myofibrillar loss (Figure 6.4, A), while micrographs from the other groups, did not show this loss. Myofibrillar loss is best assessed on transverse sections (Carpenter and Karpati, 1984). The statement by Carpenter and Karpati, 1984, that far too many micrographs have been interpreted to indicate myofibril loss, while the myofibrils have just left the plane of sectioning, initiated utmost care when interpreting myofibrillar loss in the present study.

Qualitative ultrastructural analysis could not reliably discriminate between the myofibril condition of groups that have been treated with different antioxidants at different concentrations. The present chapter therefore, solely offered qualitative information on specific and non-specific alterations in dysferlin-deficient SJL/J quadriceps muscle. The study provides evidence for alterations to mitochondria on the ultrastructural level, consistent with ultrastructural changes found in mitochondria exposed to oxidative stress (Haycock *et al*., 1996). This data therefore suggests that muscle tissue in SJL/J mice are subjected to oxidative stress. This finding provided good reason for oxidative stress analysis in muscle tissue from SJL/J mice.

Ultrastructural analysis by TEM can be regarded a useful tool in investigating and identifying non-specific alterations in dysferlin-deficient muscle. Unfortunately, it does not clearly differentiate the possible effects of different antioxidant supplementations between different groups in the SJL/J

model using a limited sample size. In addition, ultrastructural analysis by SEM, did not nearly afford qualitative analysis of non-specific changes in SJL/J mouse muscle tissue to the extent that was afforded by TEM. Nevertheless, ultrastructural analysis utilizing SEM, provided clarity on the finding of muscle fiber indentations that was left unresolved by light microscopy and TEM. It further provided a true representation of the surface morphology of specific cell structures like vesicles, myofibrils and mitochondria.

Chapter 7

Oxidative stress in the SJL/J mouse and the effect of Coenzyme Q10 and Resveratrol supplementation

7.1 INTRODUCTION

The body's antioxidant system is made up of a variety of components of both endogenous and exogenous origins (Jacob, 1995). These include small molecule antioxidants which neutralize free radicals, like enzymes which catalyze radical and peroxide quenching reactions, and metal binding proteins which sequester iron and copper ions (Jacob, 1995). The diversity of physiologic antioxidant protection apparently extends beyond endogenous-, dietary-, and metal binding protein antioxidants (Jacob, 1995). The endogenous antioxidant compounds and enzymes insure that antioxidant defence is not lacking when dietary intake of antioxidant enzymes are not sufficient (Jacob, 1995). There is compelling evidence that components of the antioxidant system interact to provide diversity and depth to the body's antioxidant protection system (Jacob, 1995).

Tidball and Wehling-Henricks, 2005, reported that although defects in the membrane repair may be a primary pathogenic mechanism in dysferlinopathy, the prominent inflammatory infiltrate in dysferlin-deficient muscle suggests that inflammation may play a significant but unexplored role in promoting muscle damage. Fanin and Angelini, 2002 reported an increased myosin heavy chain class I (MHC-1) positive reaction in association with the presence of macrophages localized to the cytoplasm of regenerating fibers in dysferlinopathy patients. This was also occasionally observed on the surface of non-necrotic and non-regenerating fibers, suggesting that the inflammatory response might precede necrosis in dysferlin-deficient fibers (Fanin and Angelini, 2002). Linnane and co-workers, 2002, predicted that small metabolic imbalances, which may not have short-term untoward effects, may lead to systemic disease when maintained over long periods of time.

The decline of mitochondrial energy production resulting in increased oxidative stress and apoptosis does play a significant role in degenerative diseases and ageing (Cenacchi *et al*., 2007). Freeman and Crapo, 1982, documented that oxidative stress can alter virtually any aspect of cellular physiology. Among the earliest evidence in support of the hypothesis that the muscular dystrophies are diseases of oxidative injury, were the findings that dietary deficiency of vitamin E, leads to many symptoms of the inherited muscular dystrophies (Murphy and Kehrer, 1989). This is indicative of oxidative

damage to the components of muscle membranes, rather than the cytoplasm, as an underlying basis of tissue damage (Murphy and Kehrer, 1989).

Oxidative stress develops when an imbalance between pro-oxidants and antioxidants exist, where an excess of pro-oxidants consumes antioxidants (Lindschinger *et al*., 2004). This imbalance is associated with a ROS attack on polyunsaturated fatty acids (PUFAs) and other biomolecules (Lindschinger *et al*., 2004). The radical induced chain reaction is called lipid peroxidation (Lindschinger *et al*., 2004). Lipid peroxidation is amongst other things, responsible for the breakdown of PUFAs, resulting in the formation of a great variety of aldehydes (Esterbauer and Cheesman, 1990). The formation of these breakdown products may react with proteins and DNA and as a result are toxic and mutagenic (Marnett, 1999).

Reactive oxygen species (ROS) can attack vital cell components, damage cell membranes, inactivate enzymes, and damage the genetic material in the cell nucleus (Jacob, 1995). Oxidative damage to body cells and molecules has been implicated in a wide variety of diseases, including degenerative diseases such as heart disease, cancer, multiple sclerosis and others (Jacob, 1995). Oxyradicals can attack proteins, thereby changing their structure and ability to function (Jacob, 1995). Increasing evidence suggests that the degenerative processes in dystrophic muscle may be due to oxidative stress (Ragusa *et al*., 1997). Ragusa and co-workers, 1997 provided indirect evidence for oxidative stress in dystrophin-deficient muscle and suggested that oxidative stress may be constitutively present in mdx mouse muscle, but may not be the principle pathogenic mechanism. Disatnik and co-workers, 1998, found evidence of increasing oxidative stress preceding the onset of muscle cell death in dystrophin-deficient mice. These results support the hypothesis of Murphy and Kehrer, 1989 that free radical-mediated injury may contribute to the pathogenesis of muscle necrosis in the muscular dystrophies (Disatnik *et al*., 1998).

Rando, 2002, reported that with any muscle sample analysed, there would be many secondary processes occurring that accompany any muscle degeneration, most notably the infiltration of inflammatory cells reflecting the immune response to tissue damage. Therefore, any, most or all the biochemical changes indicative of oxidative damage can reflect this secondary process (Rando, 2002). Rando, further stated that oxidative damage due to inflammatory cell infiltration is not insignificant given the evidence of secondary damage caused by the immune cells themselves. This can contribute to oxidative stress or to cellular damage by the release of specific cytokines (Rando, 2002). Therefore, the secondary effects should necessarily be distinguished from the primary pathogenic mechanisms that lead to cell death (Rando, 2002).

Disatnik and co-workers, 1998, reported an age-dependent increase in lipid oxidation products and compensatory induction of antioxidant enzymes, supporting oxidative stress as a primary pathogenic mechanism in the mdx mouse. Because secondary processes may confound biochemical analysis of actively degenerating tissue, studies of muscle before the onset of degeneration provide a more definitive assessment of primary pathophysiological mechanisms (Rando, 2002). The present chapter therefore paid specific attention to how the parameters assessed here differ between SJL/J mice at 14 weeks of age and 27 weeks of age. In both these age groups, the pathology has already set in, therefore the analysis of the present chapter will focus on how the parameters assessed here, were influenced as age progressed.

Although the significance and precise extent of the oxidative stress contribution in the degenerative process of dystrophic muscle is poorly understood, there is increasing evidence that the degenerative process may indeed be due to oxidative stress (Niebrój-Dobosz and Hausmanowa-Petrusewicz, 2005). The ultrastructural findings in chapter 6 of the present study provided evidence consistent with ultrastructural changes to muscle mitochondria of human skeletal muscle, experimentally subjected to oxidative damage by ROS. The findings reported in chapter 6 suggested that mitochondria in SJL/J mouse muscle are probably subjected to oxidative stress damage. Although others (Disatnik *et al.*, 1998) have confirmed oxidative stress injury as the primary pathogenic mechanism of muscle degeneration in dystrophin-deficient muscle in the mdx model, no evidence could be found from literature that dysferlin-deficient muscle is subjected to the same insult. To address the notion that muscle pathology in dysferlin-deficient muscle may be free radical-mediated, the lipid peroxidation content of quadriceps muscle in SJL/J mice, was evaluated in the present chapter. In addition, the antioxidant activity in quadriceps muscle was evaluated as the total antioxidant status (TAS), in all SJL/J mice groups. These two parameters were compared and expressed as an oxidative stress index.

7.2 Materials and Methods

After the 90 day animal study, SWR/J mice were terminated at the age of 28 weeks, SJL/J mice were 27 weeks of age. The age control group that was terminated at the beginning of the 90 day trial was 14 weeks of age. Quadriceps muscles from all groups were assessed for levels of lipid peroxidation and all SJL/J mouse groups were assessed for total antioxidant status. One quadriceps muscle from each animal was isolated and frozen in liquid nitrogen. Tissue was stored in liquid nitrogen until the assay procedures were performed. Prior to the assays, muscles were cut in half and weighed. One half was processed for TAS analysis while the other was processed for lipid peroxidation

determination. Before assay procedures were conducted, tissue was stored at -70°C, until analysis. Animals, groups, sample size, treatments and results from the assay procedures are outlined in Table 7.1.

7.2.1 Total Antioxidant Status

Total antioxidant status activity was measured by means of the Randox Kit (Antrim, United Kingdom). The kit is in the form of a colorimetric assay of which the principle is based on the inhibition of the absorbance of the radical cation of 2,2'-azinobis(3-ethylbenzothiazoline sulphonate) ($ABTS^+$) by antioxidants present in the tissue. The $ABTS^+$ radical cation forms when ABTS interacts with the ferrylmyoglobin radical species, generated by the activation of metmyoglobin with H_2O_2. The $ABTS^+$ radical cation is colorimetrically detected by its blue-green colour, and was measured on a spectrophotometer set at 595nm at 37°C. The antioxidants present in the sample suppress the formation of the radical cation to an extent and on a time scale that is proportional to the antioxidant concentration (Rice-Evans and Miller, 1994). Quadriceps muscle from each animal was homogenized individually using a Janke & Kunkel homogenizer, (IKA Werk; Ultra-Turrax) in 1 ml ice cold phosphate buffered saline (PBS). The homogenates were centrifuged at 800g for 10 min and the resultant supernatant used for TAS analysis, as per manufacturer's instruction. The protein concentration for every sample was determined with the aid of the Pierce® BCA Protein Assay Kit (Thermo Scientific) and calculated from a standard curve (Figure 7.1) using a polynomial regression analysis. The TAS of muscle samples was expressed as millimoles per gram (mM/g) of proteins for each individual. Results are given as mean TAS per group ± standard deviation (SD).

7.2.2 Lipid Peroxidation

Lipid peroxidation was measured by the thiobarbituric acid (TBA) assay, according to the method by Draper and Hadley, 1990, and Kaczor and co-workers, 2007. The assay was used to measure the level of cellular malondialdehyde (MDA) in quadriceps muscle tissue, which is proportional to the degree of lipid peroxidation (Disatnik *et al.*, 1998). The quadriceps muscles were weighed, and homogenized individually using a Janke & Kunkel homogenizer, (IKA Werk; Ultra-Turrax) in 1ml buffer containing 50mM K_2PO_4, 1mM EDTA, 1mM DTT, 1.15% KCl, and 1mM butylated hydroxytoluene (BHT) (Supelco Analytical, Bellefonte, PA, USA). The addition of BHT to the reaction mixture before processing has the ability to extensively reduce or even eliminate the oxidation of PUFAs, a process that might artefactitiously occur during the MDA determination procedures (Draper and Hadley, 1990). The homogenates were centrifuged at 8000 rpm for 10 min at 4°C. The resultant supernatant was retained and 100µl of the sample was mixed with 2 volumes (200µl) of ice cold 10% (w/v)

trichloroacetic acid (TCA) (Merck). The samples were incubated for 5 min to allow proteins to precipitate The samples were then reacted with an equal volume (300µl) of a 0.067% (w/v) solution of TBA (Sigma-Aldrich) and incubated in a boiling water bath for 10 min. Samples were cooled on ice for 5 min, and centrifuged at 7000 rpm for 1 min to remove dense particles from the supernatant. The resultant clear supernatant (200µl) was transferred to a micro plate and absorbance was measured at 550nm. The concentration of MDA was calculated using the MDA standard curve with 1,1,3,3-tetramethoxypropane (Aldrich) as a standard (Figure 7.1). A 10mM stock solution was prepared, and from the stock solution dilutions were made to range from 0 to 20µM. The standards were treated the same as the samples and the absorbance measured at 550nm. A linear regression analysis was performed and MDA tissue levels were expressed as nanomoles per gram wet weight muscle. Results are given as mean MDA concentration per group ± SD.

7.2.3 Oxidative Stress Index

Oxidative stress index is given by the ratio percentage of total lipid peroxidation to total antioxidant status. The result is an indicator of the degree of oxidative stress (Harma *et al*., 2003; Horoz *et al*., 2005) and is given in arbitrary units (AU) ± SD.

7.2.4 Statistical Analysis

TAS Assay

The TAS assay, in duplicate and total protein concentration from the quadriceps muscle of the SJL/J mice assays was preformed and utilized for the calculation of the total antioxidant capacity per gram of protein. The average total antioxidant capacity per gram of protein for each experimental group is presented in Table 7.1. The calculated total millimolar antioxidant capacity per gram of protein values was statistically compared between the various experimental groups, via a one-way ANOVA in NCSS. A significance level of 0.05 was used.

TBA Assay

The TBA assay, in triplicate, was performed upon a weighed mass of wet muscle derived from quadriceps muscle of experimental mice. The data was utilized in order to calculate the quantity of MDA present per gram of muscle tissue. The average MDA content per gram of wet muscle mass, for each experimental group, is presented in Table 7.1. The quantified MDA levels were statistically compared between the various experimental groups, via a Kruskal-Wallis one-way ANOVA in NCSS due to the lack of normal data distribution. A significance level of 0.05 was used.

OSI

Unequal sample size could be utilized during this statistical assessment as a Modified-Levene Equal-Variance Test proved all the OSI data possessed equal variance. Due to the data failing to meet a normal distribution pattern, the non-parametric Kruskal-Wallis One-way ANOVA was utilized. A significant difference (P = 0.004082) was found to exist between two or more of these groups. The Tukey-Kramer Multiple-Comparison *pos hoc* test was employed to determine where this difference lay. A significance level of 0.05 was used.

7.3 Results and Discussion

The mean values for antioxidant activity, levels of lipid peroxidation detected, and oxidative stress index in each group are presented in Table 7.1.

Table 7.1 A summary of groups assessed for antioxidant status, lipid peroxidation, and oxidative stress index. Specification of animal age, treatment doses, and results from the TAS and TBA assays, as well as the OSI calculations are presented

	Group	Age (weeks)	Treatment	TAS ± SD (mmol/g)	MDA ± SD (nmol/g)	OSI (AU)
Control groups	**Negative control** (SWR/J mice) (n = 6)	*28*	Placebo	-	248.49 ± 78.91	
	Positive control (n = 6)	*27*	Placebo	0.24 ± 0.04	480.02 ± 199.89	0.22 ± 0.13
	Age control (n = 3)	*14*	No	0.11 ± 0.02	941.81 ± 93.14	0.86 ± 0.15
Treatment groups	**Resveratrol** (n = 6)	*27*	Resveratrol 60mg/kg/day	0.28 ± 0.08	292.04 ± 73.14	0.11 ± 0.05
	CoQ10 (low) (n = 5)	*27*	CoQ10 40mg/kg/day	0.32 ± 0.05	303.60 ± 83.97	0.10 ± 0.02
	CoQ10 (high) (n = 6)	*27*	CoQ10 120mg/kg/day	0.28 ± 0.08	328.47 ± 148.01	0.12 ± 0.08
	Resveratrol/CoQ10 combination (n = 6)	*27*	Resveratrol (60mg/kg/day) + CoQ10 (40mg/kg/day)	0.21 ± 0.03	302.74 ± 65.00	0.15 ± 0.03

OSI = Oxidative stress index; AU = arbitrary unit; MDA = Malondialdehyde; TAS = total antioxidant status; TBA = thiobarbituric acid

Figure 7.1: Standard curves for protein and malondialdehyde (MDA) standards. The formulas on the graphs were used for polynomial and linear regression analysis, respectively.

7.3.1 Total Antioxidant Status

To determine whether the supplementation of SJL/J mice with various concentrations of antioxidants will result in elevated levels of antioxidant activity in the muscle tissue, the total antioxidant status was determined in quadriceps muscle from SJL/J mice (Figure 7.2). An increase in TAS was observed in the resveratrol (0.28 ± 0.08mmol/g), low CoQ10 (0.32 ± 0.05mmol/g) and high CoQ10 (0.28 ± 0.08mmol/g) groups when compared to the positive control (0.24 ± 0.04mmol/g) group. The age control (0.11 ± 0.02mmol/g) group showed the lowest level of TAS compared to all the other groups. The resveratrol/CoQ10 combination (0.21 ± 0.03mmol/g) group displayed the lowest TAS compared to the other antioxidant supplemented groups, as well as the positive control group.

A significant difference (P = 0.000477) was found in terms of the total millimolar antioxidant activity per gram of protein between the six experimental groups when assessed by means of a one-way ANOVA. The data was normally distributed and although of unequal sample size was proved to be of equal variance with the use of the Modified-Levene Equal-Variance Test. The use of Tukey-Kramer Multiple-Comparison *pos hoc* test revealed that the age control group showed a significantly smaller total antioxidant activity per gram of protein than all the other experimental groups except the resveratrol/CoQ10 combination group. The resveratrol/CoQ10 combination group was significantly smaller, in terms of its total antioxidant activity, than the low CoQ10 group. All the other experimental groups were statistically indifferent to each other.

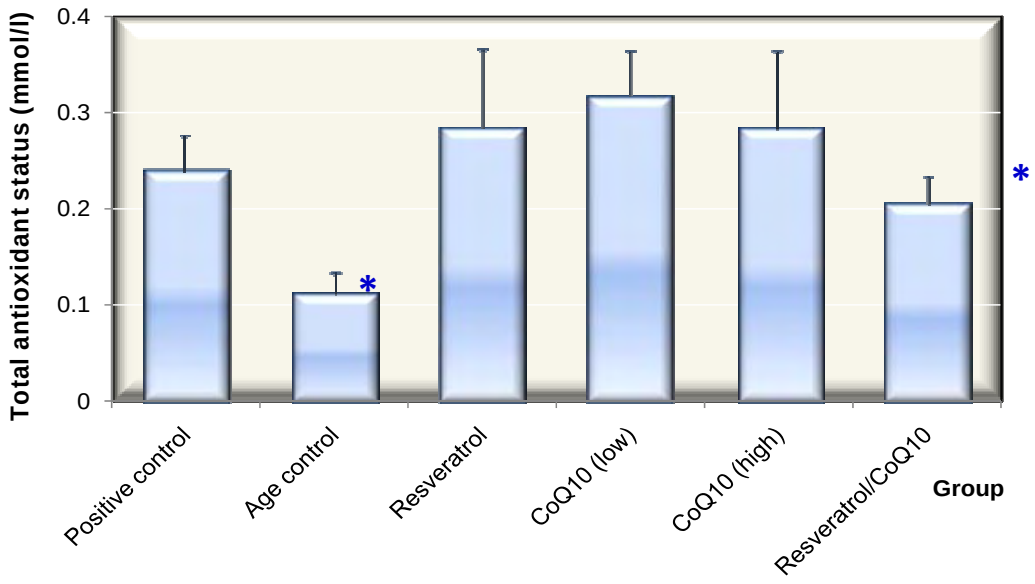

Figure 7.2: Levels of total antioxidant status in quadriceps muscles of SJL/J mice. The lowest antioxidant activity is observed in muscle samples from the age control group. The resveratrol/CoQ10 combination group shows a significantly lower antioxidant activity than the low CoQ10 group. The resveratrol and both CoQ10 groups all display higher antioxidant activity than what is observed in the untreated positive control group, although this difference is not significant. Significance at a level of 0.05 is indicated by *

7.3.2 Lipid Peroxidation

To directly test for the presence of oxidative stress in the SJL/J mice after the 90 days of supplementation with various concentrations of antioxidants, the level of lipid peroxidation was evaluated for each group. The TBA assay, to assess oxidative injury, was performed on quadriceps muscle from all groups and measured for each individual animal (Figure 7.3). The positive control (480.02 ± 199.89nmol/g) and age control (941.81 ± 93.14nmol/g) groups displayed markedly elevated levels of tissue MDA, compared to the antioxidant treated groups, as well as the negative control group.

All the antioxidant supplemented groups displayed levels of tissue MDA, comparable to that found in the negative control group (Figure 7.3). The resveratrol group (292.04 ± 73.14nmol/g), the low CoQ10 group (303.60 ± 83.97nmol/g), and resveratrol/CoQ10 combination group (302.74 ± 65.00nmol/g) showed the lowest levels of MDA compared to the positive control group. In the high CoQ10 group (328.47 ± 148.01nmol/g), MDA levels is only slightly higher than that detected in the

negative control group and other treatment groups, but still much lower than that detected in both the positive and age control groups.

Unequal sample size could be utilized during this statistical assessment as a Modified-Levene Equal-Variance Test which proved that all the data possessed equal variance. Due to the data failing to meet a normal distribution pattern, the non-parametric Kruskal-Wallis One-way ANOVA was utilized. A significant difference (P = 0.0190911) was found in terms of the total nanomolar MDA content per gram of wet muscle mass between the experiential groups. The use of Tukey-Kramer Multiple-Comparison *pos hoc* tests revealed that the age control group showed a significantly higher MDA content within their quadriceps muscles in comparison to all the other groups assessed. The negative control group showed significantly lower MDA values than the positive control. All the other experimental groups were statistically indifferent to one another.

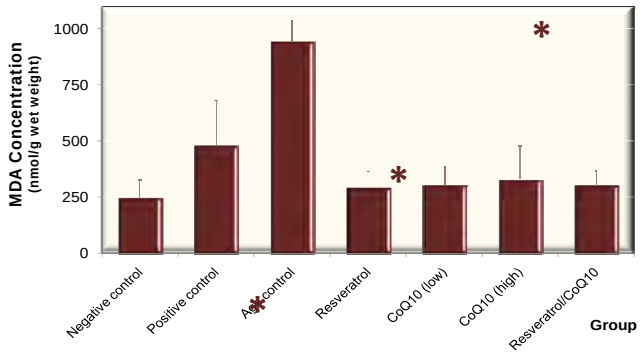

Figure 7.3: Levels of lipid peroxidation in quadriceps muscles of all groups in the present study. An increase in MDA levels was detected in the positive and age control groups, when compared to the negative control and the treatment groups. All groups supplemented with antioxidants showed decreased levels of MDA when compared to the positive and age control groups and similar to MDA levels in the negative control group. Significance at a level of 0.05 is indicated by *

Figure 7.3 shows the level of MDA to be greater in the untreated positive and age control groups, than in the negative control and antioxidant treated groups. The level of MDA was markedly elevated in the younger SJL/J mice (14 weeks of age). These results indicate that oxidative stress

levels in 14 week-old SJL/J quadriceps muscles are higher than that detected in older animals. The data suggest that these levels can be detected from 14 weeks of age, and perhaps earlier. This is in contrast with the findings of Disatnik and co-workers, 1998, who found an age dependent increase in lipid oxidation products in mdx mice.

7.3.3 Degree of Oxidative Stress

An enormous increase in the degree of oxidative stress in the age control group (0.86 ± 0.15), compared to all other groups was shown by calculation of the OSI. The Tukey-Kramer Multiple-Comparison *pos hoc* test revealed that the age control group showed a significantly higher OSI in comparison to all the other groups assessed. All groups treated with antioxidants; the resveratrol (0.11 ± 0.05), the low CoQ10 (0.1 ± 0.02), the high CoQ10 (0.12 ± 0.08), and the resvertrol/CoQ10 combination (0.15 ± 0.03) groups, all showed reduced levels of the degree of oxidative stress when compared to the positive control (0.22 ± 0.13) group, although not statistically significant.

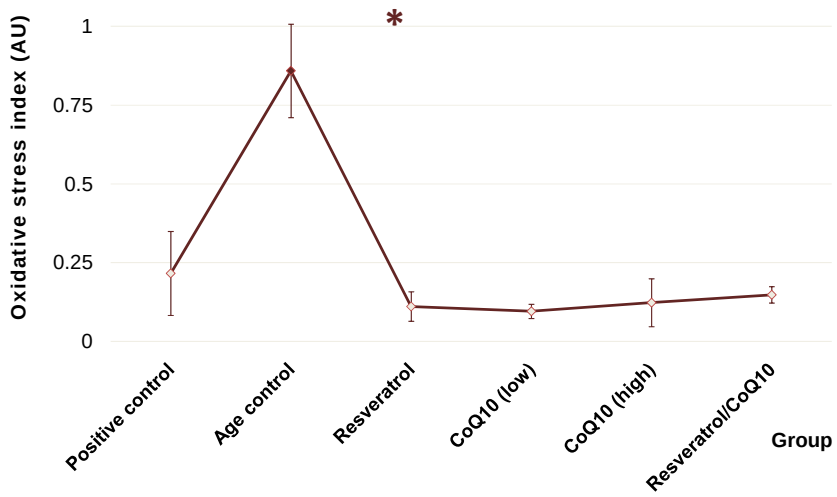

Figure 7.4: The tendency in the degree of oxidative stress in SJL/J mice untreated and supplemented with antioxidants. The age control group showed a significantly higher OSI in comparison to all the other groups assessed. OSI is expressed in arbitrary units (AU). Significance at a level of 0.05 is indicated by *

7.3. 4 JUSTIFICATION OF THE APPROACH FOLLOWED

A complex variety of products, many of which are reactive electrophiles are generated by lipid peroxidation (Marnett, 1999). The basic reactions of lipid peroxidation result in the formation of isoprostanes and MDA (Marnett, 1999). MDA occurs in biological samples in the free state and in various covalently bound forms (Draper and Hadley, 1990). Its levels can be estimated by the TBA reaction which yields a group of chromophores known as TBA reactive substances (TBARS) (Murphy and Kehrer, 1989).

Murphy and Kehrer, 1989, reviewed the role of oxidative stress in dystrophic muscle and reported that many studies have found dystrophic human-, mouse-, and chicken muscle to contain higher levels of TBARS than normal subjects. The study further revealed that the presence of TBARS and other indexes of oxidative stress in inherited muscular dystrophies is probably not due to the secondary pathological effects of inherited muscular dystrophy. It more likely indicates oxidative stress ongoing in the muscle tissue (Murphy and Kehrer, 1989).

The validity of MDA as an index of lipid peroxidation has been clouded by controversy regarding its formation as an artefact of analysis, and as a product of enzyme reactions, its occurrence in various bound forms, and the specificity of methods used for its measurement (Draper and Hadley, 1990). Nevertheless, widespread interest has been attracted to the determination of MDA in biological samples as it appears to offer a facile means of assessing lipid peroxidation in biological materials (Draper and Hadley, 1990). It is furthermore one of the most frequently used indicators of lipid peroxidation (Nielsen *et al*., 1997). Nielsen and co-workers suggested that MDA be used only as a biomarker for the degree of lipid peroxidation on a group basis.

Methods for measurement of the antioxidant activity of fluids are all essentially inhibition methods; a free radical species is generated, there is an endpoint by which the presence of the radical is detected, and the antioxidant activity of the added sample inhibits the end point by scavenging the free radical (Rice-Evans and Miller, 1994). These methods have been reported to vary greatly as to the radical that is generated, the reproducibility of the generation process, and the endpoint that is used (Rice-Evans and Miller, 1994). Since there is not yet an accepted 'gold standard' reference method for measuring TAS (Hubel, 1999; Horoz *et al*., 2005), it was decided to determine the antioxidant activity of quadriceps muscle with aid of the Randox TAS kit. The kit is one of the widely used methods for antioxidant activity/response measurement (Horoz *et al*., 2005). Lantos and co-workers, 1997, suggested TAS to be a valuable and reproducible method for measurement of the actual antioxidant status in different diseases and as a tool to monitor treatment.

The findings of mitochondrial alterations in chapter 6 indicated that the muscle tissue of SJL/J mice is subjected to oxidative damage. Therefore, analysis of lipid peroxidation levels in quadriceps muscles was performed, as a parameter for the presence of oxidative stress, in all groups in the present study. Lindschinger and co-workers, 2004, suggested that a statement about oxidative stress should be based on an antioxidant status, in the context of multiple oxidative stress parameters. In conjunction with determination of MDA levels, the TAS in muscle tissue was determined. These two parameters were used to calculate the OSI, which represents the degree of oxidative stress in the muscle tissue.

7.3.5 Denotation of the Results

The highest levels of MDA were detected in the age control group, while the lowest antioxidant activity was present in this group. The positive control group displayed markedly lower levels of MDA than that detected in the 14 week-old mice. The TAS levels in the positive control group were not significantly different from that detected in the antioxidant treatment groups. On the contrary the levels of MDA in the positive control group were markedly elevated compared to the antioxidant treatment groups, and the negative control group.

The data showed a relation between the antioxidant status and the amount of lipid peroxidation in the SJL/J mouse consistent with the findings of Lindschinger and co-workers, 2004, who reported that a decrease in TAS indicates an excess of ROS and therefore a consumption of antioxidants. At age 14 weeks, the very low levels of antioxidants are associated with the very high levels of lipid peroxidation in the age control group. These findings suggest that at the age of 14 weeks, the pathological changes has already set in and resulted in production of oxidative stress in the quadriceps muscles of SJL/J mice. Even though the dystrophic changes were only minimally present in the age control group, as observed by morphological and ultrastructural analysis in chapters 5 and 6. It can be further expected that these very high levels of oxidative stress will initiate severe tissue disruption that will manifest at the cellular level as age progress, consistent with the histopathology described for the positive control group in chapter 5.

Seeing that age control group received no antioxidant treatment, a decreased antioxidant status was expected. The antioxidant status in the age control group was nevertheless, significantly lower than the TAS measured in all the other SJL/J mice. This might indicate that at the age of 14 weeks, the endogenous antioxidant system has not yet been activated to address the high levels of oxidative stress in the tissue, or it is not yet responding. While in the positive control group, the TAS values

were similar to that of the treatment groups. This observation indicates that since this group did not receive any antioxidant supplementation, the endogenous antioxidant system must have been responding to high levels of oxidative stress. Induction of antioxidant enzymes is a common cellular response to increased levels of oxidative stress (Harris, 1992).Therefore the endogenous antioxidant response should be responsible for the increased antioxidant activity observed in 27 week-old untreated SJL/J mice. These results might further suggest that there is a delayed activation or response of the endogenous antioxidant system in the SJL/J mouse. As an effect of this late response, increasing oxidative stress levels resulted in the tissue deterioration, and in fact the ongoing dystrophic processes seen in the untreated 27 week-old SJL/J mice.

A similarity in MDA levels was observed in the negative control and antioxidant treatment groups. These results are indicative of the ability of antioxidant supplementation to address the degree of lipid peroxidation, and thereby, decrease the levels of MDA. It appears from the results that the decrease in MDA levels were independent of the dose of antioxidants administered. Structural analysis of quadriceps showed major differences between groups (chapter 5). It is therefore possible that the antioxidant supplementation at lower doses (resveratrol and low CoQ10 groups), lowered the levels of oxidative stress present in the muscle tissue. However, these concentrations were unable to delay the progression of tissue damage that was initiated by the presence of high oxidative stress levels, before the supplementation started.

It can therefore be stated that the onset of disease on a molecular level, occurred before 14 weeks of age in the SJL/J mouse, as the highest oxidative stress levels were measured in this group. The results are further suggesting that when oxidative stress in muscle tissue reaches a specific level, the endogenous antioxidant systems are activated to address this imbalance. This suggestion explains the reduced levels of MDA and increased levels of antioxidant activity measured in the untreated positive control group, when compared to the age control group. These results also suggest that if supplementation with antioxidants begins after the onset of this molecular cascade of events, responsible for oxidative stress increase in muscle, the degree of tissue damage will not be decreased by lower doses of antioxidant supplementation.

On the contrary, a lower oxidative stress profile was observed in groups treated with high doses of antioxidants (high CoQ10 and resvertarol/CoQ10 combination groups). This observation supports the findings of a lesser degree of tissue damage observed at microscopic level (chapter 5). The levels of MDA in antioxidant treatment groups suggest that the reduction of lipid peroxidation in the muscle is independent on the concentration of antioxidants administered. But histopathological

investigations (chapter 5) revealed that only very high levels of antioxidant supplementation were able to reduce the cellular disruption. This observation revisits the suggestion that a delayed activation or response of the endogenous antioxidant system might be present in the SJL/J mouse. It is therefore suggested that the higher doses of antioxidant supplementation might compensate for this delayed response, resulting in sparing of muscle tissue.

To evaluate the relationship between the levels of oxidative stress, and antioxidant response in the SJL/J mice in the present study, the two parameters assessed were compared to determine the OSI for each group. As an indicator of the degree of oxidative stress, calculation of the OSI revealed that the oxidative/antioxidative balance shifted towards antioxidative balance in 27 week-old untreated SJL/J mice compared to 14 week-old counterparts. This is probably the result of an activated endogenous antioxidant system. Furthermore, another shift was observed towards antioxidative balance in all 27 week-old SJL/J mice supplemented with antioxidants compared to the untreated 27 week-old SJL/J mice. These results showed that supplementation of SJL/J mice with antioxidants from an age of 14 weeks for 90 days result in a shift towards antioxidant balance.

7.4 Concluding Remarks

The current chapter investigated the presence of oxidative stress in the quadriceps muscle tissue as an additional parameter of the cellular effects afforded by CoQ10 and resveratrol supplementation. The benefit for dystrophic muscle from any individual antioxidant treatment would depend on the actual nature of the oxidative stress occurring in the muscle tissue (Rando, 2002). Rando, 2002, stated that different susceptibilities to oxidative stress are not identical. Even if oxidative stress is indeed the primary pathophysiological process leading to muscle cell death in the dystrophies, effective treatment with antioxidants will need to be targeted to the specific deficit in antioxidant defence (Rando, 2002). From the results obtained here, it is evident that there is a relationship between the very high levels of oxidative stress in 14 week-old SJL/J mice and the degree of pathology in 27 week-old counterparts. In addition, the results suggested that the possibility for a delayed endogenous antioxidant response exist, and that this delay is in part responsible for the severity of dystrophic progression. It is therefore possible that the specific deficit in antioxidant defence in SJL/J mice are this delayed antioxidant response. Therefore, application of low dose antioxidant supplementation might permeate a protective effect onto the cellular level, if supplementation is started before onset of the disease.

The results obtained in chapter 6 proposed the mitochondria as an organelle particularly susceptible to oxidative stress. It might not be the only organelle, but the ultrastructural alterations to the mitochondria were more pronounced. CoQ10 is present in the innermembrane of mitochondria, where the major part of ATP production occurs (Crane, 2001). The unique function of CoQ10 as an essential part of the cellular machinery is given by its ability to transfer electrons from the primary substrates to the oxidase system. At the same time CoQ10 transfers protons to the outside of the mitochondrial membrane (Crane, 2001). This results in a proton gradient across the membrane. As the protons return to the interior through the enzymatic machinery for making ATP, they drive the formation of ATP (Crane, 2001). CoQ10 is therefore the antioxidant of choice to target the specific organelle proposed to be deficient in antioxidant defence, in SJL/J quadriceps muscle.

Since the ultrastructural analysis (chapter 6) only provided qualitative information, it was decided to analyse SJL/J quadriceps muscle for the presence of oxidative stress, represented by the level of MDA present per gram of muscle, and quantify the findings. These results suggest that the endogenous antioxidant defence system in tissue subjected to oxidative stress insult is activated in response to the tissue damage in subjects not supplemented with antioxidants. The large amount of MDA detected in 14 week-old SJL/J mice showed that quadriceps muscle in these animals is subjected to oxidative stress injury before this age. These results further suggest that once oxidative stress is present in the muscle, it will result in dystrophic changes in the tissue that cannot effectively be reduced by lower antioxidant doses.

It was established that the supplementation with CoQ10 and resveratrol resulted in an increase in antioxidant activity and a decrease in lipid peroxidation levels in the quadriceps muscle of SJL/J mice. This gave rise to a shift in the oxidative/antioxidative balance towards an antioxidative balance in 27 week-old SJL/J mice.

It is evident from the present findings that the ultrastructural mitochondrial alterations in the SJL/J mouse are largely due to oxidative stress insult. The OSI suggests that antioxidant supplementation at all doses has the ability to shift oxidative/antioxidative balance towards an antioxidative balance. However, only higher doses of antioxidants (CoQ10 or a combination of resveratrol/CoQ10) are able to permeate this effect onto the cellular level.

The OSI might become a useful tool for oxidative stress assessment in the dysferlinopathies, the MDs, and other conditions, especially the lifestyle diseases.

From the results of this chapter, evidence is provided supporting the notion that metabolic disturbances are brought about by the increased levels of oxidative stress. In addition, very high levels of oxidative stress are present even before inflammation could be detected at the cellular level. This is indicative that the generation of oxidative stress in quadriceps muscle is preceding the inflammatory events in SJL/J mice. The ultrastructural changes to mitochondria, suggestive of oxidative stress injury (chapter 6) are most likely the result of oxidative stress present in the muscle. The level of oxidative stress was successfully reduced in SJL/J mice by all doses of antioxidants used in the present study, but transformation at the cellular level were afforded only by the higher antioxidant doses. This observation supports the suggestion that endogenous antioxidant response might be delayed in the SJL/J mouse. Therefore only very high levels of antioxidants will afford protection against tissue deterioration after onset of disease.

Future research might be conducted to establish whether antioxidant supplementation from a younger age will provide a more pronounced protective effect in dysferlin-deficient muscle tissue. Also, if antioxidant supplementation is started at a pre-pathological stage in the SJL/J mouse model, whether lower levels of antioxidants will then be able to maintain muscle integrity at cellular level.

Chapter 8

Concluding Discussion

The dysferlinopathies encompass a group of disorders that are not responsible for early mortality, but for a devastating deterioration of mobility in the affected. During the course of this disease this loss of ambulation results in an escalating decreased quality of life. To date, there is no curative treatment for this group of inherited disorders.

With the identification of the novel skeletal muscle gene dysferlin that is mutated in the dysferlinopathies (Liu *et al*., 1998; Bashir *et al*., 1998), the need for a therapy to restore the expression of the protein dysferlin has become indispensable. Rando, 2002, reported that although the genetic basis of many of the muscular dystrophies has been known for over a decade, the pathogenic mechanisms leading to muscle cell death in the dystrophies remain a mystery. The gene mutation responsible for the clinical pathology in the dysferlinopathies has been identified a decade ago (Bashir *et al*., 1999; Liu *et al*., 1999). However, the exact pathogenic mechanism remains to be elucidated and therefore the effective application of therapeutic strategies, lingers.

The decision to employ CoQ10 as an antioxidant was based on its known potent antioxidant potential, bearing in mind that oxidative stress may contribute to the pathological events in this disease. The decision to employ resveratrol, a rather weak antioxidant (Hu *et al*., 2007), in the same study for the same application, was based on its known ability to mediate inhibition of the detrimental effects caused by amongst others, oxidative stress ((Fauconneau *et al*., 1997; Kirimlioglu *et al*., 2008; Robb *et al*., 2008).

It has previously been shown that presymptomatic supplementation with CoQ10 in primary CoQ10 deficiency has revealed an unparalleled outcome (Montini *et al*., 2008). No clear benefit has been found in clinical trials of antioxidant therapy in human DMD that included treatments with ascorbate, penicillamine, tocopherols and SOD (Murphy and Kehrer, 1989; Walton and Nattrass, 1954; Stern *et al*., 1982; Roelofs *et al*., 1979; Fenichel *et al*., 1988). However, these trials have been limited in size and duration and almost always included subjects with advanced disease progression. On the contrary, Folkers and Simonsen, 1995, reported definite increase in physical performance of patients with various muscular dystrophies following treatment with CoQ10.

Murphy and Kehrer, 1989, clearly stated that if lipid- and water-soluble antioxidants are applied as treatment strategy in the muscular dystrophies, such treatments would only be symptomatic. They added that the underlying biochemical defect of muscular dystrophy, as with nearly all inherited diseases, can only be cured if techniques are developed to repair or replace the defective genetic material.

As early as 1989, mounting evidence revealed that oxidative processes play a fundamental role in the inherited dystrophies, either directly or indirectly (Murphy and Kehrer, 1989). Disatnik and co-workers, 1998, stated that the beneficial effect of antioxidant therapy would be compelling support of the hypothesis that oxidative stress contributes to the initiation of muscle cell necrosis in the muscular dystrophies. The present study, by the use of various parameters, confirmed that not only is oxidative stress present in skeletal muscle of dysferlinopathic mice, but it is very likely responsible for the initiation of the dystrophic process.

Assessment of non-specific parameters in chapter 4 provided valuable additional knowledge that strengthens the observations made on a cellular level in this study. Evaluation of animal weight in the present study provided an effective means of condition evaluation, to ensure animal well-being was maintained at all times. The animal weights of all experimental groups increased over the 90 day period due to supplementary food provided for their convenience. Weight increase was independent of the antioxidant supplementation.

No significant conclusion on the effect of antioxidant supplementation in SJL/J mouse model could be derived from the CK and LDH blood levels in the present study. The reason being, abnormally high values in the negative control groups could not be explained. This was in part due to the sample size utilized for these laboratory tests.

Significantly higher eosinophil counts were measured in the age control group compared to all other groups assessed. In addition, this group displayed significantly higher neutrophil counts compared to the resveratrol group, and the highest basophil count was also detected in this group. This finding correlates with the highest levels of MDA measured in this group, as well as the lowest antioxidant status. These results indicate that the highest inflammatory response was present at the age of 14 weeks and can be related to the highest degree of oxidative stress, measured for this group. On the contrary, the histopathological analysis of 14 week-old animals displayed only minimal to mild dystrophic changes. This leads to the suggestion that the deployment of inflammatory cells at the

age of 14 weeks might be in response to the high levels of oxidative stress. This inflammatory reaction, not yet detectable at cellular level at the age of 14 weeks, suggests that this cascade of events is activated around the age of 14 weeks, and give rise to the histopathology observed in untreated 27 week-old SJL/J mice.

The lowest monocyte, neutrophil, eosinophil and non-zero basophil counts, were detected in the resveratrol/CoQ10 group. This observation gave rise to the hypothesis that the lowest inflammatory activities would be observed on tissue level in this group. Consistent with the histopathological observations from this group, that displayed, from a qualitative perspective, the least inflammatory changes, the hypothesis could not be rejected. The observation of the highest physical strength displayed by this group supported this statement. Although not statistically significant, this group showed the highest tensile strength, in addition to the high CoQ10 group, compared to all other groups. A decrease in the degree of oxidative stress compared to the positive control and age control groups further strengthens the suggestion that supplementation with resveratrol and CoQ10 in combination, was able to afford physical and cellular improvement of the dystrophic alteration pattern in the SJL/J mouse.

Haematological analysis of the high CoQ10 group showed the highest similarity to that of the negative control group. At microscopic level, tissue analysis revealed a striking similarity to what was observed in the resveratrol/CoQ10 combination group, with reduced levels of inflammatory changes compared to other groups. The physical strength measured for animals on high dose CoQ10 supplementation was also stronger compared to all other groups, in addition to the resveratrol/CoQ10 combination group. The OSI measured about half of that in the positive control group. These results support the suggestion that supplementation with high doses of CoQ10 was also able to afford physical and cellular improvement of the dystrophic alteration pattern in the SJL/J mouse. This improvement was afforded almost to the same extent as that seen with resveratrol/CoQ10 combination treatment.

Morphometric assessment suggested that active regeneration occurred in the high CoQ10 and resveratrol/COQ10 combination groups, followed by maturation of fibers towards larger fiber diameters. Other groups did not display this observation. These results indicate that while quadriceps muscle fibers had a tendency towards smaller diameters in untreated and low dose antioxidant supplemented groups, CoQ10 at high dose and resveratrol/CoQ10 in combination allow for fiber maturation, indicated by the tendency of fibers towards larger diameters.

The differences in white blood cell counts detected between the high CoQ10 and resveratrol/CoQ10 combination groups, probably suggest that the mechanism whereby enhancement in condition of SJL/J mice was brought about, differs between these two supplementation strategies. The presence of minimal to mild inflammatory changes at cellular level of these two groups suggests that the dystrophic progression will probably be delayed and not reversed, following antioxidant treatment.

Resveratrol alone and low dose CoQ10 supplementation resulted in similar reduction of oxidative stress levels than that afforded by high CoQ10 doses and resveratrol/CoQ10 in combination. These two antioxidants at low doses were also able to increase antioxidant status in the muscle tissue to the same extent as high doses of antioxidants. Nevertheless, the supplementation of SJL/J mice with resveratrol alone or low dose CoQ10 was not able to decrease dystrophic alterations at cellular level to the same extent than what was afforded by high dose CoQ10 and resvertarol/CoQ10 in combination. Consistent with the histopathology data obtained from these two groups, was the reduction in physical strength that was lower than all other experimental groups. Collectively, the results from the resveratrol and low CoQ10 groups suggest that antioxidant supplementation at these doses will not result in enhanced physical condition in the SJL/J mouse. Neither will it afford protection at the cellular level. It is therefore possible that supplementation from the age of 14 weeks was too late to result in beneficial effects from these antioxidant doses. This notion further implicates that only high doses of CoQ10 or low doses of resveratrol and CoQ10 in combination will be effective in slowing disease progression in the SJL/J mouse, if supplementation is started after onset of disease.

Ultrastructural analysis of SJL/J quadriceps muscles confirmed the hallmarks of the disease at this level, previously described by others (Selcen *et al.*, 2001; Cennachi *et al*., 2005). Focussing on non-specific ultrastructural alterations in the present study resulted in the valuable observation that non-specific ultrastructural changes in muscle mitochondria of SJL/J mice are indicative of oxidative stress injury. This observation provided useful evidence that oxidative stress might also be, in addition to the deficit in membrane repair, and chemotactic response, a causative mechanism for the ongoing muscle cell necrosis in the SJL/J mouse. It can also not be excluded that oxidative stress, might even be the primary pathogenic mechanism in the SJL/J mouse. This finding directed the assessment of oxidative stress levels in quadriceps muscles of SJL/J mice, and how these levels were affected by the administration of different concentrations of antioxidants.

The results from oxidative stress assessment revealed significantly higher levels of oxidative stress in 14 week-old animals, while in the 27 week-old counter parts only about half this level was measured. Calculation of the oxidative stress index revealed that the degree of oxidative stress in 27 week-old SJL/J mice is about a quarter of that detected in 14 week-old animals. These results provide strong evidence that the endogenous antioxidant system respond to the initial elevated oxidative stress levels. When comparing the high OSI in the age control group to the histopathological data of the positive control group, it was revealed that this initial elevated OSI can be correlated to the severe disruption of tissue integrity at cellular level. This finding indicates that oxidative stress is accumulating in muscle tissue of the SJL/J mouse before the age of 14 weeks. Thereafter it reaches peak levels at around this age, triggering the endogenous antioxidant system to respond. A matter of concern with this observation is that although the OSI in 27 week-old animals is much lower, the tissue disruption at cellular level is most severe. This provides evidence that the endogenous antioxidant system might respond too late to prevent the onset of tissue damage. From these results it can be suggested that very high levels of oxidative stress at the age of 14 weeks leads to tissue deterioratiom, as displayed by histopathology data of untreated 27 week-old animals. Therefore, it is probable that the initiation of the necrotic process in the SJL/J mouse is due to very high levels of oxidative stress, in conjunction with a delayed endogenous antioxidant response.

The results from this research provide evidence that high levels of CoQ10 and a combination of resveratrol/CoQ10 are able to manipulate this defect, and as a result delay the dystrophic progression. Antioxidant supplementations at these two concentrations lead to:

- White blood cell counts, reflecting i) similarity to that observed in the negative control group, and ii) levels suggestive of very low inflammatory response at the tissue level.
- Stronger physical strength, where tensile strength exceeded that measured in the negative control group.
- A reduced occurrence of inflammatory incidence and dystrophic changes at cellular level, resulting in enhanced tissue quality.
- A reduced oxidative stress index, where levels of lipid peroxidation were lowered to a profile similar to that measured for the negative control group. In addition, TAS was elevated, compared to the positive control group.

It can be concluded that increased oxidative stress levels are present in the SJL/J mouse. All antioxidant supplementation doses were able to decrease the levels of oxidative stress following 90 days of supplementation. Only a high dose of CoQ10 and/or resveratrol/CoQ10 in combination were able to permeate this effect onto a cellular level. This statement is supported by the observation of i) decreased leukocytes in the circulation of the high dose combination group; ii) higher physical strength observations with both the single antioxidant at high dose as well as the combination of antioxidants at high dose; iii) decreased levels of dystrophic markers observed at the light microscopic level, and iv) a reduced oxidative stress index.

The hypothesis of this study stating that, the supplementation of SJL/J mice with the antioxidants CoQ10 and resveratrol would be beneficial to the animals, and that the beneficial effect would be evident at cellular level, was not rejected.

Oxidative stress may also be viewed as a condition in which the production of oxidative products exceeds their removal by cellular repair mechanisms, which may lead to acute cellular metabolic disturbances and even cell death, if such changes accumulate (Rando, 2002). From the results obtained it can be suggested that the current therapeutic strategy might hold significant value in combination with cell-based therapies in the dysferlinopathies. It is suggested that the antioxidant protection offered by high dose CoQ10 and resveratrol/CoQ10 in combination, will afford modulation of the internal cellular environment in dysferlin-deficient tissue. This adjustment at cellular level creates a host environment where there is a reduced level of oxidative stress, and therefore a more favourable environment to accommodate transplanted cells.

This thesis provides evidence to create a new platform for combination therapeutic strategies. The supplementation of subjects with antioxidants is unlikely to reverse the pathological process. However, high doses afford the manipulation of dystrophic progression. In combination with cell transplantation therapeutic strategies, high dose antioxidant supplementation might provide an optimal environment for donor cell differentiation and maturation in dysferlin-deficient muscle tissue.

This thesis therefore concludes with the proposition that the unfavourable state in muscle tissue, brought about by inevitable, and to date, irreversible dystrophic processes that sets in after disease onset in the dysferlinopathies and progress gradually over the lifespan, might be manipulated by supplementation with high dose antioxidants. Presumably, the effect will be superior if

supplementation starts before the pathology sets in. In addition, this supplementation might offer a favourable environment for donor cell maturation and differentiation in cell transplantation therapies.

This thesis harmonizes the statement of Bermúdez-Crespo and López, 2007, that it takes a broad, comprehensive and systematic approach to understand biology that is generally unbiased and not dependent on existing knowledge. This study succeeded in manipulating at least three alterations in the dysferlinopathies. By application of high dose antioxidant supplementation, higher physical strength, reduced dystrophic changes at cellular level, and a reduced oxidative stress index were attained in the SJL/J mouse model. The supplementation of CoQ10 at 120mg/kg/day and resveratrol/CoQ10 in combination at 40 and 60mg/kg/day, respectively, directed dystrophic changes at cellular and physical levels towards a normal phenotype. The present study succeeds in providing an alternative treatment strategy to address metabolic derangements at cellular level, and provides a new platform for advances in cell-based therapies.

References

Aberg F, Appelkvist EL, Dallner G, Ernster L. Distribution and redox state of ubiquinones in rat and human tissues. *Arch Biochem Biophys* 1992;295(2):230-234.

Achanzar WE, Ward S. A nematode gene required for sperm vesicle fusion. *J Cell Sci* 1997;110(9):1073-1081.

Allamand V, Campbell KP. Animal models for muscular dystrophy: Valuable tools for the development of therapies. Hum Mol Genet 2000;9(16):2459-2467.

Ampong BN, Imamura M, Matsumiya T, Yoshida M, Takeda S. Intracellular localization of dysferlin and its association with the dihydropyridine receptor. *Acta Myol* 2005;24:134-144.

Anderson LVB, Davison K, Moss JA, Young K, Cullen MJ, Walsh J, *et al*. Dysferlin is a plasma membrane protein and is expressed early in human development. *Hum Mol Genet* 1999;8(6):855-861.

Anderson LVB, Harrison RM, Pogue R, Vafiadaki E, Pollitt C, Davison K, *et al.* Secondary reduction in calpain 3 expression in patients with limb girdle muscular dystrophy type 2B and Miyoshi myopathy (primary dysferlinopathies). *Neuromuscul Disord* 2000;10(8):553-559.

Ando Y, Imamura S, Hong YM, Owada MK, Kakunaga T, Kannagi R. Enhancement of calcium sensitivity of lipocortin I in phospholipid binding induced by limited proteolysis and phosphorylation at the amino terminus as analyzed by phospholipid affinity column chromatography. *J Biol Chem* 1989;264(12):6948-6955.

Aoki M, Liu J, Richard I, Bashir R, Britton S, Keers SM, *et al.* Genomic organization of the dysferlin gene and novel mutations in Miyoshi myopathy. *Nerurology* 2001;57:271-278.

Aragno M, Tamagno E, Gatto V, Brignardello E, Parola S, Danni O, *et al.* Dehydroepiandrosterone protects tissues of streptozotocin-treated rats against oxidative stress. *Free Radic Biol Med* 1999;26(11-12):1767-1747.

Aragno M, Mastrocola R, Brignardello E, Catalano M, Robino G, Manti R, *et al.* Dehydroepiandrosterone modulates nuclear factor-κB activation in hippocampus of diabetic rats. *Endocrinology* 2002;143(9):3250-3258.

Aragno M, Mastrocola R, Catalano MG, Brignardello E, Danni O, Boccuzzi G. Oxidative stress impairs skeletal muscle repair in diabetic rats. *Diabetes* 2004;53(4):1082-1088.

Argov Z, Sadeh M, Mazor K, Soffer D, Kahana E, Eisenberg I, *et al.* Muscular dystrophy due to dysferlin deficiency in Libyan Jews. Clinical and genetic features. *Brain* 2000;123(6):1229-1237.

Arnold L, Henry A, Poron F, Baba-Amer Y, van Rooijen N, Plonquet A, *et al*. Inflammatory monocytes recruited after skeletal muscle injury switch into anti-inflammatory macrophages to support myogenesis. *J Exp Med* 2007;204(5):1057-1069.

Babiychuk EB, Draeger A. Annexins in cell membrane dynamics: Ca^{2+}-regulated association of lipid microdomains. *J Cell Biol* 2000;150(5):1113-1124.

Bai J, Wang P, Chapman ER. C_2A activates a cryptic Ca^{2+}-triggered membrane penetration activity within the C_2B-domain of synaptotagmin I. *Proc Natl Acad Sci USA* 2002;99(3):1665-1670.

Bansal D, Miyake K, Vogel SS, Groh S, Chen CC, Williamson R, *et al*. Defective membrane repair in dysferlin-deficient muscular dystrophy. *Nature* 2003;423:168-172.

Bansal D, Campbell KP. Dysferlin and the plasma membrane repair in muscular dystrophy. *Trends Cell Biol.* 2004;14(4):206-213.

Barnes JA, Gomes AV. Proteolytic signals in the primary structure of annexins. *Mol Cell Biochem* 2002;231(1-2):1-7.

Bashir R, Britton S, Strachan T, Keers S, Vafiadaki E, Lako M, *et al*. A gene related to Caenorhabditis elegans spermatogenesis factor fer-1 is mutated in limb-girdle muscular dystrophy type 2B. *Nat Genet* 1998;20:37-42.

Baulieu EE, Thomas G, Legrain S, Lahlou N, Roger M, Debuire B, *et al.* Dehydroepiandrosterone (DHEA), DHEA sulphate , and aging: Contribution of DHEAge study to a sociobiomedical issue. *Proc Natl Acad Sci USA* 2000;97:4279-4284.

Baur JA, Sinclair DA. Therapeutic potential of resveratrol: The *in vivo* evidence. *Nat Rev Drug Discov* 2006;5:493-506.

Beal MF. Mitochondrial dysfunction and oxidative damage in Alzheimer's and Parkinson's diseases and coenzyme Q10 as a potential treatment. *J Bioenerg Biomembr* 2004;36(4):381-386.

Beckman JS, Koppenol WH. Nitric oxide, superoxide, and peroxynitrite: The good, the bad, and ugly. *Am J Physiol* 1996;271(5):C1424-C1437.

Beckman KB, Ames BN. The free radical theory of aging matures. *Physiol Rev* 1998; 78:547-581.

Bejaoui K, Hirabayashi K, Hentati F, Haines JL, Ben Hamida C, Belal S, *et al.* Linkage of Miyoshi myopathy (distal autosomal recessive muscular dystrophy) locus to chromosome 2p12-14. *Neurology* 1995;45:768-772.

Ben Hamida M, Fardeau M, Attia N. Severe childhood muscular dystrophy affecting both sexes and frequent in Tunisia. *Muscle Nerve* 1983;6(7):469-480.

Bentinger M, Brismar K, Dallner G. The antioxidant role of coenzyme Q. *Mitochondrion* 2007;7(Suppl 1):S41-S50.

Bermúdez-Crespo J, López JL. A better understanding of molecular mechanisms underlying human disease. *Proteomics* 2007;1(9):983-1003.

Bernard CCA, Carnegie PR. Experimental autoimmune encephalomyelitis in mice: Immunologic response to mouse spinal cord and myelin basic proteins. *J Immunol* 1975;114:1537-1540.

Bethlem J, van Wijngaarden GK. The incidence of ringed fibers and sarcoplasmic masses in normal and diseased muscle. *J Neurol Neurosurg Psychiat* 1963;26(4):326-332.

Bhakgavan HN, Chopra RK. Coenzyme Q10: absorption, tissue uptake, metabolism and pharmacokinetics. *Free Radic Res* 2006;40(5):445-453.

Biggar WD, Gingras M, Fehling DL, Harris VA, Steele CA. Deflazacort treatment of Duchenne muscular dystrophy. *J Pediatr* 2001;138:45-50.

Birell MA, McCluskie K, Wong S, Donnelly LE, Barnes PJ, Belvisi MG. Resveratrol, an extract of red wine, inhibits lipopolysaccharide induced airway neutrophilia and inflammatory mediators through and NF-κB-independent mechanism. *FASEB J* 2005;19:840-841.

Bittner RE, Anderson LVB, Burkhardt E, Bashir R, Vafiadaki E, Ivanova S, *et al*. Dysferlin deletion in SJL mice (SJL-*Dysf*) defines a natural model for limb girdle muscular dystrophy 2B. *Nat Genet* 1999;23(2):141-142.

Blau HM, Webster C, Pavlath GK. Defective myoblasts identified in Duchenne muscular dystrophy. *Proc Natl Acad Sci USA* 1983;80:4856-4860.

Bliznakov EG, Hunt GL. The miracle nutrient coenzyme Q. *New York*: Bantam Books, 1987

Bliznakov EG. Cardiovascular diseases, oxidative stress and antioxidants: The decisive role of coenzyme Q10. *Cardiovasc Res* 1999;43(1):248-249.

Bockhold KJ, Rosenblatt JD, Partridge TA. Aging normal and dystrophic mouse muscle: Analysis of myogenicity in cultures of living sing fibers. *Muscle Nerve* 1998;21(2):173-183.

Borgonovo B, Cocucci E, Racchetti G, Podini P, Bachi A, Meldolesi J. Regulated exocytosis: A novel, widely expressed system. *Nat Cell Biol* 2002;4:955-962.

Bork P, Sudol M. The WW domain: A signalling site in dystrophin? *Trends Biochem Sci* 1994;19(12):531-533.

Borsato C, Padoan R, Stramare R, Fanin M, Angelini C. Limb-girdle muscular dystrophies type 2A and 2B: Clinical and radiological aspects. *Basic Appl Myol* 2006;16(1):17-25.

Bradamante S, Barenghi L, Villa A. Cardiovascular protective effects of resveratrol. *Cardiovasc Drug Rev* 2004;22(3):169-188.

Brea-Calvo G, Roderiíguez-Hernández Á, Fernández-Ayala DJM, Navas P, Sánchez-Alcázar JA. Chemotherapy induces an increase in coenzyme Q10 levels in cancer cell lines. *Free Radic Biol Med* 2006;40(8):1293-1302.

Briguet A, Courdier-Fruh I, Foster M, Meier T, Magyar JP. Histological parameters for the quantitative assessment of muscular dystrophy in the *mdx*-mouse. *Neuromuscul Disord* 2004;14(10):675-682.

Britton S, Freeman T, Vafiadaki E, Keers S, Harrison R, Bushby K, *et al.* The third human FER-1-like protein is highly similar to dysferlin. *Genomics* 2000;68(3):313-321.

Brooke MH, Fenichel GM, Griggs RC, Mendell JR, Moxley R, Florence J, *et al.* Duchenne muscular dystrophy: Patterns of clinical progression and effects of supportive therapy. *Neurology* 1989;39:475-481.

Brummer D, Walter MC, Palmbach M, Knirsch U, Karitzky J, Tomczak R, *et al.* Long-term MRI and clinical follow-up of symptomatic and presymptomatic carriers of dysferlin gene mutation. *Acta Myol* 2005;24(1):6-16.

Brunn A, Schröder R, Deckert M. The inflammatory reaction pattern distinguishes primary dysferlinopathies from idiopathic inflammatory myopathies: An important role for the membrane attack complex. *Acta Neuropathol* 2006;112(3):325-332.

Bruss M, Homann J, Molderings GJ. Dysferlinopathy as an extra-hepatic cause for the elevation of serum transminases. *Med Klin (Munich)* 2004;99(6):326-329.

Buck M, Chojkier M. Muscle wasting and dedifferentiation induced by oxidative stress in a murine model of cachexia is prevented by inhibitors of nitric oxide synthesis and antioxidants. *EMBO J* 1996;15(8):1753-1765.

Buetler TM, Renard M, Offord EA, Schneider H, Rüegg UT. Green tea extract decreases muscle necrosis in mdx mice and protects against reactive oxygen species. *Am J Clin Nutr* 2002;75(4):749-753.

Bushby K. Making sense of the limb-girdle muscular dystrophies. *Brain* 1999(a);122:1403-1420.

Bushby K. The limb-girdle muscular dystrophies – multiple genes, multiple mechanisms. *Hum Mol Genet* 1999(b);8(10):1875-1882.

Bushby K. Genetics and the muscular dystrophies. *Dev Med Child Neurol* 2000(a);42(11):780-784.

Bushby K. Dysferlin and muscular dystrophy. Acta Neurol Belg 2000(b);100:142-145.

Bushby K, Straub V. Nonmolecular treatment for muscular dystrophies. *Curr Opin Neurol* 2005;18(5):511-518.

Cagliani R, Magri F, Toscano A, Merlini L, Fortunato F, Lamperti C, *et al*. Mutation finding in patients with dysferlin deficiency and role of the dyserlin interacting proteins annexin A1 and A2 in muscular dystrophies. *Hum Mutat* 2005;26(3):283

Campanaro S, Romualdi C, Fanin M, Celegato B, Pacchioni B, Trevisan S, *et al*. Gene expression profiling in dysferlinopathies using a dedicated muscle array. *Hum Mol Genet* 2002;11:3283-3298.

Carpenter S, Karpati G. Pathology of skeletal muscle. *New York*: Churchill Livingston, 1984.

Carpenter S. Muscle pathology on semithin resin sections. In: Karpati G, Hilton-Jones D, Griggs RC, editors. Disorders of voluntary muscle, 7th Ed. *Cambridge*: University Press, 2001.

Carpenter S. Electron microscopy in the study of normal and diseased muscle. In: Karpati G, Hilton-Jones D, Griggs RC, editors. Disorders of voluntary muscle, 7th Ed. *Cambridge*: University Press, 2001.

Cenacchi G, Fanin M, De Giorgi LB, Angelini C. Ultrastructural changes in dysferlinopathy support defective membrane repair mechanism. *J Clin Pathol* 2005;58:190-195.

Cenacchi G, Tarantino L, Corbu A, De Giorgi LB, Fanin M, Pegoraro E, *et al*. The contemporary role of electron microscopy in neuromuscular pathology. *Basic Appl Myol* 2007;17(3-4):167-171.

Chapman ER, Jahn R. Calcium-dependent interaction of the cytoplasmic region of synaptotagmin with membranes: Autonomous function of a single C2-homologous domain. *J Biol Chem* 1994;269(8):5735-5741.

Chapman ER, Hanson PI, An S, Jahn R. Ca2+ regulates the interaction between synaptotagmin and syntaxin I. *J Biol Chem* 1995;270(40):23667-23671.

Chazot G, Fournis Y, Robert JM, Aimard G, Devic M. Serum creatine phosphokinase changes during lithium therapy on patients with muscular dystrophy Duchenne type. *Lyon Med* 1972; 228:421-425.

Chiu YH, Hornsey MA, Klinge L, Jorgensen LH, Laval SH, Charlton R, *et al*. Attenuated muscle regeneration is a key factor in dysferlin-deficient muscular dystrophy. *Hum Mol Genet* 2009;18(11):1976-1989.

Cho IJ, Ahn JY, Kim S, Choi MS, Ha TY. Resveratrol attenuates the expression of HMG-CoA reductase mRNA in hamsters. *Biochem Biophys Res Commun* 2008;367(1):290-294.

Chrobáková T, Hermanová M, Kroupová I, Vondráček P, Mařiková T, Mazanec R, *et al.* Mutations in Czech LGMD2A patients revealed by analysis of calpain3 mRNA and their phenotypic outcome. *Neuromuscul Disord* 2004;14(10):659-665.

Cohen L, Morgan J, Schulman S. Diethylstilbestrol: Observations on its use in Duchenne's muscular dystrophy. *Proc Soc Exp Biol Med* 1972;140(3):830-835.

Cohen L, Morgan J. Diethylstilbestrol effects on serum enzymes and isozymes in muscular dystrophy. *Arch Neurol* 1976;33(7):480-484.

Cohn RD, Campbell KP. Molecular basis of muscular dystrophies. *Muscle Nerve* 2000;23:1456-1471.

Comerlato EA; Scola RH, Werneck LC. Limb-girdle muscular dystrophy. An immunohistochemical diagnostic approach. *Arq Neuropsiquiatr* 2005;63(2-A):235-245.

Cooper RN, Tajbakhsh S, Mouly V, Cossu G, Buckingham M, Butler-Browne GS. *In vivo* satellite cell activation via Myf 5 and MyoD in regenerating mouse skeletal muscle. *J Cell Sci* 1999;112(17):2895-2901.

Copenhaver WM, Kelly DE, Wood RL. Bailey's textbook of histology, 17th Ed. *Baltimore*: Williams and Wilkins, 1978.

Crane FL. Biochemical functions of coenzyme Q10. *J Am Coll Nutr* 2001;20(6):591-598.

Crane FL. Discovery of ubiquinone (coenzyme Q) and an overview of function. *Mitochondrion* 2007;7(Suppl 1):S2-S7.

Crowell JA, Korytko PJ, Morrissey RL, Booth TD, Levine BS. Resveratrol-associated renal toxicity. *Toxicol Sci* 2004;82(2):614-619.

Cumming G, Fidler F, Vaux DL. Error bars in experimental biology. *J Cell Biol* 2007;177(1):7-11.

Dalkilic I, Kunkel LM. Muscular dystrophies: Genes to pathogenesis. *Curr Opin Genet Dev* 2003;13(3):231-238.

Dallner G, Sindelar PJ. Regulation of ubiquinone metabolism. *Free Radic Biol Med* 2000;29(3-4):285-294.

Danièle N, Richard I, Bartoli M. Ins and outs of therapy in limb girdle muscular dystrophies. *Int J Biochem Cell Biol* 2007;39(9):1608-1624.

Davis DB, Deltmonte AJ, Ly CT, McNally EM. Myoferlin, a candidate gene and potential modifier of muscular dystrophy. *Hum Mol Genet* 2000;9(2):217-226.

Davis DB, Doherty KR, Delmonte AJ, McNally EM. Calcium-sensitive phospholipid binding properties of normal and mutant ferlin C2 domains. *J Biol Chem* 2002;277(25):22883-22888.

Davletov BA, Sudhof TC. A single C2 domain from synaptotagmin I is sufficient for high affinity Ca^{2+}/ phospholipid binding. *J Biol Chem* 1993;268(35):26386-26390.

De Gruchy GC. Clinical Hematology in medical practice. *Acad Med* 1965; 40(3):318

De Luna N, Gallardo E, Illa I. *In vivo* and *in vitro* dysferlin expression in human muscle satellite cells. *J Neuropathol Exp Neurol* 2004;63(10):1104-1113.

De Luna N, Gallardo E, Soriano M, Dominque-Perles R, de la Torre C, Rojas-García R, e*t al*. Absence of dysferlin alters myogenin expression and delays human muscle differentiation '*in vivo*'. *J Biol Chem* 2006;281(25):17092-17098.

De Palma S, Morandi L, Mariani E, Begum S, Cerretelli P, Wait R, *et al*. Proteomic investigation of the molecular pahtophysiology of dysferlinopathy. *Proteomics* 2006;6(1):379-385.

Denk W, Horstmann H. Serial block-face scanning electron microscopy to reconstruct three-dimensional tissue nanostructure. PLoS Biology 2004;2(11):e329.

Diers A, Carl M, Stoltenburg-Didinger G, Vorgerd M, Spuler S. Painful enlargement of the calf muscles in limb girdle muscular dystrophy type 2B (LGMD 2B) with a novel compound heterozygous mutation in DYSF. *Neuromuscul Disord* 2007;17(2):157-162.

Disatnik MH, Dhawan J, Yu Y, Beal MF, Whirl MM, Franco AA, *et al*. Evidence of oxidative stress in *mdx* mouse muscle: Studies of the pre-necrotic state. *J Neurol Sci* 1998;161(1):77-84.

Doherty KR, McNally EM. Repairing the tears: Dysferlin in muscle membrane repair. *Trends Mol Med* 2003;9(8):327-330.

Doherty KR, Cave A, Davis DB, Delmonte AJ, Posey A, Earley JU, *et al.* Normal myoblast fusion requires myoferlin. *Development* 2005;132(24):5565-5575.

Doran P, Gannon J, O'Connell K, Ohlendieck K. Proteomic profiling of animal models mimicking skeletal muscle disorders. *Proteomics* 2007;1(9):1169-1184.

Draper HH, Hadley M. Malondialdehyde determination as index of lipid peroxidation. *Methods Enzymol* 1990;186:421-431.

Duchenne GB. *L'Electrisation localisee at de son application a la pathologie at a la therapeutique*. *Paris, France*: Bailliere et Fils, 1861.

Duguez S, Bartoli M, Richard I. Calpain 3: A key regulator of the sarcomere? *FEBS J* 2006;273(15):3427-3436.

Durbeej M, Campbell KP. Muscular dystrophies involving the dystrophin-glycoprotein complex: An overview of current mouse models. *Curr Opin Genet Dev* 2002;12(3):349-361.

Ehmsen J, Poon E, Davies K. The dystrophin-associated protein complex. *J Cell Sci* 2002;115:2801-2803.

Engel AG, Franzini Armstrong C. Myology: Basic and Applied, 2nd Ed. *New York*: McGrawhill, 1994.

Engel AG, Franzini-Armstrong C. Myology. *New York*: McGraw-Hill, 2004.

Engelman JA, Zhang X, Galbiati F, Volonté D, Sotgia F, Pestell R, *et al.* Molecular genetics of the caveolin gene family: Implications for human cancers, diabetes, Alzheimer's disease, and muscular dystrophy. *Am J Hum Genet* 1998;63(6):1578-1587.

Eriksson UJ, Simán CM. Pregnant diabetic rats fed the antioxidant butylated hydroxytoluene show decreased occurrence of malformations in offspring. *Diabetes* 1996;45(11):1497-1502.

Ernster L, Dallner G. Biochemical, physiological and medical aspects of ubiquinone function. *Biochim Biophys Acta* 1995;1271(1):195-204.

Esterbauer H, Cheeseman KH. Determination of aldehydic lipid peroxidation products: Malondialdehyde and 4-hydroxynonenal. *Methods Enzymol* 1990;186:407-421

Eymard B, Romero NB, Leturcq F, Piccolo F, Carrie A, Jeanpierre M, *et al*. Primary adhalinopathy (alpha-sarcoglycanopathy): Clinical, pathological and genetic correlation in 20 patients with autosomal recessive muscular dystrophy. *Neurology* 1997;48:1227-1234.

Fanin M, Angelini C. Muscle pathololgy in dysferlin deficiency. *Neuropathol Appl Neurobiol* 2002;28(6):461-470.

Fauconneau B, Waffo-Teguo P, Huguet F, Barrier L, Decendit A, Merillon JM. Comparative study of radical scavenger and antioxidant properties of phenolic compounds from *Vitis vinifera* cell cultures using *in vitro* tests. *Life Sci* 1997;61(21):2103-2110.

Fenichel GM, Brooke MH, Griggs RC, Mendell JR, Miller JP, Moxley III RT, *et al.* Clinical investigation in Duchenne muscular dystrophy: Penicillamine and vitamin E. *Muscle Nerve* 1988;11(11):1164-1168.

Fernandez I, Arac D, Ubach J, Gerber SH, Shin O, Gao Y, *et al.* Three-dimensional structure of the synaptotagmin I C_2B-domain: Synaptotagmin I as a phospholipid binding machine. *Neuron* 2001;32:1057-1069.

Fernandez-Chacon R, Konigstrofer A, Gerber SH, Garcia J, Matos MF, Stevens CF, *et al.* Synaptotagmin I functions as a calcium regulator of release probability. *Nature* 2001;410:41-49.

Fisher D, Schroers A, Blümcke I, Urbach H, Zerres K, Mortier W, *et al.* Consequences of a novel caveolin-3 mutation in a large German family. *Ann Neurol* 2003;53(2):233-241.

Flucher BE, Terasaki M, Chin HM, Beeler TJ, Daniels MP. Biogenesis of transverse tubules in skeletal muscle *in vitro*. *Dev Biol* 1991;145(1):77-90.

Flucher BE, Takekura H, Franzini-Armstrong C. Development of the excitation-contraction coupling apparatus in skeletal muscle: Association of sarcoplasmic reticulum and transverse tubules with myofibrils. *Dev Biol* 1993;160(1):135-147.

Folkers K, Wolaniuk J, Simonsen R, Morishita M, Vadhanavikit S. Biochemical rationale and the cardiac response of patients with muscle disease to therapy with coenzyme Q10. *Proc Natl Acad Sci* 1985;82(13):4513-4516.

Folkers K, Simonsen R. Two successful double-blind trials with coenzyme Q10 (vitamin Q10) on muscular dystrophies and neurogenic atrophies. *Biochim Biophys Acta* 1995;1271(1):281-286.

Folkers K. Relevance of the biosynthesis of coenzyme Q10 and of the four bases of DNA as a rationale for the molecular causes of cancer therapy. *Biochem Biophys Res Commun* 1996;224(2):358-361.

Foltz CJ, Ullman-Cullere M. Guidelines for assessing the health and condition of mice. *Lab Anim* 1999;28(4):28-32.

Fox JG. The mouse in biomedical research, 2nd Ed. *Bartholds* SW, Davisson MT, Newcomer CE, Quimby FW, Smith AL, editors. *Burlington, USA*: Academic Press, Elsevier Inc., 2007.

Frankel EN, Kanner J, German JB, Parks E, Kinsella JE. Inhibition of oxidation of human low-density lipoprotein by phenolic substances in red wine. *Lancet* 1993(a);341(8843):454-457.

Frankel EN, Waterhouse AL, Kinsella JE. Inhibition of human LDL oxidation by resveratrol. *Lancet* 1993(b);341(8852):1103-1104.

Freeman BA, Crapo JD. Biology of disease. Free radicals and tissue injury. *Lab Invest* 1982;47(5):412-426.

Fujita E, Kouroku Y, Isoai A, Kumagai H, Misutani A, Matsuda C, *et al*. Two endoplasmic reticulum-associated degradation (ERAD) systems for the novel variant of the mutant dysferlin: Ubiquitin/proteasome ERAD(I) and autophagy/lysosome ERAD(II). *Hum Mol Genet* 2007;16(6):618-629.

Gabay C. Cytokine inhibitors in the treatment of rheumatoid arthritis. *Expert Opin Biol Ther* 2002;2(2):135-149.

Gad SC. Animal models in toxicology. *USA, Cary, North Carolina*, Gad Consulting Services, 2006.

Galbiati F, Volonté D, Minetti C, Chu JB, Lisanti MP. Phenotypic behaviour of caveolin-3 mutations that cause autosomal dominant limb girdle muscular dystrophy (LGMD 1C). Retention of LGMD 1C caveolin-3 mutants within the Golgi complex. *J Biol Chem* 1999;274(36):25632-25641.

Galbiati F, Engelman JA, D, Volonté D, Zhang XL, Minetti C, Li M, *et al.* Caveolin-3 null mice show a loss of caveolae, changes in the microdomain distribution of the dystrophin-glycoprotein complex, and t-tubule abnormalities. *J Biol Chem* 2001(a);276(24):21425-21433.

Galbiati F, Razani B, Lisanti MP. Caveolae and caveolin-3 in muscular dystrophy. *Trends Mol Med* 2001(b);7(10):435-441.

Gallardo E, Rojas-García R, de Luna N, Pou A, Brown RH Jr, Illa I. Inflammation in dysferlin myopathy: Immunohistochemical characterization of 13 patients. *Neurology* 2001;57:2136-2138.

Gehm BD, McAndrews JM, Chien PY, Jameson JL. Resveratrol, a polyphenolic compound found in grapes and wine, is an agonist for the estrogen receptor. *Proc Natl Acad Sci* 1997;94(25):14138-14143.

Gempel K, Topaloglu H, Talim B, Schneiderat P, Schoser BGH, Hans VH, *et al*. The myopathic form of coenzyme Q10 deficiency is caused by mutations in the electron-transferring-flavoprotein dehydrogenase (ETFDH) gene. *Brain* 2007;130(8):2037-2044.

Gentil BJ, Delphin C, Mbele GO, Deloulme JC, Ferro M, Garin J, *et al.* The giant protein AHNAK is a specific target for the calcium- and zinc-binding S100B protein: Potential implications for Ca^{2+} homeostasis regulation by S100B. *J Biol Chem* 2001;276(26):23253-23261.

Gentil BJ, Delphin C, Benaud C, Baudier J. Expression of the giant protein AHNAK (desmoyokin) in muscle and lining epithelial cells. *J Histochem Cytochem* 2003;51(3):339-348.

Gerke V, Moss SE. Annexins: From structure to function. *Physiol Rev* 2002;82(2):331-371.

Glenny JR Jr. Tyrosine phosphorylation of a 22 kDa protein is correlated with transformation by Rous sarcoma virus. *J Biol Chem* 1989;264(34):20163-20166.

Glenny JR, Soppet D. Sequence and expression of caveolin, a protein component of caveolae plasma membrane domains phosphorylated on tyrosine in RSV-transformed fibroblasts. *Proc Natl Acad Sci USA* 1992;89:10517-10521.

Glover L, Brown RH Jr. Dysferlin in membrane trafficking and patch repair. *Traffic* 2007;8(7):785-794.

Godell CM, Smyers ME, Eddleman CS, Ballinger ML, Fishman HM, Bittner GD. Calpain activity promotes the sealing of severed giant axons. *Proc Natl Acad Sci USA* 1997;94(9):4751-4756.

Goll DE, Thompson VF, Li H, Wei W, Cong J. The calpain system. *Physiol Rev* 2003;83(3):731-801.

Gómez-Díaz C, Barroso MP, Navas P. Plasma membrane coenzyme Q10 and growth control. *Protoplasma* 2000;214(1-2):19-23.

Gowers WR. A manual of disease of the nervous system. *London*: Churchill Livinstone 1886;1:391-394. In Pearce JMS. Gower's sign. *J Neurol Neurosurg Psychiatry* 2000;68(2):149.

Grounds MD, McGeachie JK. A comparison of muscle precursor replication in crush-injured skeletal muscle of Swiss and BALBc mice. *Cell Tissue Res* 1989;255(2):385-391.

Grounds MD, Torrisi JO. Anti-TNFα (Remicade®) therapy protects dystrophic skeletal muscle from necrosis. *FASEB J* 2004;18(6):676-682.

Grounds MD, Radley HG, Lynch GS, Nagaraju K, De Luca A. Towards developing standard operating procedures for pre-clinical testing in the mdx mouse model of Duchenne muscular dystrophy. *Neurobiol Dis* 2008;31(1):1-19.

Grounds MD. Complexity of extracellular matrix and skeletal muscle regeneration. In: Schiaffino S, Partridge TA, editors. Skeletal muscle repair and regeneration. *Dordrecht, The Netherlands*: Springer, 2008.

Guglieri M, Bushby K. How to go about diagnosing and managing the limb-girdle muscular dystrophies. *Neurol India* 2008;56(3):271-280.

Guyon JR, Kudryashova E, Potts A, Dalkilic I, Brosius MA, Thompson TG, *et al.* Calpain 3 cleaves filamin C and regulates its ability to inter with gamma- and delta- sarcoglycans. *Muscle Ner*ve 2003;28(4):472-483.

Hahn KA. Chemotherapy dose calculation and administration in exotic animal species. *Semin Avian Exot Pet* 2005;14(3):193-198.

Hall-Craggs EC. The significance of longitudinal fiber division in skeletal muscle. *J Neurol Sci* 1972;15(1):27-33. In: Carpenter S, Karpati G. Pathology of skeletal muscle. *New York*: Churchill Livingston, 1984.

Halliwell B, Gutteridge JMC. Free radicals in biology and medicine. 2nd Ed. *Oxford*: Clarendon Press; 1989.

Halliwell B, Gutteridge JMC. Role of free radicals and catalytic metal ions in human disease: An overview. *Methods Enzymol* 1990;186:1-85.

Halliwell B. The wanderings of a free radical. *Free Radic Biol Med* 2009;46:531-542.

Han R, Campbell KP. Dysferlin and muscle membrane repair. *Curr Opin Cell Biol* 2007;19(4):409-416.

Harma M, Harma M, Erel O. Increased oxidative stress in patients with hydatidiform mole. *Swiss Med Wkly* 2003;133:563-566.

Harris ED. Regulation of antioxidant enzymes. *FASEB J* 1992;6(9):2675-2683.

Hartman GH, Renaud DL, Sundaram M, Reed AM. Spondyloarthropathy presenting at a young age: Case report and review. *Skeletal Radiol* 2007;36(2):161-164.

Hasty P, Bradley A, Morris JH, Edmondson DG, Venuti JM, Olson EN, *et al*. Muscle deficiency and neonatal death in mice with a targeted mutation in the myogenin gene. *Nature* 1993;364:501-506.

Hattersley PG, Ragusa D. Don't forget morphology: The importance of evaluation of blood smears. *Calif Med* 1965;103(3):175-177.

Hayashi YK. Membrane-repair machinery and muscular dystrophy. *Lancet* 2003;362(9387):843-844.

Haycock JW, Neil SM, Jones P, Harris JB, Mantle D. Oxidative damage to muscle protein in Duchenne muscular dystrophy. *Neuroreport* 1996;8(1):357-361.

Hernández-Daviez DJ, Martin A, Laval SH, Lo HP, Cooper ST, North KN, *et al.* Aberrant dysferlin trafficking in cells lacking caveolin or expressing dystrophy mutants of caveolin-3. *Hum Mol Genet* 2006;15(1):129-142.

Ho M, Gallardo E, McKenna-Yasek D, De Luna N, Illa I, Brown RH Jr. A novel, blood-based diagnostic assay for limb girdle muscular dystrophy 2B and Miyoshi myopathy. *Ann Neurol* 2002;51(1):129-133.

Hodges S, Hertz N, Lochwood K, Lister R. CoQ10: Could it have a role in cancer management? *Biofactors* 1999;9(2-4):365-370.

Hodgson JM, Watts GF, Playford DA, Burke V, Croft KD. Coenzyme Q10 improves blood pressure and glycaemic control: A trial in subjects with type 2 diabetes. *Eur J Clin Nutr* 2002;56(11):1137-1142.

Hoffman EP, Brown RH Jr, Kunkel LM. Dystrophin: The protein product of the Duchenne muscular dystrophy locus. *Cell* 1987;51(6):919-928.

Hohaus A, Person V, Behlke J, Schaper J, Morano I, Haase H. The carboxyl-terminal region of ahnak provides a link between cardiac L-type Ca^{2+} channels and the actin-based cytoskeleton. *FASEB J* 2002;16(10):1205-1216.

Hohlfeld R, Müller W, Toyka KV. Necrotizing myopathy in SJL mice. *Muscle Nerve* 1988;11(2):184-185.

Horoz M, Bolukbas C, Bolukbas FF, Sabuncu T, Aslan M, Sarifakiogullari S, *et al*. Measurement of the total antioxidant response using a novel automated method in subjects with non-alcoholic steatohepatitis. *BMC Gastroenterol* 2005;5:35-41.

Howitz KT, Bitterman KJ, Cohen HY, Lamming DW, Lavu S, Wood JG, *et al.* Small molecule activators of sirtuins extend *Saccharomyces cerevisiae* lifespan. *Nature* 2003;425:191-196.

Hsieh TC, Juan G, Darzynkiewicz Z, Wu JM. Resveratrol increases nitric oxide synthase, induces accumulation of p53 and $p21^{WAF1/CIP1}$, and suppresses cultured bovine pulmonary artery endothelial cell proliferation by perturbing progression through S and G_2. *Cancer Res* 1999;59(11):2596-2601.

Hu Y, Rahlfs S, Mersh-Sundermann V, Becker K. Resveratrol modulates mRNA transcripts of genes related to redox metabolism and cell proliferation in non-small-cell carcinoma cells. Bi*ol Chem* 2007;388(2):207-219.

Huang Y, Verheesen P, Roussis A, Frankhuizen W, Ginjaar I, Haldane F, *et al.* Protein studies in dysferlinopathy patients using llama-derived antibody fragments selected by phage display. *Eur J Hum Genet* 2005;13:721-730.

Huang YC, Laval SH, van Remoortere A, Baudier J, Benaud C, Anderson LVB, *et al.* AHNAK, a novel component of the dysferlin protein complex, redistributes to the cytoplasm with dysferlin during skeletal muscle regeneration. *FASEB J* 2007;21(3):732-742.

Huang Y, De Morrée A, Van Remoortere A, Bushby K, Frants RR, Den Dunnen JT, *et al.* Calpain 3 is a modulator of the dysferlin protein complex in skeletal muscle. *Hum Mol Genet* 2008;17(12):1855-1866.

Hubel CA. Oxidative stress in the pathogenesis of preeclampsia. *Proc Soc Exp Biol Med* 1999;222(3):222-235.

Illa I, Serrano-Munuera C, Gallardo E, Lasa A, Rojas-García R, Palmer J, *et al*. Distal anterior compartment myopathy: A dysferlin mutation causing a new muscular dystrophy phenotype. *Ann Neurol* 2001;49(1):130-134.

Illarioshkin SN, Ivanova-Smolenskaya IA, Greenberg CR, Nylen E, Sukhorukov VS, Poleshchuk VV, *et al.* Identical dysferlin mutation in limb-girdle muscular dystrophy type 2B and distal myopathy. *Neurology* 2000;55:1931-1933.

Inoue M, Wakayama Y, Kojima H, Shibuya S, Jimi T, Oniki H, *et al*. Expression of myoferlin in skeletal muscles of patients with dysferlinopathy. *Tohoku J Exp Med* 2006;209(2):109-116.

Isfort RJ. Proteomic analysis of striated muscle. *J Chromatogr B Analyt Technol Biomed Life Sci* 2002;771(1-2):155-165.

Ishikawa H. Formation of elaborate networks of T-system tubules in cultured skeletal muscle with special reference to the T-system formation. *J Cell Biol* 1968;38(1):51-66.

Jackson MJ, Jones DA, Edwards RH. Techniques for studying free radical damage in muscular dystrophy. *Med Biol* 1984;62(2):135-138.

Jacob RA. The integrated antioxidant system. *Nutr Res* 1995;15(5):755-766.

Jaiswal JK, Andrews NW, Simon SM. Membrane proximal lysosomes are the major vesicle responsible for calcium-dependent exocytosis in nonsecretory cells. *J Cell Biol* 2002;159(4):625-635.

Janeway CA Jr, Travers P, Walport M, Shlomchik MJ. Immunobiology, the immune system in health and disease. 6th Ed. *London*: Churchill Livingstone, 2005.

Jang M,Cai L, Udeani GO, Slowing KV, Thomas CF, Beecher CWW, *et al*. Cancer chemopreventive activity of resveratrol, a natural product derived from grapes. *Science* 1997;275(5297):218-220.

Jung D, Yang B, Meyer J, Chamberlain JS, Campbell KP. Identification and characterization of the dystrophin anchoring site on beta-dystroglycan. *J Biol Chem* 1995;270:27350-27310.

Kaczor JJ, Hall JE, Payne E, Tarnopolsky MA. Low intensity training decreases markers of oxidative stress in skeletal muscle of mdx mice. *Free Rad Biol Med* 2007;43:145-154.

Kagan V, Serbinova E, Packer L. Antioxidant effects of ubiquinones in microsomes and mitochondria are mediated by tocopherol recycling. *Biochem Biophys Res Commun* 1990;169(3):851-857.

Kakulas BA. Problems and solutions in the rehabilitation of patients with progressive muscular dystrophy. *Scand J Rehabil Med Suppl* 1999;39:23-37.

Kar NC, Pearson CM. Catalase, superoxide dismutase, glutathione reductase and thiobarbituric acid-reactive products in normal and dystrophic human muscle. *Clin Chim Acta* 1979;94(3):277-280.

Kelly DE, Wood RL, Enders AC. Bailey's textbook of microscopic anatomy. 18th Ed. *Baltimore, London*: Williams and Wilkins, 1984.

Kesper K, Kornblum C, Reimann J, Lutterbey G, Schröder R, Wattjes MP. Pattern of skeletal muscle involvement in primary dysferlinopathies: A whole-body 3.0-T magnetic resonance imaging study. *Acta Neurol Scand* 2008;120(2):111-118.

Kettawan A, Takahashi T, Kongkachuichai R, Charoenkiatku S, Kishi T, Okamoto T. Protective effects of coenzyme Q10 on decreased oxidative stress resistance induced by simvastatin. *J Clin Biochem Nutr* 2007;40(3):194-202.

Kirimlioglu V, Karakayali H, Turkoglu S, Haberal M. Effect of resveratrol on oxidative stress enzymes in rats subjected to 70% partial hepatectomy. *Transplant Proc* 2008;40(1):293-296.

Klinge L, Laval S, Keers S, Haldane F, Straub V, Barresi R, *et al.* From T-tubule to sarcolemma: Damage-induced dysferlin translocation in early myogenesis. *FASEB J* 2007;21(8):1768-1776.

Kobayashi K, Izawa T, Kuwamura M, Yamate J. The distribution and characterization of skeletal muscle lesions in dysferlin-deficient SJL and A/J mice. *Exp Toxicol Pathol* 2009; In Press.

Komuro A, Masuda Y, Kobayashi K, Babbitt R, Gunel M, Flavell RA, *et al.* The AHNAKs are a class of giant propeller-like proteins that associate with Ca^{2+} channel proteins of cardiomyocytes and other cells. *Proc Natl Acad Sci USA* 2004;101(12):4053-4058.

Kong KY, Ren J, Kraus M, Finklestein SP, Brown RH Jr. Human umbilical cord blood cells differentiate into muscle in sjl muscular dystrophy mice. *Stem Cells* 2004;22:981-993.

Kopp P. Resveratrol, a phytoestrogen found in red wine. A possible explanation for the conundrum of the 'French paradox'? *Eur J Endocrinol* 1998;138:619-620.

Kouno T, Katsumata N, Mukai H, Ando M, Watanabe T. Standardization of the body surface area (BSA) formula to calculate the dose of anticancer agents in Japan. *Jpn J Clin Oncol* 2003;33(6):309-313.

Kudoh J, Wang Y, Minoshima S, Hashimoto T, Amagai M, Nishikawa T, *et al.* Localization of the human AHNAK/desmoyokin gene (AHNAK) to chromosome band 11q12 by somatic cell hybrid analysis and fluorescence in situ hybridization. *Cytogenet Cell Genet* 1995;70(3-4):218-220.

Kunkel LM, Monaco AP, Middlesworth W, Ochs HD, Latt SA. Specific cloning of DNA fragments absent from the DNA of a male patient with an X chromosome deletion. *Proc Natl Acad Sci* USA 1985;82(14):4778-4782.

Lambert O, Gerke V, Bader MF, Porte F, Brisson A. Structural analysis of junctions formed between lipid membranes and several annexins by cryo-electron microscopy. *J Mol Biol* 1997;272(1):42-55.

Langsjoen PH, Langsjoen AM. Coenzyme Q10 in cardiovascular disease with emphasis on heart failure and myocardial ischemia. *Asia Pac Heart J* 1998;7(3):160-168.

Lantos J, Röth E, Czopf L, Nemes J, Gál I. Monitoring of plasma total antioxidant status in different diseases. *Acta Chir Hung* 1997;36(1-4):188-189.

Laval SH, Bushby K. Limb-girdle muscular dystrophies-from genetics to molecular pathology. *Neuropathol Appl Neurobiol* 2004;30:91-105.

Le Ber I, Dubourg O, Benoist JF, Jardel C, Mochel F, Koenig M, *et al*. Muscle coenzyme Q10 deficiencies in ataxia with oculomotor apraxia 1. *Neurology* 2007;68:295-297.

Lee E, Marcucci M, Daniell L, Pypaert M, Weisz OA, Ochoa GC, *et al*. Amphiphysin 2 (Bin 1) and T-tubule biogenesis in muscle. *Science* 2002;297(5584):1193-1196.

Leeson TS, Leeson CR, Paparo AA. Text/Atlas of Histology. *Canada*, Saunders Company, 1988.

Lennon NJ, Kho A, Bacskai BJ, Perlmutter SL, Hyman BT, Brown RH Jr. Dysferlin interacts with annexins A1 and A2 and mediates sarcolemmal wound-healing. *J Biol Chem* 2003;278(50):50466-50473.

Li ZF, Shelton GD, Engvall E. Elimination of myostatin does not combat muscular dystrophy in dy mice but increases postnatal lethality. *Am J Pathol* 2005;166(2):491-497.

Liewluck T, Pongpakdee S, Witoonpanich R, Sangruchi T, Pho-iam T, Limwongse C, *et al.* Novel DYSF mutation in Thai patients with distal myopathy. *Clin Neurol Neurosurg* 2009;111(7):613-618.

Lindschinger M, Nadlinger K, Adelwöhrer N, Holweg K, Wögerbauer M, Birkmayer J, *et al.* Oxidative stress: Potential of distinct peroxide determination systems. Clin *Chem Lab Med* 2004;42(8):907-914.

Linnane AW, Kopsidas G, Zhang C, Yarovaya N, Kovalenko S, Papakostopoulos, *et al*. Cellular redox activity of coenzyme Q10: Effect of CoQ10 supplementation on human skeletal muscle. *Free Radic Res* 2002;36(4):445-453.

Linssen WH, Notermans NC, Van der Graaf Y, Wokke JH, Van Doorn PA, Howeler CJ, *et al.* Miyoshi-type distal muscular dystrophy. Clinical spectrum in 24 Dutch patients. *Brain* 1997;120(11):1989-1996.

Littarru GP, Jones D, Scholler J, Folkers K. Deficiency of coenzyme Q9 in mice having hereditary muscular dystrophy. *Biochem Biophys Res Commun* 1970;41(5):1306-1313.

Littarru GP, Tiano L. Clinical aspects of coenzyme Q10: An update. *Curr Opin Clin Nutr Metab Care* 2005;8(6):641-646.

Liu J, Aoki M, Illa I, Wu C, Fardeau M, Angelini C, *et al*. Dysferlin, a novel skeletal muscle gene, is mutated in Miyoshi myopathy and limb girdle muscular dystrophy. *Nat Genet* 1998;20:31-36.

Lovering RM, De Deyne PG. Contractile function, sarcolemma integrity, and the loss of dystrophin after skeletal muscle eccentric contraction-induced injury. *Am J Physiol Cell Physiol* 2004;286:C230-C238.

Lovering RM, Porter NC, Bloch RJ. The muscular dystrophies: From genes to therapies. *Phys Ther* 2005;85(12):1372-1388.

Mader S. Biology. 7th Ed. *Avenue of the Americas, New York:* McGraw-Hill; 2001.

Mahjneh I, Marconi G, Bushby K, Anderson LV, Tolvanen-Mahjneh H, Somer H. Dysferlinopathy (LGMD 2B): A 23-year follow-up study of 10 patients homozygous for the same frameshift dysferlin mutations. *Neuromuscul Disord* 2001;11(1):20-26.

Marinova EM, Yanishlieva NV, Totseva IR. Anti-oxidant activity and mechanism of action of trans-resveratrol in different lipid systems. *Int J Food Sci Technol* 2002;37:145-152.

Marnett LJ. Lipid peroxidation-DNA damage by malondialdehyde. *Mutat Res* 1999;424(1-2):83-95.

Martensson J, Meister A. Mitochondrial damage in muscle occurs after marked depletion of glutathione and is prevented by giving glutathione monoester. *Proc Natl Acad Sci* USA 1989;86(2):471-475.

Matsuda C, Hayashi YK, Ogawa M, Aoki M, Muaryama K, Nishino I, *et al*. The sarcolemmal proteins dysferlin and caveolin-3 interact in skeletal muscle. *Hum Mol Genet* 2001;10(17):1761-1766.

Matsuda C, Kameyama K, Tagawa K, Ogawa M, Suzuki A, Yamaji S, *et al.* Dysferlin interacts with Affixin (β-Parvin) at the sarcolemma. *J Neuropathol Exp Neurol* 2005;64(4):334-340.

Matsuoka A, Kodama Y, Fukuhara K, Honda S, Hayashi M, Sai K, *et al*. A pilot study of evaluation of the antioxidant activity of resveratrol and its analogue in a 6-month old feeding test in young adult mice. *Food Chem Toxicol* 2008;46(3):1125-1130.

Maurissen JPJ, Marable BR, Andrus AK, Stebbins KE. Factors affecting grip strength testing. *Neurotoxicol Teratol* 2003;25(5):543-553.

Mayne R. Muscle. In: Weiss JB, Ayad S, editors. Collagen in health and disease. *New York:* Churchill Livingston, 1982.

McDonald CM, Abresch RT, Carter GT, Fowler WM Jr, Johnson ER, Kilmer DD, *et al.* Profiles of neuromuscular diseases: Duchenne muscular dystrophy. *Am J Phys Med Rehabil* 1995;74(5):S70-S92.

McNally EM, de Sa Moreira E, Duggan DJ, Bonnemann CG, Lisanti MP, Lidov HGW, *et al*. Caveolin-3 in muscular dystrophy. *Hum Mol Genet* 1998;7:871-877.

McNeil PL. Repairing a torn cell surface: make way, lysosomes to the rescue. *J Cell Sci* 2002;115(5):873-879.

McNeil AK, Rescher U, Gerke V, McNeil PL. Requirement for annexin A1 in plasma membrane repair. *J Biol Chem* 2006;281(46):35202-35207.

Mechler F, Imre S, Dioszeghy P. Lipid peroxidation and superoxide dismutase activity in muscle and erythrocytes in Duchenne muscular dystrophy. *J Neurol Sci* 1984;63(3):279-283.

Mendell JR, Engel WK, Derrer EC. Duchenne muscular dystrophy: Functional ischemia reproduces characteristic lesions. *Science* 1971;172(3988):1143-1145.

Mercuri E, Pichiecchio A, Allisop J, Messina S, Pane M, Muntoni F. Muscle MRI in inherited neuromuscular disorders: Past, present and future. *J Magn Reson Imaging* 2007;25(2):433-440.

Metules T. Duchenne muscular dystrophy. *RN* 2002;65(10):39-44,47.

Michele DE, Barresi R, Kanagawa M, Saito F, Cohn RD, Satz JS, *et al.* Post-translational disruption of dystroglycan-ligand interactions in congenital muscular dystrophies. *Nature* 2002;418:417-422.

Minetti E, Sotgia F, Bruno C, Scartzzini P, Broda P, Bado M, *et al*. Mutations in the caveolin-3 gene cause autosomal dominant limb girdle muscular dystrophy. *Nat Genet* 1998;18:365-368.

Mitchell P. The protonmotive Q cycle: A general formulation. *FEBS Lett* 1975;59(2):137-139.

Mitchell CA, McGeachie JK, Grounds MD. Cellular differences in the regeneration of murine skeletal muscle: A quantitative histological study in SJL/J and Balb/c mice. *Cell Tissue Res* 1992;269(1):159-166.

Mitchell CA, Grounds MD, Papadimitriou JM. The genotype of bone marrow-derived inflammatory cells does not account for differences in skeletal muscle regeneration between SJL/J and Balb/c mice. *Cell Tissue Res* 1995;280(1):407-413.

Miyoshi K, Saijo K, Kuryu Y, Tada Y, Otsuka Y, Oshima Y, *et al*. Four cases of distal myopathy in two families. *Jpn J Hum Genet* 1967;12:113.

Miyoshi K, Kawai H, Iwasa M, Kusaka K, Nishino H. Autosomal recessive distal muscular dystrophy as a new type of progressive muscular dystrophy: Seventeen cases in eight families including an autopsied case. *Brain* 1986;109(1):31-54.

Montini G, Malaventura C, Salviati L. Early coenzyme Q10 supplementation in primary coenzyme Q10 deficiency. *N Engl Med* 2008;358(26):2849-2850.

Morgan J, Shanahan W, Cohen L. Plasma enzyme determinations in normal and dystrophic mice. *Res Commun Chem Pathol Pharmacol* 1981;31(2):341-356.

Muller AJ, Baker JF, DuHadaway JB, Ge K, Farmer G, Donover PS, *et al.* Targeted disruption of the murine Bin 1/Amphiphysin II gene does not disable endocytosis but results in embryonic cardiomyopathy with aberrant myofibril formation. *Mol Cell Biol* 2003;23(12):4295-4306.

Murphy ED. Replica of Hodgkin's Disease in SJL/J Mice. 34th Ann Rept. *Bar Harbor, Maine*: Jackson Lab, 1962-1963:p.26.

Murphy ME, Kehrer JP. Oxidative stress and muscular dystrophy. *Chem Biol Interact* 1989;69(2-3):101-173.

Murray JM, Davies KE, Harper PS, Meredith L, Mueller CR, Williamson R. Linkage relationship of a cloned DNA sequence on the short arm of the X chromosome to Duchenne muscular dystrophy. *Nature* 1982;300:69-71.

Nagashima T, Chuma T, Mano Y, Goto Y, Hayashi YK, Minami N, *et al.* Dysferlinopathy associated with rigid spine syndrome. *Neuropathology* 2004;24(4):341-346.

Nalefski EA, Falke JJ. The C_2 domain calcium-binding motif: structure and functional diversity. *Protein Sci* 1996;5(12):2375-2390.

Nemoto H, Konno S, Nakazora H, Miura H, Kurihara T. Histological and immunological changes of the skeletal muscles in older SJL/J mice. *Eur Neurol* 2007;57(1):19-25.

Nguyen K, Bassez G, Bernard R, Krahn M, Labelle V, Figarella-Branger D, *et al.* Dysferlin mutations in LGMD 2B, Miyoshi Myopathy, and atypical dysferlinopathies. *Hum Mutat* 2005;26(2):165-176.

Nguyen F, Guigand L, Goubault-Leroux I, Wyers M, Cherel Y. Microvessel density in muscles of dogs with golden retriever muscular dystrophy. *Neuromuscul Disord* 2005;15(2):154-163.

Nguyen K, Bassez G, Krahn M, Bernard R, Laforet P, Labelle V, *et al.* Phenotypic study in 40 patients with dysferlin gene mutations: High frequency of atypical phenotypes. *Arch Neurol* 2007;64(8):1176-1182.

Niebrój-Dobosz I, Hausmanowa-Petrusewicz. The involvement of oxidative stress in determining the severity and progress of pathological processes in dystrophin-deficient muscles. *Acta Biochim Pol* 2005;52(2):449-452.

Nielsen F, Mikkelsen BB, Nielsen JB, Andersen HR, Grandjean P. Plasma malondialdehyde as biomarker for oxidative stress: Reference interval and effects of life-style factors. *Clinl Chem* 1997;43(7):1209-1214.

Norwood FL, Sutherland-Smith AJ, Keep NH, Kendrick-Jones J. The structure of the N-terminal actin-binding domain of human dystrophin and how mutations in this domain may cause Duchenne or Becker muscular dystrophy. *Structure* 2000;8:481-491.

Okahashi S, Ogawa G, Suzuki M, Ogata K, Nishino I, Kawai M. Asymptomatic sporadic dysferlinopathy presenting with elevation of serum creatine kinase. Typical distribution of muscle involvement shown by MRI but not by CT. *Intern Med* 2008;47(4):305-307.

Ostdal H, Skibsted LH, Andersen HJ. Formation of long-lived proteins radicals in the reaction between H_2O_2-activated metmyoglobin and other proteins. *Free Radic Biol Med* 1997;23(5):754-761.

Ovalle WK, Nahirney PC, Netter FH. Muscle Tissue. Netter's essential histology. *Philadelphia*: Saunders/Elsevier, 2008

Pace-Asciak CR, Rounova O, Hahn SE, Diamandis EP, Goldberg DM. Wines and grape juices as modulators of platelet aggregation in healthy human subjects. *Clin Chim Acta* 1996;246(1-2):163-182.

Papa S, Schulachev VP. Reactive oxygen species, mitochondria, apoptosis and aging. *Mol Cell Biochem* 1997;174(1-2):305-319.

Paradas C, González-Quereda L, De Luna N, Gallardo E, García-Consuegra I, Gómez H, *et al.* A new phenotype of dysferlinopathy with congenital onset. *Neuromuscul Disord* 2009;19(1):21-25.

Parton RG, Way M, Zorzi N, Stang E. Caveolin-3 associates with developing T-tubules during muscle differentiation. *J Cell Biol* 1997;136(1):137-154.

Passaquin AC, Renard M, Kay L, Challet C, Mokhtarian A, Wallimann T, *et al.* Creatine supplementation reduces skeletal muscle degeneration and enhances mitochondrial function in *mdx* mice. *Neuromuscul Disord* 2002;12(2):174-182.

Patel TJ, Lieber RL. Force transmission in skeletal muscle: From actomyosin to external tendons. *Exerc Sport Sci Rev* 1997;25:321-363.

Patel P, Harris R, Geddes SM, Strehle E, Watson JD, Bashir R, *et al*. Solution structure of the inner DysF domain of myoferlin and implications for limb girdle muscular dystrophy type 2B. *J Mol Biol* 2008;379(5):981-990.

Paul AC, Rosenthal N. Different modes of hypertrophy in skeletal muscle fibers. *J Cell Biol* 2002;156(4):751-760.

Pearce JMS. Gower's sign. *J Neurol Neurosurg Psychiatry* 2000;68(2):149.

Petrof BJ, Shrager JB, Stedman HH, Kelly AM, Sweeney HL. Dystrophin protects the sarcolemma form stresses developed during muscle contraction. *Proc Natl Acad Sci USA* 1993;90:3710-3714.

Petrucci TC, Macchia G, Macioce P, Brancaccio A, Paggi P, Ceccarini M. Functional flexibility of dystroglycan, a transmembrane linker between the extracellular matrix and the cytoskeleton. *Cell Mol Biol Lett* 2001;6(2):226.

Piccolo F, Moore SA, Ford GC, Campbell KP. Intracellular accumulation and reduced sarcolemmal expression of dysferlin in limb-girdle muscular dystrophies. *Ann Neurol* 2000;48(6):902-912.

Pongpakdee S, Sopassathit V, Phudhichareonrat S, Suthiponpaisan U, Goto K, Hayashi Y, *et al*. G.P.4.03 Dysferlinopathy in Thai patients and its unusual pathological findings. *Neuromuscul Disord* 2007;12(9-10):788.

Potgieter M, Pretorius E, Oberholzer HM. Qualitative electron microscopic analysis of cultured chick embryonic cardiac and skeletal muscle cells: The cellular effect of coenzyme Q10 after exposure to Triton X-100. *Ultrastructural Pathology* 2009;33:93-101.

Pradhan S. Calf-head sign in miyoshi myopathy. *Arch Neurol* 2006;63(10):1414-1417.

Pradhan S. Diamond on quadriceps: A frequent sign in dysferlinopathy. *Neurology* 2008;70(4):322.

Pulido SM, Passaquin AC, Leijendekker WJ, Challet C, Wallimann T, Rüegg UT. Creatine supplementation improves intracellular Ca^{2+} handling and survival in *mdx* skeletal muscle cell. *FEBS Lett* 1998;439(3):357-362.

Quinzii C, Naini A, Salviati L, Trevisson E, Navas P, Di Mauro S, *et al*. A mutation in para-hydroxybenzoate-polyprenyl transferase (CoQ2) causes primary Coenzyme Q10 deficiency. *Am J Hum Genet* 2006;78(2):345-349.

Quinzii CM, Hirano M, DiMauro S. CoQ10 deficiency diseases in adults. *Mitochondrion* 2007;7(Suppl 1):S122–S126.

Ragusa RJ, Chow CK, Porter JD. Oxidative stress as a potential pathogenic mechanism in animal model of Duchenne muscular dystrophy. *Neuromuscul Disord* 1997;7(6-7):379-380.

Rando TA. Oxidative stress and the pathogenesis of muscular dystrophies. *Am J Phys Med Rehabil* 2002;81(Suppl 1):S175-S186.

Raynal P, Pollard HB. Annexins: The problem of assessing the biological role for a gene family of multifunctional Ca^{2+}- and phospholipid-binding proteins. *Biochim Biophys Acta* 1994;1197(1):63-93.

Reagan-Shaw S, Nihal M, Ahmad N. Dose translation from animal to human studies revisited. *FASEB J* 2008;22(3):659-661.

Reynolds ES. The use of lead citrate at high pH as an electron-opaque stain in electron microscopy. *J Cell Biol* 1963;17:208-211.

Rice-Evans C, Miller NJ. Total antioxidant status in plasma and body fluids. *Methods Enzymol* 1994;234:279-293.

Rizo J, Sudhof TC. C2-domains, structure and function of a universal Ca^{2+}-binding domain. J Biol Chem 1998;273(26):15879-15882.

Robb EL, Page MM, Wiens BE, Stuart JA. Molecular mechanisms of oxidative stress resistance induced by resveratrol: Specific and progressive induction of MnSOD. *Biochem Biophys Res Commun* 2008;367(2):406-412.

Robertson TA, Maley MAL, Grounds MD, Papadimitriou JM. The role of macrophages in skeletal muscle regeneration with particular reference to chemotaxis. *Exp Cell Res* 1993;207:321-331.

Roelofs RI, de Arango GS, Law PK, Kinsman D, Buchanan DC, Park JH. Treatment of Duchenne's muscular dystrophy with penicillamine: Results of a double-blind trial. *Arch Neurol* 1979;36(5):266-268.

Rosenberg NL, Ringel SP, Kotzin BL. Experimental autoimmune myositis in SJL/J mice. *Clin Exp Immunol* 1987;68(1):117-129.

Ross MH, Kaye GI, Pawlina W. Histology. A text and atlas. 4th Ed. *Baltimore, MD*: Lipppincott Williams & Wilkins; 2003.

Rothberg KG, Heuser JE, Donzell WC, Ying YS, Glenney JR, Anderson RG, *et al.* Caveolin, a protein componenet of caveolae membrane coats. *Cell* 1992;68(4):673-682.

Rötig A, Appelkvist EL, Geromel V, Chretien D, Kadhom N, Edery P, *et al*. Quinone-responsive multiple respiratory-chain dysfunction due to widespread coenzyme Q10 deficiency. *Lancet* 2000;356(9227):391-395.

Rötig A, Mollet J, Rio M, Munnich A. Infantile and pediatric quinone deficiency diseases. *Mitochondrion* 2007;7(Suppl 1):S112-S121.

Rouger K, Fornasari B, Armengol V, Jouvion G, Leroux I, Dubreil L, *et al.* Progenitor cell isolation from muscle-derived cells based on adhesion properties. *J Histochem Cytochem* 2007;55(6):607-618.

Roux I, Safieddine S, Nouvian R, Grati M, Simmler MC, Bahloul A, *et al.* Otoferlin defective in a human deafness form, is essential for exocytosis at the auditory ribbon synapse. *Cell* 2006;127(2):277-289.

Rozen TD, Oshinsky ML, Gebeline CA, Bradley KC, Young WB, Shechter AL, *et al*. Open label trial of coenzyme Q10 as migraine preventive. *Cephalalgia* 2002;22(2):137-141.

Ryu H, Ferrante RJ. Emerging chemotherapeutic strategies for Huntington's disease. *Expert Opin Emerg Drugs* 2005;10(2):345-363.

Salviati L, Sacconi S, Murer L, Zacchello G, Franceschini L, Laverda AM, *et al*. Infantile encephalomyopathy and nephropathy with CoQ10 deficiency: A CoQ10-responsive condition. *Neurology* 2005;65(4):606-608.

Schiaffino S, Cantini M, Sartore S. T-system formation in cultured rat skeletal tissue. *Tissue Cell* 1977;9(3):437-446.

Schick F. Whole-body MRI at high field: Technical limits and clinicial potential. *Eur Radiol* 2005;15(5):946-959.

Scholler J, Farley TM, Folkers K. Response of mice with genetic dystrophy to therapy with coenzyme Q. *Int Z Vitaminforsch* 1968;38(3):369-375.

Schotland DL, Spiro D, Carmel P. Ultrastructural studies of ring fibers in human muscle disease. *J Neuropathol Exp Neurol* 1966;25(3):431-442.

Selcen D, Stilling G, Engel AG. The earliest pathological alterations in dysferlinopathy. *Neurology* 2001;56:1472-1481.

Shan X, Chi L, Ke Y, Luo C, Qian S, Gozal D, *et al*. Manganese superoxide dismutase protects mouse cortical neurons from chronic intermittent hypoxia-mediated oxidative damage. *Neurobiol Dis* 2007;28(2):206-215.

Shao X, Davletov BA, Sutton RB, Sudhof TC, Rizo J. Bipartite Ca^{2+}- binding motif in C_2 domains of synaptotagmin and protein kinase C. *Science* 1996;273(5272):248-251.

Shaul PW, Anderson RGW. Role of plasmalemmal caveolae in signal transduction. *Am J Physiol Lung Cell Mol Physiol* 1998;275(5):L843-L851.

Shtivelman E, Cohen FE, Bishop JM. A human gene (AHNAK) encoding an unusually large protein with a 1.2-microns polyionic rod structure. *Proc Natl Acad Sci USA* 1992;89(12):5472-5476.

Shults CW. Coenzyme Q10 in neurodegenerative diseases. *Curr Med Chem* 2003;10(19):1917-1921.

Sicinski P, Geng Y, Ryder-cook AS, Barnard EA, Darlison MG, Barnard PJ. The molecular basis of muscular dystrophy in the mdx mouse: A point mutation. *Science* 1989;244(4912):1578-1580.

Siemann EH, Creasy LL. Concentration of the phytoalexin resveratrol in wine. *Am J Enol Vitic* 1992;43:49-52.

Sies H. Oxidative stress: oxidants and antioxidants. *Exp Physiol* 1997; 82(2):291-295.

Silverthorn DU. Human physiology. An integrated approach. 3rd Ed. *San Francisco, CA*: Pearson, Benjamin Cummings; 2004.

Sinha K, Chaudhary G, Gupta YK. Protective effect of resveratrol against oxidative stress in middle cerebral artery occlusion model of stroke in rats. *Life Sci* 2002;71(6):655-665.

Smythe GM, Shavlakadze T, Roberts P, Davies JK, McGeachie JK, Grounds MD. Age influences the early events of skeletal muscle regeneration: Studies of whole muscle grafts transplanted between young (8 weeks) and old (13-21 months) mice. *Exp Gerontol* 2008;43(6):550-562.

Sohal R, Forster MJ. Coenzyme Q, oxidative stress and aging. *Mitochondrion* 2007;7(Suppl 1):S103-S111.

Soleas GJ, Diamandis EP, Goldberg DM. Resveratrol: A molecule whose time has come? And gone? *Clin Biochem* 1997;30(2):91-113.

Song KS, Scherer PE, Tang Z, Okamoto T, Li S, Chafel M, *et al*. Expression of caveolin-3 in skeletal, cardiac, and smooth muscle cells. Caveolin-3 is a component of the sarcolemma and co-fractionates with dystrophin and dystrophin-associated glycoproteins. *J Biol Chem* 1996;271(25):15160-15165.

Sorimachi H, Kinbara K, Kimura S, Takahashi M, Ishiura S, Sasagawa N, *et al*. Muscle-specific calpain, p94, responsible for limb girdle muscular dystrophy type 2A, associates with connectin through IS2, a p94-specific sequence. *J Biol Chem* 1995;270(52):31158-31162.

Spuler S, Carl M, Zabojszcza J, Straub V, Bushby K, Moore SA*, et al.* Dysferlin-deficient muscular dystrophy features amyloidosis. *Ann Neurol* 2008;63(3):323-328.

Stadtman ER, Levine RL. Protein oxidation. *Ann N Y Acad Sci* 2000;899:191-208.

Steen MS, Adams ME, Tesch Y, Froehner SC. Amelioration of muscular dystrophy by transgenic expression of Niemann-Pick C1. *Mol Biol Cell* 2009;20(10):146-152.

Stern LZ, Ringel SP, Ziter FA, Menander-Hube KB, Ionasescu V, Pellegrino RJ, *et al.* Drug trial of superoxide dismutase in Duchenne's muscular dystrophy. *Arch Neurol* 1982;39(6):342-346.

Straub V, Rafael JA, Chamberlain JS, Campbell KP. Animal models for muscular dystrophy show different patterns of sarcolemmal disruption. *J Cell Biol* 1997;139(2):375-385.

Straub V, Bushby K. Therapeutic possibilities in the autosomal recessive limb-girdle muscular dystrophies. *NeuroRx* 2008;5(4):619-626.

Stübgen JP, Stipp A. Limb girdle muscular dystrophy: A prospective follow-up study of functional impairment. *Muscle Nerve* 1997;20(4):453-460.

Stübgen JP. Limb girdle muscular dystrophy: An interval study of weakness and functional impairment. *J Clin Neuromusc Dis* 2008;9(3):333-340.

Sugita S, Han W, Butz S, Liu X, Fernandez-Chacon R, Lao Y, *et al.* Synaptotagmin VII as a pasma membrane Ca^{2+} sensor in exocytosis. *Neuron* 2001;30(2):459-473.

Summan M, Warren GL, Mercer RR, Chapman R, Hulderman T, van Rooijen N, *et al.* Macrophages and skeletal muscle regeneration: A clodronate-containing liposome depletion study. *Am J Physiol Regul Integr Comp Physiol* 2006;290(6):R1488-R1495.

Sun IL, Sun EE, Crane FL, Morrè DJ, Lindgren A, Löw H. Requirement for coenzyme Q in plasma membrane electron transport. *Proc Natl Acad Sci USA* 1992;89(23):11126-11130.

Sutton RB, Davletov BA, Berhuis AM, Sudhof TC, Sprang SR. Structure of the first C2 domain of synaptotagmin I: A novel Ca^{2+} / phospholipids-binding fold. *Cell* 1995;80(6):929-938.

Suzuki N, Aoki M, Hinuma Y, Takahashi T, Onodera Y, Ishigaki A, *et al*. Expression profiling with progression of dystrophic change in dysferlin-deficient mice (SJL). *Neurosci Res* 2005;52(1):47-60.

Tagawa K, Ogawa M, Kawabe K, Yamanaka G, Matsumura T, Goto K, *et al.* Protein and gene analyses of dysferlinopathy in a large group of Japanese muscular dystrophy patients. *J Neurol Sci* 2003;211(1):23-28.

Takahashi T, Aoki M, Tateyama M, Kondo E, Mizuno T, Onodera Y, *et al.* Dysferlin mutations in Japanese Miyoshi myopathy: relationship to phenotype. *Neurology* 2003;60:1799-17804.

Takaoka MJ. Of the phenolic substances of white hellebore (*Veratrum grandiflorum Loes. Fil.*). *Journal of the Faculty of Science, Hokkaido Imperial University*, 1941;3:1-16.

Takekura H, Flucher BE, Franzini-Armstrong C. Sequential docking, molecular differentiation, and positioning of T-Tubule/SR junctions in developing mouse skeletal muscle. *Dev Biol* 2001;239(2):204-214.

Tateyama M, Aoki M, Nishino I, Hayashi YK, Sekiguchi S, Shiga Y, *et al.* Mutation in the caveolin-3 gene causes a peculiar form of distal myopathy. *Neurology* 2002;58:323-325.

Taveau M, Bourg N, Sillon G, Roundaut C, Bartoli M, Richard I. Calpain 3 is activated through autolysis within the active site and lyses sarcomeric and sarcolemmal components. *Mol Cell Biol* 2003;23(24):9127-9135.

The Jackson Laboratory. *Bar Harbor, Main, USA*: JAX Mice Database – 000686 SJL/J, c2007- 2009 [updated 2009; cited 11 November, 2009], www.jax.org/jaxmice

Theate LG, Crouch RK, Spicer SS. Immunolocalization of CuZn superoxide dismutase in striated muscle. *Histochem J* 1985;17(2):259-262.

Therrien C, Dodig D, Karpati G, Sinnreich M. Mutation impact on dysferlin inferred from database analysis and computer-based structural predictions. *J Neurol Sci* 2006;250(1):71-78.

Thomson WHS, Leyburn P, Walton JN. Serum enzyme activity in muscular dystrophy. *Br Med J* 1960;2(5208):1276-1281.

Tidball JG. Force transmission across muscle cell membranes. *J Biomech* 1991;24(Suppl 1):43-52.

Tidball JG, Wehling-Henricks M. Damage and inflammation in muscular dystrophy: Potential implications and relationships with autoimmune myositis. *Curr Opin Rheumatol* 2005;17(6):707-713.

Totsuka T, Watanabe K, Uramoto I, Sakuma K, Mizutani T. Muscular Dystrophy: Centronucleation may reflect a compensatory activation of defective myonuclei. *J Biomed Sci* 1998;5(1):54-61.

Tran UC, Clarke FC. Endogenous synthesis of coenzyme Q in eukaryotes. *Mitochondrion* 2007;7(Suppl 1):S62-S71.

Turunen M, Olsen J, Dallner G. Metabolism and function of coenzyme Q. *Biochim Biophys Acta* 2004;1660(1-2):171-199.

Ueyama H, Kumamoto T, Horinouchi H, Fujimoto S, Aono H, Tsuda T. Clinical heterogeneity in dysferlinopathy. *Intern Med* 2002;41(7):532-536.

Urtizberea JA, Bassez G, Leturcq F, Nguyen K, Krahn M, Lévy N. Dysferlinopathies. *Neurol India* 2008;56(3):289-297.

Valenzano DR, Terzibasi E, Genade T, Cattaneo A, Domenici L, Cellerino A, *et al*. Resveratrol prolongs lifespan and retards the onset of age-related markers in a short lived vertebrate. *Curr Biol* 2006;16(3):296-300.

Van der Merwe CF, Coetzee J. Quetol651 for general use: a revised formulation. *Comm E M Soc S Afr* 1992;22:31-32.

Venkat Ratnam D, Ankola DD, Bhardwaj V, Sahana DK, Ravi Kumar MNV. Role of antioxiants in prophylaxis and therapy: A pharmaceutical perspective. *J Control Release* 2006;113(3):189-207.

Vieira NM, Bueno CR Jr, Brandalise V, Moraes LV, Zucconi E, Secco M, *et al*. SJL dystrophic mice express a significant amount of human muscle proteins following systemic delivery of human adipose-derived stromal cells without immunosuppression. *Stem Cells* 2008;26:2391-2398.

Von der Hagen M, Laval SH, Cree LM, Haldane F, Pocock M, Wappler I, *et al*. The differential gene expression profiles of proximal and distal groups are altered in pre-pathological dysferlin-deficient mice. *Neuromuscul Disord* 2005;15(12):863-877.

Wagner KR. Genetic disease of muscle. *Neurol Clin* 2002;20(3):645-678.

Walton JN, Nattrass FJ. On the classification, natural history and treatment of the myopathies. *Brain* 1954;77(2):169-231.

Walton JN. Clinical voluntary muscle. *London*: Churchill Livingstone; 1981.

Wang Q, Xu J, Rottinghaus GE, Simonyi A, Lubahn D, Sun GY, *et al*. Resveratrol protects against global ischemic injury in gerbils. *Brain Res* 2002;958(2):439-447.

Ward S, Argon Y, Nelson GA. Sperm morphogenesis in wild-type and fertilization-defective mutants of *Caenorhabditis elegans*. *J Cell Biol* 1981;91(1):26-44.

Washington NL, Ward S. FER-1 regulates Ca2+-mediated membrane fusion during *C. elegans* spermatogenesis. *J Cell Sci* 2006;119(12):2552-2562.

Webster C, Blau HM. Accelerated age-related decline in replicative life-span of Duchenne muscular dystrophy myoblasts: Implications for cell and gene therapy. *Somat Cell Mol Genet* 1990;16(6):557-565.

Weiler T, Greenberg CR, Nylen E, Halliday W, Morgan D, Eggerston D, *et al.* Limb-girdle muscular dystrophy and Miyoshi myopathy in an aboriginal Canadian kindred map to LGMD 2B and segregate with the same haplotype. *Am J Hum Genet* 1996;59(4):872-878.

Weiler T, Bashir R, Anderson LV, Davison K, Moss JA, Britton S, *et al.* Identical mutation in patients with limb girdle muscular dystrophy type 2B or Miyoshi myopathy suggests a role for modifier gene(s). *Hum Mol Genet* 1999;8(5):871-877.

Weller AH, Magliato SA, Bell KP, Rosenberg NL. Spontaneous myopathy in the SJL/J mouse: Pathology and strength loss. *Muscle Nerve* 1997;20(1):72-82.

Wenzel K, Zabojszcza J, Carl M, Taubert S, Lass A, Harris CL, *et al.* Increased susceptibility to complement attack due to down-regulation of decay-accelerating factor/CD55 in dysferlin-deficient muscular dystrophy. *J Immunol* 2005;175:6219-6225.

Yabe I, Kawashima A, Kikuchi S, Higashi T, Fukazawa T, Hamada T, *et al.* Caveolin-3 gene mutation in Japanese with rippling muscle disease. *Acta Neurol Scand* 2003;108(1):47-51.

Yamaji S, Suzuki A, Sugiyama Y, Koide YI, Yoshida M, Kanamori H, *et al*. A novel integrin-linked kinase-binding protein, affixin, is involved in the early stage of cell-substrate interaction. *J Cell Biol* 2001;153(6):1251-1264.

Yamaji S, Suzuki A, Kanamori H, Mishima W, Yoshimi R, Takasaki H, *et al*. Affixin interacts with alpha-actinin and mediates integrin signalling for reorganization of F-actin induced by initial cell-substrate interaction. *J Cell Biol* 2004;165(4):539-551.

Yasunaga S, Grati M, Cohen-Salmon M, El-Amraoui A, Mustapha M, Salem N, *et al*. A mutation in OTOF, encoding otoferlin, a FER-1-like protein, causes DFNB9, a non-syndromic form of deafness. *Nat Genet* 1999;21(4):363-369.

Yasunaga S, Grati M, Chardenoux S, Smith TN, Friedman TB, Lalwani AK, *et al.* OTOF encodes multiple long and short isoforms: Genetic evidence that the long ones underlie recessive deafness DFNB9. *Am J Hum Genet* 2000;67(3):591-600.

Young B, Lowe JS, Stevens A, Heath JW. Wheater's functional histology. A text and colour atlas. 5th Ed. *Elsevier*: Churchill Livingstone; 2006.

Yumoto T, Dmochowski L. Light and electron microscope studies of organs and tissues of SJL/J strain mice with reticulum cell neoplasms resembling Hodgkin's disease. *Cancer Res* 1967;27(1):2098-2112.